XUV PHOTOABSORPTION STUDIES ALONG EXTENDED ISOELECTRONIC SEQUENCES USING A DUAL LASER PRODUCED PLASMA TECHNIQUE.

BY JAMES BRILLY. M.Sc.

ABSTRACT.

Hot dense plasmas produced when the output of powerful pulsed laser systems are focused onto targets located in vacuum have been the subject of extensive study for a number of years. Such plasmas have found applications both as intense sources of continuum radiation in the XUV and as a versatile source of ionic species. In the work reported here the above properties of the laser produced plasma were exploited and enabled many new photoabsorption spectra of ionic species to be recorded in the XUV region.

Using a dual laser produced plasma technique the XUV radiation emitted from laser plasmas created on the surface of a high Z material was used to backlight a second laser plasma and carry out ionic photoabsorption studies at wavelengths below 300Å. An extensive examination of a number of isoelectronic sequences was undertaken. XUV photoabsorption studies were carried out on members of the neon, sodium, argon, krypton, bromine, selenium and xenon sequences.

Absorption along the neon like sequence was extended to the fifth member; Si V. We report here the first unambiguous photoabsorption spectrum of the neon like Al^{3+} ion showing the principal outer shell transitions together with 2s inner shell autoionizing features. Detailed XUV photoabsorption spectra of the Si^{4+} ion are reported here for the first time, excitations involving an inner 2s electron were classified and in the case of the 2s→3p transition found to be an example of *forced autoionization.* An intensity anomaly in the Beutler Fano line shape of the 2s→3p member of the autoionizing series in Si^{4+} was studied with varying plasma conditions.

Absorption studies along the sodium isoelectronic sequence have resulted in the classification of new lines arising from transitions to core excited autoionizing levels in the Al^{2+} and Si^{3+} ions; transitions from ground and excited states were observed.

XUV photoabsorption spectra of plasmas formed on targets of elements following argon (scandium and titanium) in the periodic table were found to be of a complex nature and to contain contributions from a number of different ion stages

Elements following krypton were also studied Absorption spectra of laser produced plasmas formed on targets of strontium, yttrium and zirconium were recorded The strontium and yttrium work resulted in 3d→4p transitions being observed in a number of ion stages for the first time

Work along the xenon sequence was found to be in agreement with previous Ba^{2+} observations Absorption studies along the sequence were extended to the fifth member Ce^{4+} An extensive analysis of the 4d photoabsorption spectrum of La^{3+} was carried out and revealed that the 4d→4f transition, expected to be the strongest was not observed The interpretation of the spectrum showed that the feature possessed a large autoionization width and was not present in the experimental spectrum The analysis further confirmed that the 4f wave function in Ba^{2+} is only partially collapsed

The work reported here has clearly shown the dual laser produced plasma technique to be a powerful and versatile method for recording XUV photoabsorption spectra of ionized species

XUV PHOTOABSORPTION STUDIES ALONG EXTENDED ISOELECTRONIC SEQUENCES USING A DUAL LASER PRODUCED PLASMA TECHNIQUE.

A THESIS FOR THE DEGREE OF

DOCTOR OF PHILOSOPHY

BY

JAMES BRILLY. M.Sc.

SCHOOL OF PHYSICAL SCIENCES
DUBLIN CITY UNIVERSITY

RESEARCH SUPERVISOR
PROF EUGENE T KENNEDY B Sc Ph D C Phys F Inst P
APRIL 1990

DECLARATION

THIS THESIS IS BASED ON THE WORK OF THE AUTHOR

DEDICATION

THIS THESIS IS DEDICATED TO MY PARENTS.

Kathleen and Jack

Contribution, ocean vast, drop of rain
Effect, molecule, hurricane
Important work, these pages contain
Balance of all Oceanic, molecular
Nothing, God nor atomic physics,
could bar a man from heaven for

Jim Brilly

Ever try
Ever fail
Never mind
Try again
Fail better

Samuel Beckett

TABLE OF CONTENTS

CHAPTER FOUR: THE SODIUM ISOELECTRONIC SEQUENCE.

CHAPTER FIVE: THE ARGON ISOELECTRONIC SEQUENCE.

CHAPTER SIX THE Kr, Br and Se ISOELECTRONIC SEQUENCES

CHAPTER SEVEN: THE XENON ISOELECTRONIC SEQUENCE.

CHAPTER EIGHT: COMMENTS AND CONCLUSIONS.

XUV PHOTOABSORPTION STUDIES ALONG EXTENDED ISOELECTRONIC SEQUENCES USING A DUAL LASER PRODUCED PLASMA TECHNIQUE.

ABSTRACT

Hot dense plasmas produced when the output of powerful pulsed laser systems are focused onto targets located in vacuum have been the subject of extensive study for a number of years Such plasmas have found applications both as intense sources of continuum radiation in the XUV and as a versatile source of ionic species. In the work reported here the above properties of the laser produced plasma were exploited and enabled many new photoabsorption spectra of ionic species to be recorded in the XUV region

Using a dual laser produced plasma technique the XUV radiation emitted from laser plasmas created on the surface of a high Z material was used to backlight a second laser plasma and carry out ionic photoabsorption studies at wavelengths below 300Å An extensive examination of a number of isoelectronic sequences was undertaken. XUV photoabsorption studies were carried out on members of the neon, sodium, argon, krypton, bromine, selenium and xenon sequences

Absorption along the neon like sequence was extended to the fifth member, Si V We report here the first unambiguous photoabsorption spectrum of the neon like Al^{3+} ion showing the principal outer shell transitions together with 2s inner shell autoionizing features. Detailed XUV photoabsorption spectra of the Si^{4+} ion are reported here for the first time, excitations involving an inner 2s electron were classified and in the case of the 2s→3p transition found to be an example of *forced autoionization* An intensity anomaly in the Beutler Fano line shape of the 2s→3p member of the autoionizing series in Si^{4+} was studied with varying plasma conditions.

Absorption studies along the sodium isoelectronic sequence have resulted in the classification of new lines

arising from transitions to core excited autoionizing levels in the Al^{2+} and Si^{3+} ions, transitions from ground and excited states were observed

XUV photoabsorption spectra of plasmas formed on targets of elements following argon (scandium and titanium) in the periodic table were found to be of a complex nature and to contain contributions from a number of different ion stages.

Elements following krypton were also studied Absorption spectra of laser produced plasmas formed on targets of strontium, yttrium and zirconium were recorded The strontium and yttrium work resulted in 3d→4p transitions being observed in a number of ion stages for the first time.

Work along the xenon sequence was found to be in agreement with previous Ba^{2+} observations Absorption studies along the sequence were extended to the fifth member Ce^{4+} An extensive analysis of the 4d photoabsorption spectrum of La^{3+} was carried out and revealed that the 4d→4f transition, expected to be the strongest was not observed The interpretation of the spectrum showed that the feature possessed a large autoionization width and was not present in the experimental spectrum. The analysis further confirmed that the 4f wave function in Ba^{2+} is only partially collapsed.

The work reported here has clearly shown the dual laser produced plasma technique to be a powerful and versatile method for recording XUV photoabsorption spectra of ionized species

CHAPTER ONE INTRODUCTION

1 1 INTRODUCTION

The work reported in this thesis is concerned with photoabsorption studies of ionized species and the extension of these studies along isoelectronic sequences We have employed a dual laser produced plasma technique to record the XUV absorption spectra of a number of different ionized species, using targets of different elements It is the intention of this chapter to provide a comprehensive introduction to the thesis by firstly outlining the scope of the work reported in succeeding chapters and secondly, by reviewing those areas of physics which overlap with or may otherwise be considered relevant to the work reported here The areas reviewed include, absorption spectroscopy of ions and of neutral species, recent relevant advances in experimental atomic spectroscopy and VUV and soft X-ray laser schemes Chapter two deals with the experimental method employed to record the spectra discussed in later chapters The various component parts of the experimental set up are described including the laser, target chamber and the spectrograph used Concise and detailed explanations of the many aspects of the various types of experiment carried out are given

The remainder of the thesis deals with work undertaken along the different isoelectronic sequences, the classification of the various elements studied is in order of increasing atomic number Absorption spectra of laser produced plasmas of elements following neon, argon, krypton and xenon in the periodic table have been studied and many new spectra of ions of these elements are presented and discussed Many of the absorption spectra presented in the succeeding chapters are reported here

for the first time. The results are grouped by isoelectronic sequence so that for each member of a sequence, the work carried out is discussed and where appropriate, trends along the sequence are examined. The new spectra presented may be classified into four distinct groups· The first group are ions of those elements following neon in the periodic table and which form the neon like sequence. Of particular interest along this sequence is the spectrum of Si^{4+} where we report what we believe to be the first observation of forced autoionization in a laser produced plasma Other ions of the elements which follow neon and which are members of the sodium sequence have been extensively investigated and in this case a full and detailed report on experimental observations and analyses of photoabsorption involving core excited autoionizing levels is given

Ions of the argon like isoelectronic sequence have been investigated and in the particular case of scandium and titanium ions new absorption features have been observed The third group of elements studied here are those elements which follow krypton in the periodic table New absorption features thought to arise from inner shell excitations in ions of strontium and yttrium have been observed and are discussed.

The last isoelectronic sequence presented in this study is that of xenon The xenon sequence has been the subject of extensive experimental investigation and chapter seven comprises a full and detailed report on the work carried out including the recent analysis of the 4d photoabsorption results for higher members of the xenon sequence.

The table given below includes the members of the various isoelectronic sequences for which absorption spectra have been recorded and which are reported in subsequent chapters of this work

TABLE 11

FOLLOWING THE ELEMENT:	IONS STUDIED:
NEON	Mg^{2+} Al^{2+} Al^{3+} Si^{3+} Si^{4+}
ARGON	Sc^{2+} Sc^{3+} Ti^{3+} Ti^{4+}.
KRYPTON.	Sr^{2+} Sr^{3+} Y^{3+} Y^{4+} Y^{5+} Zr^{4+}.
XENON.	Ba^{2+} La^{3+} (Ce^{4+}).

In all of the above cases an analysis of the observed features has been attempted, for many of the spectra reported this analysis may be considered fairly complete However, for a number of the ions involved the recorded spectra were found to be of an exceedingly complex nature, or were extremely weak, or both and for these cases only a tentative or partial analysis is reported

1 2 ABSORPTION SPECTROSCOPY OF IONS IN THE VUV REGION

Experiments leading to photoabsorption spectra of ionized species in the XUV region of the spectrum are a potentially vast source of new and fundamental information on various atomic processes Such experiments can provide valuable information which cannot be obtained from emission spectra alone In recent years there has been a growing and sustained interest in photoabsorption experiments involving both neutral and ionic species Information concerning the excitation of inner shell electrons, double electron excitations and photo-ionization continua can be readily obtained from the absorption spectra of neutrals and ionized species This is easily seen from the fact that to record an emission spectrum containing information on inner shell transitions would require that the inner shell contains a vacancy, this situation is rarely the case. Although the number of reported experiments in this field is increasing every year with increasing numbers of spectra

being published, relatively few elements have been studied in this way when compared to the more established techniques of emission spectroscopy The reason for this is due largely to the experimental difficulties involved For ionic species these difficulties center around obtaining a sufficiently high ion density in the absorbing column together with the added problem of providing a suitable line free continuum light source in the XUV region.

Photoabsorption spectroscopy of neutral species.
Early work on the photoionization spectroscopy of gases (Madden and Codling 1963, 1964, 1965, Codling and Madden 1964, 1965) and later on vapors (Garton et al 1969, Connerade et al 1971, Wolff et al 1972, Connerade and Mansfield 1972, 1973) paved the way for absorption studies of ionized species. The experiments performed were straightforward in principle, though perhaps more difficult in practice The apparatus consisted of a radiation source, a sample chamber and a spectrometer equipped with a suitable detector normally a photographic plate The information obtained was for the most part wavelength information concerning unidentified features, in certain cases if the photographic plates were calibrated, cross sections and line profiles could be measured. In many of the experiments the light source consisted of a synchrotron Fig.(1 1) shows a typical experimental set up used to obtain the absorption spectra of the rare gases using synchrotron radiation as the background source Indeed synchrotron radiation has played a key role in advances in absorption spectroscopy of neutral species This source is ideally suited to absorption studies of neutrals because it is a powerful, clean (i e., line free) and reproducible source of continuum radiation covering the wavelength range 10-1000Å, see Codling (1973). Connerade (1978) discusses the many early absorption results obtained for both gases and vapors using synchrotron radiation as a back lighting source.

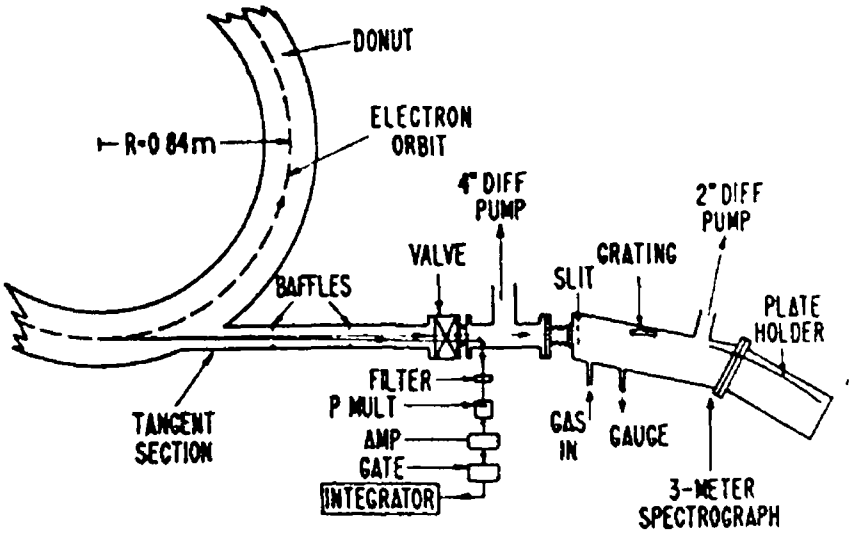

FIG 11

The experimental set up used by Madden and Codling to record the absorption spectra of the rare gases in the VUV region using synchrotron radiation. (after Madden and Codling 1963)

The BRV (Balloffet, Romand and Vodar 1960) source provides a relatively clean windowless continuum source at wavelengths between 150-600Å and has been used as a continuum light source in this wavelength region for a number of years Fig (1 2 a b) shows the source and illustrates a typical experimental arrangement used to record the VUV absorption spectrum of a vapor, (Garton et al 1969) The source uses a triggered discharge between a uranium anode and a brass cathode. Many absorption experiments which utilize this source have been reported and photoabsorption spectra of both neutral and ionized species have been extensively studied, (Esteva and Mehlman 1974, Sugar et al 1979, Lucatorto et al 1981)

The BRV source has now been superseded to a large extent by the laser produced plasma as a table top continuum light source in the XUV region. Laser produced plasmas were found (Carroll and Kennedy 1977, Carroll et al 1978, 1980) to have strong emission spectra in the VUV region which, for certain elements consist of almost completely

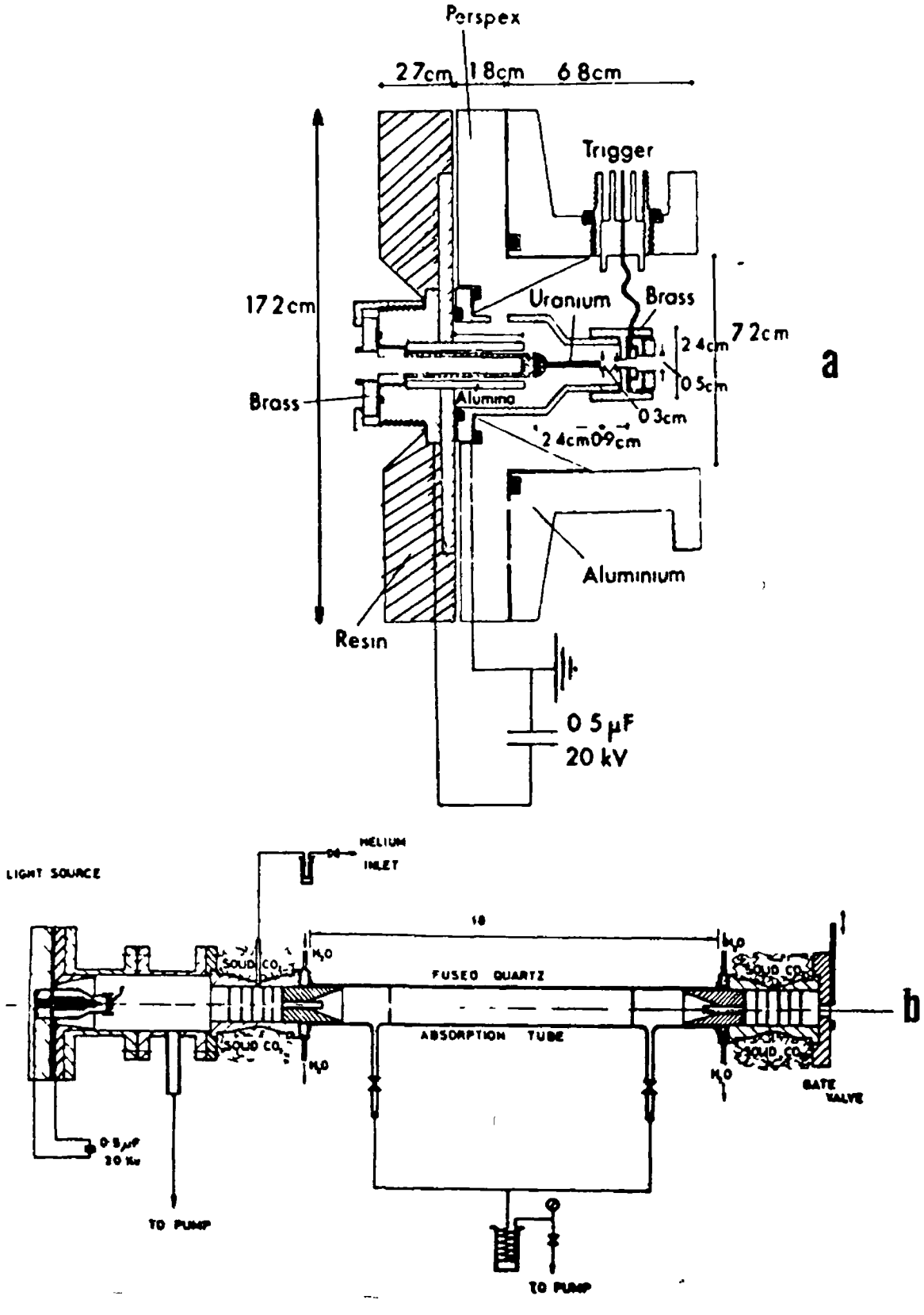

FIG 12

(a). Shows a BRV spark source in cross section, the source was used as a backlighting continuum for early absorption experiments in the VUV region. (b). Shows an experimental arrangement used to record the photoabsorption spectra of metal vapours in the VUV. (After Garton et al 1969).

line free continua. Such a versatile short wavelength continuum source has found many and varied applications some of which will be further discussed in a later section of this chapter

XUV Photoabsorption spectroscopy of ions.

A variety of techniques have been developed and used to record XUV photoabsorption spectra of ions As mentioned above, the need to create a sufficient absorbing column density of ionic species means that each approach which has been employed to date uses a dual plasma technique, i.e., one plasma is created to provide the column of absorbing ions while the second plasma acts as the continuum light source used to probe the absorbing plasma.

Some early work on the absorption spectroscopy of ionized species in the VUV was carried out using *single discharge plasmas* (Feldman et al 1967) where the absorption was along the plasma length. Kastner et al (1977) used such a discharge to record absorption spectra of ions from the neon and argon isoelectronic sequences. However, there are essentially only three methods which have been successfully employed over the years to carry out extensive studies of ionic absorption. These methods are (1) a synchronized *dual vacuum spark technique,* (2) *resonant laser driven ionization (RLDI)* and (3) the use of two *laser produced plasmas*

The earliest report of an absorption experiment involving the use of two plasmas was that of Hildum and Cooper (1972) who used a z-pinch discharge as the absorption cell with a theta-pinch plasma as the background light source They studied absorption features in a number of ions including C^{+}, Si^{+} and Si^{2+} Fig (1.3 a) shows the experimental set up for this early two plasma experiment The first absorption experiment to use two synchronized vacuum spark discharges was reported by Mehlman and Esteva (1974). Using this technique originally proposed

by Mehlman et al (1969) the VUV absorption spectra of a number of light ions and neutral species were recorded Fig (1.3 b) shows the method with the two spark sources aligned such that the axes of the two devices form a right angle. One of the sources used a uranium anode to provide the back lighting continuum while the other was used as an absorbing medium. The ions to be studied were generated at the tip of the second BRV spark device simply by replacing the uranium anode with an anode of the appropriate material By using a time delay between the two sparks it was possible to obtain time resolved spectra of neutral and singly ionized beryllium (Mehlman and Esteva 1974) and neutral, singly ionized and doubly ionized magnesium (Esteva and Mehlman 1974) This technique has not been extended to other ions

The technique of *flash pyrolysis* was used by Cantu et al (1977) to study the absorption spectra of neutral and singly ionized lithium Finely divided Li_2N, Li_2O or LiH was placed in a quartz or glass absorption tube which was surrounded by a helical flash lamp, the material in the tube was heated, vaporised and ionized by the strong luminous flux emitted by the flash lamp A BRV source synchronized with the flash lamp provided the back lighting continuum

The technique of *resonant laser driven ionization (RLDI)* uses one or more high powered pulsed tunable lasers to ionize a column of vapor, contained within a heat pipe (See Fig 1 4) This technique has proven to be a versatile and productive method for obtaining the absorption spectra of singly and doubly ionized species By tuning the lasers to resonance lines of the atoms present in the vapor ($\rho \simeq 10^{15}$ atoms, cm^{-3}) it was found (Lucatorto and McIlrath 1976) that a column of metal vapor could be completely ionized This technique has been widely used to study the absorption spectra of a number of ions including Li^+ (McIlrath and Lucatorto 1977), Na^+ (Sugar et al 1979), Ba^+ and Ba^{2+} (Lucatorto et

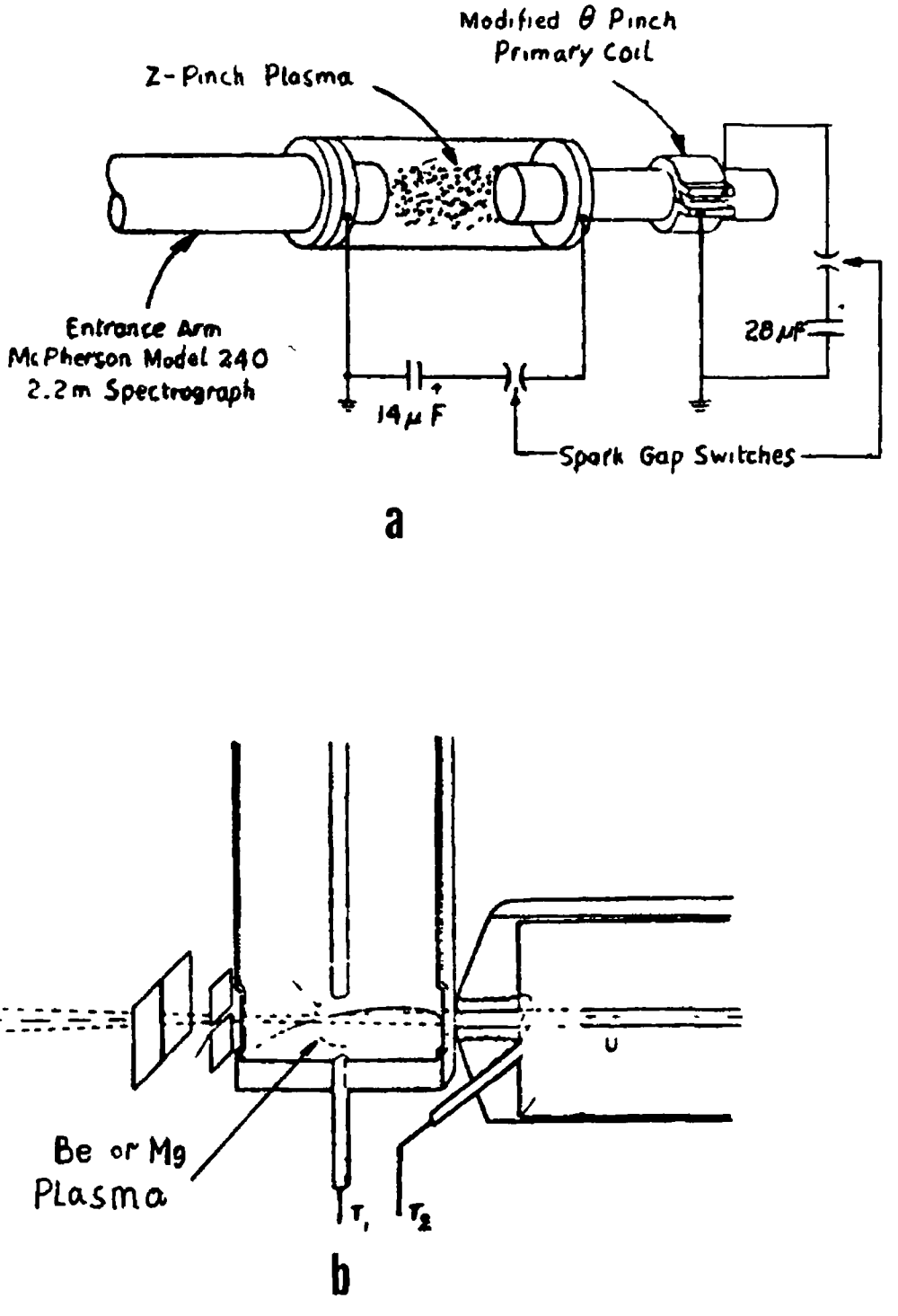

FIG 13

(a). Shows an early two plasma method used to record the absorption spectra of Si ions in the VUV region. (After Hildum and Cooper 1972). (b). Shows a dual BRV spark experiment which was used to record absorption spectra of a number of ionized species. T_1 and T_2 are the trigger electrodes used to initiate the discharges. (After Esteva and Mehlman 1974).

al 1981). Over the cycle of the laser pulse, resonant photoabsorption of the laser light occurs and causes a population build up in the upper level of the transition. These excited atoms then become ionized either by multi photon absorption or by collisions with other excited atoms; the various mechanisms involved in the process have been discussed by Lucatorto and McIlrath (1980) and more recently by Clark and Lucatorto (1987). Multi photon ionization produces a small number of free electrons which become rapidly heated by super elastic collisions with excited atoms within the vapor column, the atoms are in turn re-excited by the laser. When the free electrons acquire sufficient energy, electron impact ionization of ground and excited state atoms then becomes important and a chain reaction follows. As a function of time after the initiation of the laser pulse the population of ground state atoms will decrease more or less monotonically, the population of ions, on the other hand, increases from zero to as much as 100%. By suitable timing of a VUV pulse with respect to the laser pulse the absorption spectra of various mixtures of ground state, excited and ionized atoms can be recorded. This is one of the principal advantages of the technique, i.e. that by employing suitable time delay circuitry to control the two pulses one may observe absorption from either the ground state or from excited states. A number of papers have reported results of absorption from excited states of either ions or neutrals, see for example Sugar et al (1979) and Sonntag et al (1986). The pulsed VUV continuum source used in early work with this technique was a uranium anode (BRV) spark; the current version of the experimental arrangement employs a Nd:YAG laser to create a back lighting plasma on the surface of a high Z target, (Cromer et al 1985, Sonntag et al 1986, Cooper et al 1989). The laser produced plasma continuum source is well suited to time resolved absorption studies (Carroll and Costello 1986) because it provides an intense pulse of quasi continuum radiation with a pulse duration similar to that of the laser used to create the plasma, typically 15-40nsec.

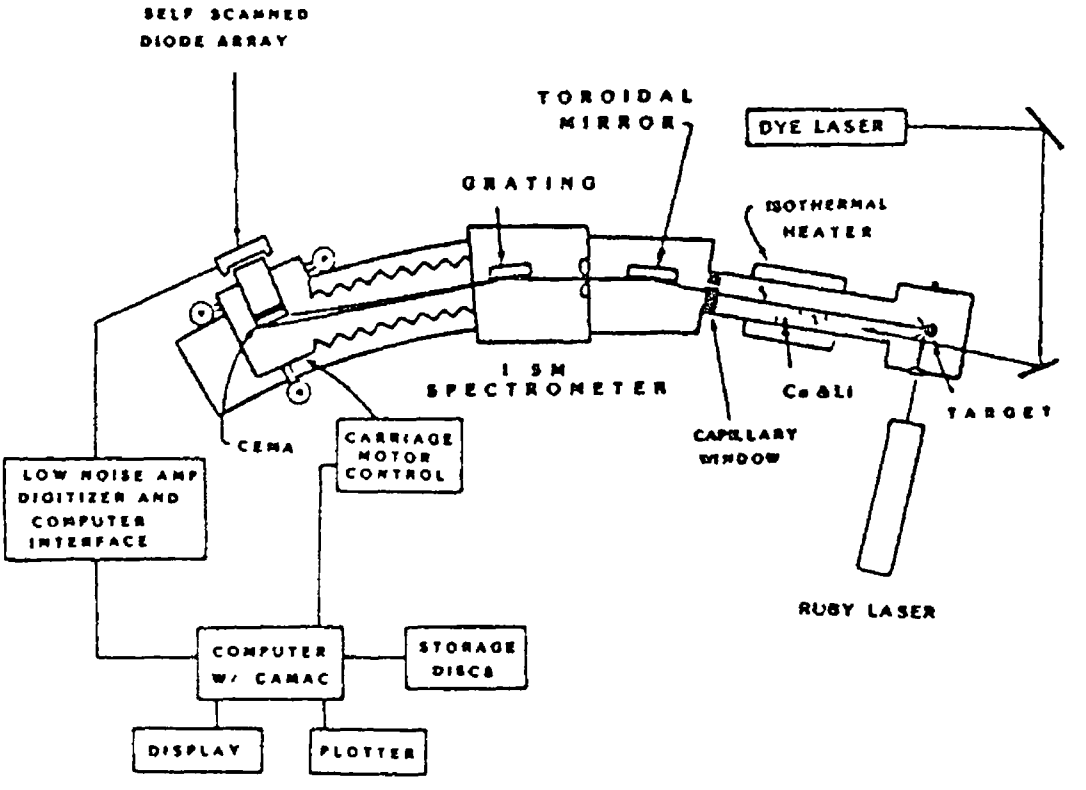

FIG 14
Shows the experimental set up of the RLDI technique which uses a laser produced plasma as the backlight, see text After Cromer et al (1985).

The basic underlying mechanisms of RLDI are not as yet entirely understood, however, the technique has found wide application and many atomic and ionic species have been studied The technique has the considerable disadvantage of only being applicable to neutrals and to singly and doubly ionized species The lack of laser technology at short wavelengths and the fact that the tunable lasers used in the approach cannot be readily frequently doubled into the VUV prevents the extension of this absorption work to higher members of those isoelectronic sequences studied

By far the most versatile absorption technique which has yet been applied to record the absorption spectra of ionized species is the *dual laser produced plasma technique* This technique has been applied by a number of different groups with the result that many new spectra have thus far been reported This technique was first

employed by Carillon et al (1970) to study the absorption of XUV radiation emitted by one aluminium laser produced plasma by another aluminium laser produced plasma. Ions in the absorbing plasma particularly the neon like Al^{3+} ion were seen to absorb radiation emitted from the hot central core of the backlighter plasma.

The experiment used the output of a single high power Q-switched laser divided by an optical delay line between two separated aluminium targets. In these experiments (Carillon et al 1970, 1972, Jamelot et al 1972) both principal series absorption as well as autoionizing structures were reported for the Al^{3+} ion. However, because of the intense line emissions from other ion stages present in both of the plasmas very little quantitative information about the absorption spectrum of Al^{3+} was obtained. Fig.(1.5.a) illustrates the main features of the experiment of Carillon et al (1970).

The dual laser produced plasma technique became a more fruitful approach when it was discovered (Carroll and Kennedy 1977, Carroll et al 1978, 1980) that when a moderate to high powered (>300mJ of optical energy per pulse) Q-switched laser pulse was focused onto the surface of certain metal targets (Z>62) in a vacuum, a hot dense plasma was formed; the spectral output of such plasmas in the XUV region were found to be largely continuum in nature. These laser produced continua were also found (Carroll et al 1983) to cover the wavelength range 40-2000Å depending on the specific target material. The rare earth elements as well as elements such as tungsten, hafnium and tantalum were found to produce particularly clean (i.e., line free) continua in the XUV region. The origin of these continua has been discussed (O'Sullivan 1980, 1987, Nicolosi et al 1981); they may be thought of as essentially a recombining continuum originating due to free bound transitions within the expanding laser produced plasma. The laser plasma has the highest spectral radiance of any XUV light source available. This fact alone makes the laser plasma ideal

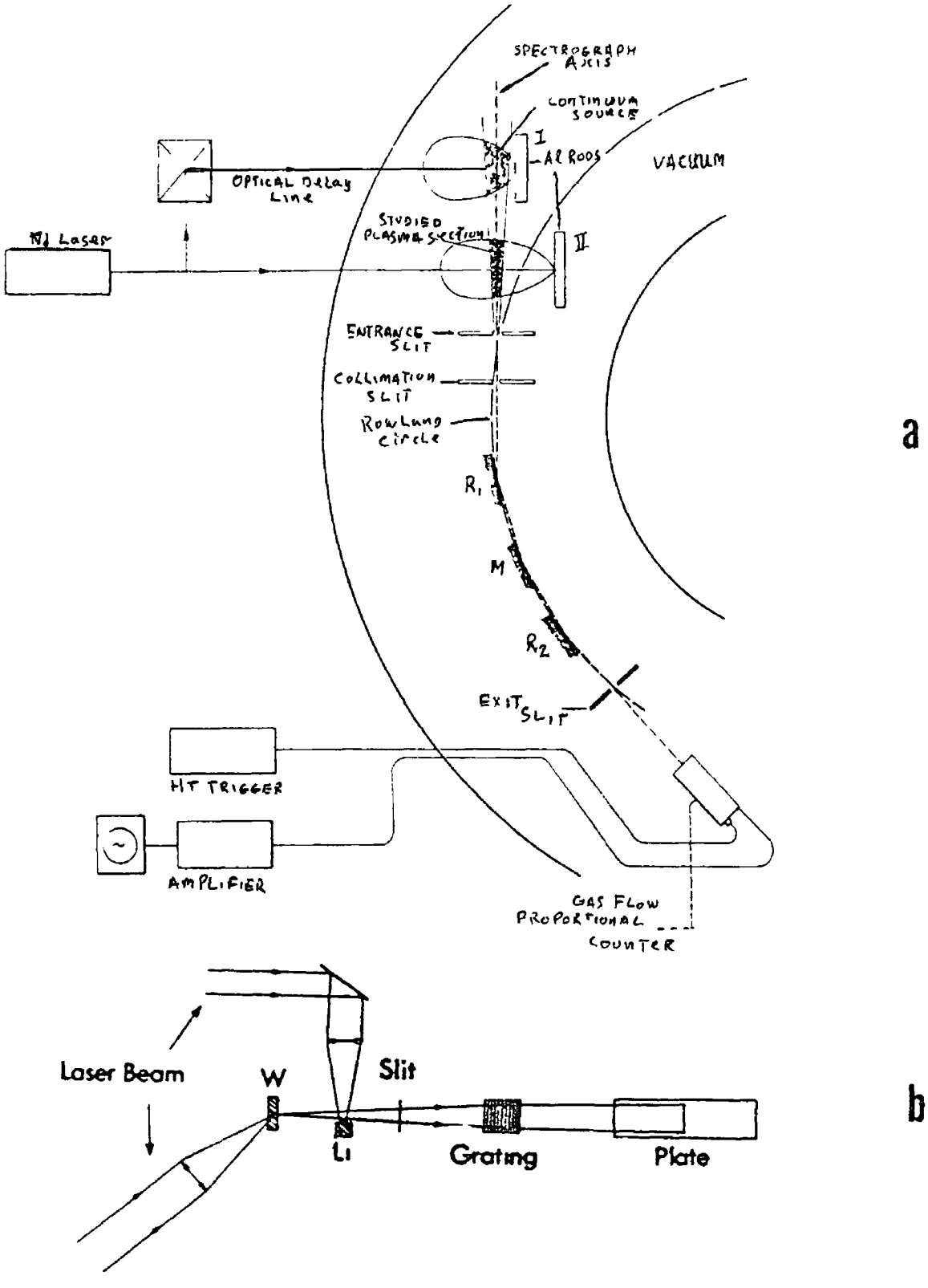

FIG 15

(a). Shows the experimental arrangement of the first dual laser produced plasma absorption experiment, radiation from the rear aluminium plasma was used to probe the second aluminium plasma, see text. After Carillon et al (1970). (b). The first dual laser produced plasma absorption experiment to employ a continuum emitting plasma as the backlighting source. (After Carroll and Kennedy 1977).

for use as a back-lighting source in ionic absorption studies The fact that such plasmas may be readily created using even a moderately high powered pulsed laser means that unlike the synchrotron the laser produced plasma XUV source is accessible to most researchers

By employing a tungsten target and creating the back-lighting plasma on the tungsten surface in a dual laser produced plasma absorption experiment, the first XUV absorption spectrum of a laser plasma free from superimposed emission lines was recorded by Carroll and Kennedy (1977). They used a crossed target configuration in which the incident ruby laser beam (1 5J,30nsec) was divided with a beam splitter and focused to each of the targets to create two separated plasmas which were orthogonally opposed to each other, the method is schematically illustrated in Fig (1 5 b). The resulting spectrum was as a consequence spatially resolved They observed in the absorption spectrum of a lithium plasma the principal series together with the adjoining photoionization continuum in helium like Li^{+} Also observed in Li^{+} were the doubly excited autoionizing resonances, $1s^2\ ^1S \rightarrow 2snp\ ^1p$

The group of Jannitti et al (1984, 1985, 1986 and 1988) have undertaken absorption studies further along the He isoelectronic sequence and have extended the absorption spectra to the fifth member C^{4+}. They use a two laser produced plasma method with the continuum radiation being produced some way from the absorbing plasma A toroidal mirror is used to focus the continuum radiation through the absorbing plasma and onto the entrance slit of a 2m grazing incidence spectrograph The detection system employed consists of a VUV sensitive scintillator which lies along the Rowland cylinder of the spectrograph. The visible scintillator emissions are taken from the spectrograph via a fiber optic bundle to an image intensifier and from there to a 512 element photo diode array coupled to an optical multi channel analyser (OMA)

A schematic diagram of the apparatus which indicates the salient features of the set up is given in Fig (1 6).

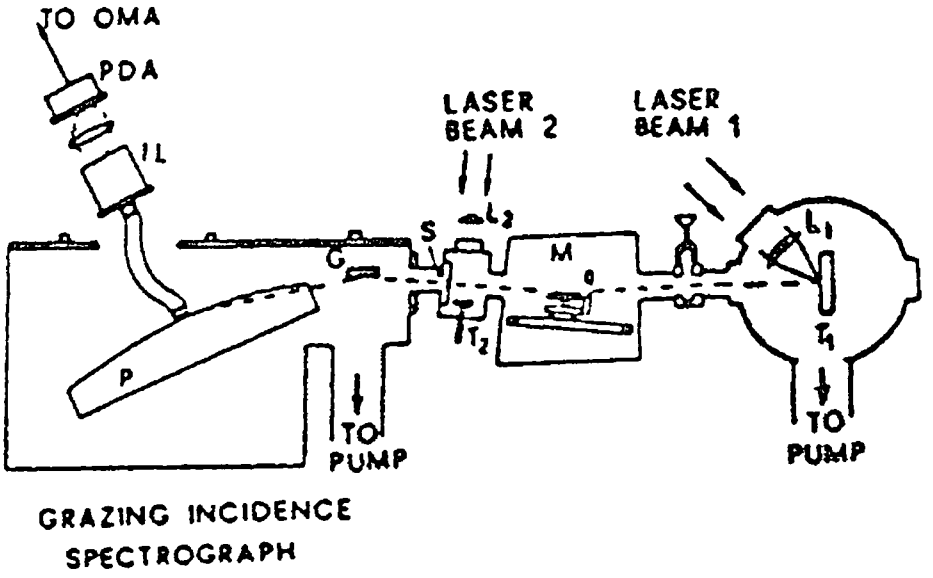

FIG 1 6

A dual laser produced plasma experiment which uses a toroidal mirror to focus the XUV continuum radiation onto the slit of the spectrograph and then to the photodiode array (PDA) to detect the spectrum. After Jannitti et al (1988).

Because of the detection system used the subtraction of background noise is a matter of simplicity and hence photoionization cross sections and line profile measurements are more easily made than with photographic plates

Carroll and Costello (1986) presented photoabsorption results obtained with a dual laser produced plasma system which used two separate lasers to create the plasmas In this twin laser system one laser was used to create the absorbing plasma while the second laser was brought to a focus on the surface of a high Z target to produce the back lighting VUV radiation In the experiment the pumping pulses of both laser systems were synchronized. A continuously variable time delay from 250nsec to 10msec could be introduced between the output pulses of both lasers For short time delays it was found that the dominant absorption occurred for ionized species whereas

for longer time differences neutral species dominated in the absorbing plasma The experimental set up used is represented in Fig (1 7) This technique has proved to be of particular importance in the study of those elements (e g , U, Th, W) which are either so highly refractory and/or corrosive that the conventional methods used to obtain the absorption spectrum of a vapor are not applicable. Carroll and Costello (1986) used the technique to record the absorption spectrum of neutral thorium (a highly refractory material) in the 80-140eV region, which was the first recording of that spectrum In later work the authors carried out the first absorption study of uranium in the vapor phase, (Carroll and Costello 1987) They found in agreement with theory that the VUV absorption spectrum of neutral uranium in the vapor phase, in common with solid uranium (Cukier et al 1978) and UF_4 (Connerade et al 1980) contained a giant 5d → 5,6f resonance.

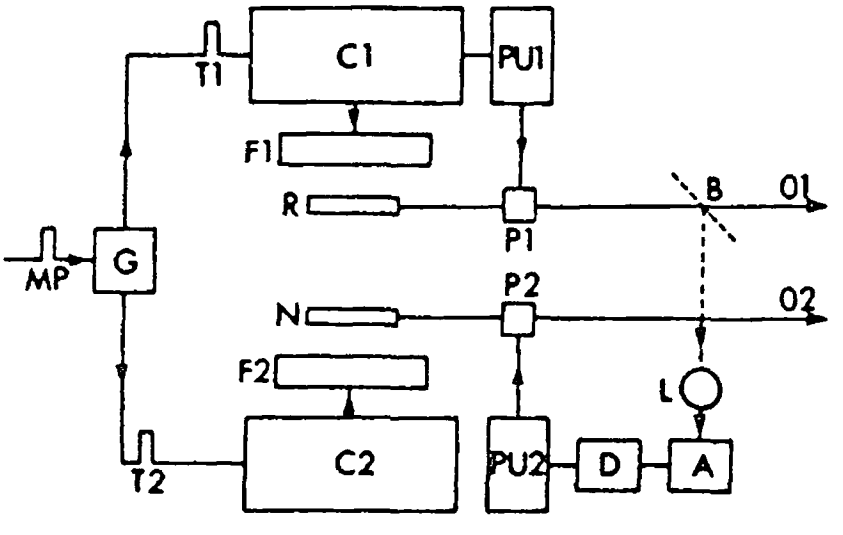

FIG 1 7
The twin laser system used to record XUV absorption spectra of refractory metal vapors. After Carroll and Costello (1986).

Lacey et al (1986) have employed a dual laser produced plasma technique to study an indium laser plasma produced on the surface of a molten indium target The object of the experiment was to probe the plasma which was intended to form the medium for a proposed short wavelength laser scheme. One important feature of this experiment is the illustration that by employing a liquid metal target the problem of surface wear is averted The experimental method used by Lacy and his co-workers is shown graphically in Fig (1 8 a b)

More recently Balmer et al (1989) have used a sophisticated experimental set up to study laser produced plasmas in absorption. The apparatus used is shown in Fig (1 9). Two high powered lasers were used in the experiment One of the lasers creates the main absorbing plasma on a slab of material at t=0, while the second laser was used to create the back-lighting plasma at t>0 by irradiating a thin (approximately 20μm) diameter wire of a second material The experiment resulted in both spatial and temporal resolution measurements of the absorbing plasma and from these results it was possible to determine ground state populations of specific ions within the plasma as well as providing detailed information about the ionization balance and temperature of the absorbing plasma as a function of time and space Such involved experiments are clearly a step forward in plasma diagnostics and should provide important information which may be useful in x-ray laser experiments A review of absorption diognostic techniques for dense laser produced plasmas has recently been given by Willi (1988), in which are described the various methods by which dense laser produced plasmas have been characterised by absorption

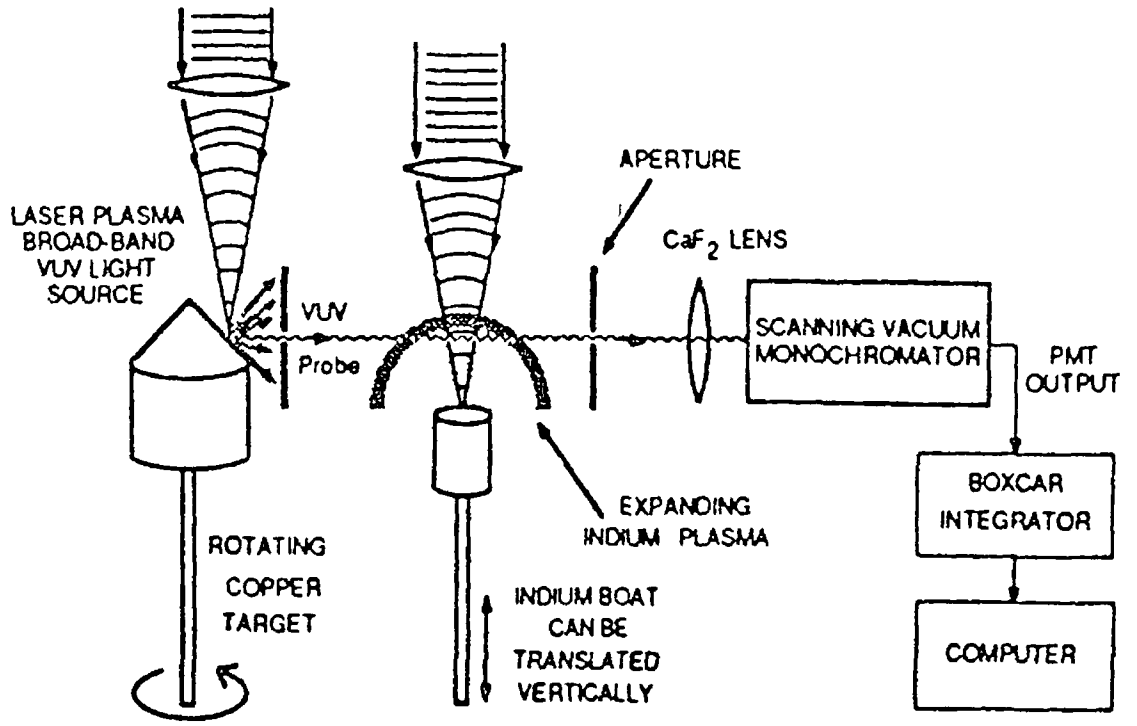

a

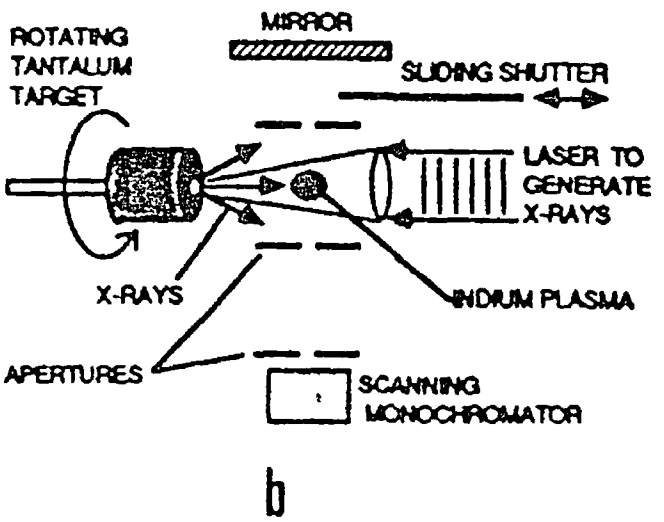

b

FIG 18

(a). Is a schematic of a dual laser produced plasma experiment used to obtain time and space resolved spectra of an indium laser produced plasma created on the surface of a molten indium target. (b). Is the set up used by the same group for photoionization pumping of the indium plasma and the measurement of gain at 185nm. (After Lacey et al 1986).

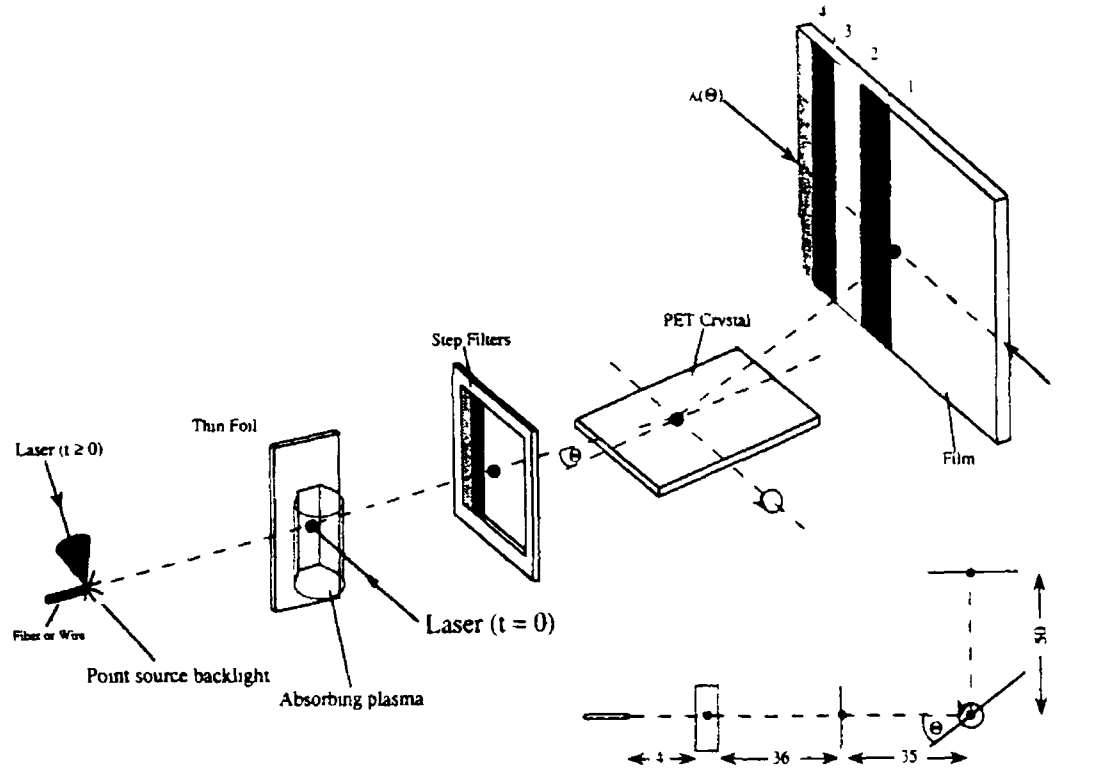

FIG 19
Shows a more sophisticated experimental set up used to record time and space resolved absorption spectra of laser produced plasmas After Balmer et al (1989).

The most recent published reports of photoabsorption experiments using the dual laser produced plasma technique are those of Hansen et al (1989) and Brilly et al (1990) in which the 4d photoabsorption spectrum of the La^{3+} ion, and excited state absorption in sodium like ions were respectively recorded for the first time This work forms the bulk of subsequent chapters of this thesis and so will not be discussed further here

1 3 RECENT ADVANCES IN EXPERIMENTAL ATOMIC SPECTROSCOPY

The last twenty years have seen a resurgence in experimental atomic spectroscopy with the result that the subject has advanced considerably Research in atomic spectroscopy produces primary data such as positions widths and strengths of spectral lines, together with structural information which derives from these data. By carrying out such studies a vast knowledge base has been accumulated which has relevance, and is indeed of vital

importance to a number of different areas of endeavor The purpose of this section of the thesis is to outline some of the most recent advances in atomic spectroscopy For reasons of brevity the discussion will be confined to the vacuum ultraviolet (VUV) spectral region and to experimental arrangements which incorporate XUV radiation generated using laser produced plasmas or synchrotrons

The use of lasers has transformed many areas of experimental atomic physics as exemplified by the many experiments performed since the invention of this versatile light source Many examples of fundamental experiments have been reported, for example the work carried out on Rydberg and planetary atoms Lasers have also been used to slow and cool atoms to milli-kelvin temperatures (Philips et al 1984), and also to prepare atoms and molecules in specific well characterized quantum states, (Hurst et al 1979) Such experiments would perhaps be impossible to perform without the particular qualities of laser radiation. In its own way synchrotron radiation has also had a major impact on experimental techniques This versatile XUV source has been applied to such fields as x-ray lithography (Nagel 1984) for the production of micro structures on surfaces Also synchrotron radiation has been applied to soft x-ray microscopy (Grobman 1983, Kirtz and Sayer 1986); to determine the structure of proteins and virus (Vshe et al 1984) The source has also found a wide application in the recording of a very broad range of absorption spectra of gases, vapours and solid materials which have shown the source to be of immense importance to such studies

The combination of lasers and synchrotron radiation sources has opened up a new field of study, significant photoionization experiments on laser excited atoms have been carried out, (Wuilleumier 1984) Cubaynes et al (1987) have obtained photoelectron spectra of laser excited sodium and barium atoms The oscillator strengths for several transitions of core electrons to outer orbitals were determined and photoionization cross

sections in excited atoms measured over a broad range of photon energies, (Presses et al 1985). In other studies two electron, highly excited autoionizing states were produced and studied using stepwise excitation with two cw dye lasers used to excite the outer electron and synchrotron radiation used to subsequently excite an inner electron. One of these experiments (Bizau et al 1985) has resulted in the measurement of oscillator strengths for transitions between the laser excited $2p^6 3p$ level in neutral sodium and the upper $2p^5 3s3p$ core excited autoionizing levels. Such levels in neutral sodium and along the sodium isoelectronic sequence are of importance to proposed VUV laser schemes and from an atomic physics point of view. A further more detailed discussion of these levels will be given in chapter four which reports new results for the sodium like ions of aluminium and silicon.

Very high resolution photoabsorption experiments have also been carried out on a number of neutral species in both gases and vapors over the past few years (Sommer et al 1987). In a typical experiment involving helium the principal series $1s^2 \rightarrow 1snp$ has been investigated up to n=50. The spectrum was detected in the 10^{th} order using a 6.5m spectrograph with a resolving power of greater than 2.5×10^5 , (Ito et al 1986).

Laser spectroscopy of core excited levels have been carried out using the combination of tunable lasers and laser produced plasmas. The apparatus used to study the laser spectroscopy of such levels in the alkali metals is shown in Fig.(1.10.a.b). Accurate values of autoionizing lifetimes, line widths, relative level positions and transition oscillator strengths were determined (Spong et al 1987). In these experiments quasi metastable core excited autoionizing levels in neutral lithium, sodium and rubidium were populated by the XUV emission from a laser produced plasma. The XUV radiation emitted when these levels decay is measured. When the population is transferred to an autoionizing level using a tunable

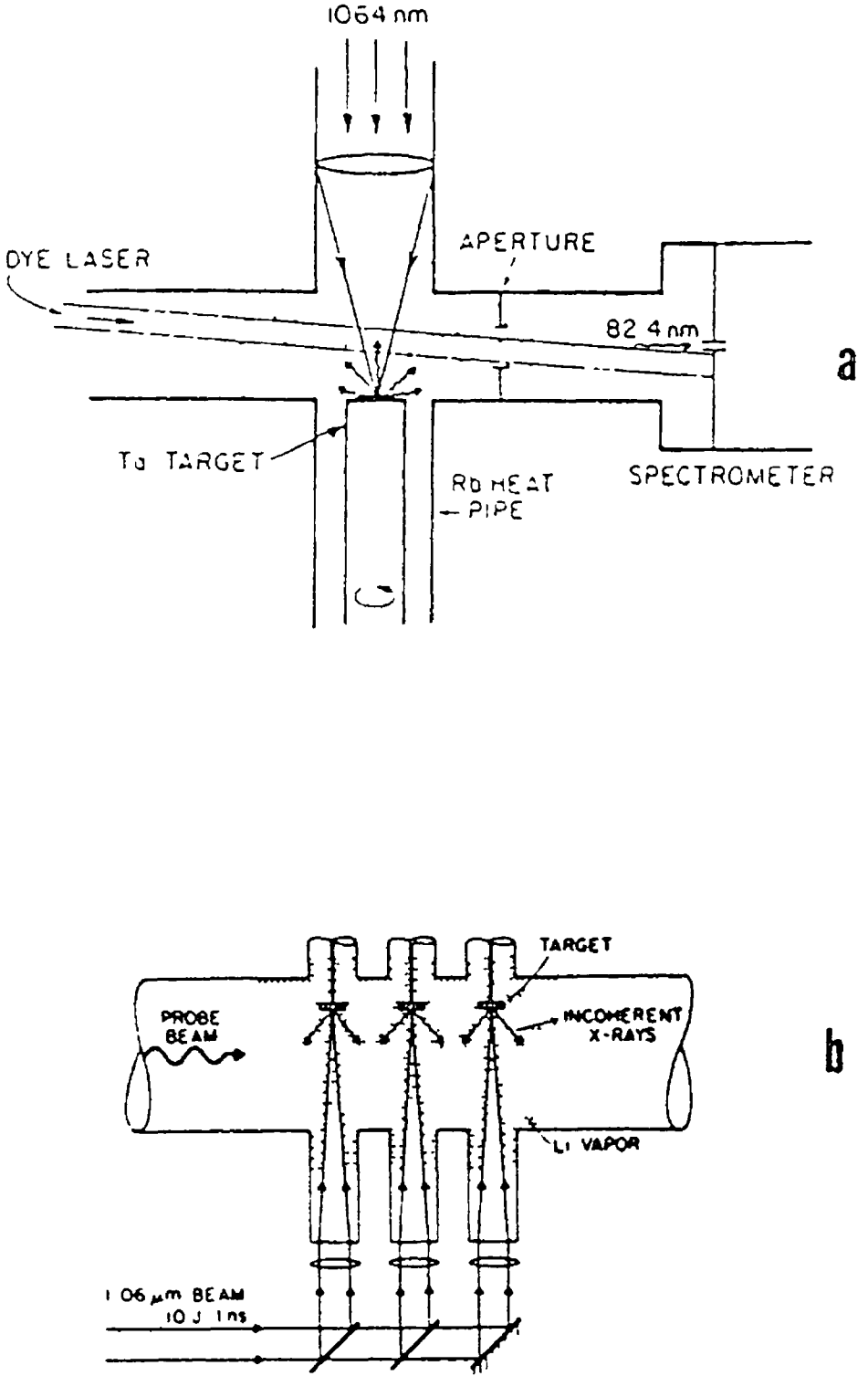

FIG 1.10

(a). The apparatus used to study the spectroscopy of core excited levels in vapours of the alkali metals (After Spong et al 1987). (b). A more sophisticated form of the method which has been used to probe inner shell excited levels in Li. (After Caro et al 1986).

laser this XUV fluorescence is depleted The shape and position of the resulting dip in the XUV emission versus dye laser wavelength determine the position and line width of the autoionizing level With this sort of experiment the accuracy of laser spectroscopy has been transferred to the XUV region.

Other important experimental methods include energy, angle and spin resolved photoelectron studies which have yielded useful information about the nature of atomic structure Total and partial cross sections and angular asymmetry parameters have been determined (Krause et al 1986). Also studied using these methods have been decay channels of core excited resonances (Lindle et al 1987), satellite emission (Svensson et al 1987) and threshold effects, (Heinzman 1987) VUV photoelectron spectroscopy on laser aligned or orientated atoms has also proven to be a fruitful technique and has been particularly applied to study core excited states in Li and Na using the combination of linearly polarized tunable lasers and synchrotron radiation, (Meyer et al 1987)

One area of experimental atomic spectroscopy which should also be discussed briefly is that of detectors in particular the recent development of the micro channel plate (MCP) and the employment of solid state area detectors based on charged coupled devices (CCD's) These detectors are the successor to the traditional photographic plate and in the near future we will see such devices become the dominant detector in the XUV region of the spectrum For discussions of the technology behind this method of detection and the various applications, together with examples of spectra obtained, see Wize (1979), Cromer et al (1985) and Colcott et al (1988)

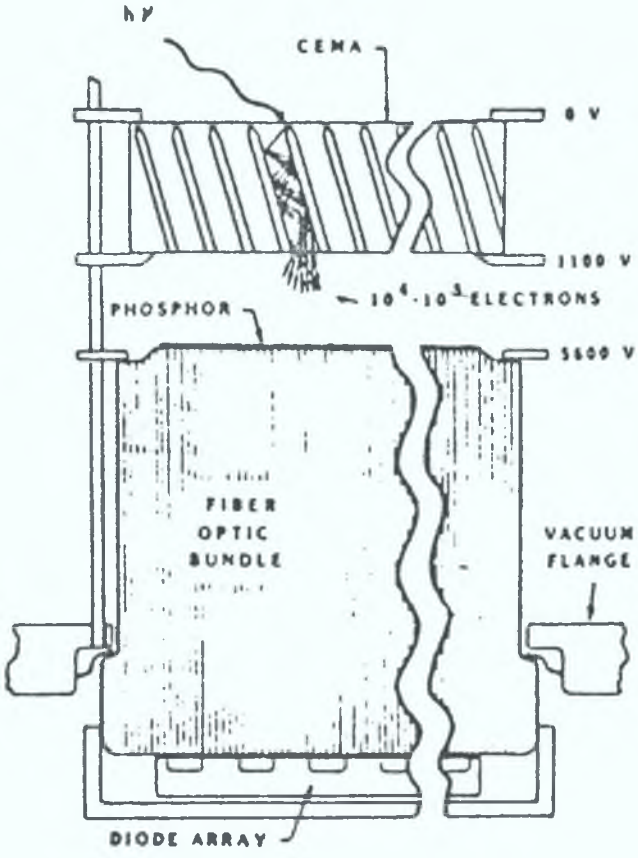

FIG 1.11

A schematic of a Channel Electron Multiplier Array (CEMA) and phosphor coupled to a fibre optic bundle which in turn is coupled to a diode array. After Cromer et al 1985).

1.4. VUV AND SOFT X-RAY LASERS.

One of the more important recent application of laser produced plasmas has been in various proposed x-ray laser schemes. The development of lasers operating at visible wavelengths revolutionized physics by providing light sources at various wavelengths throughout the visible and near uv region, which emit high powered, collimated, spectrally pure and coherent radiation. Similar dramatic consequences may be expected to follow when x-ray lasers become widely available. This brief review of the area will be confined to those schemes which employ a laser produced plasma as the gain medium, or which use the XUV emissions from laser produced plasmas to pump some other medium such as a metal vapor.

High powered pulsed lasers when focused onto solid targets located in vacuum produce plasmas which undergo adiabatic expansion into the vacuum. The expansion velocity of such a plasma is high (typically 10^3m sec^{-1}) and as a result the recombination rates will be too low to bring ionization into equilibrium with the decreasing electron temperature, with the result that a substantial density of highly charged ions will exist a few millimeters from the target surface in the super cooled region. When the plasma recombines, highly excited states may be populated and depending on the properties of these upper levels (lifetimes etc) a population inversion may exist between an excited state and the ground state, or between two excited states of the ion. The existence of a population inversion was first determined and quantified in such plasmas from intensity ratio measurements carried out on XUV transitions in carbon ions (Irons and Peacock 1974), with further measurements being carried out using both time and space resolution (Key at al 1979) for greater accuracy. However, the demonstration of a population inversion alone did not prove the presence of a net amplification due to the possibility of other competing processes such as photoionization of other ions within the laser plasma. Direct evidence of amplification was sought by using extended line plasmas formed using cylindrical lenses to focus the incident laser radiation onto the target surface.

Such experiments sought to measure values for the single transit amplification which may be denoted as exp(GL) and is explained as follows The net amplification coefficient resulting from the balance between stimulated emission and absorption in an atomic transition between two levels 1 and 2, may be given by

$$G=(n_1-n_2(g_1/g_2))(\lambda/8\pi)(A_{21}/\Delta\nu) \qquad \text{Eq (1 1)}$$

where n_1 and n_2 are the number densities of both levels with degeneracies g_1 and g_2 and A_{21} is the Einstein coefficient $\Delta\nu$ is the spectral width of the level due to Doppler broadening, L is the length of the lasing medium GL values are measured from the ratio R(L) of spectral

line intensities from the laser transition along and transverse to the axis of the plasma. This ratio is denoted R(L) and given theoretically as $R(L)=(\exp(GL)-1)/GL$; see Jacoby et al (1981) for a full discussion. Experiments were performed with various values of L so that comparisons of different lengths L_1 and L_2 could be made. From such studies values of the ratio $I(L_1)/I(L_2)$ could be obtained and hence values for the ratio $(1-\exp(GL_1))/(1-\exp(GL_2))$. The first significant report of amplification obtained in this way was that of Matthews et al (1985) using the high powered NOVA laser focused to form a 2cm long line plasma on the surface of a selenium target; lasing was observed in neon like Se^{24+} at wavelengths around 206Å. The lasing occurred between the upper $2p^5 3p$ and the lower $2p^5 3s$ levels, illustrated in Fig.1.12 for the neon like Mo^{32+} ion. In the experiment a thin (75nm) layer of selenium was used in order to avoid re-absorption of the 3s→2p resonance radiation. The selenium layer was supported by a thin (50nm) polymer

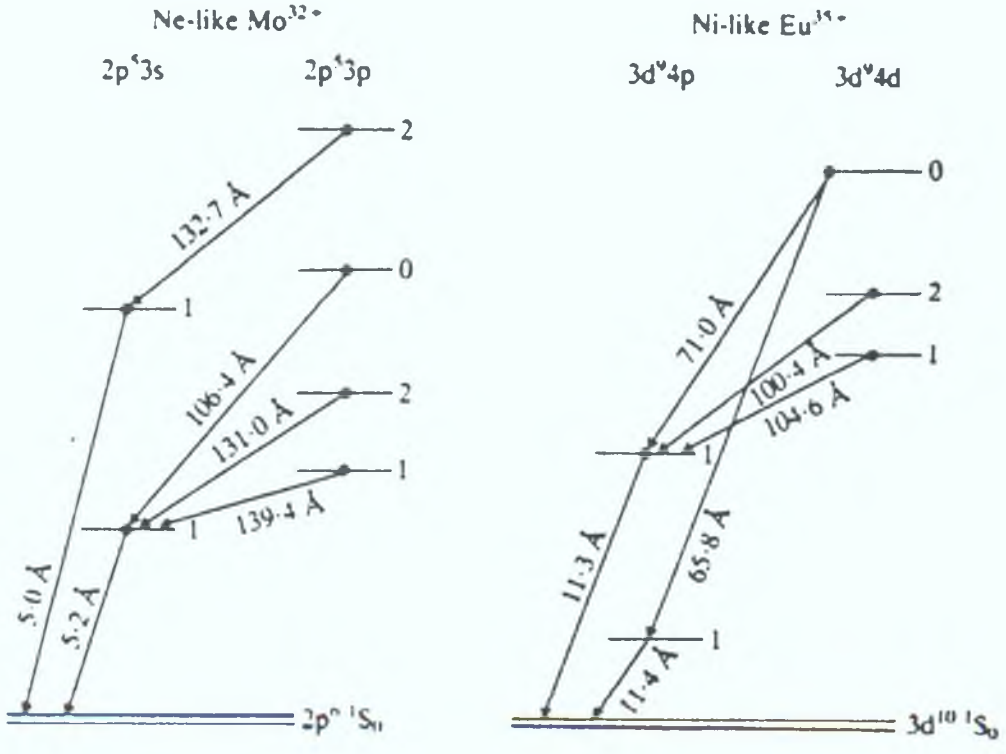

FIG 1.12

Schematic energy level diagram of the laser levels in Ne like Mo and Ni like Eu. After Mc Gowan (1987).

film so that when the target was irradiated with a dual beam 450psec pulse at $5X10^{13}Wcm^{-2}$ the whole target thickness was uniformly heated producing the Se^{24+} ions at a temperature of $5X10^{6}K$ resulting in a rapid expansion to a uniform lower density ($n_e \approx 10^{21}cm^{-3}$) at which the maximum amplification occurred A representation of the experimental set up is shown in Fig (1 13) Detailed

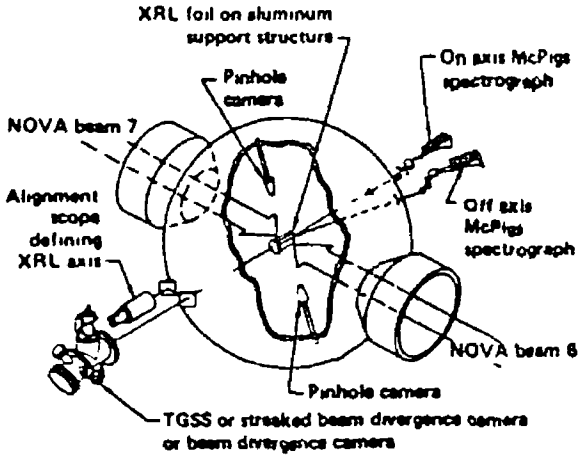

FIG 1 13

A representation of the Livermore x-ray laser experiment in which gain was observed in Ne like selenium After Matthews et al (1985).

calculations (Rosen et al 1985) suggested that amplification coefficients could be as high as $G=10cm^{-1}$ The experiment used two beams from the giant NOVA laser allowing up to 2cm of the target to be illuminated. Sophisticated time resolving XUV spectrographs viewed the plasma axially and transversely, the original results showed that two lines 206 and 210Å were amplified by up to 500 times (see Fig.1.14) along the plasma axis indicating $G=5\ 5cm^{-1}$.

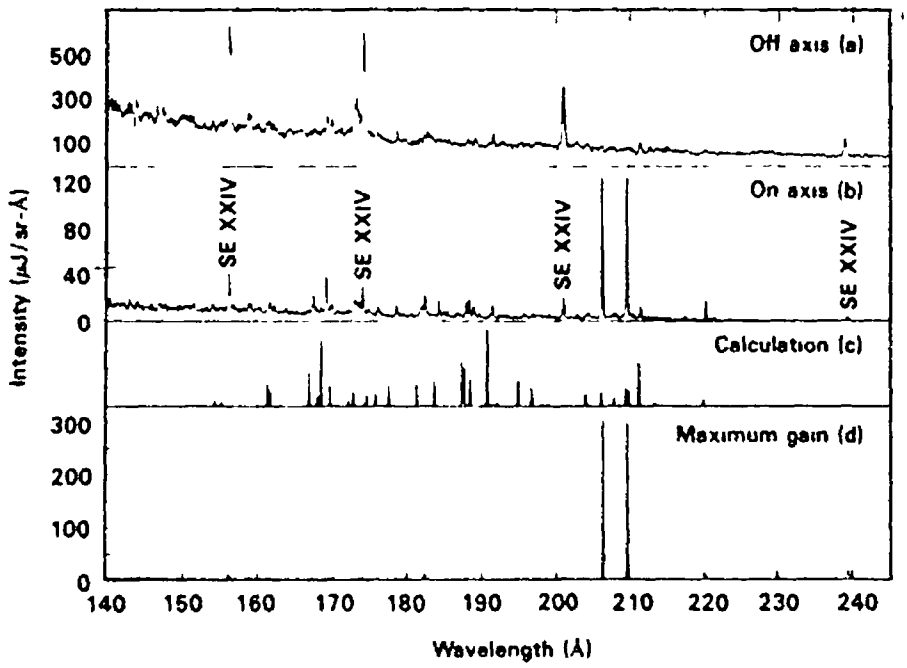

FIG 1 14
Density trace showing substantial gain at 20.6 and 21.0nm in the spectrum of a selenium laser produced plasma. After Matthews et al (1985).

Since the original experiments considerable progress has been made by the same group towards producing a working x-ray laser, (Matthews et al 1987). A successful attempt at lasing inside a cavity composed of a spherical multi layered mirror and a semi transparent multi layer thin plate has also been made, (Ceglio et al 1986) Also ions of the Ni sequence have proven to be suitable candidates (Fig 1 12) for x-ray amplifiers (McGowan et al 1987) at short wavelengths. Lasing has been demonstrated at 60Å in Ni like Eu^{35+}.

Carbon plasmas have also been extensively studied and showed early evidence of population inversions on the C VI Balmer-α transition at 182 2Å, (Irons and Peacock 1974, Key et al 1979). Chenais-Popovics et al (1987) reported XUV amplification at 182 2Å in C VI (see Fig.1 15). The experiment involved the irradiation of a thin carbon fibre (5μm) with a 70psec 0 53μm Nd.glass laser

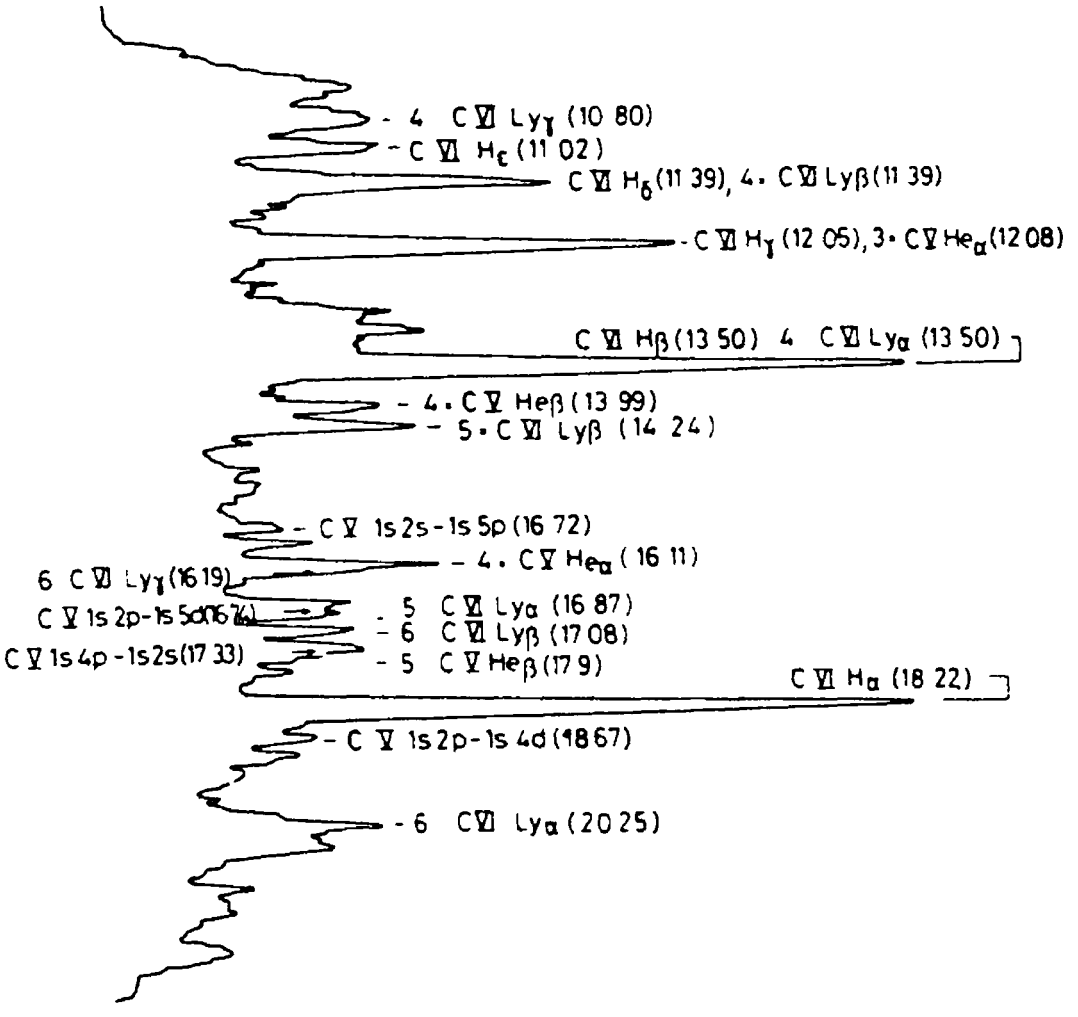

FIG 1 15

Density trace of the spectrum of a carbon laser produced plasma showing gain at 18.2nm. After Chenais-Popovics et al (1987).

The fibres were irradiated by six beams focused to a 7mm long 25μm wide aberration free line focus Measurements carried out were time resolved and resulted in a reported peak single transit amplification of about 30 times A different approach to the same laser scheme was employed by the group at Princeton (Suckewer et al 1984, 1986) An expanding plasma created on the surface of a carbon target by a high powered CO_2 laser was confined by a sinusoidal magnetic field with rapid cooling being caused by thermal radiation The experimental arrangements are shown in Fig (1 16 a b) Evidence from axial and transverse intensity ratios suggested Gl values of the order of 6. Recent measurements by the group (Kim et al 1989) have reported a gain of $8\pm2cm^{-1}$ at 182.2Å.

There have been many other suggested and in some cases implemented VUV/XUV laser schemes in several different ions as well as in neutral species, some examples are given below Jaegle et al (1986) have proposed a scheme based on the Li like Al^{10+} ion and have observed gain using a laser produced line plasma as the medium, (Jaegle 1987) Gain has also been observed in the neon like ions Cu^{19+} and Ge^{22+} (Elton et al 1987) Alkali atoms and alkali like ions have also been proposed as x-ray laser media (Harris 1980, Caro et al 1984 and Pedrotti et al 1985). These schemes involve the core excited autoionizing levels in these atoms and ions some of which are metastable against autoionization. Experiments carried out show that by using the VUV radiation generated by a laser produced plasma substantial populations of excited atoms or ions may be produced in a heat pipe containing the vapor (Caro et al 1984) Quasi metastable levels within these atoms or ions may then be populated by radiation transfer using tunable lasers Richards and Griffen (1986) have also suggested a similar scheme based on the sodium like Al^{2+} ion Clark et al (1986) have suggested that ions along the Kr isoelectronic sequence may be possible x-ray laser candidates The scheme involves the population of upper levels in Kr like ions by the absorption of many (n>10) ultraviolet photons The calculations show that there is a potential for achieving x-ray lasing from levels in Kr like ions using a Kr.F excimer laser Suckewer et al (1986) have proposed to implement this particular scheme using a two laser experiment (Fig.1 16 b) in which a high power CO_2 laser will be used to create a magnetically confined plasma containing Kr like ions Levels in these ions will in turn be excited by multi photon absorption from a second high powered psec laser. Hara et al (1989) have also reported gain on the Al XI 3d→5f transition at 105 7Å using a low power 6J 5nsec glass laser A gain of 3 4cm^{-1} was reported from a 12mm long 40μm wide line plasma and demonstrates that x-ray lasing may also be achieved in plasmas created with relatively low power lasers.

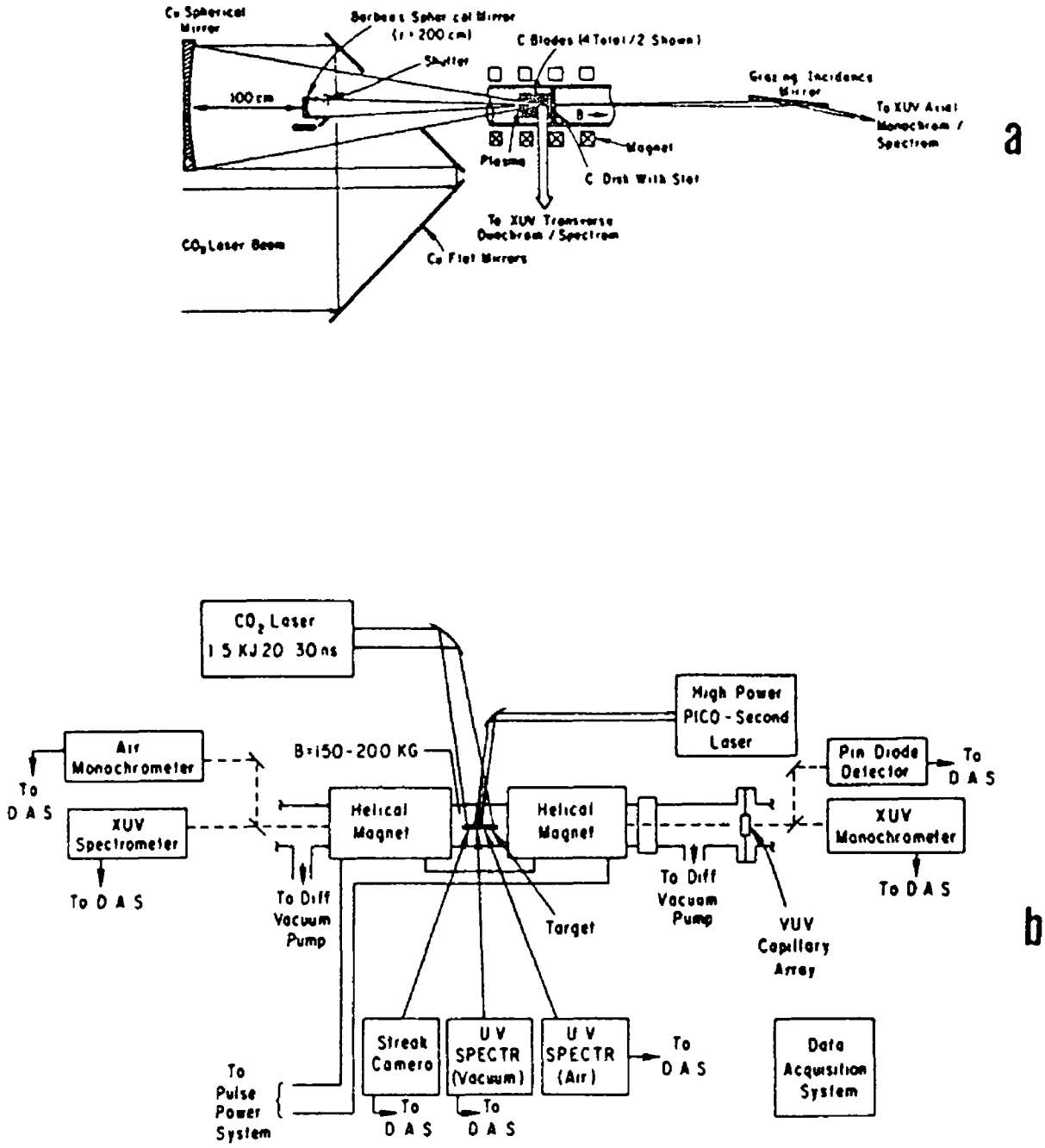

FIG 1 16

(a) Shows the experimental setup used to investigate x-ray lasing in a magnetically confined carbon laser produced plasma. (b). Shows a more sophisticated two laser plasma experiment in which the CO_2 laser produces a plasma in which energy levels are then excited by multi-photon absorption from the second high power psec laser. (After Suckewer et al 1986).

Many reviews on the subject of x-ray lasers are available detailing the developments and future applications of these devices, Hagelstein (1983), Key (1985), Sobel'man and Vinogradov (1985), Jaegle (1987) and Lewis (1988) When such lasers are fully developed and become widely available they will offer powerful MW to GW single pulses at very short wavelengths. Clearly such lasers will find many and varied applications which will include soft x-ray microscopy in biology, diffraction from crystals, materials processing and applications in atomic physics and nonlinear optics.

16 REFERENCES

Balmer, J Lewis, C L S Corbett, R E Robertson, E Saadat, S O Neill, D Killkenny, J.D Back, C A and Lee, R.W. Phys. Rev A **40**, 330 (1989)

Ballofet, G. Romand, J. Vodar, B. C R Accad Sci **252**, 4139, (1961).

Bizau, J M. Wullieumier, F.J. Ederer, D L Keller, J C LeGuoer, J.L. Picque, J.L Carre, B and Koch, P Phys Rev. Lett **55**, 1281 (1985)

Brilly, J Mosnier, J P and Kennedy, E.T Phys. Scr. **40**, 1, (1990).

Callcott, T.A Tsang, K.L Zhang, C.H. Ederer, D L Arakawa, E.T. Nucl. Instr Meth. **A226**, 578 (1988)

Cantu, Parkinson, Tondello, G. and Tozzi, J Opt Soc. Am. **67**, 8, (1977).

Carillon A Jaegle P. and Dhez P Phys Rev Lett 25 3 (1970).

Carillon A Jamelot G. Sureau A and Jaegle P Phys Lett. 38 2 (1972)

Caro, R G. Wang, J C Young, R W. and Harris, S E Phys. Rev. A. **30**, 1407 (1984)

Caro, R G. Wisoff, P J K Yin, G Y Walker, D J Sher, M H Barty, C P.J. Young R.W. and Harris, S E In *Short Wavelength Coherent Radiation Generation and Applications* AIP Conf Proc. No. 147. p 145 (1986)

Carroll, P K. and Kennedy, E T Phys. Rev. Lett **38**, 1068, (1977)

Carroll, P K and Kennedy, E T and O' Sullivan G Opt Lett **2**, 72 (1978)

Carroll, P K. and Kennedy, E.T and O' Sullivan G Appl Opt Lett. **19**, 1454 (1980)

Carroll, P K and Kennedy, E T. and O' Sullivan G IEEE J. Quant Electonics **QE-19**, 12 (1983).

Carroll, P K and Costello, J T Phys Rev Lett. **57**, 1581, (1986).

Carroll, P.K and Costello, J T J Phys B. Atom. Mol Phys **20**, L201 (1987)

Ceglio, N Gaines, D Trebes, J Hawryluk, A Stenrns, D and Howe, G. S P.I E. Vol-688, p.44, (1986).

Chenais-Popovics, C. Corbert, R. Hooker, C.J. Key, M.H. Kiehn, G.P. Lewis, C.L.S. Pert, G.J. Regan, C. Rose, S.J. Sadaat, S. Smith, R. Tomie, T. and Willi, O. Phys. Rev. Lett. **59**, 2161 (1987).

Clark, C.W. Littman, M.G. Miles, R. McIllrath, T.J. Skinner, C.H. Suckewer, S. and Valeo, E. J. Opt. Soc. Am. **3**, 371, (1986).

Clark C.W. and Lucatorto T.B NATO ASI *"Giant resonances in atoms molecules and solids."* Plenum, New York. (1987).

Codling, K. and Madden R.P. Phys. Rev. A. **155**, 1, (1964).

Codling, K. and Madden R.P. Appl. Opt. **4**, 1434 (1965).

Codling, K. Rep. Prog. Phys. **36**, 541-624, (1973).

Connerade, J.P. Garton, W.R.S and Mansfield, M.W.D Astrophys. J. **165**. 203 (1971).

Connerade, J.P. and Mansfield, M.W.D. Proc. R. Soc. Lond. A. **348**, 539, (1976).

Connerade, J.P. Contemp. Phys. **19**, 415 (1978).

Connerade, J.P. Mansfield, M.W.D. Cukier, M. and Pantelouris, M. J. Phys. B. At. Mol. Phys. **13**, L-235 (1980).

Cooper, J.W. Clark, C.W. Cromer, C.L. Lucatorto, T.B. Sonntag, B.F. Kennedy, E.T. and Costello, J.T. Phys. Rev. A. **39**, 6074 (1989).

Cromer, C.L. Bridges, J.M. Roberts, J.R. and Lucatorto, T.B. Appl. Opt. **24**, 2996 (1985).

Cubaynes, D. Bizau, J.M. Wuilleumier, F.J. Ederer, D.L. Picque, J.L. Carre, B. Ferray, and Gounand, F. Journal De Physique Colloque, C9, 12 (1987).

Cukier M. Dhez, P. Gauthe, Jaegle, P. Wekhenkel, C. and Combet-Farnoux, F. Phys. Lett. **39**, L315 (1978).

Elton, R. Lee, T, and Mc Lean, E. Journal De Physique Colloque **C9**, 12 (1987).

Esteva J.M. and Mehiman G. Astro. Phys. J. 193 1 (1974).

Feldman, U. and Cohen, L., J. Opt. Soc. Am 57, 1128-1129 (1967).

Garton W.R.S. Parkinson W.H. and Reeves E.M. Proc. Phys. Soc. London 80, 860, (1962)

Grobman, W.D. in *Handbook of Synchrotron Radiation. Vol I.* Ed. E.E. Koch, North Holland, Amsterdam, (1983). p. 1131.

Hagelstein, P.L. Plasma. Phys. 25, 12 (1983)
Hansen J E Brilly J Kennedy E T and O'Sullivan G Phys Rev. Lett 63, 1934, (1989)
Hara, T. Ando, K Kosahabe, N Yashiro, H and Aoyagi, Y Work presented at the ninth international conference on vacuum ultraviolet radiation physics VUV-9 University of Hawaii July (1989).
Harris S E Opt.Lett. 5, 1 (1980)
Heintzman, U. Phys Scr T17, 77 (1987).
Hildum, J S and Cooper, J J Quant Spec Rad Trans. 12, 1453 (1972)
Hurst, G S. Payne, M D Kramer, S P and Young, J.P Rev Mod Phys 51, 767, (1979)
Irons, F E and Peacock, N J J Phys B 7, 2084, (1974).
Ito, K Namioka, T Morioka, Y Sasaki, T Noda, H Goto, K. Katayama, T. and Koike, M Appl Opt 25, 837 (1986)
Jacoby, D Pert, G.J. Ramsden, S A Shorrock, L D and Tallents, G J Opt. Commun 37, 1265 (1981).
Jaegle P Carillon, A. Klismic, G Jamelot, G Guennou, and Sureau, A Europhysics Letters 1, 555, (1986).
Jaegle, P. Journal De Physique Colloque C9, 12 (1987)
Jamelot G Sureau A and Jaegle P Phys Lett. 41A2 (1972)
Jannitti, E Nicolosi, P Tondello, G Opt Commum 50, 225 (1984)
Jannitti, E Nicolosi, P Tondello, G Journal De Physique Colloque C9, 12 (1987)
Jannitti, E Nicolosi, P Tondello, G Phys Lett A. 131, 3 (1988).
Kastner SO Crooker AM Behring WE. and Cohen L Phys Rev A 16 2 (1977)
Key, M H *Nature (London)* 316, 314 (1985)
Key, M.H. Lewis, C L S and Lamb, M.J Opt Commun 28, 331 (1979).
Kim, D Skinner, C H Umesh, G and Suckewer, S Opt Lett. 14, 665 (1989).
Kirz, J and Sayre, D Nucl Instru and Meth 246, 695 (1986).
Krause, M.O Gerard, P and Fahlmann, A Phys. Rev. A

34, 4511 (1986).

Lacey, R.A. Byer, R.L. Silfvast, W.T. Wood O.R. and Svanberg, S. In *Short Wavelength Coherent Radiation: Generation and Applications.* AIP Conf. Proc. No. 147. p. 412. (1986).

Lewis, C.L.S. in *"Laser plasma interactions 4."* Ed M.B. Hooper. Proceedings of the Thirty-Fifth Scottish Universities Summer School in Physics. (1988).

Lindel, D.W Ferrett, T.A. Heimann, P.A. and Shirley D.A. Phys. Rev. A. **35**, 1128 (1987).

Lucatorto TB. and McIlrath TJ. Phys. Rev. Lett. 37 7 (1976).

Lucatorto T.B. and McIlrath T.J. Appl. Opt. **19**, 3948 (1980).

Lucatorto TB. McIlrath TJ. Sugar J. and Younger SM. Phys. Rev. Lett. **47**, 16, (1981).

Mehlman G. and Esteva J.M. Astrophysics. J. **157**, 945 (1969).

Mehlman G. and Esteva J.M. Astrophysics. J. **188**, 191 (1974).

MacGowan, B.J. Rosen, M. D. Ekhart, M. J. Hagelstein, P. L. Madden, R.P. and Codling, K. J. Opt. Soc. Am. **54** 268 (1964).

Matthews, D. L. Nilson, D. G. Philips, T. W. Scofield, J. H. Shimkaveg, G. Trebes, J. E. Walling, R. S. Whitten, B. L. and Woodworth, J. G. J. Appl. Phys. **61**, 12, (1987).

Madden, R.P. and Codling, K. J. Phys. Rev. Lett. **10**, 516 (1963).

Madden, R.P. and Codling, K. J. Opt. Soc. Am. **54** 268 (1964).

Madden, R.P. and Codling, K. J. Astrophysics. J. **141**, 364 (1965).

Mansfield, M.W.D. and Connerade, J.P. Proc. R. Soc. Lond. A. **324**, 421 (1975).

Matthews, D. L. Hagelstein, P. L. Rosen, M. D. Eckart, M. J. Ceglio, N. M. Hazi, A. U. Medecki, H. MacGowan, B.J. Trebes, J. E. Whitten, B. L. Campbell, E. M. Hatcher, C. W. Hawryluk, A. M. Kauffman, R. L. Pleasence, L. D. Rambach, G. Scofield, J. H. Stone, G. and Weaver, T. A. Phys. Rev. Lett. 54. 110. (1985).

Matthews, D. L Nılson, D G. Phılıps, T W. Scofıeld, J H. Shımkaveg, G Trebes, J E Wallıng, R S Whıtten, B L and Woodworth, J G J Appl Phys. 61 12 (1987).
McIlrath, T.J and Lucatorto, T B Phys Rev Lett 38, 1390 (1977)
Mehlman, G,, Weıss, A W. and Esteva, J M. Astrophys J 209, 640-641 (1976).
Meyer, M Muller, B. Nunnemann, A Prescher, T H Raven, E. Rıchter, M Schmıdt, B, Sonntag, B and Zımmermann, P Journal De Physıque Colloque C9, 12 (1988).
Nagel, D J. ın *VLSI Electronıcs mıcrostructure scıence* Vol 8, p 137, (1984)
Nıcolosı, P Jannıttı, E and Tondello, G Appl. Phys B (Germany) B26, 2, (1981)
O'Sullıvan G Ph D Thesıs Unıversity College Dublın (1980) Unpublıshed
O'Sullıvan G. In *"Gıant resonances ın atoms molecules and solıds "* Plenum, New York. (1987)
Pedrottı, K.D., Mendelsohn, A J., Falcone, R W , Young, J F and Harrıs, S E J Opt Soc. Am B 2, 1942-1947 (1985).
Phıllıps, W.D. Prodan J V. and Metcalf H. Atomıc, Physıcs, 9, 338 (1984).
Presses, J M Burkhardt, C E Corey, R.L Erson, D L Daulton, T L Garver, W P. Leventhal, J J Msezane, A Z. and Manson, S T. Phys. Rev A 32, 1264 (1985)
Rıchards, R.K and Grıffın, D C ın *Short Wavelength Coherent Radıatıon Generatıon and Applıcatıons*, Attwood, D T and Bokor J eds , AIP Conf Proc. 147, 343 (1986)
Rosen, M D Hagelstein, P L Matthews, D L Campbell, E M Hazı, A U Whıtten, B L. MacGowan, B J Turner, R E and Lee, R W Phys. Rev. Lett 54 106 (1985)
Sobel'man, I I and Vınogradov, Advances ın Atomıc and Molecular Physıcs 20, 327 (1985)
Sommer, K Baıg, M A. Garton W R S. and Hormes, J Phys Scr 35, 637 (1987).
Sonntag, B F Cromer, C L Brıdges, J M. Lucatorto T B and McIlrath T.J. In *Short Wavelength Coherent Radıatıon Generatıon and Applıcatıons* AIP Conf Proc. No 147 p 412 (1986).

Spong, J.K Kmetec, J.D. Wallace, S C Young, J F and Harrıs, S E Phys Rev. Lett 25, 2631 (1987).
Suckewar, S Skınner, C H Mılchberg, C. Keane, H and Voorhees, D. Phys Rev Lett 55, 1753 (1985).
Suckewar, S Skınner, C.H Kım, D Valeo, E Voorhees, D and Wouters, A In *Short Wavelength Coherent Radıatıon Generatıon and Applıcatıons* AIP Conf. Proc No 147 p 412. (1986)
Sugar J , Lucatorto T B , McIlrath T J and Weıss A W. Opt. Lett 4, 4 (1979)
Svensson, S. Helenlund, K and Gelıus, U Phys Rev. Lett 58, 1624 (1987)
Usha, R Johnson, J E Moras, D. Thıerry, J C Fourme, R and Kahn, R. J. Appl Cryat. 17, 147, (1984)
Wıllı, O. ın *"Laser plasma ınteractıons 4 "* Ed M B Hooper. Proceedıngs of the Thırty-Fıfth Scottısh Unıversıtıes Summer School ın Physıcs (1988)Wıza, J L Nucl. Instr Meth 162, 578 (1979).
Wolff, H W. Radler, K Sonntag, B and Haensel R. Zeıtschreıft fur Physık. 257 353 (1972).
Wuılleumıer, F J ın *Laser Techniques ın the Extreme Ultravıolet* AIP Conf Proc Ser N° 119 eds, S E Harrıs, and T.B. Lucatorto Amarıcan Instıtute of Physıcs, New York, (1984) p 220

CHAPTER TWO: EXPERIMENTAL.

2.1 INTRODUCTION.

The intention of this chapter is to describe the apparatus and experimental method used to obtain the absorption spectra of a number of different ionized species discussed in later chapters of this work. Detailed descriptions of various pieces of equipment which have been used in the experiments are given. There are many new or novel aspects to the apparatus used and these are given particular attention. An overview of the experimental arrangement is given and the general aims and achievements of the current method are outlined. The laser and spectrograph which were used to record the spectra reported in the succeeding chapters are described briefly. The target chamber along with its various attendant components are described here in considerable detail. The alignment of the targets used, with each other and with the entrance slit of the spectrograph is of considerable importance as are the type and nature of the target materials used. This area of the project is covered in detail along with detailed discussions concerning the type of optics used and the overall computer control of the experimental set up. Photographic plates have been the exclusive detector of this work, their use and some general points relating to the measurement of such plates are discussed.

2.2 EXPERIMENTAL SET UP.

The experimental technique employed in this work to record the results reported in all subsequent chapters may be summarised as follows. The output of a 1.5J, 30-40nsec, Q-switched ruby laser was passed through a lens combination composed of either a spherical and

cylindrical lens or alternatively a pair of spherical lenses The laser output was focused by the lens combination onto the prepared surfaces of two different solid targets located in an evacuated target chamber The spherical lens used to create the continuum was cut in such a way that the point plasma produced at its focus was separated from the absorbing plasma produced on the adjacent target. During this work two different target configurations were employed. The earliest and simplest of the two configurations used two flat target elements which were butt jointed together such that the two target surfaces faced the incident laser beam The arrangement is shown in Fig (2 1) A schematic diagram of the second target configuration is shown in Fig.(2 2)

In the later target arrangement the flat machined end faces of rod targets were used, these were positioned in target holders connected to drive shafts of 5mm diameter, such that an angle of 45^{0} was maintained between the planes of the two target surfaces The targets were driven about the drive shaft axis by stepping motors controlled by computer software which also controlled the firing of the laser so that a fresh target surface was presented to the laser each time it fired (Fig 2.3) When a cylindrical lens was employed in the lens combination it resulted in the formation of a line plasma of approximately 5-7mm in length on the surface of the absorber target and in line with the point plasma formed on the surface of the continuum producing target By varying the position of the lens used to create the absorbing medium with respect to the absorber target the laser power density could be varied and the absorption for a particular ionic species optimized At the power densities used to produce the absorbing plasmas emission in the VUV was usually not observed, except in the case where a spherical lens tightly focused the incident laser beam to form the absorbing medium The lens and target arrangement for the second configuration are shown in Fig (2 4)

The absorption spectra were recorded on KODAK-SWR (Short Wavelength Radiation) plates by means of a 2m grazing incidence spectrograph equipped with a 1200 lines/mm concave grating, the entrance slit of the spectrograph was varied between 5 and 30μm The dispersion of the spectrograph was of the order of 1Åmm^{-1} at 120Å. In a typical experiment of this type 100-200 laser shots were required to produce adequate plate blackening, though on occasion this number of laser pulses was exceeded In measuring the plates well known spectral lines of Al, Si, Be and O ions were used as external wavelength standards in addition to internal tungsten and hafnium lines listed by Sugar and Kaufman (1975) and Kaufman and Sugar (1976) The external references were obtained by recording emission spectra of point plasmas formed on Al, Si or BeO targets with tightly focused laser beams.

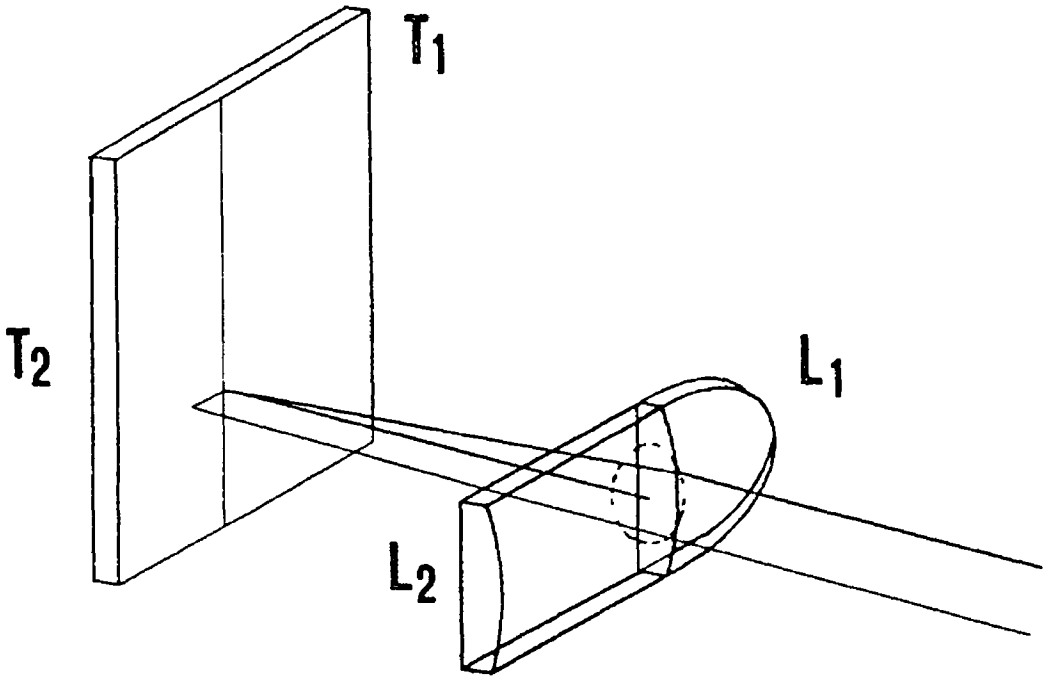

FIG 2 1

Representation of the flat target configuration used to study the absorption spectrum of a laser produced plasma created on target T_2 using the XUV continuum generated in a laser produced plasma created on target T_1.

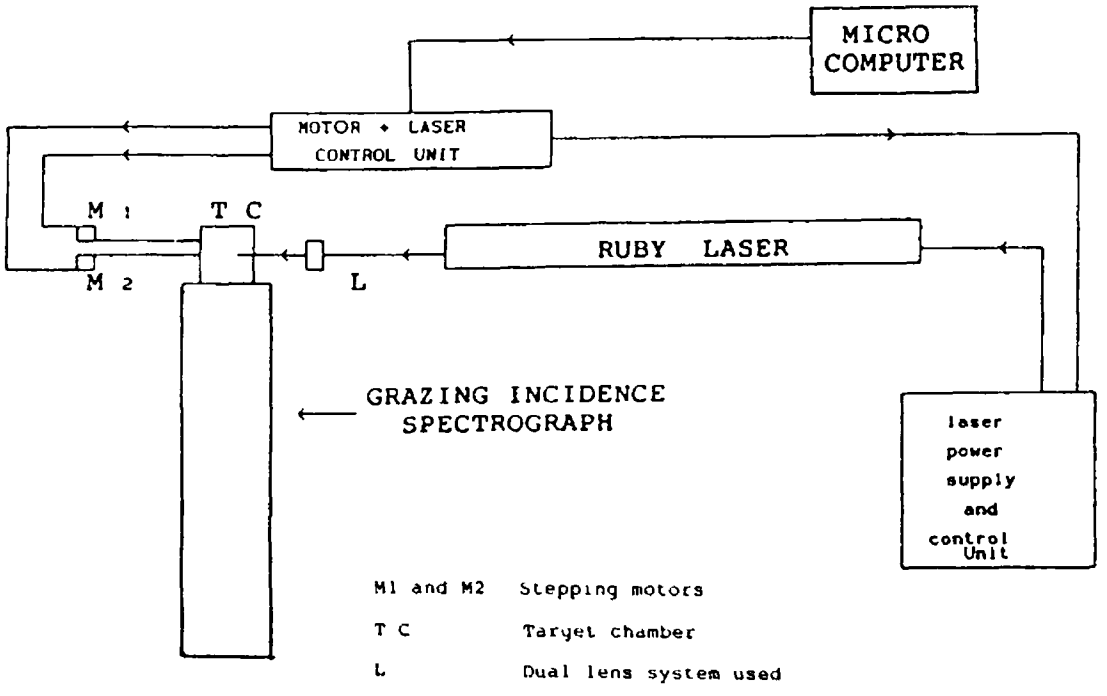

FIG 22

Schematic diagram of the experimental arrangement used to record absorption spectra of laser produced plasmas in the VUV region

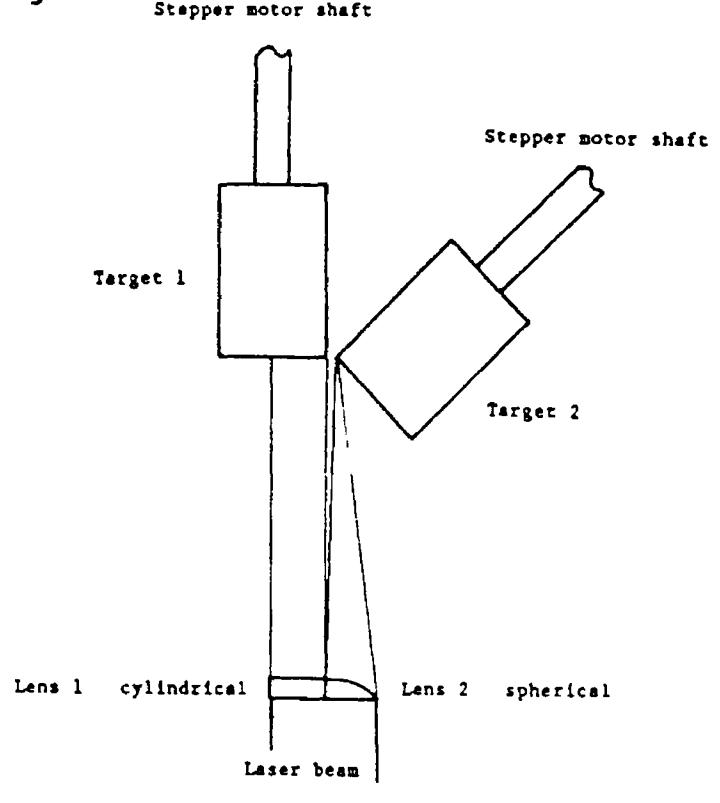

FIG 23

Plan view of the lens and target arrangement showing clearly the effect of having the spherical lens cut such that the point plasma is separated from the absorbing line plasma.

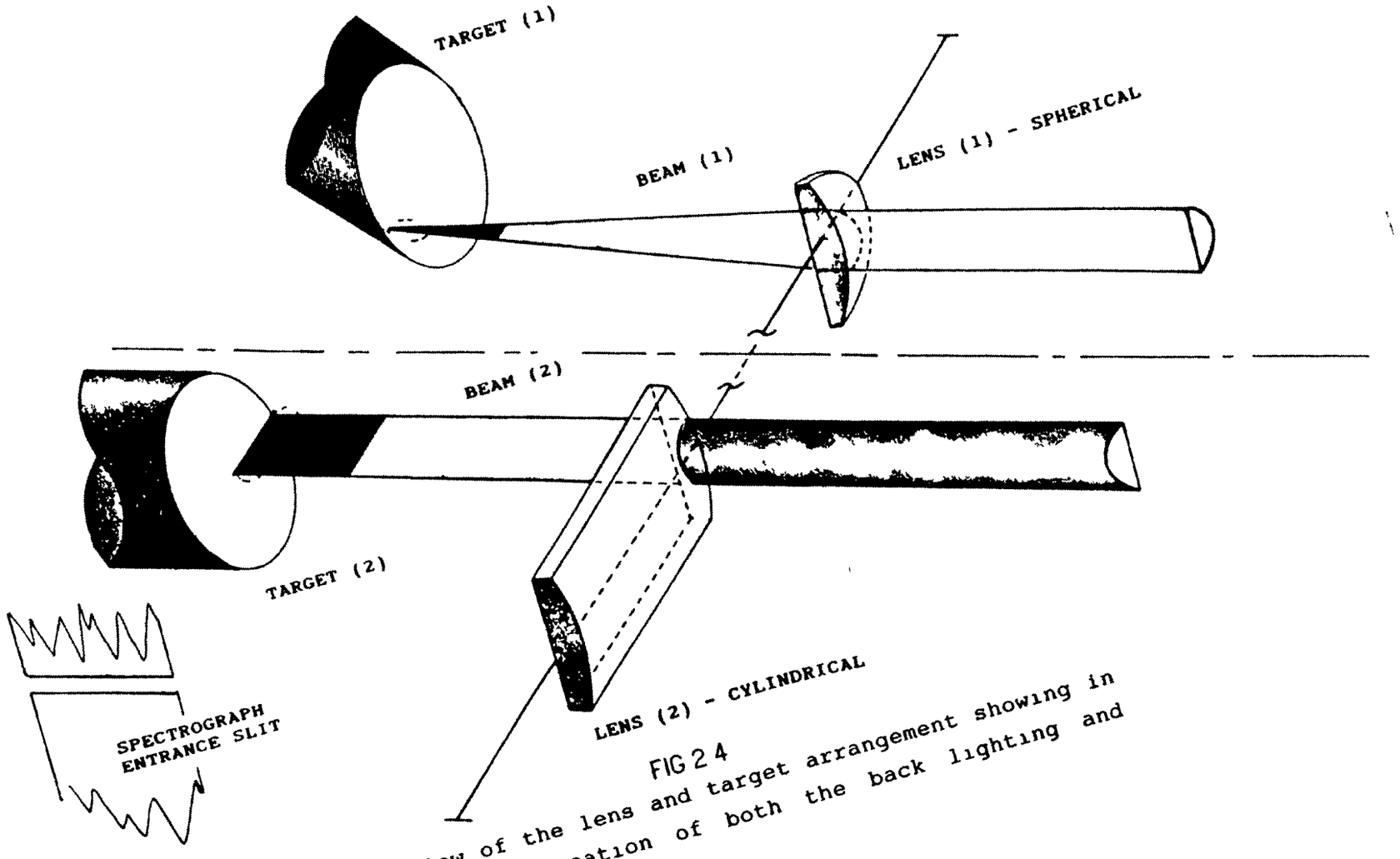

FIG 2 4

Exploded view of the lens and target arrangement showing in more detail the creation of both the back lighting and absorbing plasmas

2 3 THE LASER

The laser which was employed throughout this experimental work was a conventional commercially available model Its workings have been previously discussed at length by Brilly (1986) For the sake of completeness its operation will be briefly reviewed here

The laser used was a ruby (Series 2000) laser, supplied by J K LASERS The laser consists of a single oscillator which can deliver approximately 1 5J of optical energy in a single pulse of 30-40nsec (FWHM) duration when operated in Q-switched mode. Some details pertaining to the operation of the laser are discussed below A schematic diagram which shows the basic construction of the system is presented in Fig (2.5) The Pockels cell, which makes Q-switching possible, is located in the cavity just in front of the rear reflector and operates at a voltage of 2.7kV, which can be varied by adjusting the controls on the Pockels cell unit The output of the laser is monitored on an energy monitor which takes a small portion of the output beam and directs it to a photo diode The integrated output from the photo diode is converted to a voltage which is proportional to the laser output energy and can be read from the energy monitor

A series of apertures are spaced out along the circumference of a metal disc located within the laser cavity By reducing the aperture the number of laser modes can be progressively restricted which results in good spatial coherence and a low beam divergence, and hence a high energy density due to good focusability Throughout these experiments the smallest aperture was used.

Routine maintenance of the laser system was largely confined to the Pockels cell which is a sealed unit with anti-reflection coated windows at each end; the void between the windows of the unit and the crystal is filled

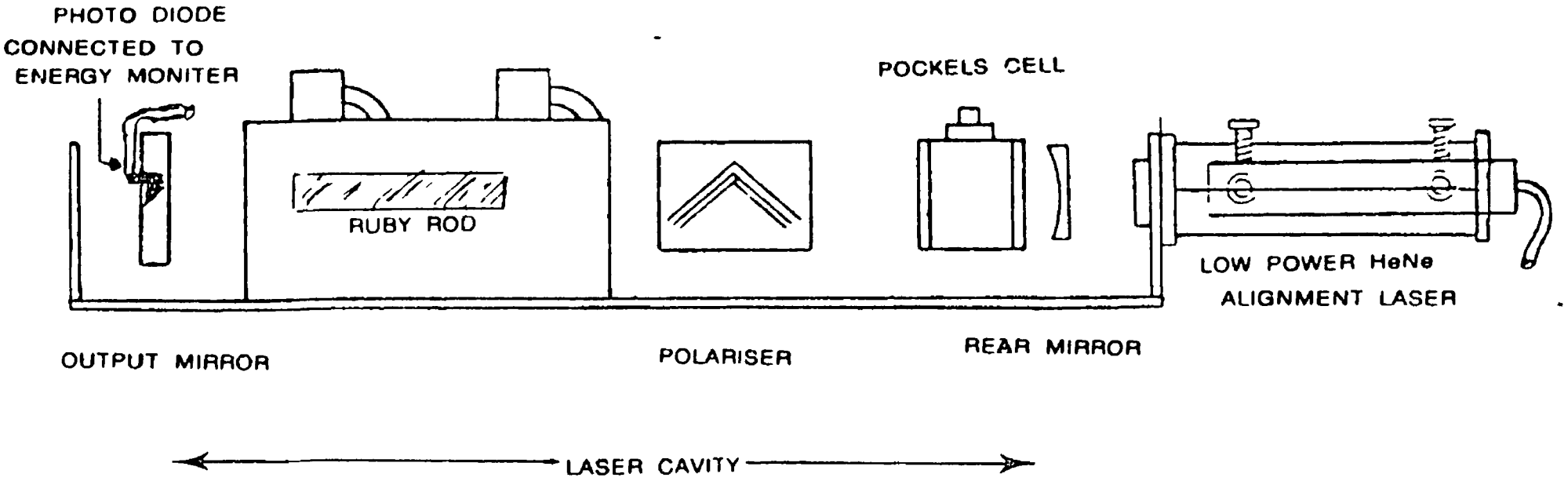

FIG 2 5

Schematic diagram showing the laser system used to create the plasmas studied in this work. Also shown is the low power helium-neon alignment laser aligned along the optic axis of the ruby laser.

with FC-104 index matching fluid to minimize transmission losses. The Pockels cell was checked at regular intervals (each week during continuous operation, but, more frequently during the summer months) to ensure that the fluid level was correct. Periodic checks were also carried out on the cavity of the laser in particular the flash tubes and electrical connectors were checked for spark damage and erosion of the electrodes. The ruby rod was also checked at regular intervals for possible damage During the work reported here both of the flash tubes as well as the ruby rod were changed.

To facilitate alignment a low power helium-neon laser was passed through the optical system of the ruby laser. This second laser was used to fix precisely the position of the optical components used in plasma production

2 4 THE SPECTROGRAPH

All of the photoabsorption studies reported here were carried out in the extreme ultraviolet and soft x-ray regions of the spectrum, below 500Å. In this wavelength region the decrease in reflectance of all materials with decreasing wavelength necessitates the use of grazing incidence spectrographs to obtain usable grating efficiency and in general, the closer the incident angle α approaches 90^{0} the lower will be the cut-off wavelength of the instrument. For example, the platinum coated grating used with the spectrograph discussed here has a critical wavelength (in Angstroms) of approximately 2 64 times the grazing angle in degrees Therefore at an angle of 4^{0} (used throughout this work) the cut-off wavelength should be approximately 10.6Å. However, due to scattered light at shorter wavelengths this theoretical cut-off minimum is never in fact achieved In practice for the spectrograph discussed here the minimum observable wavelength was about 40Å in emission while for absorption this was somewhat longer. The theory and construction of

spectrographs is well known and is dealt with in a number of texts; see for example Samson (1967). A brief summary of the salient features of the spectrometer and its operation follow.

The grating used in this work had a blaze of $1^{0}47'$ and is most efficient in the 60Å wavelength region. The instrument used for the investigations reported here was a two meter grazing incidence spectrograph model E580 supplied by HILGER ANALYTICAL and has the specifications summarised in Table.2.1 below. The grating used in the instrument was supplied by BAUSCH & LOMB and its parameters are also listed in the table below.

TABLE 2.1

Summary of the specifications of the 2m grazing incidence spectrograph used throughout the work reported here.

RANGE:	5-950Å Depending upon grating fitted.
GRATING:	BAUSCH & LOMB Radius of curvature 2m.
RULING:	1200 Groves per mm.
RULED AREA:	25 X 35mm.
BLANK SIZE:	35 X 45 X 10mm.
BLAZE ANGLE:	$1^{0}47'$
MINIMUM GRAZING ANGLE:	40 Minutes.
ANGLES OF INCIDENCE:	86^{0} 88^{0} or 90^{0}.
PLATES:	2" X 25". (max).
WORKING PRESSURE:	10^{-3} - 10^{-4}torr.
SLIT WIDTHS USED:	5-30μm.

Three interchangeable entrance slit assemblies giving angles of incidence of 86^{0}, 89^{0} or 89^{0} respectively were also supplied. The plate holder used with this instrument takes 2-inch plates with a maximum plate length of 25-inches. Although normal plates used in this work are 10-inches by 2-inches we have on occasion used two plates together in the instrument to cover a wide spectral range; the size of the plate holder permits this. The curved surface of the plate holder (on which the plates are positioned) is machined to a positional accuracy of 0.0002 inches (0.005mm). The plate holder can be replaced by a tracking slit assembly which converts the spectrograph into a scanning grazing incidence

monochrometer, thus photographic or photoelectric detection may be employed The spectrograph was, until very recently, pumped by a 5-inch water cooled diffusion pump coupled to a rotary pump which together were able to evacuate the spectrograph from atmospheric pressure to the working pressure of 10^{-4} torr in approximately fifteen minutes The pumping system currently in use consists of a smaller 4-inch diffusion pump coupled to an EDWARDS rotary pump The entire pumping operation is now manual compared with the previous semi automatic system, this has the advantage of affording greater control over the pumping of the vacuum tank, but the disadvantage of a longer turn round time than the previously used system

Fig (2 6 a) shows the spectrograph in cross section The walls of the spectrograph vacuum tank are constructed from a magnesium zirconium alloy casting. The base of the tank is shaped to reduce the internal volume and the sides are ribbed eternally to reduce distortion of the tank under vacuum. The plate holder, also shown in Fig (2.6 a) consists of two main parts both constructed from the same material as the tank Fig.(2 6.b) shows the way in which the plate A, is held against the main body B, by means of a shaped back C, assisted by two cord strips D. The entire plate holder is supported kinematically within the tank The addition of a movable baffle between the entrance slit and the plate holder allowed for several narrow spectra to be recorded on a single photographic plate by dividing the plate into sections across its width

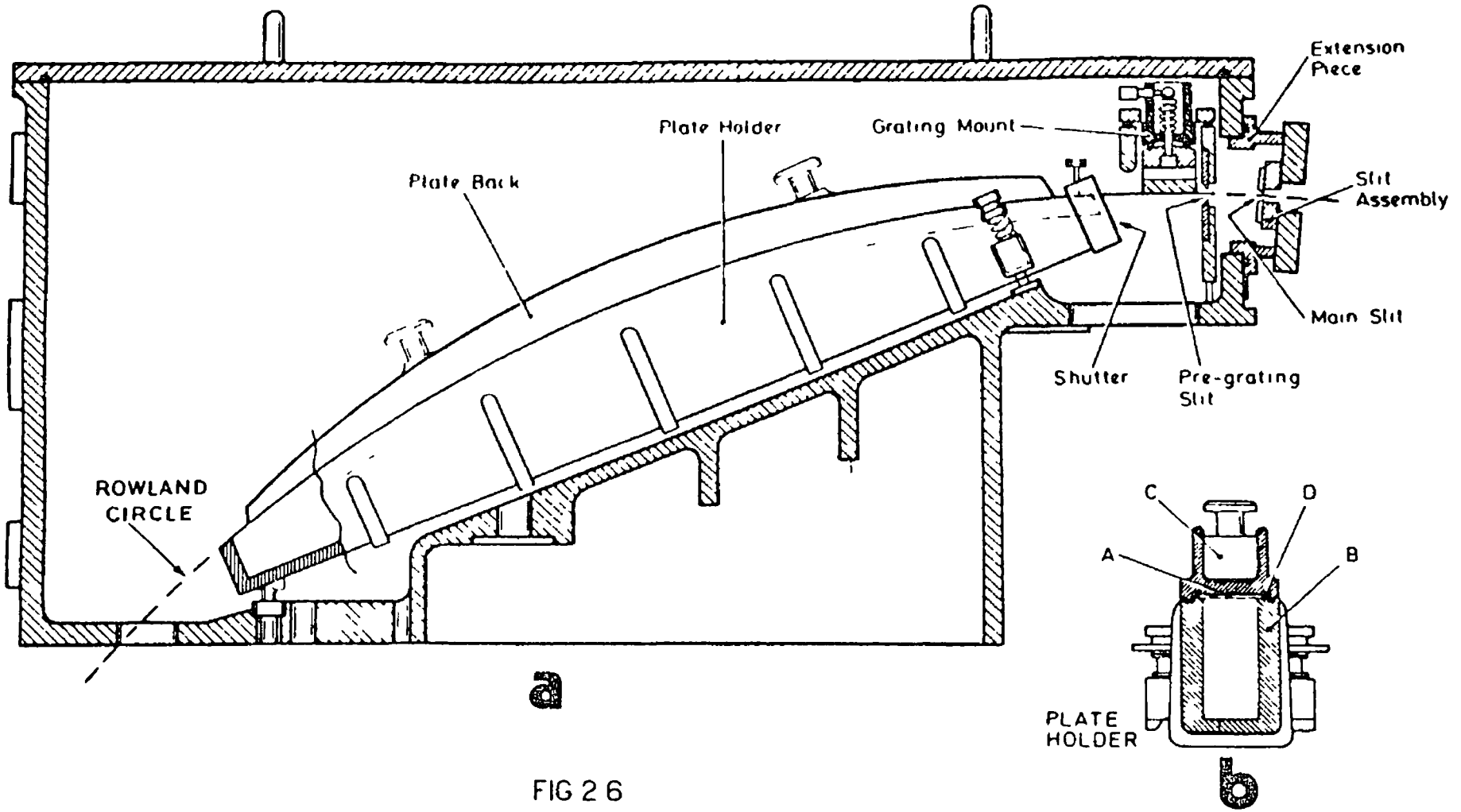

FIG 2 6

(a). Shows the vacuum tank of the 2m grazing incidence spectrograph in cross-section Also shown are the plate holder and slit and grating assemblies. **(b).** Shows the plate holder in cross-section.

2 5 THE TARGET CHAMBER

The experimental work reported here involved a series of two plasma experiments carried out in vacuum in target chambers attached to the spectrograph just in front of the entrance slit. Two target chambers were used for the experiments. The first target chamber was constructed of mild steel and allowed the plasmas to be formed approximately 5cm in front of the spectrograph entrance slit, thus increasing the intensity of the light incident on the grating This chamber was quite small having dimensions of 120 X 50 X 50mm and was used for experiments involving two flat targets butt jointed together as shown above in Fig (2.1) This chamber was constructed to allow maximum observation of the plasmas formed on the surface of the targets during the course of the experiment, and to facilitate alignment An attachment for holding a low power helium-neon laser at the rear of the chamber was also constructed, this laser was aligned along the optic axis of the spectrograph and was used for course alignment of the plasmas with the entrance slit The top plate of the chamber contained the target holder and allowed the targets to be moved such that the optimum position in front of the entrance slit was obtained. Both top and bottom plates of the target chamber were approximately 2 5cm thick and were hollowed out thus increasing the target chamber volume and allowing the target holder the greatest possible vertical motion within the chamber, this allowed relatively long (approximately 6cm) flat targets to be fabricated

The current target chamber is the most advanced construction used to date. This chamber is of a robust construction built of mild steel Several important modifications have been made to this latest chamber when compared with the previous model The present chamber is considerably larger than the previous chamber and thus allows for maximum visibility of the experiment being carried out within the chamber There is maximum

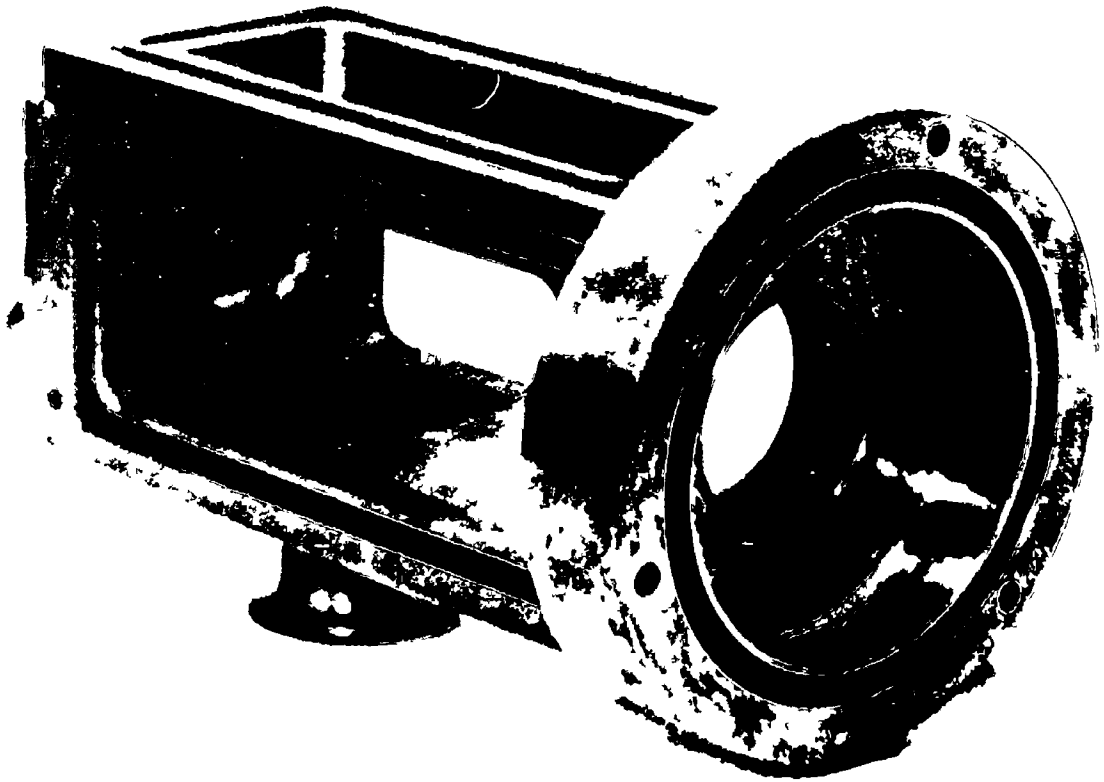

FIG 2 7
The target chamber used throughout this work

visibility of the laser plasmas under study and also of the targets and of the motion of each target with respect to the other This is of importance for alignment purposes and also for correct focusing of both lenses used to form the plasmas. Fig (2.7) shows the target chamber, the three large openings on the top and on the right and left sides have the approximate dimensions of 150 X70mm This gives an estimate of the target chamber size. A circular opening in the base of the chamber allows for a third (reference) target to be used together with the absorber and continuum emitting targets A second opening in the base of the chamber (to the rear) allows for pumping of the chamber while the opening on the end face of the chamber permits the passage of the low power helium-neon laser beam used for alignment

2 6 THE ANGLED BACK PLATE

The angled back plate shown in Fig (2.8 a) was constructed of mild steel, and bolts into the left side of the target chamber This plate has the function of holding in position the back lighting and absorber target holders The large size of the present target chamber (approximately 150X80mm) compared with only half of this size for the previous chamber enables relatively large targets to be utilized in the experimental arrangement The targets used in the present experimental set up are cylindrical in shape and are of various sizes The continuum producing targets used were either tungsten or hafnium rods with a diameter of approximately 20mm The continuum producing plasma was formed close to the edge of one of the end faces of the rod, the rod was rotated after each shot A hafnium target was employed by using a disc of the metal approximately 1mm in thickness attached to the end of the tungsten rod with an adhesive bond The continuum producing target was firmly clamped into place in the target holder which in turn was attached to the target drive shaft (Fig 2 8 b) The target drive shaft passed through a vacuum seal and had a drive gear attach

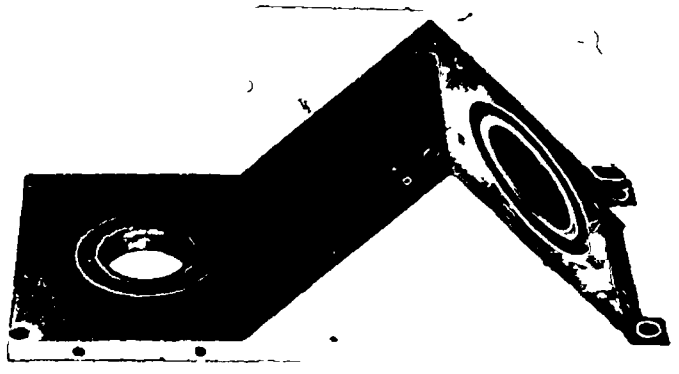

a

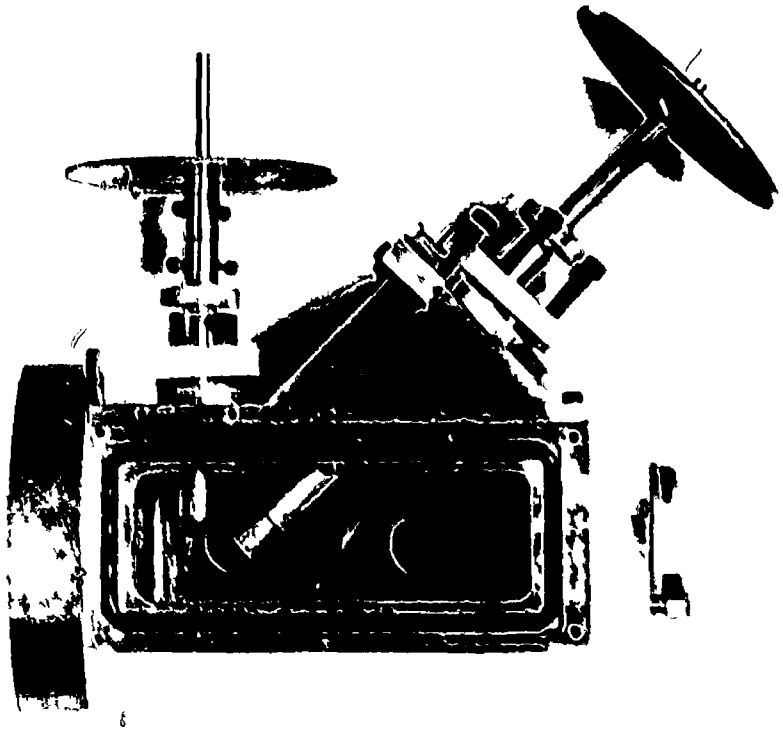

b

FIG 2 8

(a) Shows the angled target chamber back plate (b) Shows the back plate attached to the target chamber together with the targets, drive shafts and gearing

some along its length. The o-ring seal between the face plate of the target drive shaft holder and the target chamber back plate prevents the vacuum within the chamber from being breached and allows for maximum side to side displacement of the target drive shaft and hence for the target within the chamber Thus the target may be moved (±1cm) simply by sliding the target shaft holder across the o-ring seal The face plate of the target drive shaft holder was made sufficiently large that it always overlaps the o-ring contained in the target chamber back plate and so maintains the vacuum seal

The absorbing plasmas were also created on the ends of rod targets which were held in place in the chamber in much the same way as was the continuum producing target The majority of materials used as absorber targets could be readily obtained in rod form Rods of approximately 12mm in diameter were favored since the average length of the absorbing line plasma was of the order of 6mm This gave the effect of smooth wear on the surface of the absorber target over the course of the experiment Surface wear of the absorber targets was found to be important because most of the target materials used were considerably softer than either of the continuum producing targets used Materials such as calcium, barium and strontium were particularly difficult to work with, surface damage being considerable, this together with the sometimes rapid build up of an oxide layer on the surface (while the vacuum tank was being evacuated) made it important to achieve an even wear of the surface by the focused laser

Fresh surfaces of both absorber and continuum producing targets were prepared by turning away the old surface on a lathe This *facing off* process produced (with the exception of barium) a smooth fresh surface. The process also ensured that the targets were free from eccentricities in their motion.

In cases where the material could not be obtained in rod form or where due to the large expense involved only a small amount of the material could be acquired, a disc of the target material was used This disc was firmly attached to the machined end of a brass or aluminium former using an adhesive. Fig.(2.9.a) shows the worn faces of two rod targets used in the experiments reported here.

2 7 THE ABSORBER TARGET DRIVE SHAFT ATTACHMENT

Precise positional control of each of the targets with respect to the optic axis of the spectrograph was found to be one of the most important parameters in the experimental set up For the absorber target this positional control was achieved with the drive shaft attachment shown in Fig (2 9 b) which was constructed in two sections from 12mm mild steel tubing. The central bore of the tubing was made almost exactly the diameter of the drive shaft (approximately 5mm), thus giving a sliding fit between the two One section of the attachment was tapped along a short length of its bore while the other section was threaded such that both sections fitted smoothly together Both sections contain tapped holes mid-way along their lengths which enabled each of the sections to be independently fixed to the drive shaft with small bolts By fixing one of the sections and rotating the other about the drive shaft the length of the attachment could be varied by 7mm from its initial length of 49mm to a final length of 56mm This extension in the length of the attachment was achieved by seven complete revolutions of the unfixed section The threads were machined such that each full rotation of the unfixed section extended the length of the attachment by 1mm. At the junction of the two sections the circumference of the attachment was divided into twenty divisions which were indicated on the circumference by the numbers 0 through 9 with half divisions between these

numbers. Thus it was possible to increase or decrease the length of the attachment accurately by 1/20mm

When the absorber target holder was clamped to the target chamber back plate there was a metal to metal contact between the two surfaces There was also a metal to metal contact between the back plate and the target chamber Thus once securely clamped into position the absorber target was fixed and no lateral or sideways motion of the target was possible. The only allowed motions of the absorber target and drive shaft were rotation and motion with respect to the optic axis of the spectrograph The rotation of both targets was achieved by stepping motors coupled to appropriate gearing attached to the drive shafts. Therefore reproducibility in the absorber target position within the target chamber and with respect to the optic axis was assured It was possible using the drive shaft attachment to position the absorber target accurately with respect to the point plasma continuum source. It was thus possible to carry out studies of different regions of the absorbing plasma A similar mechanism was designed and constructed for the back-lighting target.

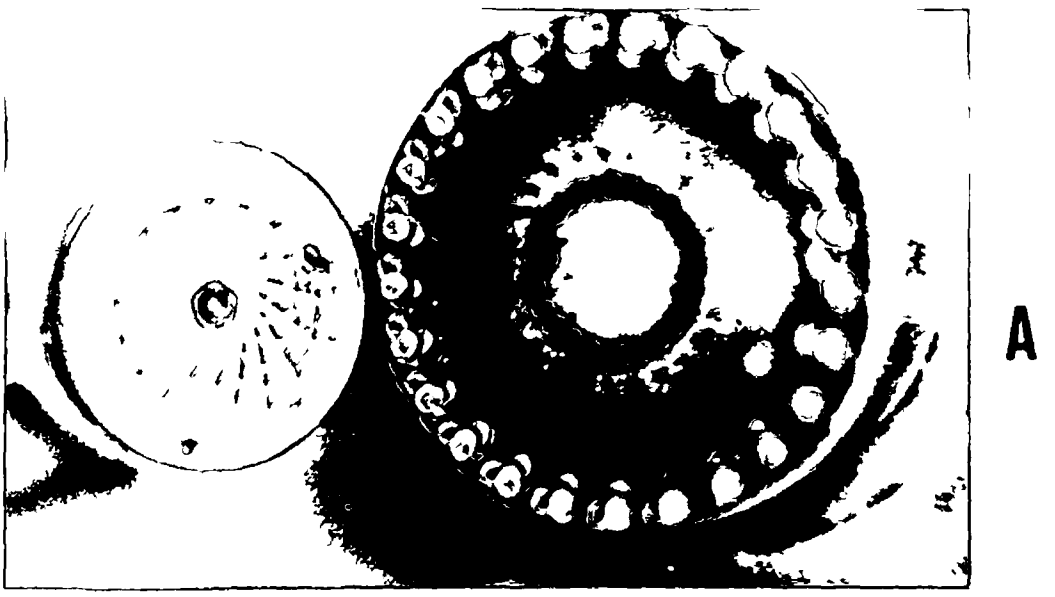

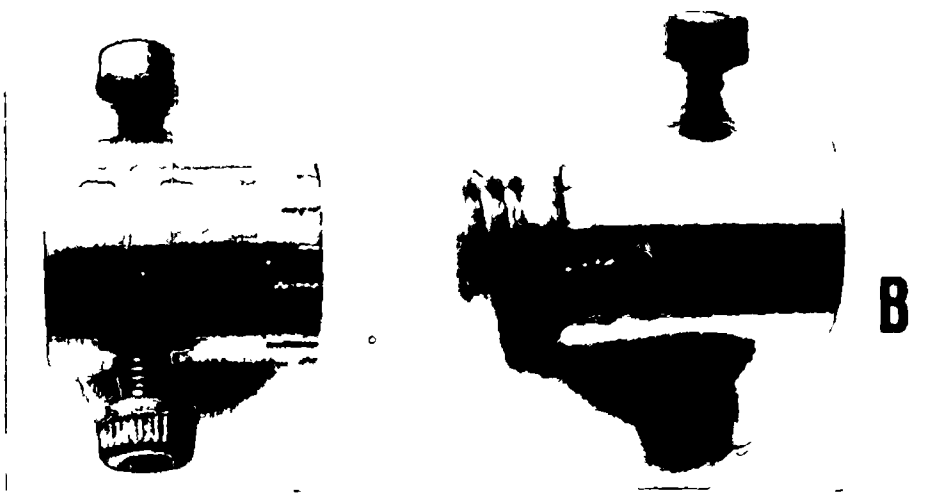

FIG 2 9

(a) Shows the damage caused by the ruby laser to the surface of each of the targets used in a typical two plasma experiment (b) Shows the absorber target drive shaft attachment used to control the lateral motion of the absorber target

2 8 ALIGNMENT OF THE TARGETS

The alignment of the plasmas both with each other and with the entrance slit of the spectrograph can be considered the most critical part of the experimental procedure The rough initial alignment of the two plasmas is described as follows and in graphic form in Fig (2.10.a.b c). Firstly the optic axis of the spectrograph was defined This was obtained with the help of a low powered helium-neon laser attached to the rear of the target chamber The output of this laser was directed through the entrance slit of the spectrograph and onto the central part of the grating.

The scattered laser light thus formed an image of maximum intensity on the back wall of the spectrograph That portion of the laser beam passing through the target chamber thus defined the optic axis of the spectrograph Hence any point source (e.g., a laser produced plasma) located along this axis within the target chamber should be in alignment with both the entrance slit and the central portion of the grating. Fig (2.10 a) shows how this was achieved. With both targets withdrawn to the far half of the chamber in the x and x' directions, the absorber target T_1 was brought back along the x direction (i e , along the absorber target axis) until the front face of the target cut the alignment beam (Fig 2 10 b) The lens L was then focused onto the surface of T_1 and its vertical position adjusted until the focal spot formed by beam (2) was located on the surface of T_1 roughly central in beam (1) A plasma produced at this point would be roughly in alignment with the entrance slit The continuum producing target T_2 was then brought back towards the optic axis in the x' direction such that both targets were in the configuration described by Fig (2 10 c) The lens L was then moved slightly in the y direction such that the focal spot formed by beam (2) was on the surface of target T_2; the fine alignment of the lens L was then carried out

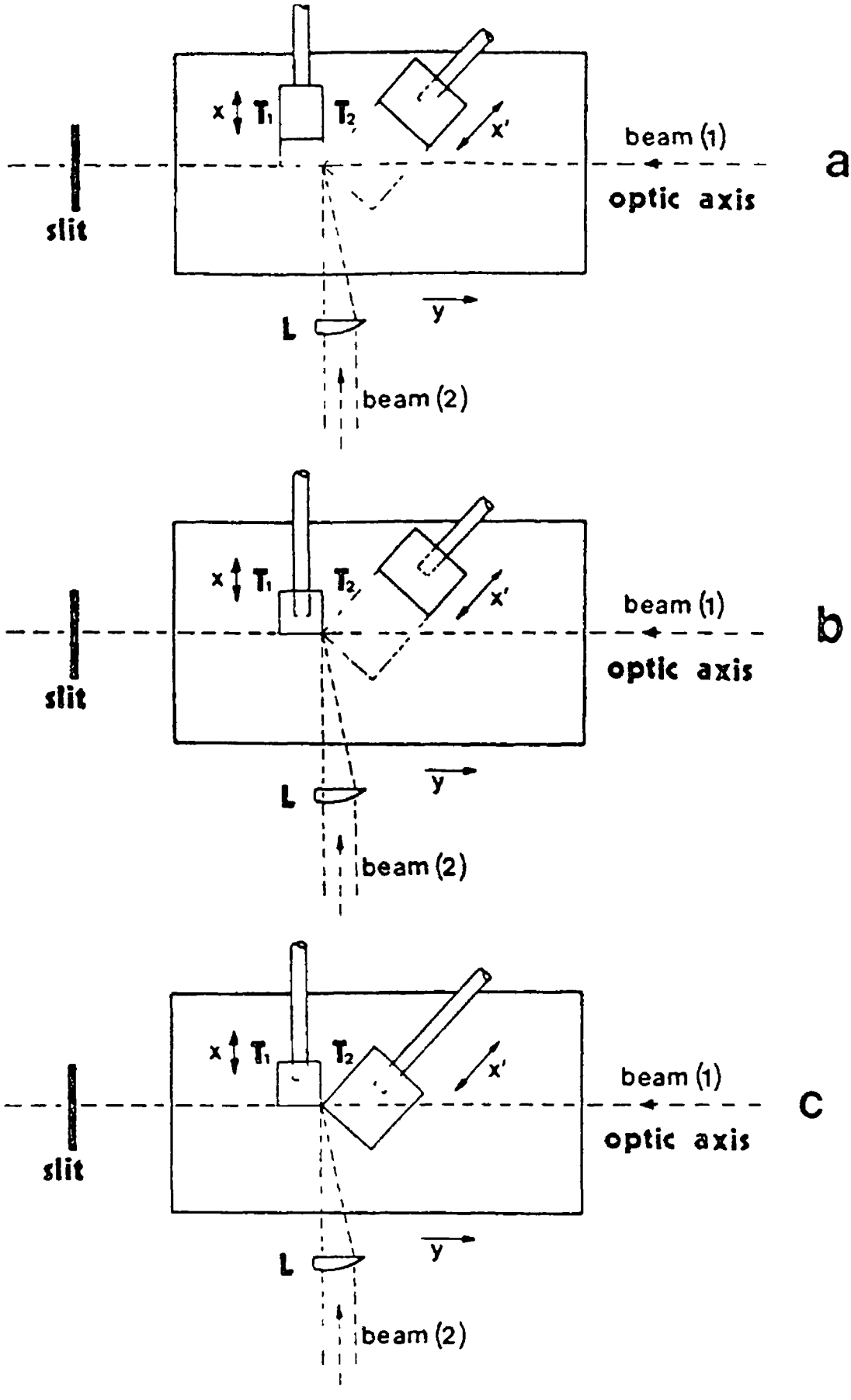

FIG 2 10

(a.b.c). A graphic illustration of the alignment method used to align the targets with each other and with the entrance slit of the 2m grazing incidence spectrograph.

The targets were illuminated from above by a white light source. The lens L was then critically focused onto the surface of T_2. At this stage it is considered that the vertical position of the lens L is accurate to within ±0 15mm and fine alignment of the lens may be carried out. Two methods of accomplishing the fine alignment of the lens L were used. The first employed a photographic technique while the second consisted of a photoelectric approach Photographic alignment of the lens requires the use of a photographic plate, or more usually a section of a plate. The lens L was focused onto the surface of the continuum producing target, or onto the surface of some other target material such as boron or aluminium Laser produced plasmas of both of these elements produce strong emission lines at short wavelengths Five or more spectra were recorded by moving the lens vertically through a series of positions about what was thought to be the optimum position After the plate was developed the spectra were compared and the lens position re-set to that position judged to be the best.

Photoelectric alignment was carried out using the monochrometer attachment fitted to the spectrograph, together with a photo multiplier tube and appropriate scintillator Most often the scintillator used was was a piece of the plastic NE102A, which fluoresces in the visible when irradiated with XUV radiation, though on occasion a glass slide coated with the scintillator sodium salicylate was employed. The slit of the monochrometer attachment was located in position on the Rowland cylinder at approximately 100Å where the continuum output from both tungsten and hafnium laser plasmas is particularly strong The lens L was then adjusted through different vertical positions in order to obtain the maximum signal output from the photo multiplier tube. The position of the lens for which maximum signal output was obtained was then taken as the optimum vertical position for the lens It was found that there was no noticeable difference between spectra

recorded after photoelectric alignment and those recorded after photographic alignment. It was further found that identical spectra were obtained for ±1/12mm about the optimum position.

Using the monochrometer attachment it was then possible to establish the correct position for the absorber target with respect to the continuum emitting source. This procedure was carried out as follows. The absorber target was placed close to the optic axis of the spectrograph such that it obscured the central continuum emitting region of the point plasma so that the photo multiplier signal dropped to zero. The target was then withdrawn from the optic axis using the drive shaft attachment until the signal again reached its maximum value. If a line plasma were to be produced on the surface of the absorber target at this stage then we might reasonably expect its absorption spectrum to be recorded. This assumes that the vertical position of the cylindrical lens with respect to the optic axis of the spectrograph is correct. This was easily found by eye since the absorbing plasma is normally deliberately broadened by de-focusing of the lens; line plasmas of width 1mm were not uncommon during these experiments. A spherical lens used to create the absorbing plasma was usually more de-focused resulting in absorbing plasmas which were 1-3mm in diameter.

2.9 COMPUTER CONTROL OF THE SYSTEM.

As was mentioned in a previous section of this chapter, the targets used in the two plasma experiments were driven from outside the vacuum by stepping motors coupled to appropriate gearing. Both of these motors were controlled by electronic circuitry which was interfaced to a small micro computer (BBC Model B). The box which controlled the motors also contained circuitry which allowed the laser to be fired from instructions issued

within the controlling program The computer program listed below made it possible to control very precisely the acquisition of experimental data This was accomplished as follows The computer program once running rotated each of the targets slightly, the amount of rotation being determined by the program variables, the laser was then fired one or more times and the targets were then rotated again This process continued until the correct number of laser shots were taken

```
 10 REM TAR AND STIP ARE THE FRACTIONS OF A REVOLUTION
 20 REM OF ABSORBING AND EMITTING TARGETS RESPECTIVELY
 40 INPUT "THE NUMBER OF SHOTS",M
 50 INPUT "ABSORBER TARGET STEP SIZE", TAR
 60 INPUT "EMITTER TSRGET STEP SIZE", STIP
 70 HOP = STIP * 2000
 80 TAR = TAR  * 240
 90 FOR G = 1 TO M
100 FOR K = 1 TO 10
110 PROCSTEP( 1,50,144,145)
120 PROCSTEP(TAR,100,144,176)
130 NEXT K
140 PROCSTEP(HOP,10,144,145)
150 PRINT G*10; "SHOTS"
160 NEXT G
170 PRINT "DATA ACQUASITION OVER."
180 END
190 DEF PROCSTEP
200 A=&FE60
210 A?2=&FF
220 FOR C = 1 TO N
230 ?A=R
240 FOR I=1 TO L: NEXT I
250 ?A=M
260 FOR J = 1 TO L  NEXT J
270 NEXT C
280 ENDPROC
```

The ability to computer control the experiment effectively accomplished the semi automation of the data acquisition, once the initial set up was completed the entire experiment ran to a conclusion without the need to interrupt the process. Because of the finite time required for each of the motors in turn to move the targets the repetition rate of the laser during these experiments was of the order of 12 shots per minute

The computer program listed above was adopted from the extensive software which was written by Mythen (1988)

The program is essentially unchanged from the original version except for some very minor modifications in input and output

2 10 THE OPTICS

The optical components in the experimental set up make it one of the more important parts of the arrangement The basic requirements of the lens system called for a pair of lenses of various focal lengths which were used to divide the incident laser beam such that different portions of the beam could be focused to the back lighting and absorber targets The position of each lens was required to be adjustable in all directions, i.e., x, y and z together with a degree of rotation about the optic axis of the ruby laser beam Rotation of the lenses only becomes important when a cylindrical lens is used to create the absorbing plasma The plasmas formed at the focal point of the cylindrical lens must lie exactly along the optic axis of the spectrograph and thus rotation of this lens was found to be necessary With the lens system currently in use all of the above requirements are fulfilled; the lens system is shown in Fig (2 11) The individual lenses were supported in holders which in turn were connected to Ealing mounts bolted to a short length of optical bench. The mounts allow for a substantial x, y and z motion of each lens and in the case of the cylindrical component of the lens system rotation is accomplished simply by loosening the clamp which holds the bar to which the lens holder is attached It was found that this lens system is well suited to the purpose for which it was designed, it was also found to be reproducible from day to day, i e , that frequent re-alignment of one or both of the lenses was not required. Throughout the experimental work described here the lenses used were in general 6cm focal length plano convex lenses

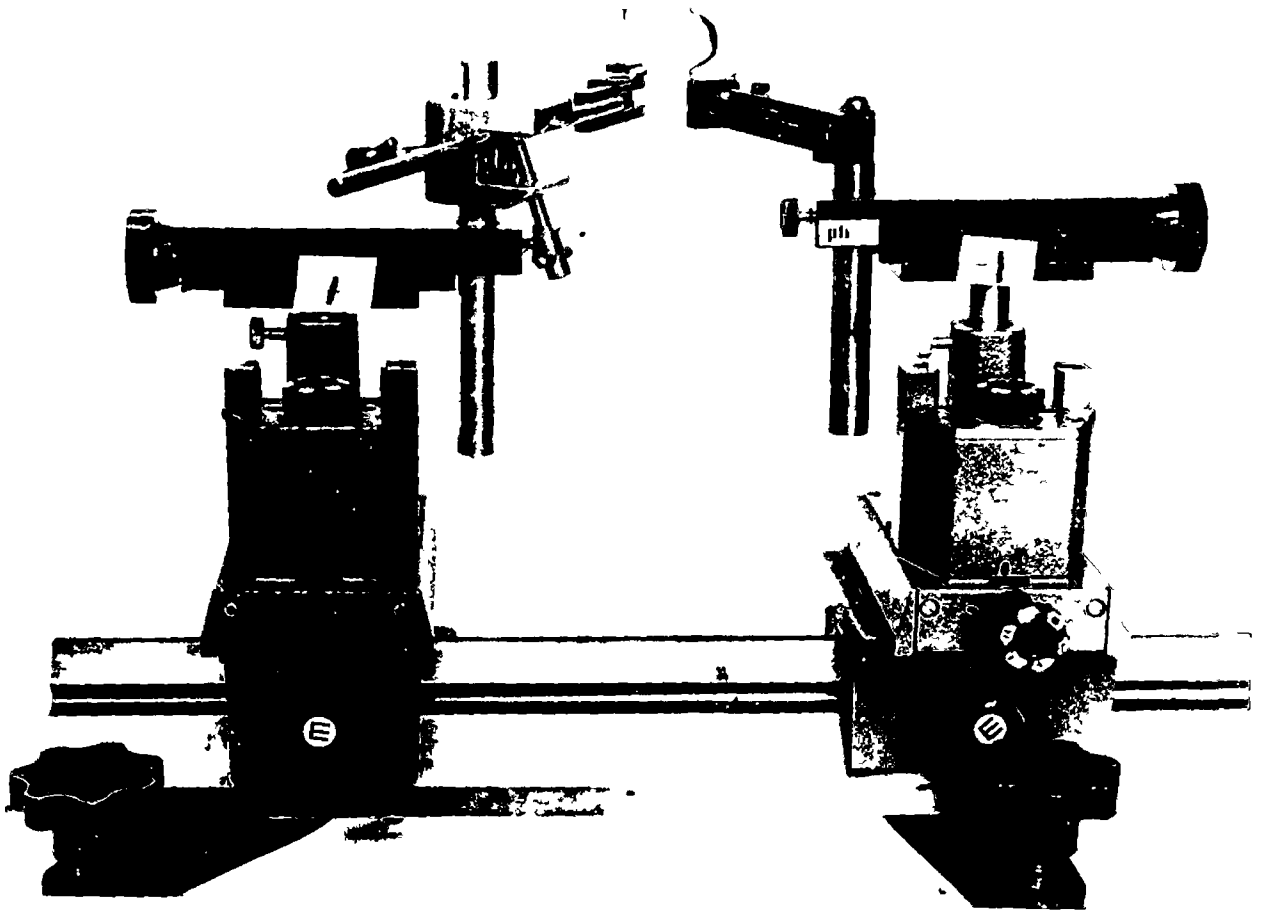

FIG 2 11

Shows the lens system used throughout this work

Motion towards or away from the targets is also important and the current arrangement allows for a large displacement of this type. This is particularly useful when an isonuclear sequence is to be studied, since successive de-focusing of the lens used to create the absorbing plasma reduces the laser irradiance at the target surface which results in lower ion stages dominating in the plasma than would otherwise be the case. This essentially gives a coarsely tunable source of ions simply by the movement of a lens in one direction or another. The lateral motion of both lenses (i.e., motion parallel to the spectrograph optical axis) allows different portions of the ruby laser output to be directed to each target. Although it was usual to split the laser beam roughly equally between both elements of the lens combination, it was found that even if as little as 30% of the beam was directed to the continuum producing target that absorption could still be seen in lower stages of ionization. For example, an absorption spectrum of Mg^{2+} ions could be obtained by splitting the laser beam such that the continuum producing target received only 30% of the output. For higher ion stages, for example, the absorption spectrum of Si^{4+} and indeed for most of the results reported in subsequent chapters of this work 50% of the incident laser beam was directed to each of the targets used.

2.11 PHOTOGRAPHIC PLATES.

The photographic plates used to record each of the spectra reported in later chapters of this work were KODAK SWR (short wavelength radiation) plates; these plates were found to produce clean and measurable spectrograms. The processing technique followed employed four trays, two of which contained water, one with developer (KODAK-D19) and one with fixer (KODAK UNIFIX). The temperature of the developer was maintained at $19^{o}C$ which was found to give adequate developing times of approximately five minutes. Lower temperatures than this

tended to produce plates in which the grain size was large; while much higher temperatures caused the plate background to become enhanced at the expense of the spectrum. The plates were first placed in the tray of distilled water for 2-3 minutes, they were then transferred to the developer tray (the developer being changed for each plate) for as long as it was felt necessary, the progress of the development was closely monitored by careful visual examination of the plate under a safe lamp. After washing in the third tray for a further 2-3 minutes the plate was transferred to the final tray and fixed for five minutes However, despite following this exact procedure for each plate, differences in plate density were found to be present even between plates of identical exposure. Scattered light from the spectrograph was also found to present problems at shorter wavelengths This therefore sets the practical limit on the minimum wavelength that can be recorded photographically in absorption with this instrument. As was mentioned in a previous section of this chapter the minimum wavelength from strong emission sources was found to be of the order of 40Å, however, in absorption this short wavelength limit seems to be of the order of 60Å. This can be accounted for by the fact that absorption spectra are in general much weaker than corresponding emission spectra

The use of SWR plates, together with developing procedures has been described by Hoag and Miller (1969), measurements of sensitivities and characteristic curves, etc., are given by Burton et al (1973). Each of the spectra recorded here had overlaying a section of it an emission spectrum which was used as an external reference (internal references were also used where possible) with known lines from which positions on the plate of the unknown features could easily be measured The following procedure was used when measuring the wavelengths of spectral features The plate was measured on the photoelectric comparator in the *Physics department at*

University College Dublin This instrument is operated by hand and essentially allows the accurate determination of the position of spectral lines along the photographic plate To compute final wavelength values for the unknown features a computer program was written to read the data in a series of x, and y coordinates where x was the position and y the wavelength The program used a least squares subroutine taken from the N.A G. (Numerical Algorithms Group) numerical subroutine library to fit an N^{th} order polynomial to the data. This program allows interpolation to be carried out so that the positions of unknown features can be converted into wavelengths The program together with sample input and output has been previously described by Brilly (1986).

The comparator described above and used to measure the plates has the major disadvantage of not being able to detect plate features below a certain intensity As many of the features recorded in the spectra of various ions during this work fall into this category it was found necessary to resort to enlarged photographic prints of the appropriate wavelength region in order to establish the the wavelengths for the weaker features in a given spectrum Because of this it is suggested that the margin of error be taken as ±0 05Å for wavelengths of those features which, for reasons of weakness, could only be measured from a photographic print of the spectrum The comparison of the wavelengths of those strong lines which were measured from both plates and photographic prints of the spectrum was also taken into account in the estimation of the probable errors in the method For plate measurements and for all subsequent wavelength measurements quoted in this work the suggested error is ±0 02Å, (unless otherwise stated) and in general it was found that comparison of print and plate measured wavelengths tended to agree to within this limit

2 12 REFERENCES

Beutler, H G. J Opt. Soc Am 35, 311, (1945)

Brilly, J M Sc Thesis *"Applications of Laser Produced Continuum Radiation "* Dublin City University. (1986). Unpublished.

Burton, W M Hatter, A T. and Ridgley, A Appl Opt 12, 1851, (1973).

Hoag, A.A. and Miller, W C Appl Opt 8, 12, (1969)

Kaufman, V and Sugar, J J Opt Soc Am. 66, 10, (1976)

Kelly, R.L. and Palumbo, L.J N R.L Report N° 7599. (1973)

Mack, J.E Stehn, J R and Edlen, B J Opt. Soc Am 22, 245, (1932).

Mythen, C. M.Sc. Thesis (Un-finished Work)

Rung, C.R. and Mannkopf, R Z *Physik* 45, 13, (1927)

Sugar, J and Kaufman, V Phys Rev. A. 12, 3, (1575)

2 13 GENERAL REFERENCES FOR CHAPTER TWO

Driscol, W G. and Vaughn, W Ed's *"O S A Handbook of Optics "* McGraw, Hill, Book Company (1978)

Ross, D. *"Lasers Light Amplifiers and Oscillators "* Academic Press (1969)

Samson, J A.R *"Techniques of Vacuum Ultraviolet Spectroscopy "* Wiley and Sons. inc (1967).

CHAPTER THREE THE NEON ISOELECTRONIC SEQUENCE

3 1 INTRODUCTION

This chapter reports the observation of photoabsorption spectra of the third, fourth and fifth members of the neon isoelectronic sequence, Mg^{2+} Al^{3+}, Si^{4+} and is the first detailed study of the VUV absorption spectrum of the Si^{4+} ion. Of particular interest in each of the ions studied were the inner shell autoionizing series ($2s^2 2p^6$ $^1S_0 \rightarrow 2s2p^6np\,^1P$). In previous studies of Al^{3+} (Carillon et al 1972 and Kastner et al 1977) outer shell transitions and inner shell autoionizing features were observed in the absorption spectra of aluminum plasmas, however, in both cases the observed features were distorted by the presence of strong emission lines from other ion stages present in the absorbing plasmas. The main thrust of this work has therefore been to record clean VUV absorption spectra of as many of the neon like ions as possible, in particular the neon like Al^{3+} and Si^{4+} spectra, neither of which had been recorded in detail previously Elements of this work have been discussed in a qualitative manner in a previous report (Brilly 1986) and so this chapter will only briefly summarise the results for Mg^{2+} and Al^{3+} The new results presented here relate to the Si^{4+} ion The unexpected observation of a Beutler Fano line profile associated with the first member of the 2s→np series is believed to be an example of *Forced Autoionization*

The spectra reported here are free from superimposed emission lines thus enabling unambiguous information about the nature of the principal and autoionizing series to be obtained. We have used the same experimental technique discussed in the preceding chapter, and conclude that absorption observations further along this sequence would present considerable difficulties due both to the nature of the substances involved and to power

limitations in the present experimental arrangement

3 2 THE NEON SEQUENCE IN EMISSION

A chapter on the neon isoelectronic sequence could not ignore the recent renewal of interest in ions of this sequence, this section briefly reviews that work Recent successful X-ray laser experiments (Matthews et al 1985) have focused considerable attention on ions of the neon sequence The resonance lines for the Ne sequence are known for most of the elements (Aglitsky et al 1984), whereas spectroscopic identifications are limited to lower Z elements for the weaker n=3, $\Delta n=0$ transitions The structure of ions along the neon sequence have been vigorously investigated in recent years In addition to the importance of this data to basic atomic physics there are interesting applications in astrophysics, for example the interpretation of solar flare spectra (Jupen 1984, Feldman et al 1985) The data also has relevance to plasma physics where Ne like ions of Cr, Fe and Ni are observed in tokamaks In neon like ions the ground state is $2p^6\ ^1S$ and the two lowest configurations are $2p^5 3s$ and $2p^5 3p$ Two of the four 3s levels (with angular momentum J=1) have much shorter radiative lifetimes than those of the 3p levels which feed them, and this fact makes it possible to obtain inverted populations The demonstration of laser action in the VUV and X-ray regions in neon like systems has provided additional strong motivation for experimental and theoretical studies along the sequence. In the X-ray laser experiments population inversions were predicted among levels of the $2p^5 3l$ configurations. The $2p^5 3p$ (J=0) to $2p^5 3s$ (J=1) transitions which were predicted to have the highest gain were not initially observed to lase, although lasing was observed for lines with weaker gain predictions, and later for those levels with the higher gain predictions leading to the demonstration of soft X-ray amplification of 3s→3p transitions in Se XXV and Y

XXX, (Matthews et al 1985, Rosen et al 1985). Laser action has also been reported more recently for neon like molybdenum ions in a laser produced plasma (Mac Gowan 1987). Goldstein and Walling (1987) have proposed a new scheme for obtaining X-ray lasing in neon like ions from inner shell ionization of sodium like ions.

Experimental studies of the n=3, Δn=0 levels e g: 3s→3p and 3p→3d transitions in neon like ions have been carried out using a variety of techniques, including, sparks, the beamfoil technique, laser produced plasmas and solar flares The available data base is now extensive and extends to Cu XX (Buchet et al 1987) Beam foil excitation spectra have been reported for Ar IX (Buchet-Poulizac et al 1983), Ti XIII (Trabert 1984, Bashkin et al 1983), Cr XV (Buchet-Poulizac et al 1986) and for Fe XVII (Buchet et al 1985). The Ar IX results stimulated revision and extension of earlier work and several $2p^5nl$ ($n\geq4$) configurations have been reported (Fawcett 1984 and Kramida 1985) Laser produced plasmas have also been extensively employed in these studies, for example, S VII (Kononov et al 1983), Ca XI (Gaiazov et al 1985, Jupen et al 1986) and Ti XIII (Jupen and Litzen 1984), in these cases energy levels were also derived The same method of study was used for neon like scandium, vanadium, chromium and manganese (Jupen and Litzen 1985, 1986 and Jupen et al 1987). Solar flare identifications of 3s→3p and 3p→3d transitions have been made in Fe XVII (Feldman et al 1985) and for a few lines in Ni XIX (Jupen 1984).

As might be expected numerous theoretical studies along the neon like sequence have been undertaken Various methods have been employed including relativistic as well as non relativistic calculations. Fawcett (1984) has employed the Hartree Fock method of Cowan (1981) to obtain energy levels along the sequence. Cogordan et al (1985, 1986) have performed *ab-initio* calculations using the multi- configurational Dirac Fock code of Grant et al (1980) for a number of ions up to Z=54 In both cases

good agreement with experimental data has been obtained The MCDF code of Grant et al has also been applied by Curtus et al (1988) to calculate energy levels and transition probabilities for the neon like ions S VII, Cl VIII and Ar IX Buchet et al (1987) have undertaken a theoretical survey of the $2p^5 3l$ configurations from Ar IX to Cu XX. A theoretical study of the principal $2p^5ns$ series along the neon like sequence using the eigen quantum defect theory (EQDT) has also been carried out by Wang and Liu (1988)

3 3 THE NEON SEQUENCE IN ABSORPTION PREVIOUS WORK

3.3.a) Neutral Neon.

The first member of the neon sequence is neutral neon which has the ground state configuration $2p^6\ ^1S_0$ The VUV absorption spectrum of this member was first studied by Madden and Codling (1964) using a 180Mev electron synchrotron to back-light a column of neon gas They observed the principal series due to the excitation of a single 2p electron to excited states of the form $2p^5ns,nd$ converging on the $^2P_{1/2,3/2}$ limits Also observed was a prominent Rydberg series of autoionizing resonances due to the promotion of a single inner shell 2s electron to levels with energies greater than the $^2P_{1/2}$ ionization limit. A number of series due to the simultaneous excitation of two of the outer p electrons in transitions of the type $2p^6 \rightarrow 2p^4ml,m'l'$ were also recorded

3.3.b) Na^+.

The VUV absorption spectrum of Na^+ was studied by Lucatorto and McIlrath (1976) using the resonant laser driven ionization technique, (RLDI). The absorption spectrum of Na^+ was observed in the 420-150Å wavelength region. They reported the observation of the $Na^+ 2p^6 \rightarrow 2p^5ns,nd$ series, together with the lowest lying autoionization resonances involving the excitation of a single 2s subshell electron $2s^22p^6 \rightarrow 2s2p^6np\ ^1P$, six

members of this series were measured.

3.3.c) Mg^{2+}.

The VUV absorption spectra of neutral and ionized magnesium (Mg, Mg^{+} and Mg^{2+}) were recorded by Esteva and Mehlman (1974) using a dual BRV technique More recently Kastner et al (1977) also obtained the absorption spectrum of Mg^{2+} using a low inductance vacuum spark as the ion source. Esteva and Mehlman identified some 68 resonances from Mg I, II and III They observed the absorption spectrum of Mg^{2+} in the 240-150Å wavelength region. The spectrum consisted of the normal series transitions involving the excitation of an outer 2p electron Also recorded by both groups of workers were the autoionizing resonances due to the inner shell 2s electron In each case the wavelengths for several members of this series were measured

3.2.d) Al^{3+}.

Some features in the absorption spectrum of Al^{3+} were studied by Carillon et al (1972) using a two laser plasma technique with one plasma acting as the continuum source and the other as the absorber Kastner et al (1977) also carried out absorption studies of aluminium plasmas in the VUV, using a single low inductance vacuum spark, they observed the $2p^6 \rightarrow 2p^5ns,nd$ series along with several members of the inner shell autoionizing transitions $2s^22p^6np\ ^{1,3}P$. However, both of these techniques failed to record an unambiguous absorption spectrum of the aluminium plasma In the case of Carillon et al, an aluminium target was employed as the backlighter to produce the continuum radiation The strong emission lines from higher ion stages in the aluminium laser produced plasma resulted in the partial obscuration of the absorption features present This led to some controversy in the literature with reports of the observation of stimulated emission and gain in the two plasma experiment of Carillon et al (1971, 1972) and Jaegle et al (1973, 1974). In the experiment in which they studied the absorption of VUV radiation emitted from

one aluminium plasma by a second aluminium plasma they suggested that their photoabsorption measurements showed the occurrence of a negative absorption at the wavelength 117 41Å corresponding to the $2p^6\ {}^1S \rightarrow 2p^5 4d\ {}^3P$ transition in Al^{3+}. The mechanism suggested by the authors to increase the population of this level was dielectronic recombination involving the $2s2p^6 4p\ {}^3P$ level followed by a collisional transfer to the $2s^2 2p^5 4d\ {}^3P$ level Valero (1974) carried out extensive studies using a cylindrical lens to produce the absorbing aluminium plasma with a point aluminium plasma to back light the ion column Valero explained the anomalous intensities observed by the group of Carillon et al as arising from the re-absorption of spectral lines in the cooler regions of the plasma. In the case of the theta-pinch technique used by Kastner et al there was also a dense line spectrum which arose from emission within the plasma from a number of different ion stages, thus tending to lead to a confusing spectrum Jamelot et al (1972) identified new lines in the $2p^6 \rightarrow 2p^5 nd$ series in Al^{3+}, in addition to those already known (Soderqvist 1934) As well as these identifications Carillon et al (1972) reported the observation of two members of the ^3P inner shell autoionizing series and three members of the ^1P series Kastner et al (1977) disputed these assignments and re-assigned the ^3P series identifying the series of strong absorption features present in their spectra as $^1S_0 \rightarrow {}^1P_1$ transitions. They based their reassessment of the data of Carillon et al on the smooth variation of effective principal quantum numbers along the isoelectronic sequence Kastner et al describes the triplet features as being narrower profiles superimposed on the longer wavelength side of the main $^1S_0 \rightarrow {}^1P_1$ resonances

3.3.e) Si^{4+}.

The fifth member of the sequence is Si^{4+} The principal series were observed in emission (Soderqvist 1934, Ferner 1941) More recently Brillet (1976) carried out an analysis of laser produced plasma spectra of silicon and

measured lines due to transitions between the $2p^5 3s$, 3p,3d and 4s configurations at long wavelengths (>500Å); the analysis was further extended by Brillet and Artru (1986). Kastner et al (1977) observed the principal series of Si^{4+} in absorption however, no observation of autoionizing structures above the $^2P_{1/2}$ limit have been reported for the Si^{4+} ion previous to this work.

3.4 THE NEON SEQUENCE IN ABSORPTION: PRESENT WORK.

An overview of the absorption studies carried out along the beginning of the neon sequence is shown in Fig.(3.1.a.b.c) which illustrates the VUV absorption spectra of Mg^{2+}, Al^{3+} and Si^{4+}. Tables listing the principal series absorption have been previously given (Brilly 1986) and are not presented here. The individual spectra are discussed in what follows.

3.4.a) Mg^{2+}.

The VUV absorption spectrum of a magnesium plasma is shown in Fig.(3.1.a). The spectrum contains lines from Mg^{2+} and Mg^{3+} but not from the neutral or singly ionized atom. This is to be expected given the experimental conditions and the low ionization potentials of the ions in question. The cylindrical lens used to create the absorbing plasma was focused either in front of or behind the magnesium target surface by up to 1.5cm. The magnesium spectrum shown in Fig.(3.1.a) was acquired using the flat target configuration discussed in chapter two, with a cylindrical lens used to form the absorbing plasma. The lens was de-focused by 5mm and 200 laser shots were required to record the spectrum. The effect of successive de-focusing of the cylindrical lens on the observed absorption spectrum was to lessen the number of features from the Mg^{3+} ion observed to short wavelengths; though there was not a corresponding enhancement of Mg^{2+} features on the plate. The spectrum shown in Fig.(3.1.a) was the most intense magnesium absorption spectrum recorded.

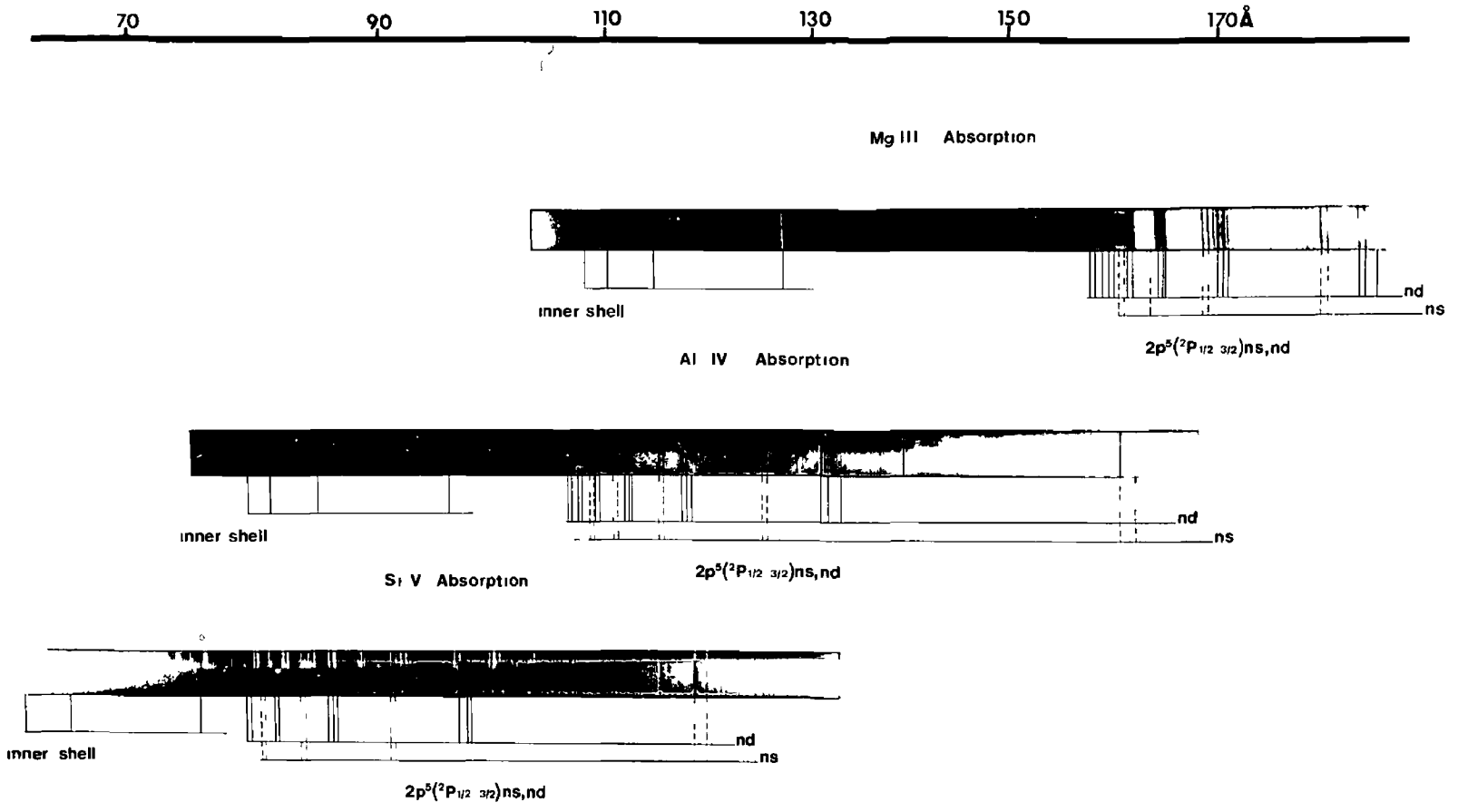

FIG 31

The third, fourth and fifth members of the neon isoelectronic sequence in absorption.

Fig (3.1 a) shows the principal series of the Mg^{2+} ion due to the excitation of an outer 2p electron (200-160Å) The lines due to these $2p^6 \rightarrow 2p^5ns,nd$ transitions are strong and in the case of the nd series are also broad indicating that the fore plasma contained a large number density of Mg^{2+} ions in the ground state. Also in Fig.(3.1 a) are lines due to transitions in the Mg^{3+} ion of the type $2p^5\ {}^2P_{1/2} \rightarrow 2p^4ns,nd$ (200-160Å). Fig.(3 1.a) shows the spectacular onset of continuum absorption after the $^2P_{1/2,3/2}$ limits in the 160Å region Above the limits are further groups of lines due to Mg^{3+} transitions of the type $2p^5\ {}^2P_{1/2} \rightarrow 2p^4ns,nd$ Also above the Mg^{2+} ionization limit, (beginning just above 130Å) are observed the Rydberg series of asymmetric resonances assigned to the inner shell transitions $2s^22p^6 \rightarrow 2s2p^6np\ ^1P$. The measured wavelengths of these are listed in Table (3.1) together with the results of Esteva and Mehlman (1974) and Kastner et al (1977)

TABLE 3 1

Wavelengths of the inner shell $2s^22p^6 \rightarrow 2s2p^6np$ autoionizing levels in Mg III observed in the absorption spectrum of a magnesium laser produced plasma.

	λ_{TW}	λ_{EM}	λ^*_{TW}	λ^*_{EM}	λ_K
n=3	126.48	126 50	125 65	125 19	126 49
n=4	114.30	114 32	113 44	113 16	114 34
n=5	110 13	110 16	109 31	109 27	110 12
n=6	108 02	108 08	107 31	107 34	.
n=7	.....	106 92		106 26	
n=8	... .	108 30	.. .	105 60	
$^2S_{1/2}$	. . .	104 50	. ..	103.61	. .

*. are calculated values.
EM are results of Esteva and Mehlman (1974).
K are results of Kastner et al (1977)
TW are results of this work
All wavelengths are in angstroms ($\Delta\lambda$=±0.02Å)

In this work four members of the series were observed The calculated values of table 3.1 and all subsequent tables of this chapter were obtained in single configuration runs of the Dirac Fock package of Grant et al (1980) Also in table 3 1 and all subsequent tables wavelengths quoted were measured at that point where the absorption cross section of the feature changes most rapidly

3.4.b) Al^{3+}.

The features observed in the absorption of an aluminium plasma are shown in the second spectrum of Fig (3 1) This is the first absorption spectrum of aluminium ions to show clearly the discrete principal $2p^5ns,nd$ series together with the strong autoionizing resonances above the $^2P_{1/2}$ limit. The spectrum is essentially the same as the isoelectronic Mg^{2+} case. The dominant absorption is again the principal $2p^6 \rightarrow 2p^5ns,nd$ series with some less intense absorption features due to the lower stage Al^{2+} ion (Mosnier et al 1987, Brilly et al 1988, 1990) The onset of the photoionization continuum is not as dramatic as the magnesium spectrum, due to the difficulty in generating large densities of Al^{3+} ions As with magnesium the Rydberg series of asymmetric resonances $2s^22p^6 \rightarrow 2s2p^6np^1P$ are clearly seen in the photoionization continuum Also noticeable from the Al^{3+} spectrum in Fig (3 1.b) is the energy gap between the $2p^5\ ^2P_{1/2,3/2}$ limits and the first member of the autoionizing series, this energy interval has decreased when compared with the Mg^{2+} case indicating that the autoionization levels lie closer to the ionization limit Also there is no absorption from the higher stage Al^{4+} observed between the ionization limit and the first member of the autoionization series as in magnesium. This spectrum was obtained using the butt jointed target configuration detailed in chapter two with a hafnium target employed to provide the back-lighting continuum radiation A tightly focused cylindrical lens was used to create the absorbing plasma on the magnesium target surface, 250 laser shots

were required to produce the observed spectrum

The list of measured wavelengths of the autoionizing features of this ion are listed in Table (3 2) along with the values obtained by Carillon et al (1972) and more recently those of Kastner et al (1977). Both Carillon et al (1972) and Kastner et al (1977) reported the observation of the $2s^2 2p^6 \rightarrow 2s2p^6np\,^3P$ autoionizing resonances in absorption spectra of aluminium plasmas, in both cases the triplet structures were reported as weak features to the long wavelength side of the ^1P profiles. This work which reports the first unambiguous absorption spectrum of Al^{3+} in this wavelength region (70-100Å) has not revealed the presence of the $^1S_0 \rightarrow {}^3P_1$ series.

TABLE 3 2

Wavelengths of the inner shell $2s^2 2p^6 \rightarrow 2s2p^6np$ autoionizing levels in Al^{3+} observed in the absorption spectrum of an aluminium laser produced plasma.

	λ_{TW}	λ_C	λ_K	λ^*_{TW}	λ^*_C
n=3	95 56	94.48	95 56	94 73	91 93
n=4	84 36	84 14	84 38	83 82	82 97
n=5	80 59	..	80 58	80.09	79.87
n=6	78.79	.	78 79	78 33	.
n=7	... ..	...	77.79	.	....
n=8	....	...	77 18	. .	. .
$^2S_{1/2}$	.	.	75 38	74.97	

*. are calculated values.
C. are results of Carillon et al (1972)
K. are results of Kastner et al (1977)
TW are results of this work.
All wavelengths are in angstroms. ($\Delta\lambda = \pm 0$ 02Å)

An enlargement of the wavelength region containing the autoionizing $^1S_0 \rightarrow {}^1P$ resonances is shown in Fig (3 2 a) and shows clearly the higher members of the principal series merging into the photoionization continuum with

the discrete series of inner shell autoionizing features being observed above the ionization limit.

An interesting observation which concerns this particular spectrum relates to the over lapping aluminium emission spectrum which was recorded to provide a source of external references. The spectrum was recorded simply by translating the aluminium target so that both lenses used in the absorption experiment were focused onto the aluminium target surface. In effect the spectrum shown is the result of emission from two aluminium plasmas, it may also be considered as the absorption spectrum of an aluminium line plasma back lit by an aluminium point plasma. In the emission spectrum of a single point plasma formed on an aluminium target the emission features in this region of the spectrum are normally of approximately equal intensity. In the spectrum shown in Fig (3 2 a) we see that from the end of the principal series in the absorption spectrum the lines in the emission spectrum are becoming progressively weaker due to absorption by the photoionization continuum of the Al^{3+} ions in the line plasma. The reason why the line which overlaps the $2s2p^6 3p\,^1P$ autoionizing member appears to be the strongest emission line in the region is that it is superimposed on the reduced absorption wing of the $2s2p^6 3p$ profile

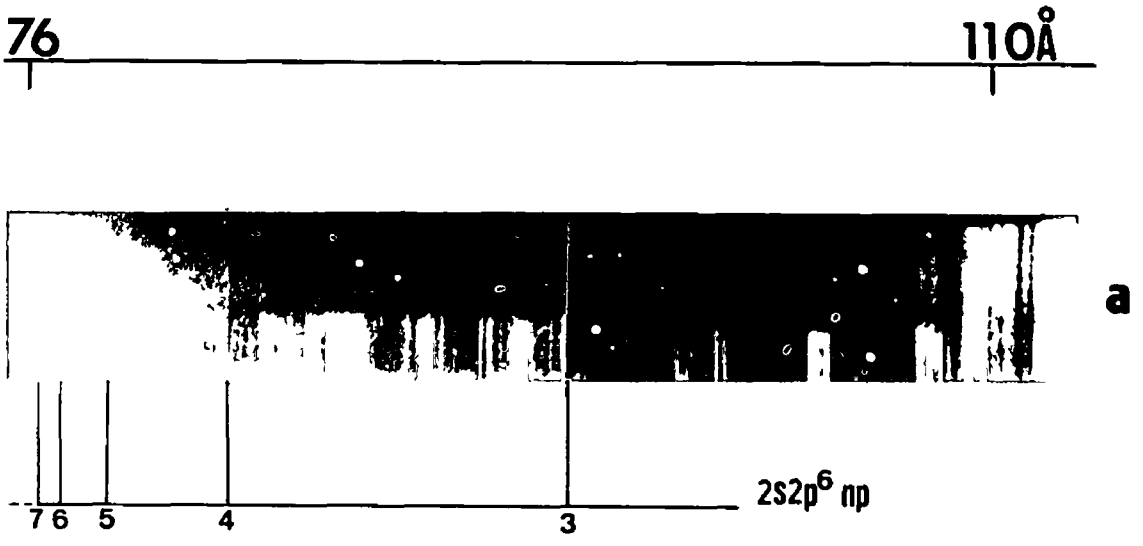

Al IV autoionizing series.

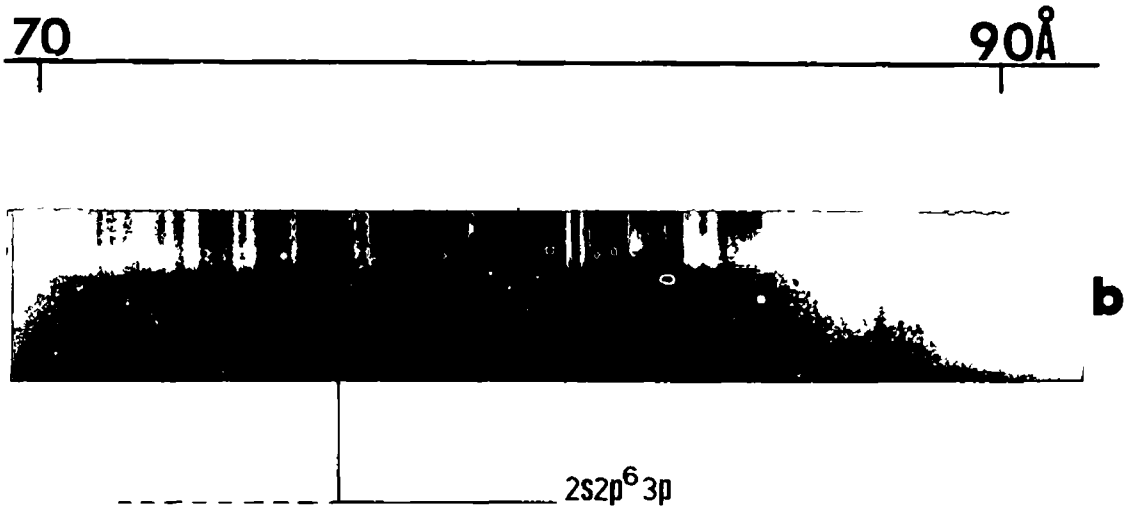

SiV autoionizing series

FIG 32

An enlargement of the wavelength regions containing the inner shell autoionizing $^1S_0 \rightarrow {}^1P$ resonances in both Al^{3+} and Si^{4+}

3 5 ABSORPTION AND EMISSION SPECTRA OF Si^{4+}

The VUV photoabsorption spectrum of a silicon laser produced plasma is shown in Fig.(3.1.c) , The spectrum was recorded using the technique described in the preceding chapter. All of the silicon absorption spectra recorded during this work were recorded using two flat targets joined together along a common edge as shown in Fig.(2.1). To record the neon like spectrum of silicon it was necessary to employ a spherical element in the lens combination in order to produce an absorbing plasma with a sufficiently high density of Si^{4+} ions Approximately 300 laser shots were required to record a typical spectrum using a tungsten or hafnium plasma to provide the background continuum Absorbing plasmas produced with a cylindrical lens were found to be dominated by Si^{3+} absorption with only the n=3, 4 and 5 members of the Si^{4+} principal series present; although these lines were generally strong. The principal series of the neon like Si^{4+} ion together with the first three members of the $2s^22p^6 \rightarrow 2s2p^6np^1P$ autoionizing series are shown in Fig (3.1 c) A large number of other absorption lines are also seen, these additional features have been assigned to the sodium like ion Si^{3+} (Mosnier et al 1988, Brilly et al 1989) and are discussed in the next chapter

Kastner et al (1977) reported the observation of inner shell autoionizing levels in the ions along the beginning of the neon-like isoelectronic sequence Their study of silicon, revealed the presence of the neon like Si^{4+} ion in the plasma under investigation, evident from observed Si^{4+} emission lines. The authors reported no evidence of the autoionizing series, suggesting that the spark used does not always produce the spatial plasma configuration needed to observe absorption lines. Kastner et al further suggest that observation of Si^{4+} absorption requires a hot central continuum emitting region surrounded by a cooler region containing Si^{4+} ions.

The series of experiments reported here enabled the observation of the first three members of the autoionizing $2s^2 2p^6 \rightarrow 2s2p^6np^1P$ series in Si^{4+} The wavelengths of the 3p, 4p and 5p members are listed in table 3.3, the values of the $^2P_{1/2,3/2}$ series limits are also given in table 3.3 in wavelength form for ease of comparison. The wavelength region containing the first member is displayed above in Fig (3.2 b) the feature clearly possesses an asymmetric profile strongly suggesting it is autoionizing

The three spectra shown in Fig.(3 3 a b c) were recorded by focusing the entire laser output onto the surface of a silicon target using a single spherical lens Each of the spectra corresponds to a successive de-focusing of the incident laser beam by changing the lens to target distance. The slit width of the spectrometer remained constant throughout this series of experiments and was approximately 10-15μm This series of spectra is important in two respects Firstly we see the fall off in the number of strong emission lines from higher ion stages in the plasma This fall off with progressive de-focusing especially at shorter wavelengths reveals the underlying recombination continuum, which although weak is clearly visible (Fig.3 3.b c). Secondly the actual size of the silicon plasma increases with progressive de-focusing Changing the lens to target distance from the original focal length of the lens (f=6mm) to f+7 5mm in steps of 2 5mm results in the plasma at the silicon target surface increasing in size from a point like plasma to a diffuse plasma of approximately 3mm in diameter This diffuse plasma is neither as dense nor does it contain large populations of highly ionized atoms, as would the plasma created with the tightly focused laser beam However, it does provide a significant path length along which lower ion stages within the plasma may absorb the recombination continuum. The strong self absorption of members of the Si^{4+} $2p^6 \rightarrow 2p^5nd$ series are observed in the spectra of the more de-focused plasmas (Fig 3.3 b.c) Two members of the

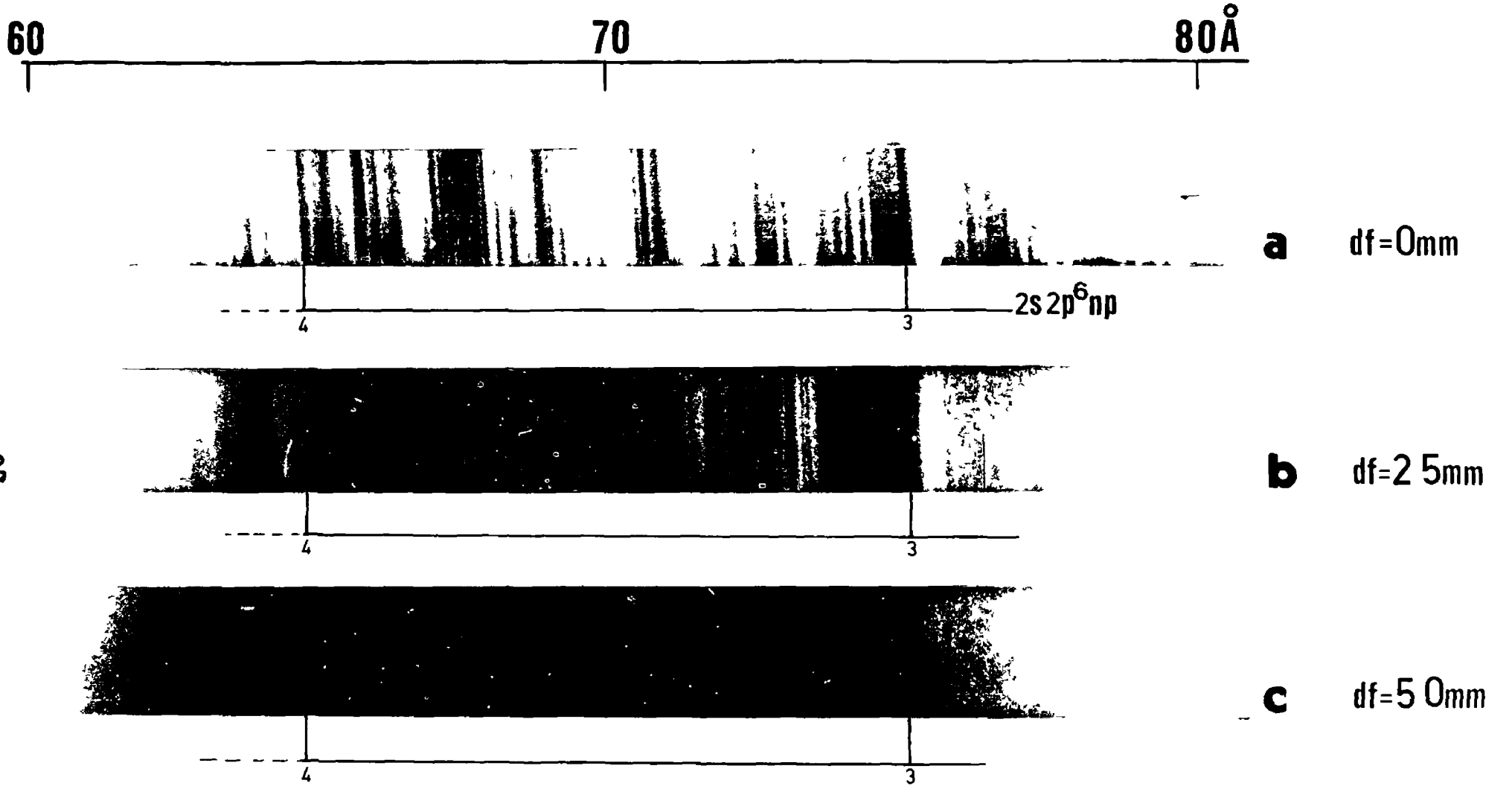

FIG 3 3

The effect of successive de-focusing on the emission spectrum of a silicon laser produced plasma. (See text)

inner shell autoionizing series are also clearly visible in the first spectrum and are indicated in Fig.(3.3.a). The n=3 member of the $2s2p^6np\,^1P_1$ series can be seen clearly in each of the spectra in Fig.(3.3.a.b.c) and as is shown in the first spectrum the structure appears asymmetric, again indicating its autoionizing nature. However with successive de-focusing (Fig.3.5.b.c) the asymmetric shape of this feature seems to recede to be replaced by what appears at first glance to be a broad absorption structure with an emission like feature superimposed centrally along it. It may also perhaps be interpreted as the emergence of a second absorption feature to the short wavelength side of the main n=3 profile. Whichever interpretation is placed upon the observation of the feature in Fig.(3.3.a.b.c) it is clear that the n=3 member of the autoionizing series in Si^{4+} appears to undergo a profile shape change with successive de-focusing, i.e., with changing plasma conditions.

TABLE 3.3.

Wavelengths of the inner shell ($2s^22p^6 \rightarrow 2s2p^6np$) autoionizing levels of Si V observed in the absorption spectrum of a silicon laser produced plasma.

	$\lambda_{MZ.}$	λ_{TW}	$\lambda^{*}_{TW.}$
$^2P_{3/2}$ limit.	74.35	74.36	74.15
$^2P_{1/2}$ limit.	74.07	74.11	74.04
n=3	.....	74.93	74.47
n=4	.....	64.96	64.71
n=5	.....	61.67	61.43
$^2S_{1/2}$ limit.	.....	.....	56.86

*. are calculated values.
MZ. are the limits given in Martin and Zalubas (1983).
TW. are the results of this work.
Measured wavelengths are in angstroms and are accurate to ±0.02Å with the exception of the n=5 member for which $\Delta\lambda$=±0.05Å.

The wavelength of the $2s2p^6 3p$ member has been measured from a number of different photographic plates containing the feature as well as from enlarged photographic prints of the region. These values are listed in table 3.3.

A quantum defect analysis of the principal series converging on the $^2P_{3/2,1/2}$ limits was carried out using a three parameter Rydberg Ritz formula (Edlen 1964) to establish the quantum defects and thereafter the series limits. This analysis resulted in values for the two limits which, as is seen in the above table are in good (±0.05Å) agreement with those given by Martin and Zalubas (1983).

Clearly the feature lies to the low energy side of the $^2P_{1/2}$ limit of the free Si^{4+} ion by some $15490cm^{-1}$ (1.92eV) and therefore the autoionizing character of the feature is at first surprising. However, if we consider the case not of the free ion but of an ion subject to plasma micro fields then we can interpret the observation as an example of *forced autoionization.*

3.6 FORCED AUTOIONIZATION.

The phenomenon of *forced autoionization* was first observed by Garton et al (1962). who found in the absorption spectrum of shock heated barium vapor that high lying members of the principal series were not observed for values of n>12 and that two known 5d8p doubly excited states appeared to have Beutler Fano profiles. To explain this apparent paradox they suggested that fields produced in the shock heating turned the n>12 states into a Stark continuum with the result that the 5d8p states appeared as autoionizing features. For over a decade the subject was largely ignored, but with the development of tunable lasers and a renewed interest in atomic Rydberg states there has been a corresponding upsurge of interest in forced autoionization. Work

carried out in the last ten years (Cole et al 1980, Sandner et al 1981, Blondel et al 1983 and Gallagher et al 1983) has shown by controlled experiment that the original suggestion of Garton et al was correct Most of the recent work on the subject involves the use of tunable lasers to probe high n states in the presence of static electric fields, (see for example, Blondel et al 1983, Saloman et al 1985, Liu et al 1985). An account of the phenomenon and recent work on the subject may be found in Sandner et al (1986) Rzazewski and Cooper (1986) have considered the problem in a fluctuating electric field and have formulated a model of the effect considering micro fields within plasmas Both dense and dilute plasmas were considered and the model has been used to derive specific expressions for broadening of Fano profiles. No experimental observation of forced autoionization as a result of micro fields in laser produced plasmas has been reported prior to this work

To transform an isolated atom in its ground state into an electron and an ion requires that the electron absorbs the ionization energy E_∞ The same transformation in an external field requires less energy This can be interpreted as the lowering of the ionization energy by an amount ΔE_∞. In a plasma an atom is exposed to the action of the Coulomb field of the ions and the electrons (the plasma micro field) Therefore a lowering of the ionization energy is to be expected In the absorbing silicon plasma used in this work which was created with a spherical lens, we would expect a high electron density to pertain over the cycle of the plasma and thus expect strong micro fields to be present. It is to be expected that such fields turn the high n states of the principal $2p^5ns,nd$ series into a Stark continuum resulting in a lowering of the effective ionization limit of Si^{4+} and thus allowing the $2s2p^6 3p\,^1P$ level to appear to be autoionizing In none of the neon like spectra studied here have we been able to measure or even observe members of the $2p^5ns,nd$ series for $n>9$ This may be due to the fact that these high n series members have low oscillator

strengths and are therefore too weak to be observed however, it is also equally likely that the high n states have been Stark broadened into a continuum by the plasma micro fields. In both the Mg^{2+} and Al^{3+} spectra of Fig (3 1 a.b) the 2s autoionizing series lie far beyond the $^2P_{1/2}$ limit and are therefore expected to be autoionizing. But for the Si^{4+} case the position of the first member lies just to the low energy side of the limit. Hence it lies in the Stark continuum of the high $2p^5ns,nd$ states and can therefore autoionize. The second (n=4) member of the Si^{4+} series has been measured at 64.96Å and is therefore sufficiently removed from the $^2P_{1/2}$ limit in energy terms to appear as an asymmetric feature in both Fig.(3.3 a) and Fig.(3.3 b) and although this feature is weak in Fig.(3 3.a b) its asymmetric profile is nonetheless maintained despite the changing plasma conditions

The concept of *forced autoionization* invoked here permits an explanation of the observation of a Beutler Fano line shape (Fig 3 1 c, 3 2 b and 3 3 a) associated with a feature measured below the ionization limit in Si^{4+} A more detailed discussion of the plasma electron density and the corresponding lowering of the Si^{4+} ionization limit is given in what follows

IONIZATION LIMIT: Electron density effects

The $^2P_{1/2}$ limit has been given by Martin and Zalubas (1983) as 167.39eV while the feature under discussion has been measured at 165 47eV We must therefore conclude *ab initio* that there is a lowering of the limit by about 2eV

The average value for the quantum defect for the principal $2p^5ns$ series converging on the $^2P_{1/2}$ limit was calculated for a number of members of the series to be 0.66. Using the Rydberg formula the value of n in the $2p^5ns$ series which corresponds to the position of the first member of the autoionizing series is n=14 From this we may infer that for values of n>14 the levels of

the $2p^5ns$ series converging on the $2p^5\ {}^2P_{1/2}$ limit are broadened into a Stark continuum, i e , n=14 sets a lower limit for the plasma electron density n_e.

As one proceeds up a given spectral series the spacing between the levels decreases, the lines overlap and eventually merge The point at which this merging occurs in the spectrum of a plasma is the well known Ingles Teller (1939) limit; see (Griem 1983) Application of equations given by Griem (1983) assuming the value of n to be 14 results in a value for the electron density n_e below which the $2p^5 14s$ level in Si^{4+} will remain discrete of $n_e \simeq 2\ 2X10^{18} cm^{-3}$, which may be considered low for a laser produced plasma created with a ruby laser. Cooper (1966) gives an expression for the amount by which the ionization energy is lowered, assuming the above value for the electron density we may estimate the value of the reduction in the ionization energy assuming some value for T_e the electron temperature

A reasonable assumption for T_e is 25eV which is consistent with the collisional radiative equilibrium model described by Colombant and Tonon (1973) We have used this model to plot the fractional ionic abundances against electron temperature; this is shown in Fig (3 4) below for the case of a silicon plasma The model is electron density dependent and for the calculated curves shown in Fig.(3 4) we have assumed a value for n_e of $1\ 0X10^{21} cm^{-3}$ which is less than half of the critical density for a ruby laser produced plasma, which can be calculated to be of the order of $n_e = 2\ 5X10^{21} cm^{-3}$

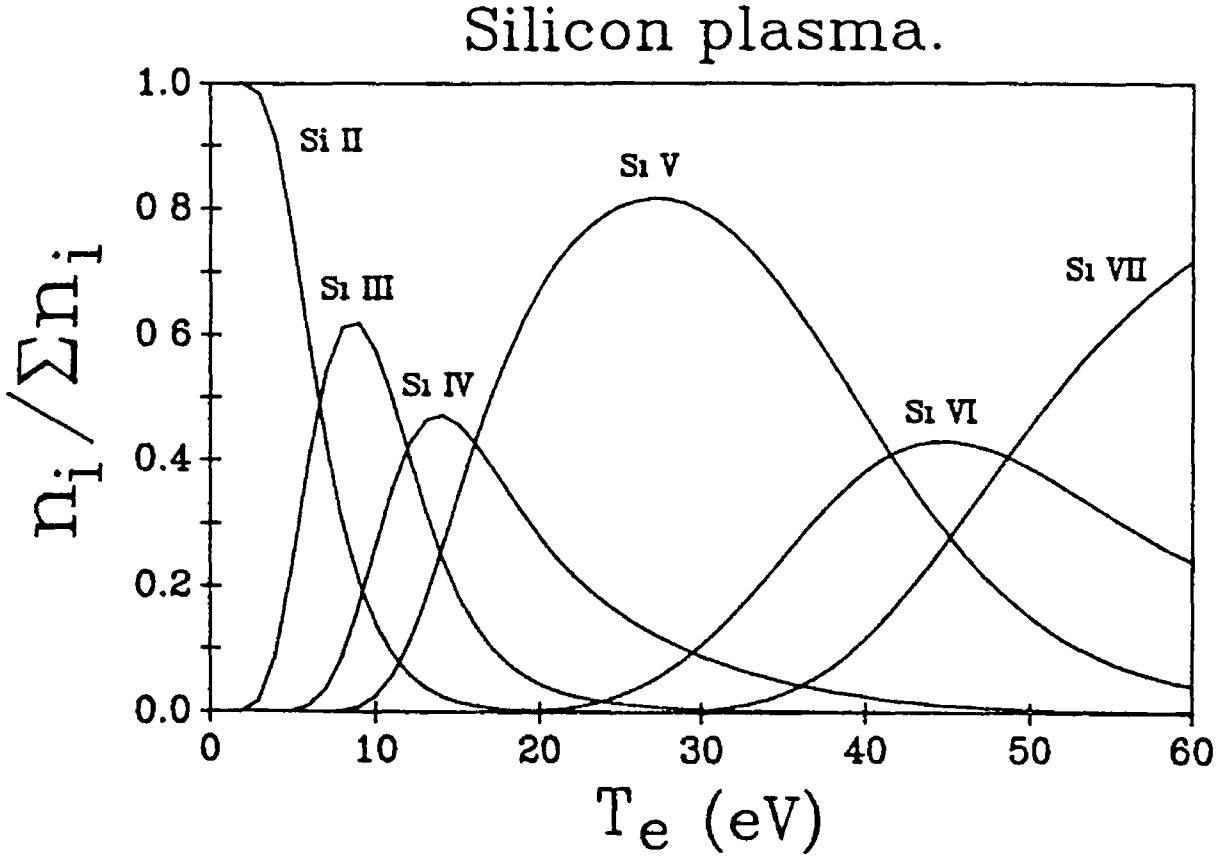

FIG 3.4

Fractional ionic abundances plotted against electron temperature for a silicon laser produced plasma, assuming the collisional radiative equilibrium model described by Colombant and Tonon (1973).

Applying the equation for the lowering of the ionization energy to the lower value of n_e given above results in a value for the lowering of the $^2P_{1/2}$ limit (ΔE) of less than 1eV, which is clearly inconsistent with the observation of the autoionizing feature

If we consider the case of the maximum visible $2p^5ns$ series member then we have a value of $n_{max}=6$. Application of the Ingles Teller relationship using this value of n_{max} results in a much higher value for the electron density which although below the critical density for a ruby laser produced plasma gives a value for ΔE of the order of 9eV, which may be considered unreasonably high It has however, been a feature of the work along the neon sequence that in none of the spectra examined have we

been able to observe members of the principal series for n>9. This observation may be the result of low oscillator strengths for these features, however, it is also a possibility that the higher series members are broadened into a Stark continuum. When we consider a value for n_{max} of 9 in the above expressions we arrive at an intermediate value for the electron density which results in a corresponding intermediate value of the order of 3eV for the lowering of the ionization limit which from the above qualitative discussion seems consistent with the observation.

The lowering of the Si V ionization limit and the concept of Forced autoionization offer an explanation for the observation of a Beutler Fano line shape associated with the 2s→3p feature discussed above. However, as is seen in Fig.(3.3.b.c) the shape of the line profile seems to alter with progressive de-focusing. This apparently anomalous behaviour will be further discussed in a tentative manner in Appendix one

Isoelectronic behaviour of 2s→3p ^{1}P level.

Fig.(3.5) below is a graphic representation of the gradual decrease in energy difference between the first member of the autoionizing series and the ionization limit as the sequence progresses to higher members. As can be seen from Fig.(3.1.a.b.c) and the tables of data presented above the energy difference between the $^2P_{1/2}$ limit and the $2s2p^6 3p\,^1P$ autoionizing level decreases along the sequence until in the fifth member Si V the positions overlap and the $2s2p^6 3p\,^1P$ level in fact lies to the low energy side of the $^2P_{1/2}$ ionization limit by about 1.92eV. In Fig.(3.5) are plotted the difference between $\Delta E/\zeta$ for the particular transition and $\Delta E/\zeta$ for the $2s^2 2p^5(^2P_{1/2})$ series limit, (ΔE is the transition energy in atomic units, ζ in the effective charge on the ion) against the particular sequence member (see Kastner et al 1977). The point relating to the 2s→3p member for Si V is the experimental measurement of this work, that of P VI is the result of a calculation. It should be

pointed out here that no experimental observation for the 2s→3p feature in the P VI spectrum has been reported in the literature, though clearly the feature lies well below the ionization limit of the ion as it does for all subsequent members of the Ne sequence

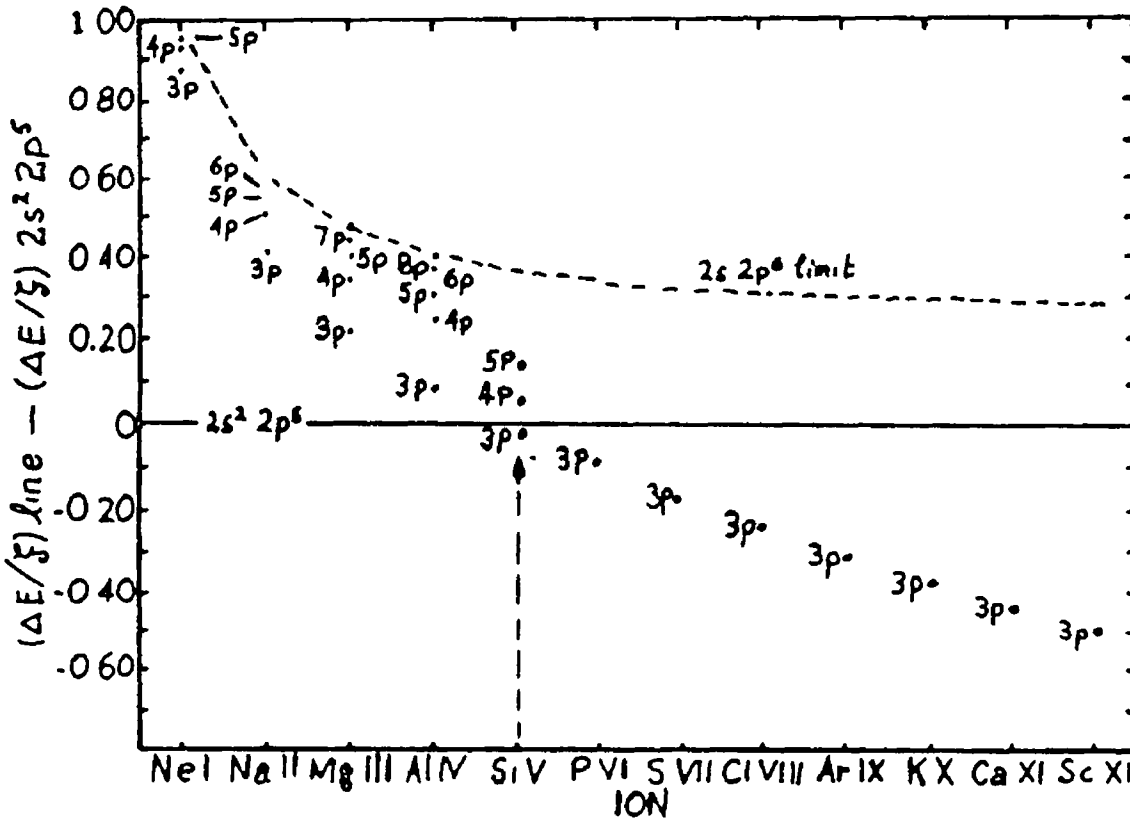

FIG 3 5
Plot showing the relationship between the inner shell, 2s→3p autoionizing series and the ionization limit along the neon isoelectronic sequence. (See text).

3 6 REFERENCES

Aglitsky, E. V. Antsiferov, P S Mandelstam, S L and Panin, A M. Can. J Phys. **62**. 1924 (1984)

Bakhkin, S. Trabert, E Hackmann, P H. and Buttlar, H Phys. Scr. **28**, 1983 (1983).

Blondel, C. Champeau, R. J. and Delsart, C Phys Rev A. **27**, 1, (1983).

Brillet, W.U L. Phys. Scr. **13**, 5, 289. (1976).

Brillet, W.U L and Artru, M C Phys. Scr. **14**, 6 285 (1976)

Brilly, J. M.Sc Thesis (*Applications of laser produced continuum radiation*) Dublin Cuty University (1986) Unpublished.

Brilly J. Kennedy E.T and Mosnier J.P. J Phys B At Mol. Opt. Phys **21**, 3685 (1988)

Brilly J Kennedy E T. and Mosnier J P *Proceedings of the ninth international conference on Vacuum ultraviolet radiation physics VUV-9 University of Hawaii 1989* Phys. Scr. **40**, 30, (1990)

Buchet, J P Buchet-Poulizac, M C. Denis, A. Desesquelles, J. Druetta, M. and Martin, M. Phys Scr **27**, 99 (1983)

Buchet-Poulizac, M C and Buchet, J P Phys Scr **27**, 99. (1983).

Buchet, J P Buchet-Poulizac, M C. Denis, A Desesquelles, J. Druetta, M. Martin, M. and Wyart, J F J. Phys B. At Mol Opt Phys **20**, 1709 (1987)

Buchet-Poulizac, M C. and Buchet, J P. Phys. Scr **27**, 99. (1983).

Buchet-Poulizac, M C Buchet, J P. and Martin, S *J Physique* **47** 407. (1986).

Carillon A Jamelot G. Sureau A and Jaegle P Phys. Lett **38**, 2 (1972)

Cogordan, J. A. Lunell, S. Jupen, C. and Litzen, U. Phys. Rev. A **32**, 1885 (1985)

Cogordan, J A Lunell, S Phys Scr. **33**, 406 (1986)

Cole, B. E. Cooper, J. W. Saloman, E. B. Phys. Rev. Lett **45**, 887. (1980).

Colombant, D. and Tonon, G F J. Appl Phys. **44**, 8 (1973).
Cowan, R D. and Dieke, H.G. Rev. Mod. Phys **20**, 2 418 (1948)
Cowan, R.D. *The Theory of Atomic Structure and Spectra* (U. California Press, Berkeley, Calif., 1981)
Curtus, L. J Haar, R. R. and Martinson, I. Nucl Instr and Methd B31 288. (1988)
Edlen. B Atomic Spectra. "*Handbauch Der Physik* " **27**, 80-220 (1964)
Esteva JM and Mehiman G. Astro. Phys J. **193**, 1 (1974)
Fawcett, B C Phys Scr. **30**, 326. (1984).
Feldman, U. Doschec, G. A. and Seeley, J F Mon. Not. R Astron Soc. **212**, 41P. (1985).
Ferner E. Ark. Mat. Astron Phys. **28A**, PP 1-21 (1941)
Gaiazov, R. R Zaikin, Yu F. Kononov, E Ya. Ryabtsev, A. N. Ragozin, E. N Chirkoc, V A and Churilov, S S Preprint N° 155 Lebedev Institute. Academy of Sciences USSR. (1985).
Gallagher, T. F Gounand, F. Kachru, R. Tran, N H and Pillet, P. Phys. Rev A **27**, 2485 (1983).
Garton W.R S Parkinson W H and Reeves E.M Proc. Phys Soc. London **80**, 860, (1962)
Goldstein, W. H. and Walling, R S. Phys Rev A **36**, 7 (1987).
Grant, I P. McKenzie, B.J Norrington, P.M. Mayers, D R. and Pyper, N.C. Comput. Phys Commun **21**, 207 (1980)
Griem, H R. Radiation processes in plasmas "Basic Plasma Physics " Vol 1 Editors. A A Galeev and R N Sudan North Holland Publishing Company. (1983)
Jaegle, P Jamelot, G Carillon, A Sureau, A and Dhez, P. Phys Rev. Lett **33**. 1070 (1974)
Jamelot G. Sureau A and Jaegle P. Phys Lett **41A**, 2, (1972).
Jupen, C Mon. Not. R Astron Soc. **208**, 1P. (1984)
Jupen, C Litzen, U. Phys Scr **30**, 112 (1984)
Jupen, C. Litzen, U and Skogvall, B Phys Scr **33**, 69 (1986)
Jupen, C. Litzen, U. Phys. Scr. **33**, 509. (1986).
Jupen, C. Litzen, U Kaufman, V and Sugar, J. Phys. Rev.

A. 35, 116 (1987).
Kastner S.O., Crooker,A M , Behring,W E , and Cohen, L. Phys. Rev. A. 16, 57 (1977).
Kononov, E Ya Kramida, A E Podobedova, L. I Ragozin, E. N. and Chirkov, V. A. Phys Scr. 28, 496. (1983).
Kramida, A. E. *Opt Spectrosc* 58, 450 (1985)
Liu, J. Y. Mc.Nicholl, P Harmin, D A Ivri, J. Bergeman, T and Metcalf, H. J. Phys Rev. Lett. 55, 2. (1985).
Lucatorto T B. and McIlrath T. J Phys Rev Lett 37, 7 (1976).
MacGowan, B J Rosen, M. D. Ekhart, M J. Hagelstein, P L. Madden, R P and Codling, K J Opt Soc Am. 54, 268 (1964)
Matthews, D L Nilson, D. G Philips, T. W. Scofield, J H Shimkaveg, G. Trebes, J E. Walling, R S. Whitten, B. L. and Woodworth, J. G. J Appl Phys 61, 12 (1987)
Matthews, D. L. Hagelstein, P L. Rosen, M D Eckart, M J Ceglio, N M Hazi, A. U. Medecki, H MacGowan, B J Trebes, J E. Whitten, B L Campbell, E M Hatcher, C W Hawryluk, A M. Kauffman, R. L Pleasence, L. D Rambach, G. Scofield, J H. Stone, G and Weaver, T A Phys. Rev. Lett 54, 110 (1985).
Martin W.C and Zalubas R J. Phys. Chem Ref Data Vol 12, 2 (1983)
Mosnier J. P. Brilly J. and Kennedy E T Journal de Physique Colloque C9, Supplement au n 12 (1987).
Rosen, M D Hagelstein, P L Matthews, D L Campbell, E. M Hazi, A. U. Whitten, B L MacGowan, B J. Turner, R E and Lee, R W Phys Rev Lett 54 106 (1985)
Rzazewski, K and Cooper, J J Opt Soc Am 3, 6 (1986).
Saloman, E. B. Cooper, J W. and Kelleher, D E Phys Rev Lett 55, 2 (1985).
Sandner, W Safinya, K A. and Gallagher, T F. Phys Rev A 24, 1647. (1981)
Sandner, W. Safinya, K. A. and Gallagher, T F Phys Rev. A. 33, 2. 1008 (1986)
Soderqvist J. Nova. Acta. Ragiae. Soc. Sci. Ups. Ser. IV. 9, PP 1-103 (1934).

Trabert, E. *Z Phys A*. 319. 25, (1984).
Valero, F P.J Appl. Phys Lett 25, 64 (1974).

CHAPTER FOUR: THE SODIUM ISOELECTRONIC SEQUENCE.

4.1 INTRODUCTION.

The work reported in this chapter involves the observation of new photoabsorption spectra of aluminium and silicon laser produced plasmas (Mosnier et al 1988, Brilly et al 1988, 1989). In both the aluminium and the silicon experiments we have observed new absorption spectra which have been assigned to the sodium like ions Al^{2+} and Si^{3+}.

Chapter three described observations along the neon like isoelectronic sequence. It was found while studying this sequence that in all cases the spectra were a good deal more complex than would have been suggested from a consideration of the structure of the neon like ions alone. In the neon like spectra shown in Fig.(3.1) the magnesium spectrum is seen to consist of strong absorption features due to the neon like Mg^{2+} ion, strong absorption was also observed from the higher ion stage Mg^{3+}. The absorption spectrum of Si^{4+} also contained contributions from more than one ion stage. This was found to be the case regardless of the focusing conditions of that portion of the laser beam incident on the silicon target. The absorption spectrum of aluminium however, only shows strong absorption in the Al^{3+} ion with only very weak contributions from another ion stage.

In each of the spectra studied the dominant ionic species were found to be the neon like ions. It was further found that successive de-focusing of the incident laser beam used to create the absorbing aluminium or silicon plasmas highlighted the non neon like absorption; this was particularly the case in aluminium. A consideration of the ionization potentials (Table 4.1) of each of the ions of Mg, Al and Si up to the fifth stage reveals the reason for this. The fact that de-focusing of the laser beam led

to the enhancement of the non neon like structures in the spectra of both aluminium and silicon led to the conclusion that the the sodium like ions Al^{2+} and Si^{3+} must be present in reasonably large densities in our absorbing plasmas.

TABLE 4 1

IONIZATION POTENTIALS FOR IONS OF Mg, Al AND Si.

	Mg.	Al.	Si.
I.	7.65	5.99	8 15
II.	15 04	18 83	16 35
III.	80.14	28 45	33.49
IV.	109.27	119.99	44 14
V	141.27	153.83	166.77

Energy values are in eV

In the absorption studies reported here and in the other chapters of this work it has been found that the rare gas like ion always dominates in the absorbing plasma and that absorption in higher ion stages was for the most part not observed. This is due to the increase in the ionization potential required in order to proceed to the next stage of ionization, (see table 4 1) For both aluminium and silicon Fig (4 1) shows a graphic representation of the fractional ionic abundances expected to pertain in the absorbing plasma. The graphs were calculated using the collisional radiative equilibrium model described by Colombant and Tonon (1973), the figure shows that over a broad electron temperature range the neon like ion dominates in the plasma. Having established qualitatively that sodium like absorption was observed we concluded that these lines were in fact due to inner shell transitions involving a single inner 2p electron with the outer 3s electron in either the ground state or in one of the lower excited states

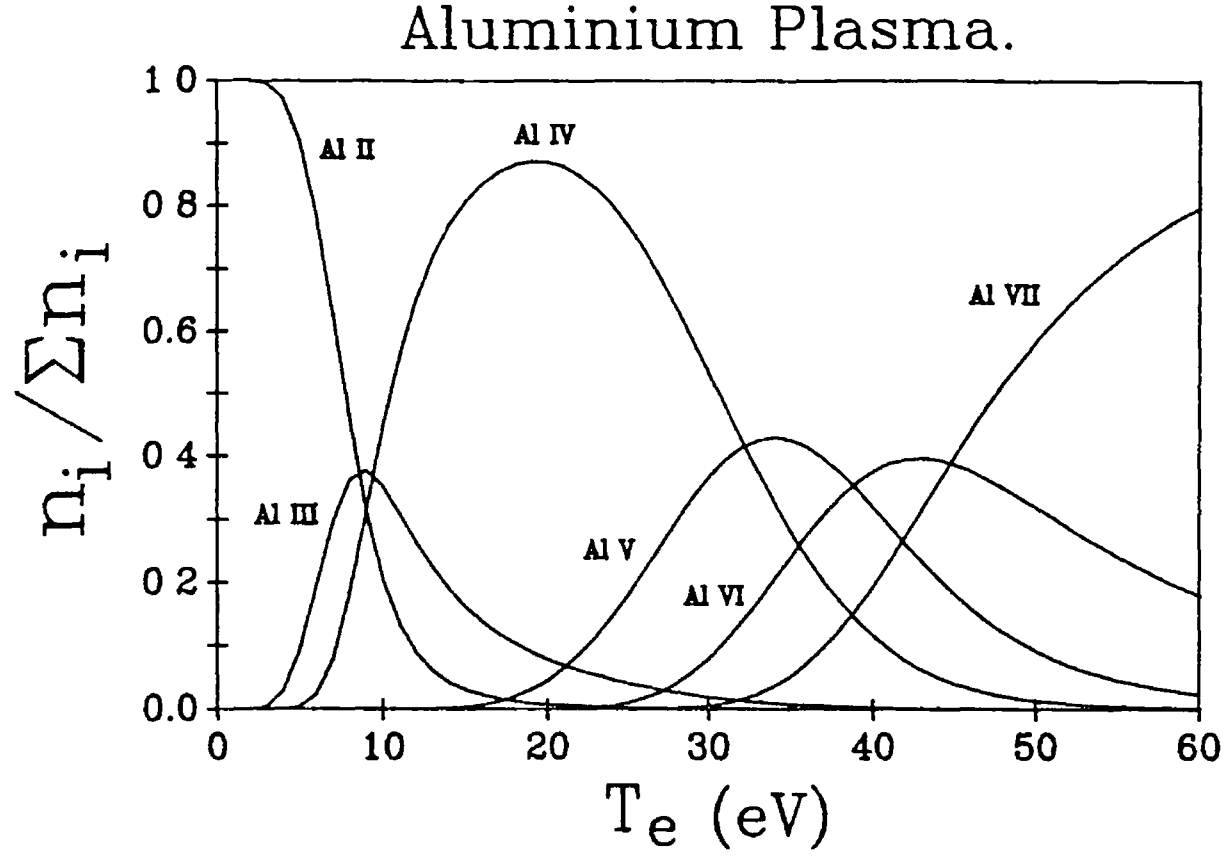

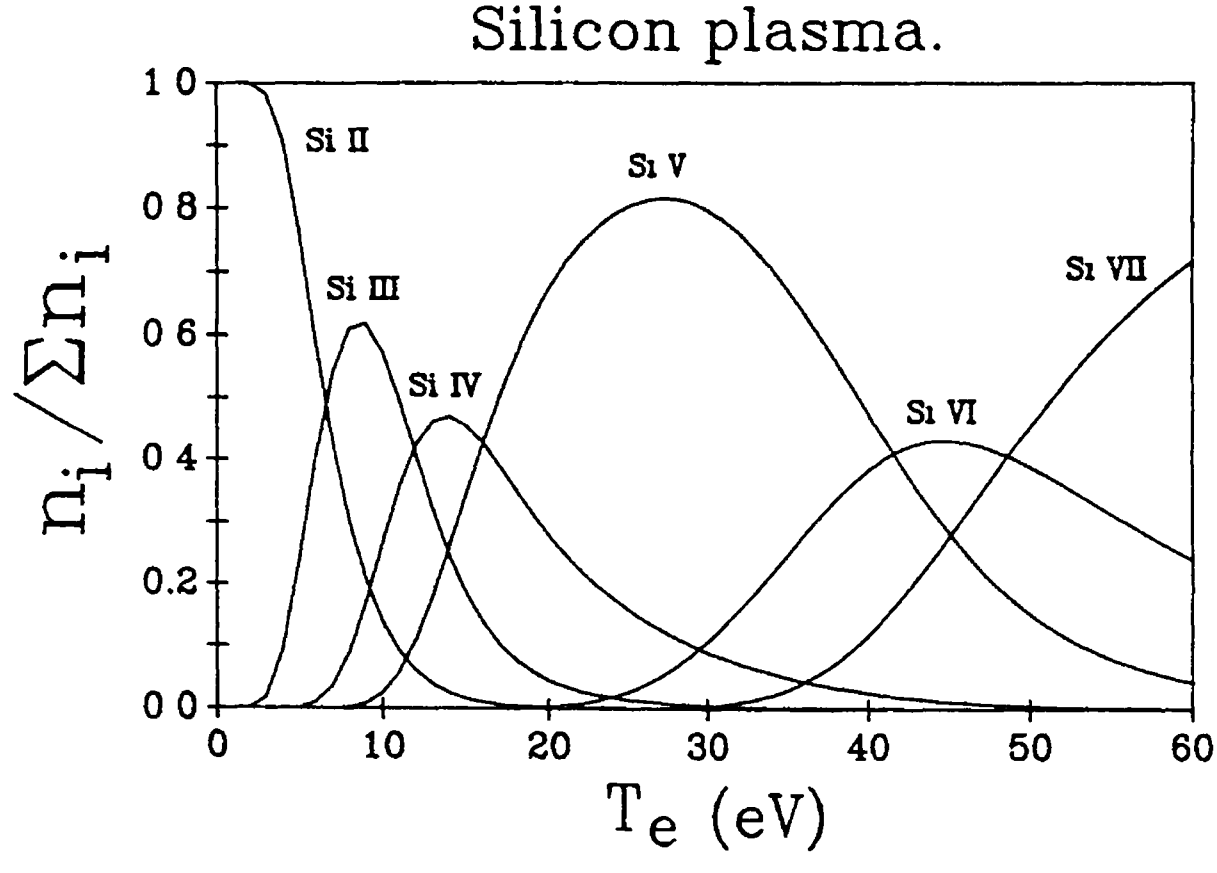

FIG 4 1

Shows graphs of calculated fractional ionic abundances calculated using the collisional radiative model described by Colombant and Tonon (1973).

A sodium like ion possesses the electronic configuration of $2p^6 3s^2 S_{1/2}$ in the ground state, the resulting absorption spectra of such ions are expected to be of a complex nature and to involve excitations of the outer 3s electron as well as the inner neon like core Excitations involving the outermost electron only, lie to very long wavelengths due to its small binding energy and so lie outside the spectral range discussed here. The type of transitions considered most likely to be responsible for the observed structures are given below.

TABLE 4 2

Types of transitions expected in sodium like ions.

FROM THE GROUND STATE	
(1) $2s^2 2p^6 3s\ ^2S_{1/2}$	$\longrightarrow\ 2s^2 2p^5 3s^2\ ^2P_{1/2,3/2}$
(2) $2s^2 2p^6 3s\ ^2S_{1/2}$	$\longrightarrow\ 2s^2 2p^5 3sns$
(3) $2s^2 2p^6 3s\ ^2S_{1/2}$	$\longrightarrow\ 2s^2 2p^5 3snd$
(4) $2s^2 2p^6 3s\ ^2S_{1/2}$	$\longrightarrow\ 2s^2 2p^5 3p^2$
FROM EXCITED STATES.	
(5) $2s^2 2p^6 3p\ ^2P_{1/2,3/2}$	$\longrightarrow\ 2s^2 2p^5 3s3p$
(6) $2s^2 2p^6 3d\ ^2D_{3/2,5/2}$	$\longrightarrow\ 2s^2 2p^5 3s3d$
(7) $2s^2 2p^6 4s\ ^2S_{1/2}$	$\longrightarrow\ 2s^2 2p^5 3s4s$

The most intense pair of lines in the sodium like spectrum are the so-called leading doublet transitions These are the result of excitations involving the 2p subshell and take the form $2p^6 3s\ ^2S_{1/2} \rightarrow 2p^5 3s^2\ ^2P_{1/2,3/2}$ These lines were observed during this work and their identification in both Al^{2+} and Si^{3+} was of crucial importance in the analysis of other more complicated structures present in the spectra of these ions

4 2 THE SODIUM SEQUENCE PREVIOUS WORK

Before describing the specific results obtained along the sodium sequence during this work, it is of value to review briefly the extent to which the sodium sequence has been studied in the past A variety of techniques have been employed by a number of different workers in obtaining spectroscopic data along the sequence Sodium, as would be expected, has been extensively studied and for this element there exists a wealth of available data.

In neutral sodium extensive work has been carried out Configurations involving excitations from the 2p subshell have been identified in photoabsorption spectra below 410Å Lines observed in absorption were assumed to arise from transitions to odd parity levels having J=1/2 or 3/2 Connerade et al (1971) measured such features in the 180-410Å region, using a windowless containment system with a BRV (Ballofet, Romand, Vodar 1961) source backlighting the vapor column Their classifications involved the outstanding $2p^6 3s^2 S_{1/2} \rightarrow 2p^5 3s^2\ ^2P_{1/2,3/2}$ leading doublet near 400Å Subsequent work was carried out by Wolff et al (1972) using a synchrotron to back light a sodium furnace They observed the ground state absorption spectrum including many (mostly weaker) lines which had not been observed in the work of Connerade et al Both Connerade et al and Wolff et al observed features in the absorption spectrum above the Na II $2p^5 3s\ ^1P$ limit due to excitations of the type $2p^5 3s\ ^2S_{1/2} \rightarrow 2p^5 nln'l'$ with neither nl nor n'l' (in the principal configuration of the upper odd parity term) being a 3s electron Most of the observed features were very asymmetric and autoionization broadened and included a number of window resonances Because the electron coupling scheme in the upper levels varies with increasing n, their labelling is particularly difficult as one has to find the most appropriate intermediate coupling scheme for each configuration Connerade et al found on the basis of Hartree-Fock calculations that the

spin-orbit interaction of the open core was small in Na I and therefore the $2p^5 3s$ configuration tends to L.S coupling Line assignments were obtained in the same paper from the computation of effective principal quantum numbers based on all four limits

Inner shell absorption in Na I involving the 2s electron was also observed by Connerade et al (1971) and Wolff et al (1972) and more recently by LaVilla et al (1981). Strong $2s^2 2p^6 3s^2 S \rightarrow 2s(^2S)2p^6 3snp(^3P)^2P$, n=3,4 resonances in the 65-72eV region were found by Wolff et al (1972) and LaVilla et al (1981). The strong n=3 resonance was found to have a striking Beutler-Fano profile with a width of some $2700cm^{-1}$

The first observation of even parity core excited states along the sodium sequence was reported by Sugar et al (1979) for neutral sodium They used the technique of resonant laser driven ionization (Lucatorto and Mc Illrath 1976) in which they employed a tunable laser to selectively populate the $2p^6 3p\ ^2P_{1/2,3/2}$ levels of the atom and studied photoabsorption to the upper levels of the $2p^5 3s3p$ and $2p^5 3s4p$ even configurations The term separation ($3p\ ^2P_{1/2} \rightarrow\ ^2P_{3/2}$) in neutral sodium is only $17cm^{-1}$ and was not resolved

Most of the very recent work which has been undertaken on neutral sodium has been with tunable lasers to probe the core excited autoionizing levels Holmgren et al (1985) carried out experimental investigations of atomic sodium using a pulsed hollow cathode discharge in conjunction with a tunable laser Metastable excited atoms produced (in the $(2p^5\ 3s3p)^4D_{7/2}$ and $(2p^5 3s3p)^4S_{3/2}$ levels) within the discharge were further excited to levels in both the $2p^5 3s3d$ and $2p^5 3s4s$ configurations, thus allowing the authors to establish a partial Grotrian diagram for the quartet system They also suggested several XUV laser schemes based on the observed spectroscopy. Following the work of Holmgren et al, Engstrom et al (1985) used the beam foil technique to determine experimental lifetimes

for eight of the levels in the core excited configurations $2p^5 3s3d$ and $2p^5 3s4s$. Pedrotti et al (1985) used a similar hollow cathode discharge to study emission spectra from excited states in both neutral sodium and Mg^+ and made use of these observations to propose XUV laser schemes in these elements, involving the same core excited levels.

Esteva and Mehlman (1974) using a dual BRV technique in which one BRV source provided the background continuum while the other served as the ion source, observed extensive magnesium photoabsorption spectra in the 100-250Å region. They used time and space scanning of the absorbing plasma to distinguish Mg I, Mg II and Mg III lines. The Mg II lines (184-248Å) were classified as transitions from the $2p^6 3s\ ^2S_{1/2}$ ground state to upper configurations based on the excited $2p^5$ core. The allowed transitions were thus to levels with J=1/2 or 3/2 and had significant $2p^5 3snl\ ^2P$ eigen vector components (nl=ns or nd), the system beginning with the $2p^5 3s^2\ ^2P$ leading doublet pair a little above 250Å. The same authors computed energy levels in the J:L coupling scheme to identify the features observed in the Mg II spectrum. A subsequent paper by Mehlman et al (1976) showed that identifications of transitions within these complex spectra were more difficult than is expected from the rather simple excitation scheme which has been described above. Subsequently the classifications were revised for ten of the low lying core excited levels on the basis of intermediate coupling configuration interaction calculations based on center of gravity Hartree Fock orbitals.

Core excited levels of Mg^+ were also observed in the ejected electron work of Pegg et al (1975) and Pejcev et al (1977); they assigned these levels to the $2p^5 3s3p$ configuration of Mg^+.

The most recent work along the sodium sequence (excluding the present work) has been by Finkenthal et al (1988) who

nave carrıed out studıes of both the Mg^{+} and Al^{2+} excıted states. The arrangement used by Fınkenthal and hıs co workers consısted of a Pennıng ıonızatıon dıscharge tube, the anode of whıch was set at ground potentıal and the two cathodes whıch opposed each other set at voltages of between 1 and 2kV. In order to confıne the charged partıcles of the dıscharge plasma, an external magnetıc fıeld of the order of 1kG, coaxıal wıth the symmetry axıs of the dıscharge, was applıed The dıscharge was operated at pressures of 5-10 torr wıth argon as the workıng gas The Pennıng source was attached dırectly to the spectrograph and pumped vıa the spectrograph's pumpıng system In order to successfully record spectra the dıscharge was run contınuously for 5-40 mınutes. The spectra were recorded wıth a 2m grazıng ıncıdence ınstrument They observed emıssıon lınes from transıtıons between levels of the upper $2p^{5}3s3p$ confıguratıon and the lower $2p^{6}3p$ level ın both the Mg^{+} and Al^{2+} ıons The spectra showed partıcularly strong emıssıon from those levels wıth quartet parent term The fıne structure splıttıng of the lower $^{2}P_{1/2,3/2}$ term was not observed

Emıssıon lınes ın Al III observed from Pennıng dıscharges ın the wavelength regıon around 170Å were also previously reported by Warden and Moos (1977) and assıgned to the $2p^{5}3s3p$ confıguratıon although no precıse spectroscopıc assıgnments were gıven by these authors Rıchards and Grıffın (1986) have made sımılar observatıons ın emıssıon from aluminıum ımpurıtıes present ın the ELMO Bumpy Torus experıment and have suggested a possıble XUV laser scheme based on the $2p^{5}3s3p$ confıguratıon ın Al^{2+}. Other recent work on Al^{2+} has ıncluded the paper by Martınson et al (1988) ın whıch they report the use of the beam foıl method to search for transıtıons between the doubly excıted quartet states ın Al III The authors proposed prelımınary ıdentıfıcatıons for a number of levels However, we have found that many of the assıgnments of Martınson et al (1988) are ın conflıct wıth the work reported ın thıs chapter

Berry et al (1978) used the beam foil technique to study highly ionized argon and chlorine and observed features in the sodium like spectra of Cl VII and Ar VIII, including the leading doublet transitions Emission data for some of the autoionizing transitions of interest here were also reported by Feldman and Cohen (1967) for the highly ionized atoms from Ti to Cu In addition Burkhalter et al (1975) reported work on highly ionized Ge.

4 3 THE SODIUM SEQUENCE PRESENT WORK

Before the specific results of this work for Al^{2+} and Si^{3+} are discussed in detail it is appropriate here to recapitulate both the precise experimental conditions under which the spectra were obtained and also the method of calculation which was used to assign the observed spectral features

The experiments carried out on aluminium and silicon targets have been largely described in the previous chapter In both cases the flat target configuration discussed in chapter two was employed to record most of the spectra described here, however, in the case of the aluminium work the rotating target configuration was also employed. For both the aluminium and the silicon experiments, tungsten or hafnium continua were used with approximately 50% of the available laser beam energy directed towards each of the targets. Both targets were on average 5cm from the entrance slit of the 2m grazing incidence spectrograph. The width of the entrance slit was varied between 5 and 20μm. In obtaining the absorption spectra that portion of the incident ruby laser beam used to create the absorbing plasma was brought to a focus away from the front surface of the absorber target by amounts of up to 10mm using a 6cm focal length lens 100-200 laser shots were on average required A silicon emission spectrum showing transitions

between excited states is also presented For this experiment the laser beam was defocused by approximately 5mm and required the expenditure of 50 laser shots

The Multi-Configuration Dirac Fock (MCDF) approach was used to obtain theoretical energy levels, (Grant et al 1980). Particular features of the MCDF method which are relevant to the present study are now described An atomic state electron wave function is represented by a linear combination of Configuration state Functions (CSF), these CSF'S are linear combinations of Slater determinants of the orbitals (central-field Dirac orbitals) and are eigenfunctions of the total angular momentum operators as well as parity. Within one CSF electrons are assigned to subshells by specifying the orbital occupation numbers and jj coupled within each of the subshells. The total angular momentum J is then given by the coupling of the angular momentum of all the shells involved according to the chosen intermediate coupling scheme; the latter can therefore be easily varied We have mainly used two of the extensions of the MCDF method namely the MCDF-AL (average level) and EAL (extended average level) methods (Grant et al 1976, Das and Grant 1986). In these methods all the levels are built from the same set of orthornomal orbitals determined self-consistently by using the variational principle on an energy functional proportional to the trace of the Hamiltonian matrix (AL) or to a weighted sum of the diagonal matrix elements if the configurations included have differing total angular momenta (EAL). The Hamiltonian matrix is then set up and diagonalised to obtain the eigen energy levels and configuration mixing coefficients The problem of electron correlation is usually treated as a multiconfiguration expansion built on the same set of orbitals (see for example Das and Grant 1986) using multiple orbitals with the same quantum numbers to take account of correlation and relaxation effects

4 4 TRANSITIONS FROM THE GROUND STATE

Fig.(4 2) shows the photoabsorption spectrum of an Al plasma in the wavelength range 120-170Å. The strongest lines in the spectrum belong to the neon like ion Al IV and arise due to transitions of the type $2p^6\ {}^1S_0 \rightarrow 2p^5ns,nd\ {}^{1,3}P$ (n=3,4,5 ..). There is extensive structure to the long wavelength end of the spectrum as well as to shorter wavelengths which we have classified as arising from both ground state and excited state transitions in the Al^{2+} ion.

The compilation of experimental data by Martin and Zalubas (1979) for the ions of aluminium enables us to present a schematic energy level diagram for Al III and Al IV (Fig 4.3). The various continua are indicated as well as the value of the relevant ionization limits

4.4.a) Absorption from the Al^{2+} ground state: $2p^63s\ {}^2S_{1/2}$
The starting point in the analysis of the spectrum according to the electron excitation scheme described in the preceding section, was to identify the $2p^53s^2\ {}^2P_{1/2,3/2}$ leading doublet transitions The corresponding pair of lines were found in the spectrum to the long wavelength side of the Al IV $2p^6\ {}^1S_0$- $2p^53s\ {}^{1,3}P$ resonances Several other resonances with substantial intensity were also found in this wavelength region, these lines are the excited state transitions arising from the $2p^63p$ and $2p^63d$ states in Al^{2+} and are the subject of section 4 5. Calculations performed gave a value of some 3560cm^{-1} for the fine structure splitting of the $2p^63s^2\ {}^2P$ term, the experimental value was found to be 3340±200cm^{-1} The positions of the two members were found to be 591580cm^{-1} for the $^2P_{1/2}$ component with the $^2P_{3/2}$ component measured at 588240cm^{-1} From the positions of these levels we have obtained a value for ζ_{2p} (the core spin-orbit interaction) of 2230cm^{-1} All known data for these transitions along the sodium sequence are shown on the Moseley plot shown in Fig.(4.4).

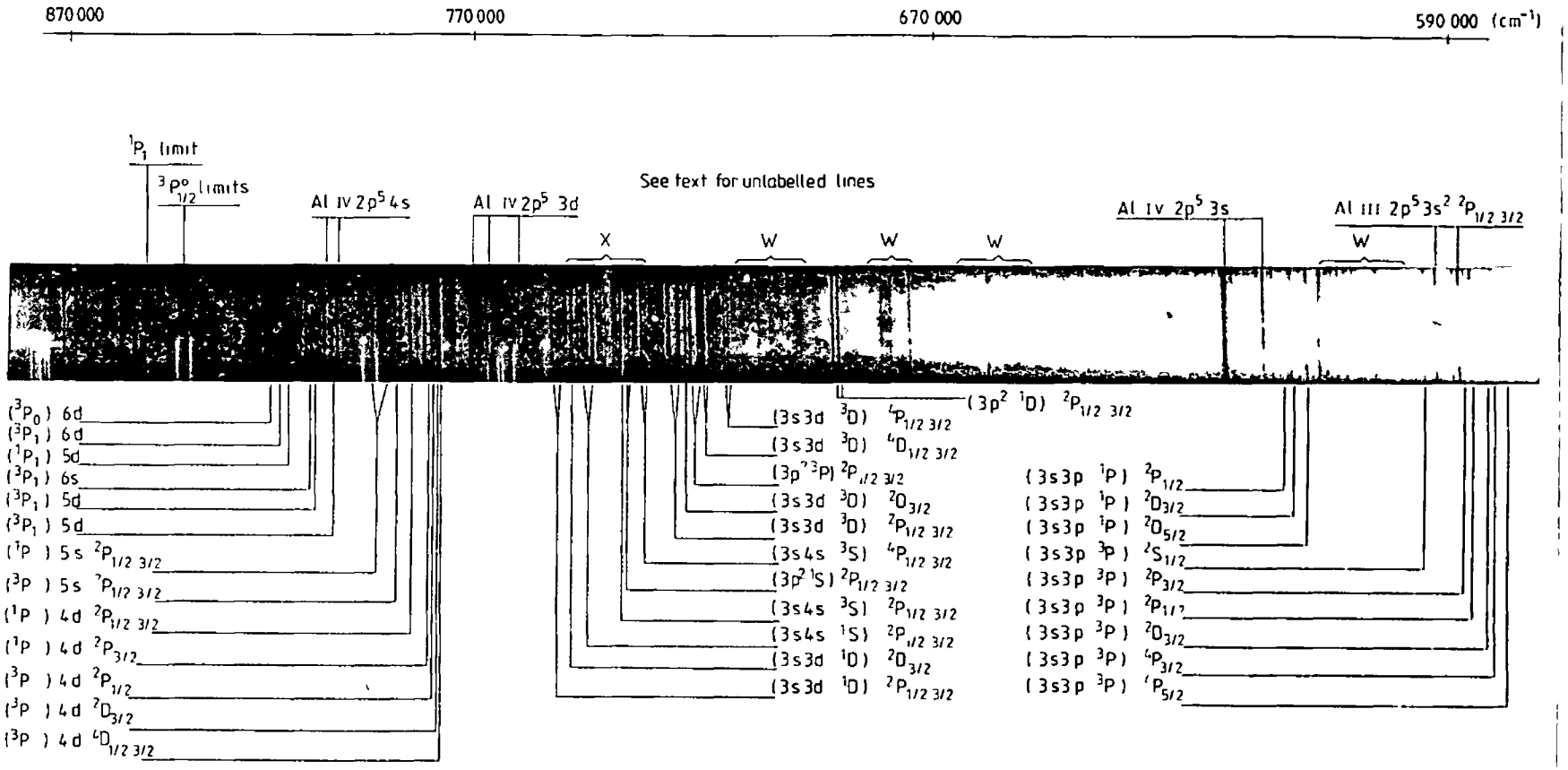

FIG 4 2

The photoabsorption spectrum of an aluminium laser plasma in the wavelength range 120-170Å. The strongest lines are the neon like Al IV principal series. Also shown is the extensive structure to the long wavelength end of the spectrum as well as the complex absorption seen to shorter wavelengths which has been attributed to excitations in the sodium like Al III ion.

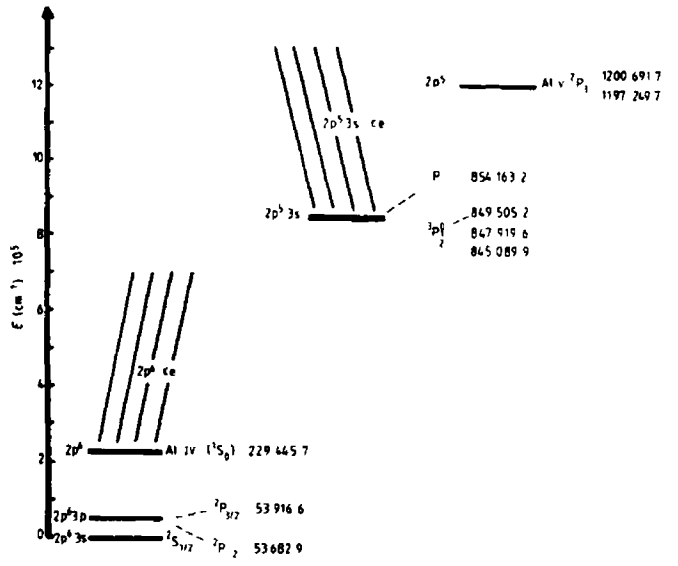

FIG 4 3

Schematic energy level diagram of the Al III and Al IV ions. The various continua are indicated together with values of the relevant ionization limits.

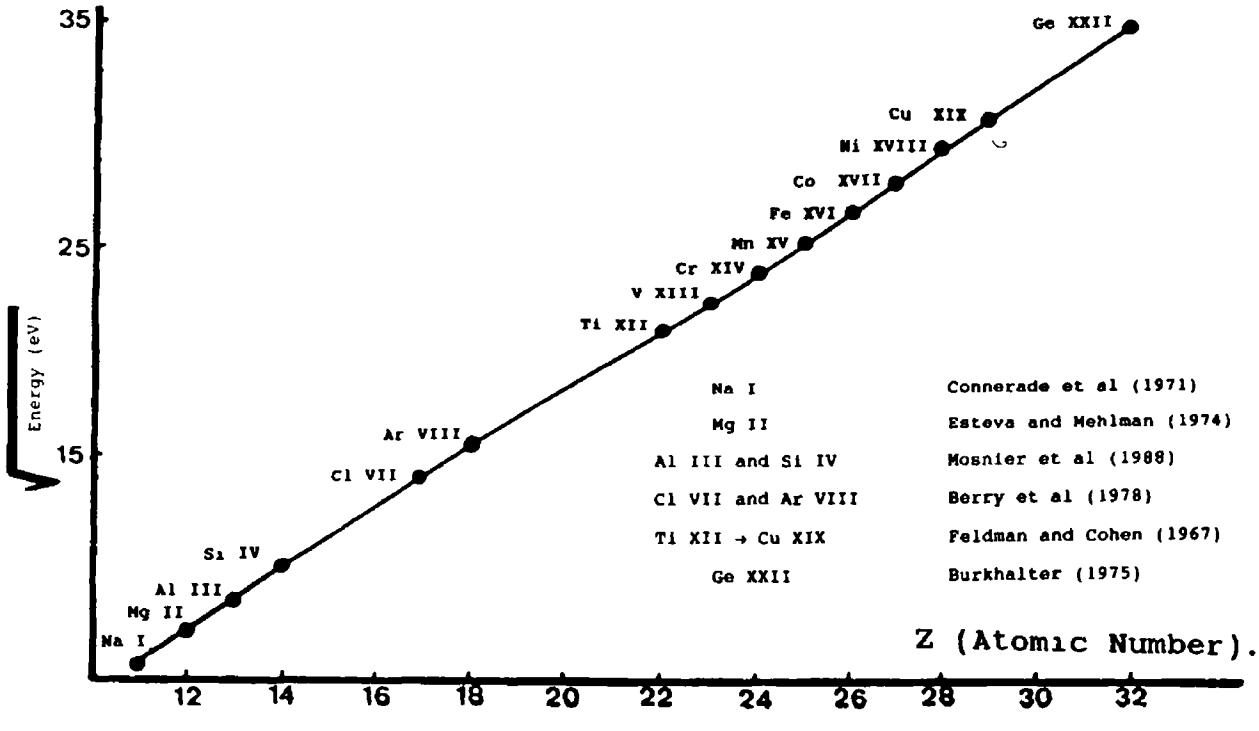

FIG 4 4

Moseley plot of the $2p^6 3s \rightarrow 2p^5 3s^2$ transitions along the sodium isoelectronic sequence.

Lines corresponding to the levels of the $2p^5 3s,ns$ (n>3) configuration are located in the complex region of the spectrum between 125 and 140Å. Line identifications are listed in table 4.3 together with the calculated L:S compositions of the corresponding upper levels and calculated term energies relative to the $2p^6 3s\ ^2S_{1/2}$ ground state. These were obtained from MCDF runs including all the states with J=1/2, 3/2 and 5/2 of the eleven odd parity configurations: $2p^5 3s^2$, $2p^5 3s4s$, $2p^5 3s5s$, $2p^5 3p^2$, $2p^5 3p4p$, $2p^5 3s3d$, $2p^5 3s4d$, $2p^5 3s5d$, $2p^5 3d^2$, $2p^5 3d4d$ and $2p^5 3d4s$. Usually the energy matrix was diagonalised separately for each value of J, although EAL runs were also performed in order to obtain more accurate values of the fine structure splittings. In all cases very good agreement was found between these two different methods. The $2p^6 3s^2 S_{1/2}$ ground state energy was obtained in a separate optimization calculation. Energy values for all the levels were shifted by about $9000cm^{-1}$ in order to obtain a correct position for the $2p^5 3s^2\ ^2P$ term; we found this energy shift to vary systematically along the sodium sequence. In these calculations the left-to-right coupling scheme of the subshells was used for all configurations mentioned above with the exception of the $2p^5 3s3d$ and $2p^5 3s4s$. That is the $2p^5$ subshell was coupled first to the 3s electron and the resulting term value (^1P or ^3P) then coupled to the outermost electron. In the case of the $2p^5 3s3d$ and $2p^5 3s4s$ configurations the 3s electron was first coupled to the outer electron. In this way parentage mixing of terms within a configuration was found to be less than for any other intermediate coupling scheme.

4.4.b) The $2p^5 3sns$ series in Al III.

When progressing along an isoelectronic sequence the increase in nuclear charge causes the corresponding spectra to become more hydrogenic and in Al III the $2p^5(3s4s\ ^3S)^2P$ term lies above the $(3s3d\ ^3D)^2P$ term in contrast to Na I and Mg II. Two spin forbidden transitions to the ^4P term of the $2p^5 3s4s$ configuration were observed. This observation is attributable to

intermediate coupling as $^4P_{1/2}$ and $^4P_{3/2}$ both contain about 12% ^2P character (see table 4 3) The $(3p^2\ ^1S)^2P$ term is energetically close to the levels of the 3s4s configuration and electrostatic mixing with the $(3s4s\ ^1S)^2P$ term as expected, was found to be quite substantial Our calculated eigenvector compositions indicate that $(3p^2\ ^1S)^2P_{3/2}$ and $(3p^2\ ^1S)^2P_{1/2}$ contain respectively 16% and 14% $(3s4s\ ^1S)^2P$ character The lines observed at 734800 and 735950cm^{-1} are therefore classified accordingly, (see table 4 3). Table 4.3 also reports the assignments of three levels belonging to the $2p^5 3s5s$ configuration The values of effective principal quantum numbers for the lines observed at 792550 and 794000cm^{-1} (relative to the $^1P_1$ limit) are 4 00 and 4 04 respectively A tentative assignment of the $2p^5 3s6s$ configuration based on the values of quantum defects is also presented in table 4.4

TABLE 4 3

Classification of the levels of the $2p^5 3s4s$ and $2p^5 3s5s$ configurations in the Al^{2+} ion (see text). Energies are relative to the ground state $2p^6 3s^2 S_{1/2}$

Wavelength of transition (Å)	Term energy (cm^{-1})		Term	*LS* composition (leading percentages)
	Measured	Calculated		
136 50	732 600	732 880	$^4P_{3/2}$	$-83\%(3s4s\ ^3S)\ ^4P + 11\%(3s4s\ ^1S)\ ^2P$
136 39	733 200	733 080	$^4P_{1/2}$	$-85\%(3s4s\ ^1S)\ ^4P + 13\%(3s4s\ ^3S)\ ^2P$
136 09	734 800	734 250	$^2P_{3/2}$	$56\%(3p^2\ ^1S)\ ^2P + 16\%(3s4s\ ^1S)\ ^2P + 13\%(3p^2\ ^3P)\ P - 7\%(3s4s\ ^3S)\ ^4P$
135 88	735 950	735 500	$^2P_{1/}$	$51\%(3p^2\ ^1S)\ ^2P + 14\%(3s4s\ ^1S)\ P + 10\%(3s4s\ ^3S)\ ^2P - 7\%(3s4s\ ^3S)\ ^4P$
135 56	737 700	738 040	$^2P_{1/2}$	$-69\%(3s4s\ ^3S)\ ^2P - 16\%(3p^2\ ^1S)\ ^2P - 10\%(3s4s\ ^1S)\ ^4P$
		738 190	$^2P_{3/2}$	$53\%(3s4s\ ^3S)\ ^2P - 27\%(3s4s\ ^1S)\ ^2P + 10\%(3s4s\ ^3S)\ ^4P$
134 49	743 550	743 300	$^2P_{3/2}$	$56\%(3s4s\ ^1S)\ ^2P + 36\%(3s4s\ ^3S)\ ^2P$
134 05	746 000	746 000	$^2P_{1/2}$	$81\%(3s4s\ ^1S)\ ^2P + 9\%(3s4s\ ^3S)\ ^2P$
126 76	788 900	784 510	$^2P_{3/2}$	$66\%(^3P)5s\ ^2P - 26\%(^3P)5s\ ^4P$
		785 970	$^2P_{1/2}$	$61\%(^3P)5s\ ^2P - 30\%(^3P)5s\ ^4P$
126 19	792 450	790 040	$^2P_{3/2}$	$94\%(^1P)5s\ ^2P + 6\%(^3P)5s\ ^4P$
125 94	794 000	790 720	$^2P_{1/2}$	$83\%(^1P)5s\ ^2P + 16\%(^3P)5s\ ^2P$

TABLE 4.4.

Tentative assignment of $2p^5 3s5d$, $2p^5 3s6s$ and $2p^5 3s6d$ levels in the Al^{2+} ion based on the experimental values of quantum defects.

Wavelength (Å) of transition.	Term energy (cm^{-1})	n^*	Tentative assignment.
124.27	804700	4.79	$(^3P_1)5d$
123.56	809300	5.06	$(^3P_1)6s$
123.34	810750	4.77	$(^1P_1)5d$
122.83	814150	4.98	$(^1P_1)6s$
122.19	818400	5.78	$(^3P_1)6d$
121.89	820400	5.83	$(^3P_0)6d$

4.4.c) The $2p^5 3snd$ series in Al III.

Perturbation of $3s3d\ ^1D$ by $3p^2\ ^1D$ in the Mg I sequence which leads to an inversion of the ^3D and ^1D terms has been known for a long time and has been discussed extensively in the open literature, (see for example Froese Fisher 1975.a.b). As the $3p^2$ perturbing configuration belongs to the same complex as 3s3d the interaction between the two does not diminish when the electronic charge of the core is decreased by one unit and the effect should therefore prevail in the core excited spectra along the Na I sequence as pointed out by Hansen (1975) who studied the $2p^5(3p^2+3s3d)\ ^2P$ mixing in Mg II and reinterpreted the data of Esteva and Mehlman (1974) obtaining a satisfactory agreement between measured and calculated values.

A calculation of all possible states built on the $2p^5 3p^2$ configuration yielded the value $733440cm^{-1}$ for the position of the unperturbed $(3p^2\ ^1D)\ ^2P$ term and showed substantial mixing with $(3p^2\ ^3P)\ ^2P$. The position of the unperturbed $(3s3d\ ^1D)\ ^2P$ term is $732280cm^{-1}$. When the multiconfiguration calculation described above is

performed the interaction between $(3p^2\ ^1D)^2P$ and $(3s3d\ ^1D)^2P$ turns out to be so strong that the eigenvectors composition gives $(3p^2\ ^1D)^2P$ (58%) as the lowest term with about 28%$(3s3d\ ^1D)^2P$ and 16%$(3p^2\ ^3P)^2P$ components, (see table 4 5) The perturbation therefore amounts to about 38500cm^{-1} The two corresponding fine structure levels $^2P_{1/2,3/2}$ were observed at 693650 and 694700cm^{-1} As expected, the multiconfigurational calculation shows that $(3p^2\ ^3P)$ has a substantial $(3s3d\ ^1D)^2P$ component (see table 4 5) due to electrostatic mixing, and we consequently assign the two resonances observed at 721500 and 723050cm^{-1} to this term

TABLE 4 5

Classification of energy levels belonging to the $2p^5 3s3d$ configuration of Al^{2+} (see text). Energies are relative to the $2p^6 3s^2 S_{1/2}$ ground state.

Wavelength of transition (Å)	Term energy (cm^{-1})		Term	*LS* composition (leading percentages)
	Measured	Calculated		
144 17	693 650	692 760	$^2P_{1/2}$	58%$(3p^2\ ^1D)\ ^3P-28\%(3s3d\ ^1D)\ P$ $-16\%(3p\ ^3P)\ ^3P$
143 95	694 700	693 820	$^2P_{3/2}$	$-53\%(3p^2\ ^1D)\ ^2P+23\%(3s3d\ ^1D)\ ^2P$ $+16\%(3p\ ^3P)\ ^2P$
139 83	714 950	714 990	$^4P_{1/2}$	$97\%(3s3d\ ^3D)\ ^4P$
139 67	716 000	715 400	$^4P_{3/2}$	$94\%(3s3d\ ^3D)\ ^4P+3\%(3s3d\ ^3D)\ ^4D$
138 83	720 300	720 880	$^4D_{1/2}$	$-87\%(3s3d\ ^3D)\ ^4D+8\%(3s3d\ ^3D)\ P$
138 77	720 600	721 190	$^4D_{3/2}$	$79\%(3s3d\ ^3D)\ ^4D+9\%(3s3d\ ^3D)\ ^4F$ $+7\%(3s3d\ ^3D)\ ^2P$
138 60	721 500	722 090	$^2P_{1/2}$	$64\%(3p^-\ ^3P)\ P-18\%(3s3d\ ^1D)\ ^2P$ $-8\%(3p\ ^1S)\ ^3P$
138 30	723 050	722 640	$^2P_{1/2}$	$53\%(3p^2\ ^3P)\ ^2P-18\%(3s3d\ ^1D)\ ^2P$ $-18\%(3p^2\ ^1S)\ ^3P$
138 10	724 100	725 040	$^2D_{3/2}$	$-76\%(3s3d\ ^3D)\ D+14\%(3s3d\ ^3D)\ P$ $-5\%(3s3d\ ^3D)\ ^4F$
137 83	725 550	726 860	$^2P_{3/2}$	$74\%(3s3d\ ^3D)\ P+15\%(3s3d\ ^3D)\ ^2D$ $+5\%(3s3d\ ^3D)\ ^4D$
137 46	727 500	727 350	$^2P_{1/2}$	$-87\%(3s3d\ ^3D)\ ^2P+7\%(3s3d\ ^3D)\ ^4D$
133 67	748 100	748 960	$^2D_{3/2}$	$49\%(3s3d\ ^1D)\ ^2D+25\%(3p^2\ ^1D)\ ^2D$ $+9\%(3s3d\ ^1D)\ ^2P+8\%(3p^2\ ^1D)\ P$
133 13	751 150	750 050	$^2P_{1/2}$	$-44\%(3s3d\ ^1D)\ ^2P-34\%(3p^2\ ^1D)\ ^2P$ $-13\%(^3P)4d\ ^2P$
132 89	752 500	752 870	$^2P_{3/2}$	$-37\%(3s3d\ ^1D)\ ^2P-25\%(3p^2\ ^1D)\ ^2P$ $-10\%(^3P)4d\ ^2P+13\%(3s3d\ ^1D)\ ^2D$

We have attributed the two fairly weak and broad lines at 751150 and 752500cm^{-1} to the fine structure levels of the high ^2P term with principal $(3s3d^1D)^2P$ component (see

table 4.5). Compositions of these levels show the importance of configuration mixing with $2p^5 3p^2$ and $2p^5 3s4d$. The contribution of $(3p^2\ ^1D)^2P$ amounts to about 25%. From table 4 5 we see that $2p^5(3s3d^1D)^2P$ and $2p^5(3s3d^3D)^2P$ are not inverted in Al III. Also, for levels with $(3s3d^1D)$ parent term, correlation mixing of different configurations with the same term value is the dominant interaction

In contrast, for levels with $(3s3d^3D)$ parent term, spin-orbit mixing of different terms of the same configuration predominates Thus the spin forbidden transitions to the $(3s3d^3D)^4D_{1/2,3/2}$ levels are observed, these have about 8% $(3s3d^3D)^2P$ component (see table 4 5). The assignments of the $(3s3d^3D)^4P$ are tentative as the corresponding expansions indicate almost pure quartet composition.

Line identifications and wave function compositions for the 3s4d series are given in table 4 6. The coupling scheme has been changed here to $(2p^5 3s\ ^{3,1}P)nd$. Four resonances are attributed to n=4 upper levels with ^3P parent term and one with ^1P parent term namely the $(2p^5 3s\ ^1P)4d\ ^2P$ term. Wave function composition indicates departure from L·S coupling as should be expected, since the excited electron tends to be on average at a comparatively greater distance from the other electrons of the core Therefore the spin orbit interaction of the core electrons begins to predominate over their electrostatic interaction with the excited electron

TABLE 4 6

Classification of energy levels belonging to the $2p^5 3s4d$ configuration of Al^{2+} (see text). Energies are relative to the $2p^6 3s^2 S_{1/2}$ ground state.

Wavelength of transition (Å)	Term energy (cm^{-1})		Term	*LS* composition (leading percentages)
	Measured	Calculated		
128 53	778 000	777 165	$^4D_{1/2}$	84%(^{3}P)4d ^{4}D + 6%(^{1}P)4d ^{2}P − 5%(^{3}P)4d ^{2}P
		777 940	$^4D_{3/2}$	51%(^{3}P)4d ^{4}D + 29%(^{3}P)4d ^{4}F + 6%(^{1}P)4d ^{2}P + 5%(^{3}P)4d ^{4}P
128 42	778 700	779 900	$^2D_{3/2}$	56%(^{3}P)4d ^{2}D + 12%(^{3}P)4d ^{2}P − 12%(^{3}P)4d ^{4}F − 5%(3s3d^{1}D) ^{2}D
128 17	780 200	780 160	$^2P_{1/2}$	−71%(^{3}P)4d ^{2}P + 9%(3s3d^{1}D) ^{2}P + 5%(^{1}P)4d ^{2}P − 5%(3p4p^{1}D) ^{2}P
127 92	781 750	781 210	$^2P_{3/2}$	−54%(^{3}P)4d ^{2}P + 15%(^{1}P)4d ^{2}D + 5%(3s3d^{1}D) ^{2}P − 5%(^{3}P)4d ^{2}D
127 36	785 200	783 960	$^2P_{3/2}$	81%(^{1}P)4d ^{2}P − 9%(^{1}P)4d ^{2}D
		784 170	$^2P_{1/2}$	56%(^{1}P)4d ^{2}P − 28%(^{3}P)5s ^{4}P − 6%(^{3}P)5s ^{2}P

Unidentified lines

A few lines in the range 733000-755000cm^{-1} do not appear to be continuum background features and must therefore be classified as probable Aluminium features The possible presence of lines due to inner-shell absorption in Al II was investigated since the 2p excitation energy is roughly the same in Al II and Al III and the two spectra should consequently overlap Spectral series in Al II due to the excitation of a 2p electron converge on the Al III limits $2p^5 3s^2\ ^2P_{1/2}$ and $2p^5 3s^2\ ^2P_{3/2}$ which we computed respectively at 734100 and 743440cm^{-1} Once these limits were determined a Rydberg formula was used to calculate effective principal quantum numbers However, no evidence could be found for a series of quantum defects characteristic of excitation processes of the type $2p^6 3s^2$- $2p^5 3s^2$nd or $2p^6 3s^2$- $2p^5 3s^2$n'd A tentative suggestion as to the origin of these features might be that they belong to the $2p^5 3p3d$ transition array. We have calculated the transitions $2p^6 3p \rightarrow 2p^5 3p3d$ and found that they lie in the 690000-712000cm^{-1} energy range. However,

in previous work involving excited states along the sodium sequence (Sugar et al (1979)) no such transitions were reported

4.4.d) Si IV Ground State Absorption.

Much of the proceeding discussion will also apply to transitions from the ground state of Si IV. For the Si IV case we have observed the $2p^6 3s^2 S_{1/2} \rightarrow 2p^5 3s^2\ ^2P_{1/2,3/2}$ leading doublet levels at 809400cm-1 ($^2P_{1/2}$) and 804400cm^{-1} ($^2P_{3/2}$) which in this case gives a fine structure splitting of 5000cm^{-1} and a value for ζ_{2p} of 3333cm^{-1}. However, in the silicon spectra which have been recorded as part of this work there were considerably more absorption lines in the short wavelength region than there were for the Al III case. Also this region of the silicon spectrum was found to be more compacted than the aluminium case, with many of the features being poorly resolved. We have not as yet undertaken an analysis of the Si IV ground state features to the same degree of rigor as has been presented above for the Al III spectrum. However a few of the more prominent features in the region have been assigned and these are listed in table 4.7 below along with leading percentages and calculated oscillator strengths.

Extensive absorption has also been attributed to excitations from the lower $2p^6 3p$ and $2p^6 3d$ excited states in Si IV, this work forms a major portion of the next section of this chapter.

TABLE 4 7

Observed and calculated $2p^6 3s \rightarrow 2p^5 3p^2$, 3s3d and 3s4s transitions in the Si^{3+} ion observed in the absorption spectrum of a silicon laser produced plasma.

(a)	(b)	(c)	(d)
934000	938918	1.45(-2)	57.2%$(3s3d\,^1D)\,^2P$ +20%$(3p^2\,^3P)\,^2P$
935800	940332	2.58(-2)	52.2%$(3p^2\,^3P)\,^2P$ +18%$(3s3d\,^1D)\,^2P$
978900	980367	1.99(-2)	62.2%$(3p^2\,^3P)\,^1P$ +7%$(3s3d\,^3D)\,^2P$
	980502	3 28(-2)	82 7%$(3s3d\,^3D)\,^4F$ +7%$(3s3d\,^3D)\,^2P$
975700	978464	2.93(-3)	44 3%$(3p^2\,^1S)\,^2P$ +14%$(3s3d\,^1D)\,^2P$
	979350	1.37(-3)	32 3%$(3s3d\,^3D)\,^4D$ +13%$(3s3d\,^1D)\,^2P$
983400	985096	3 54(-2)	85%$(3s3d\,^3D)\,^2P$
986400	988454	3 09(-1)	67 1%$(3p^2\,^1S)\,^2P$ +8%$(3s3d\,^3D)\,^2D$
	989719	2 10(-1)	82 9%$(3p^2\,^1S)\,^2P$ +7%$(3s3d\,^3D)\,^2D$
	1018432	2.20(-4)	82 1%$(3s4s\,^3S)\,^2P$
	1020502	<1(-4)	77 2%$(3s4s\,^3S)\,^2P$
994000	992757	1.41(-1)	34%$(3p^2\,^3P)\,^2P$ +14%$(3s3d\,^3D)\,^2P$
	994600	3 06(-2)	57 2%$(3p^2\,^3P)\,^2P$ +8%$(3s3d\,^3D)\,^2P$
1025100	1024502	2.46(-3)	70 2%$(3s4s\,^3S)\,^4P$ +6%$(3s4s\,^1S)\,^2P$
	1024997	8.01(-3)	43 3%$(3s4s\,^1S)\,^2P$ +8%$(3s4s^2S)\,^4P$
	1209656	2 2(-4)	49 5%$(3s4s\,^3S)\,^2P$
	1032763	1 1(-4)	88 7%$(3s4s\,^3S)\,^2P$
101290	1016074	1.82(-2)	51 2%$(3p^2\,^1D)\,^2D$ +11%$(3s3d\,^1D)\,^2P$
1017400	1017891	4 18(-2)	50 3%$(3p^2\,^1D)\,^2P$ +9%$(3p^2\,^3P)\,^2P$
	1021899	6 52(-2)	34.2%$(3p^2\,^1D)\,^2P$ +14%$(3s3d\,^1D)\,^2D$

(a) Measured values (cm^{-1}).
(b) Calculated values (cm^{-1}).
(c) Calculated oscillator strength The figure in brackets indicates power of ten
(d). Leading percentages.

4 5 TRANSITIONS FROM EXCITED STATES

In the previous section of this chapter we have dealt with absorption from the ground states of both Al III and Si IV. As was pointed out both spectra contain a number of resonances to the long wavelength side of the neon-like $2p^6\ ^1S \rightarrow 2p^5 3s\ ^{3,1}P$ pair. These lines have been classified by us as arising from the excited states $2p^6 3p$ and $2p^6 3d$ in the sodium like ions Al^{2+} and $Si.^{3+}$ These spectra are discussed at length below

The Al III spectrum is displayed in Fig (4 5), with the corresponding Si IV spectra in both emission and absorption shown in Fig.(4.6 a b) Fig (4 7) shows the two spectra presented for isoelectronic comparison The dominant features in both spectra are the neon like 3s resonances together with the sodium-like $2p^6 3s\ ^2S_{1/2} \rightarrow 2p^5 3s^2\ ^2P_{1/2,3/2}$ doublet In addition many other absorption features are observed, most of which can be interpreted as arising from 2p excitation in the $2p^6 3p$ and $2p^6 3d$ excited configurations in sodium-like ions In the following we successively describe the transition arrays which result from these two excitation processes

4.5.a) $2p^6 3p \longrightarrow 2p^5 3s3p$ transitions.

A listing of the optical spectra observed in this experiment are presented in tables 4 8 and 4 9, together with the results of a multiconfiguration calculation of all the energy levels of the $2p^5 3s3p$ configuration For this calculation the following procedure was used Six configurations were included in the calculation, these were; $2p^5 3s3p$, $2p^5 3s4p$, $2p^5 3s3d$, $2p^5 3p4d$, $2p^5 3p4s$ and $2p^5 3d4p$ We followed the same procedure as has been outlined in section 4 4 but the MCDF-Extended Average Level (EAL) option was favored over the MCDF-Average Level (AL) option Because of the small number of configurations used as input it was possible to calculate all levels with J=1/2, 3/2 and 5/2 together with the

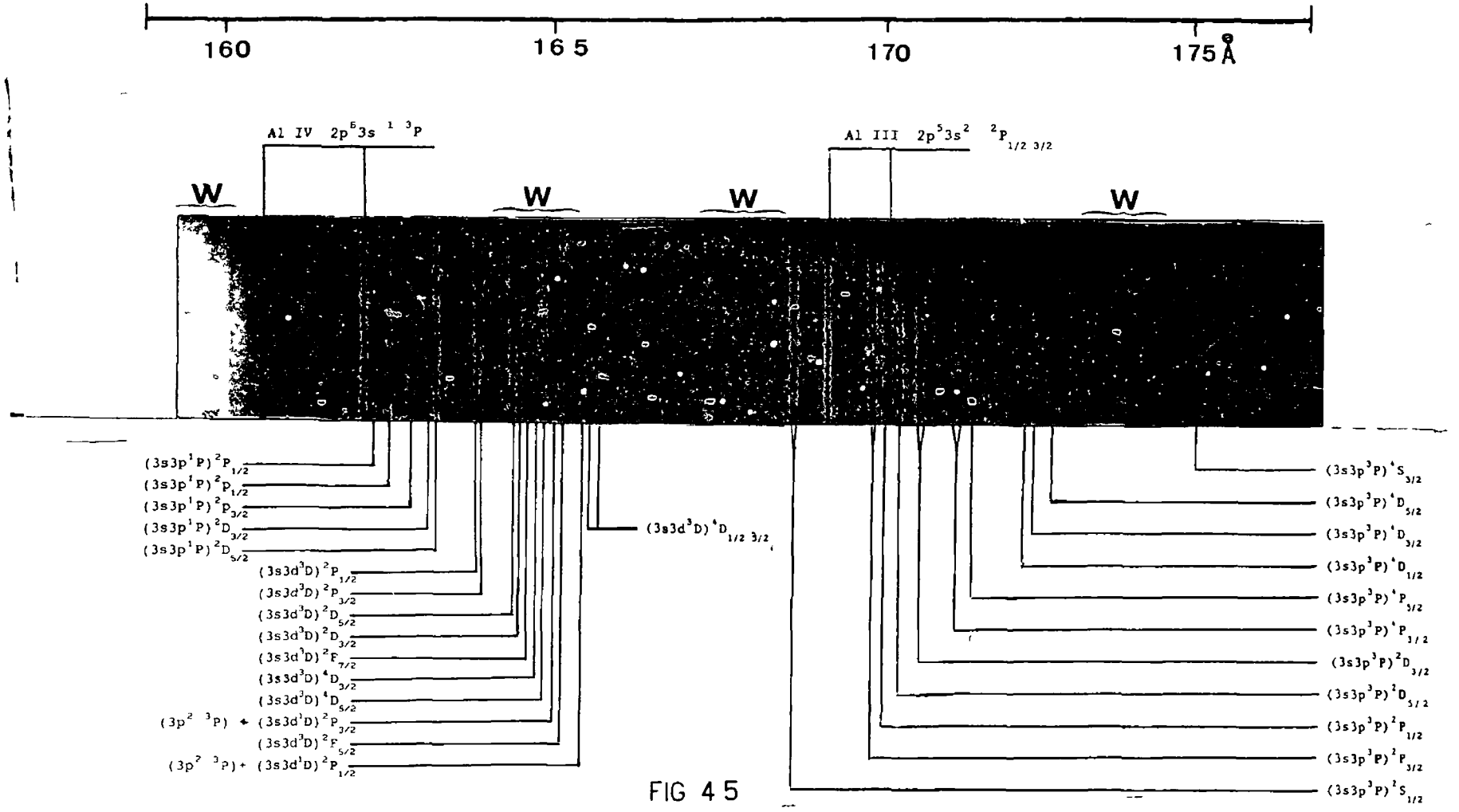

FIG 45

The absorption spectrum of an aluminium laser produced plasma in the 160-175Å region, most of the structure in this wavelength range arises from excited state transitions in the Al^{2+} ion (See text)

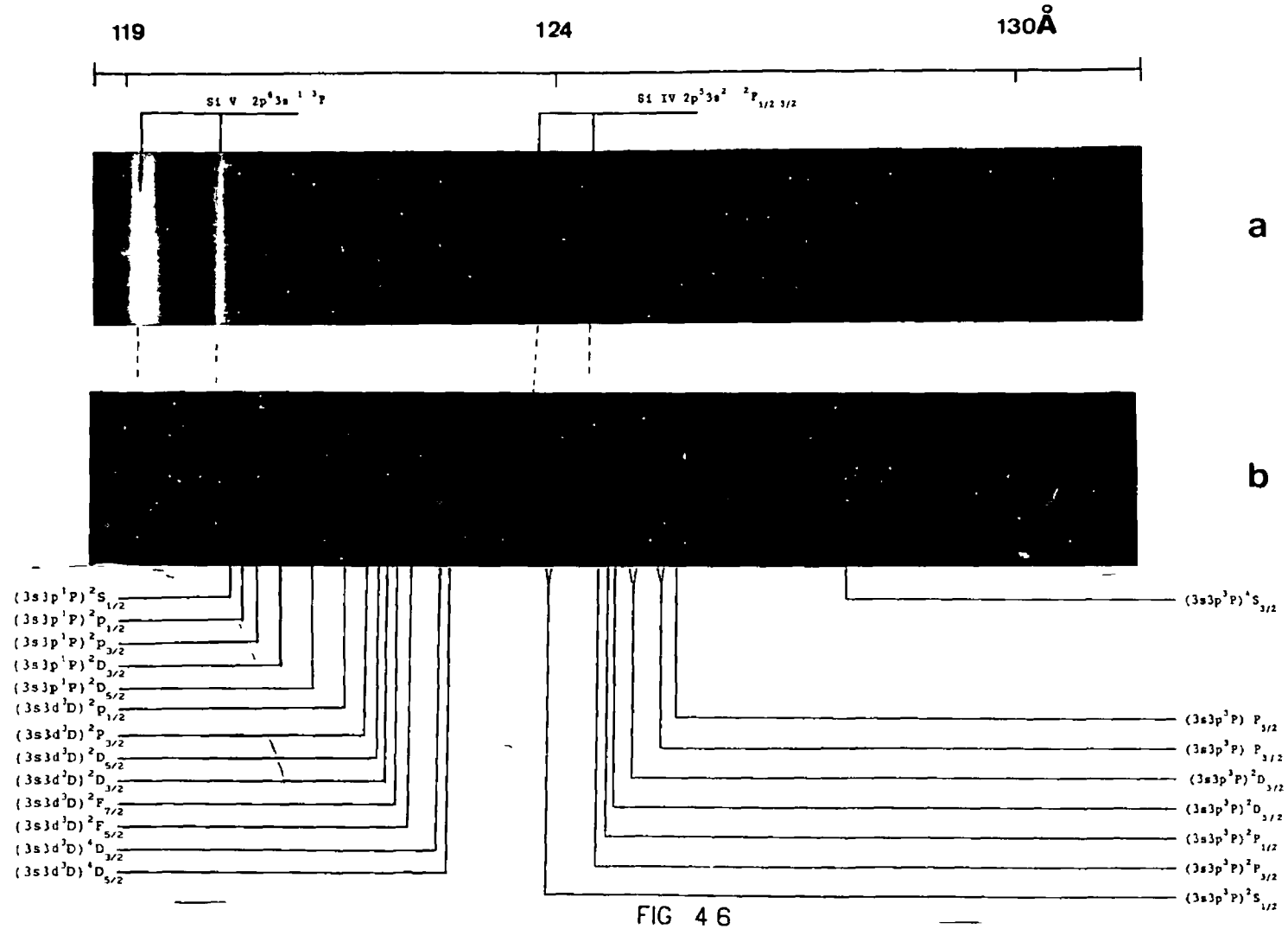

FIG 46

Emission and absorption spectra of silicon laser produced plasmas in the 119-130Å region, most of the observed structure can be assigned to the Si^{3+} ion (See text)

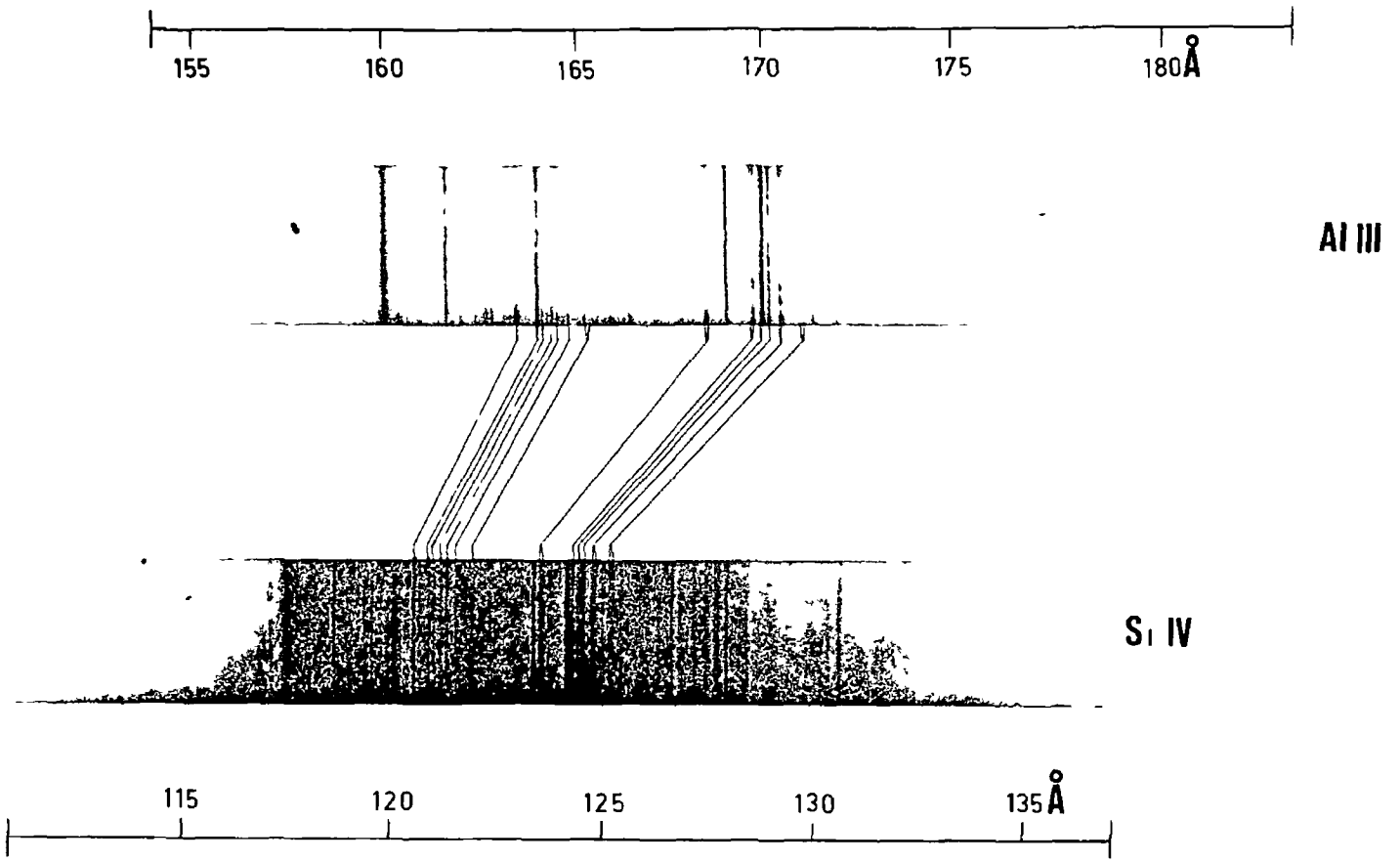

FIG 4 7
Photoabsorption spectra of an aluminium laser plasma in the range 160-175Å and of a silicon laser plasma in the range 119-130A Both spectra were obtained using a tungsten laser plasma as the continuum source Identical features in each of the spectra are connected by solid lines

inclusion of both lower levels in the case of the $2p^5 3p\ ^2P$ and $2p^6 3d\ ^2D$ terms. The wave functions obtained in the above manner were used to generate oscillator strengths (gf values) for all the transitions. The calculated gf values were plotted against wavelength for both the $2p^5 3s3p$ and $2p^5 3s3d$ configurations. We then plotted the estimated intensities of each of the known aluminium and silicon lines observed against wavelength. This series of plots is shown in Fig.(4.8) and as can be seen in both cases there are similarities between the calculated and experimental stick diagrams. This was of help in confirming the fact that the observed spectra were indeed due to excitations from the $2p^6 3p$ and $2p^6 3d$ levels.

In table 4.8 and 4.9 are also listed the Penning ionisation discharge emission data of Finkenthal et al (1988) which in general show good agreement with the present photoabsorption data for Al III. However a closer examination of the table calls for a few comments. As is obvious from Fig.(4.6) and Fig.(4.7) the spin forbidden transitions to quartet terms ^4S and ^4D are very faint for most of the levels in both spectra as should be expected in a photoabsorption experiment; this is in contrast with the emission work of Finkenthal et al where the radiative transitions from quartet terms are dominant as these are less likely to autoionize than doublet terms. In the case of Al III we tentatively assign the weak line measured at 174.88Å to the $^4S_{3/2}$ level, however the disagreement with Finkenthal et al amounts to 0.14Å in this case. A problem also exists with the assignment of this transition in Si IV. We have measured a line at 128.05Å in agreement with the calculated position, however it is much stronger than expected on the basis of our Al III observation and our calculated gf value. Therefore this assignment must still be considered tentative. The Al III lines measured at 172.60Å, 172.45Å and 172.32Å are also observed with very weak intensities; however due to the wavelength agreement with Finkenthal et al, we follow the assignments given therein and hence label the features $^4D_{5/2}$ and $^4D_{3/2}$. Unlike the Penning discharge emission work however, we do

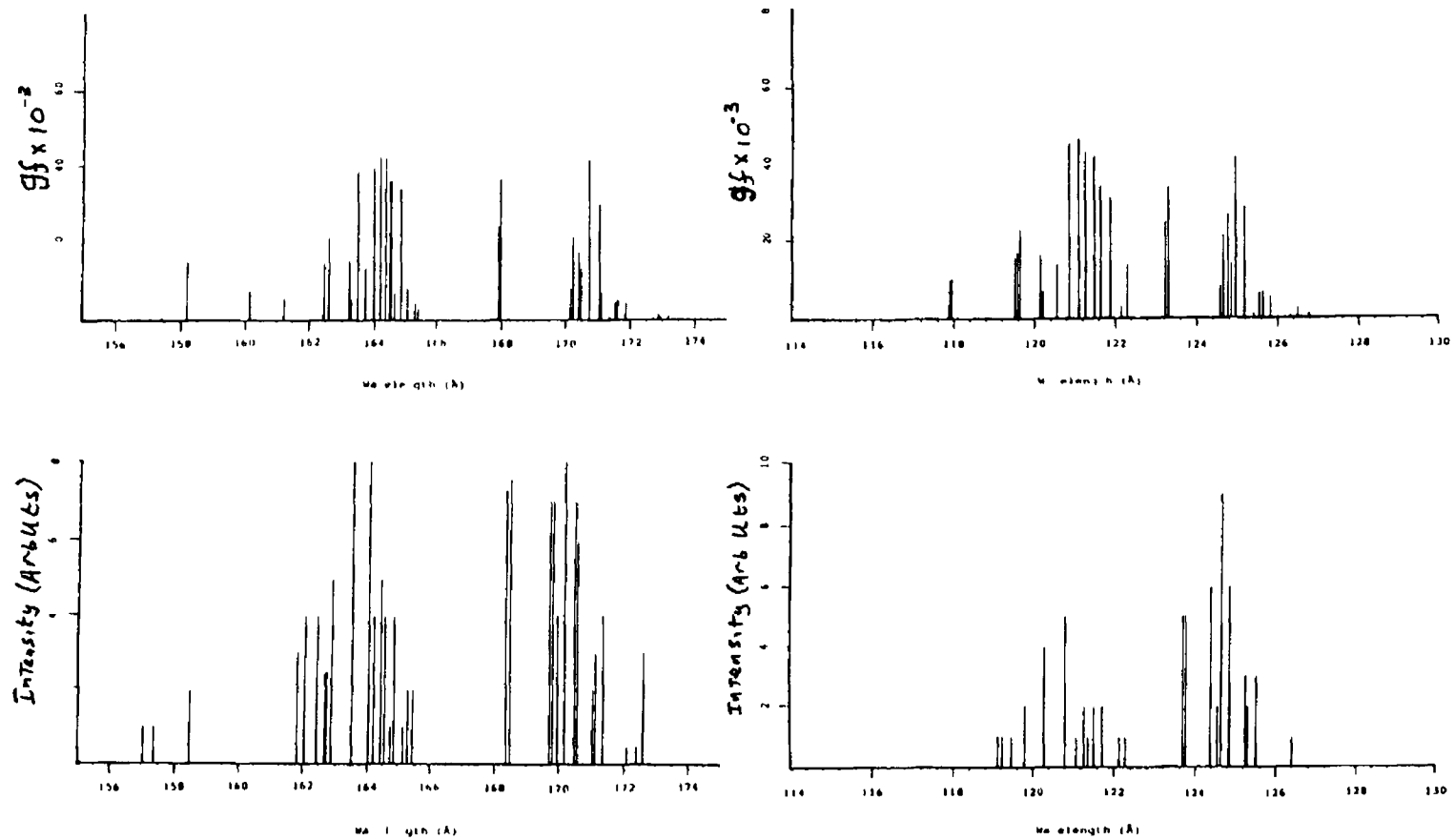

FIG 4 8

Calculated gf values plotted against wavelength for both the $2p^5 3s3p$ and $2p^5 3s3d$ configurations Also plotted against wavelength are the experimentally estimated intensities of each of all known aluminium and silicon lines observed in the respective wavelength regions The series of plots shows clearly the similarities between the calculated and experimental spectra

Table 4.8 *Measured wavelengths, calculated wavelengths, intensities and calculated oscillator strengths for the $2p^6 3p$–$2p^5(3s3p^3P)$ transitions in the Al^{2+} and Si^{3+} ions*

	Al III					Si IV			
$2p^6 3p \rightarrow 2p^5(3s3p^1P)$	λ_{Exp}	$\lambda_{Fink.}$	$\lambda_{Calc.}$	I	$gf \times 10^{-3}$	λ_{Exp}	λ_{Calc}	I	$gf \times 10^{-3}$
$^2P_{3/2} \rightarrow {}^4S_{3/2}$	–	175.02	175.52	–	0.10	128.05	128.36	8.0	0.12
$^2P_{1/2} \rightarrow {}^4S_{3/2}$	174.88 (P)		175.45	2.0	0.02		128.29		0.03
$^2P_{3/2} \rightarrow {}^4D_{5/2}$	172.60	172.62	173.23	3.0	1.47	126.47	126.79	1.0	1.79
$^2P_{3/2} \rightarrow {}^4D_{3/2}$	172.45*	172.31	172.99	1.0	1.00		126.60		1.00
$^2P_{1/2} \rightarrow {}^4D_{3/2}$	172.32*		172.92	1.0	2.14	–	126.52	–	2.80
$^2P_{3/2} \rightarrow {}^4D_{1/2}$	172.13*	172.1	172.76	1.0	0.71	–	126.41	–	0.35
$^2P_{1/2} \rightarrow {}^4D_{1/2}$			172.69		0.27	–	126.34	–	0.96
$^2P_{3/2} \rightarrow {}^4P_{5/2}$	171.36	171.37	171.89	4.0	4.93	125.58	125.84	3.0	5.90
$^2P_{3/2} \rightarrow {}^4P_{3/2}$	171.12	171.09	171.63	3.0	5.69	125.37	125.65	2.0	7.48
$^2P_{1/2} \rightarrow {}^4P_{3/2}$	171.04		171.56	2.0	4.99	125.32	125.58	3.0	7.07
$^2P_{3/2} \rightarrow {}^4P_{1/2}$	–	170.80	171.46	–	0.14	–	125.50	–	0.24
$^2P_{1/2} \rightarrow {}^4P_{1/2}$	–		171.39	–	1.16	–	125.43	–	1.54
$^2P_{3/2} \rightarrow {}^2D_{3/2}$	170.57	170.52	171.12	6.0	7.35	124.94	125.27	3.0	6.19
$^2P_{1/2} \rightarrow {}^2D_{3/2}$	170.49		171.06	7.0	30.50	124.92	125.20	6.0	28.90
$^2P_{3/2} \rightarrow {}^2D_{5/2}$	170.19	170.26	170.75	8.0	41.90	124.71	124.98	9.0	41.70
$^2P_{3/2} \rightarrow {}^2P_{1/2}$	–	170.11	170.49	–	13.76	–	124.87	–	14.18
$^2P_{1/2} \rightarrow {}^2P_{1/2}$	169.97		170.43	4.0	17.92	124.63	124.79	2.0	26.80
$^2P_{3/2} \rightarrow {}^2P_{3/2}$	169.82	169.81	170.26	7.0	21.98	124.45	124.67	6.0	21.10
$^2P_{1/2} \rightarrow {}^2P_{3/2}$	169.73		170.19	7.0	8.60	–	124.60	–	8.54
$^2P_{3/2} \rightarrow {}^2S_{1/2}$	168.57	168.7	168.05	7.0	36.90	123.83	123.32	5.0	33.90
$^2P_{1/2} \rightarrow {}^2S_{1/2}$	168.49		167.99	7.0	24.85	123.76	123.25	5.0	24.90

* Lines where $\Delta\lambda$ may be taken to be ± 0.05 Å.
(P) Lines proposed as tentative assignments only.
The wavelength accuracy may be quoted as ± 0.02 Å (see text).

$\lambda_{Fink.}$ Are the results of Finkenthal et al (1988).

Table 4 9 *Measured wavelengths, calculated wavelengths, intensities and calculated oscillator strengths for the* $2p^6 3p - 2p^5(3s3p^1P)$ *transitions in the* Al^{2+} *and* Si^{3+} *ions*

	Al III					Si IV			
$2p^6 3p \rightarrow 2p^5(3s3p^1P)$	λ_{Exp}	λFink	λ_{Calc}	I	$gf \times 10^{-3}$	λ_{Exp}	λ_{Calc}	I	$gf \times 10^{-3}$
$^2P_{3/2} \rightarrow {}^2D_{5/2}$	162 89	163 0	163 77	5 0	14 07	120 33	120 57 W	4 0	14 28
$^2P_{3/2} \rightarrow {}^2D_{3/2}$	162 75	162 47	163 33	2 5	6 00	119 85	120 22	2 0	7 33
$^2P_{1/2} \rightarrow {}^2D_{3/2}$	162 69		163 26	2 5	15 90		120 16		16 32
$^2P_{3/2} \rightarrow {}^2P_{3/2}$	162 45 (P)	162 2	162 62	4 0	21 78	119 53 (P)	119 66	1 0	22 74
$^2P_{1/2} \rightarrow {}^2P_{3/2}$	162 08		162 56	4 0	0 44	119 31 (P)	119 60	1 0	0 07
$^2P_{3/2} \rightarrow {}^2P_{1/2}$			162 55		14 95		119 60		17 04
$^2P_{1/2} \rightarrow {}^2P_{1/2}$	161 85 (P)	162 0	162 48	3 0	15 10	119 20 (P)	119 54	1 0	15 76
$^2P_{3/2} \rightarrow {}^2S_{1/2}$	–	–	161 23		5 96	–	117 95	–	10 50
$^2P_{1/2} \rightarrow {}^2S_{1/2}$	–		160 17		7 97	–	117 90	–	10 00

W Features which coincide with a background feature
(P) Lines proposed as tentative assignments only

λFink. Are the results of Finkenthal et al (1988).

not observe any possible candidate line for the $^4P_{1/2}$ level in either spectrum.

One of the features of the present work is that we have been able to clearly resolve the fine structure of the $2p^6 3p\ ^2P_{1/2,3/2}$ levels when these are connected to the same $(3s3p\ ^{3,1}P)^{4,2}L_{3/2}$ upper levels in both Al III and Si IV spectra. To illustrate this consider the intense emission measured at 171 09Å by Finkenthal et al and assigned to $(3s3p\ ^3P)^4P_{3/2}$. In the present work we instead observe two strong absorption features at 171 12A and 171.04Å which clearly correspond to the $2p^6 3p\ ^2P_{3/2} \rightarrow {}^4P_{3/2}$ and $2p^6 3p\ ^2P_{1/2} \rightarrow\ ^4P_{3/2}$ transitions respectively The fine structure splitting of the lower term is 234cm^{-1} in Al^{2+} and 461cm^{-1} in Si^{3+}.

The line measured at 162.89Å in the Al III spectrum is definitely assigned to $(3s3p\ ^1P)^2D_{5/2}$ which confirms the previous tentative assignment given by Finkenthal et al For the other levels having $(3s3p\ ^1P)$ parent term our work does differ in some respects from that work The $(^1P)^2D_{3/2}$ level in particular has been attributed to the lines observed at 162.75Å and 162 69Å and we also propose that the $(^1P)^2P_{1/2,3/2}$ levels give rise to the lines measured at 162 08Å and 161 85Å. The classification of the same levels in Si^{3+} is also tentatively proposed and in this case the corresponding lines are weak (see Fig 4 6)

The work described here allows us to present isoelectronic plots of the levels of the $2p^5 3s3p$ configuration from Na I (Sugar et al 1979) through Si IV The data for Mg II are taken from Finkenthal et al and Pedrotti et al Such plots provide valuable information for extrapolation purposes, also, it is well known that if series perturbation is present, this will most likely occur at the beginning of the series. This situation is well exemplified in Fig.(4.9) in the case of the levels with ^1P parent term, where several level crossing effects are observed. Although there remain uncertainties for

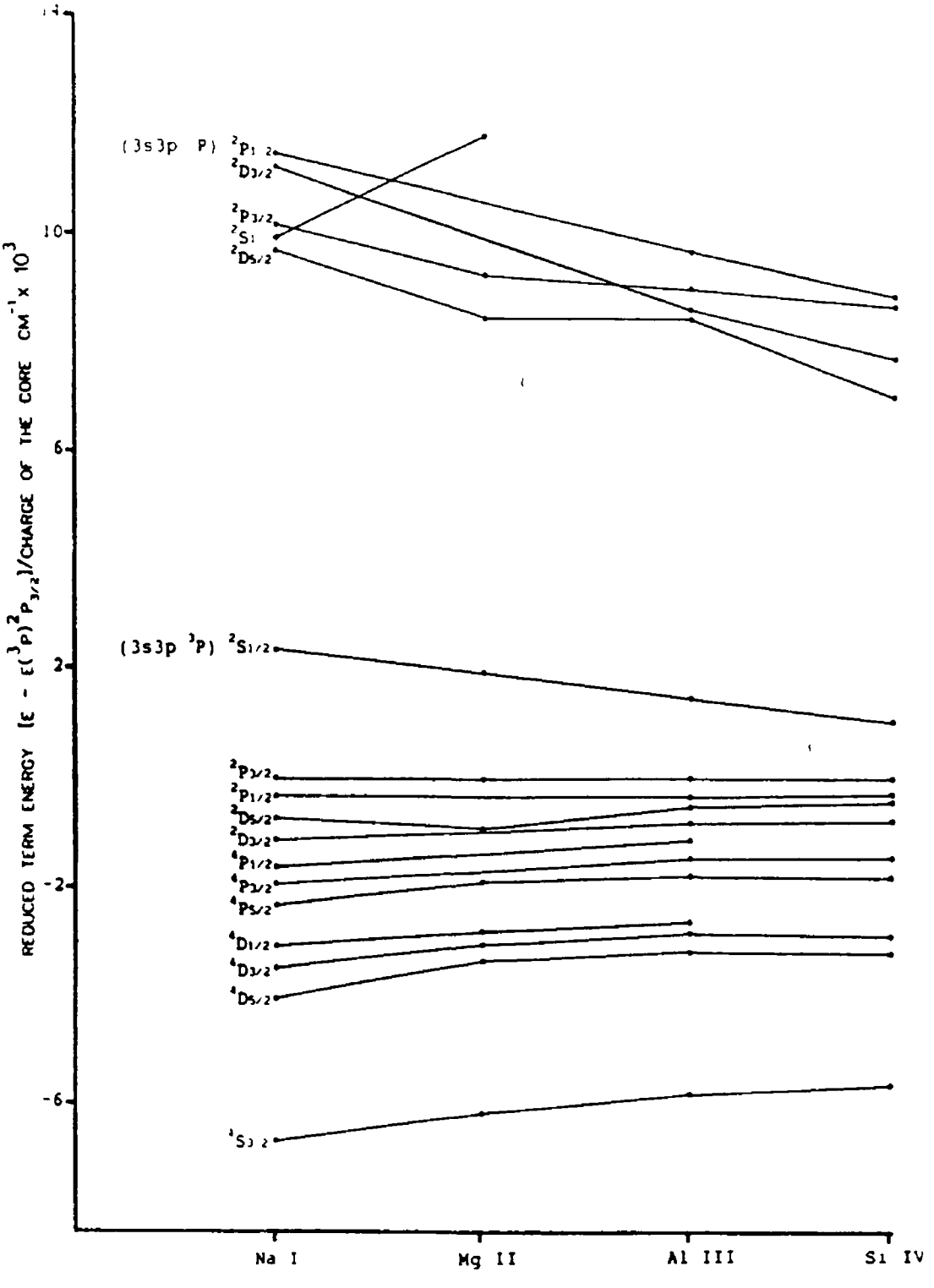

FIG 4 9

Isoelectronic plot of the levels of the $2p^5 3s3p$ configuration from Na I through Si IV.

some of the levels (see above) and the corresponding data in Mg II is rather scarce, it is nevertheless possible to make some qualitative remarks as the observed pattern of behavior is mimicked by calculations (tables 4 8 and 4 9).

The apparent anomalous behavior of the $^2P_{3/2}$ and $^2D_{3/2}$ levels observed when progressing along the sequence is due to relativistic interactions which strongly mix them. The interaction is indeed so strong in Al III and Si IV that the labelling becomes rather arbitrary The corresponding LSJ wave function composition as obtained in our calculations is given in table 4 10 for the doublet structures in Al III and Si IV The leading percentage composition for all of the terms of the $2p^5 3s3p$ are listed in table 4.11.a and b for Al III and Si IV respectively For the $^2P_{1/2}$ level, the main interaction is correlation mixing with (3p3d ^1P) $^2P_{1/2}$ the contribution of which for both Al III and Si IV amounts to about 7%. The (^1P) $^2S_{1/2}$ level is predicted to lie above (^1P) $^2P_{1/2}$ in Al III and Si IV and although it is not reported in the present work, this result is supported by the experimental observation in Mg II (see Fig.4 9). The repulsive behavior of the two ^2S terms is due to the effects of parental mixing Indeed a gradual breakdown of parentage assignments for these levels is observed in table 4.10 which can be readily understood in terms of increased core penetration by the running electron. This view is supported by calculations of the Hartree-Fock mean radius of the 3s and 3p electrons in the $2p^5 3s3p$ configuration of neutral sodium by Froese fisher (1986).

TABLE 4 10

LSJ composition of the $(^1P)^2D_{3/2}$, $(^1P)^2P_{3/2}$, $(^1P)^2S_{1/2}$ and $(^3P)^2S_{1/2}$ levels in Al^{2+} and Si^{3+}

	Al^{2+}
$^2D_{3/2}$	$0.70(^1P)^2D + 0.65(^1P)^2P + 0.18(3p3d^1P)^2D + 0.18(3p3d^1P)^2P$
$^2P_{3/2}$	$-0.69(^1P)^2P + 0.66(^1D)^2D - 0.19(3p3d^1P)^2P + 0.17(3p3d^1P)^2D$
$^2S_{1/2}$	$0.80(^3P)^2S + 0.55(^1P)^2S + 0.12(^3P)^4P + 0.12(3p3d^1P)^2S$
$^2S_{1/2}$	$0.77(^1P)^2S - 0.52(^3P)^2S + 0.20(3p3d^1P)^2S - 0.18(3s4p^3P)^2S$
	Si^{3+}
$^2D_{3/2}$	$0.69(^1P)^2D + 0.67(^1P)^2P + 0.18(3p3d^1P)^2D + 0.17(3p3d^1P)^2P$
$^2P_{3/2}$	$0.69(^1P)^2P - 0.67(^1P)^2D + 0.17(3p3d^1P)^2D - 0.18(3p3d^1P)^2P$
$^2S_{1/2}$	$-0.77(^3P)^2S - 0.57(^1P)^2S - 0.14(^3P)^4P - 0.12(3p3d^1P)^2S$
$^2S_{1/2}$	$-0.75(^1P)^2S + 0.58(^3P)^2S - 0.19(3p3d^1P)^2S - 0.16(3s4p^3P)^2S$

4.5.b) $2p^63d \rightarrow 2p^53s3d$ transitions.

Many of the remaining lines in the spectra of Fig (4.5) and Fig.(4.6) can be interpreted according to the $2p^63d \rightarrow 2p^53s3d$ excitation scheme. The bulk of the corresponding lines are found in the range 163-166A in Al III and 120-123Å in Si IV

The levels with J=1/2 or 3/2 built on the $2p^53s3d$ configuration are readily accessible from the ground state via dipole radiation as has been discussed for both Al III and Si IV in the previous section Table 4 12 lists the measured positions of the $2p^63d \rightarrow 2p^53s3d$ lines observed in this experiment for Al^{2+} and Si^{3+}. For levels with J=1/2 and 3/2 the position of these lines can be predicted from our previous measurements and there is good agreement between both sets of data Energies of the levels of the $2p^53s3d$ configuration in Al III relative to the ground state were calculated and have been presented

TABLE 4 11 A B

L:S Composition and leading percentages for the $2p^5 3s3p$ configuration in Al^{2+} and Si^{3+}

L S Composition of the $2p^5 3s3p$ configuration in Al^{2+}

Term	L S Composition (leading percentages)
$^4S_{3/2}$	97% $(3s3p^3P)^4S$
$^4D_{5/2}$	93% $(3s3p^3P)^4D$
$^4D_{3/2}$	-91% $(3s3p^3P)^4D$
$^4D_{1/2}$	-95% $(3s3p^3P)^4D$
$^4P_{5/2}$	88% $(3s3p^3P)^4P$ +10% $(3s3p^3P)^2D$
$^4P_{3/2}$	74% $(3s3p^3P)^4P$ +18% $(3s3p^3P)^2D$ -5% $(3s3p^3P)^2P$
$^4P_{1/2}$	94% $(3s3p^3P)^4P$
$^2D_{3/2}$	-76% $(3s3p^3P)^2D$ +17% $(3s3p^3P)^4P$ -6% $(3s3p^3P)^4D$
^2D	86% $(3s3p^3P)^2D$ -8% $(3s3p^3P)^4P$ +5% $(3s3p^3P)^4D$
$^2P_{1/2}$	-94% $(3s3p^3P)^2P$
$^2P_{3/2}$	92% $(3s3p^3P)^2P$
$^2S_{1/2}$	64% $(3s3p^3P)^2S$ +31% $(3s3p^1P)^2S$
^2D	92% $(3s3p^1P)^2D$ +6% $(3p3d^1P)^2D$
$^2D_{3/2}$	48% $(3s3p^1P)^2D$ +43% $(3s3p^1P)^2P$
$^2P_{3/2}$	-47% $(3s3p^1P)^2P$ +44% $(3s3p^1P)^2D$
$^2P_{1/2}$	88% $(3s3p^1P)^2P$ +7% $(3p3d^1P)^2P$
$^2S_{1/2}$	59% $(3s3p^1P)^2S$ -27% $(3s3p^3P)^2S$ +4% $(3p3d^1P)^2S$

L S Composition of the $2p^5 3s3p$ configuration in Si^{3+}

Term	L S Composition (leading percentages)
$^4S_{3/2}$	97% $(3s3p^3P)^4S$
$^4D_{5/2}$	92% $(3s3p^3P)^4D$
$^4D_{3/2}$	-89% $(3s3p^3P)^4D$
$^4D_{1/2}$	-93% $(3s3p^3P)^4D$
$^4P_{5/2}$	86% $(3s3p^3P)^4P$ +12% $(3s3p^3P)^2D$
$^4P_{3/2}$	67% $(3s3p^3P)^4P$ +25% $(3s3p^3P)^2D$ -6% $(3s3p^3P)^2P$
$^4P_{1/2}$	93% $(3s3p^3P)^4P$
$^2D_{3/2}$	-68% $(3s3p^3P)^2D$ +22% $(3s3p^3P)^4P$ -8% $(3s3p^3P)^4D$
$^2D_{5/2}$	84% $(3s3p^3P)^2D$ -9% $(3s3p^3P)^4P$
$^2P_{1/2}$	-93% $(3s3p^3P)^2P$
$^2P_{3/2}$	90% $(3s3p^3P)^2P$
$^2S_{1/2}$	58% $(3s3p^3P)^2S$ +36% $(3s3p^1P)^2S$
$^2D_{5/2}$	93% $(3s3p^1P)^2D$
$^2D_{3/2}$	47% $(3s3p^1P)^2D$ +46% $(3s3p^1P)^2P$
$^2P_{3/2}$	47% $(3s3p^1P)^2D$ -46% $(3s3p^1P)^2P$
$^2P_{1/2}$	90% $(3s3p^1P)^2P$ +6% $(3p3d^1P)^2P$
$^2S_{1/2}$	59% $(3s3p^1P)^2S$ -34% $(3s3p^3P)^2S$ +3% $(3p3d^1P)^2S$

Table 4 12 *Measured wavelengths, calculated wavelengths, intensities and oscillator strengths for the* $2p^6 3d$–$2p^6 3s3d$ *transitions in* Al^{2+} *and* Si^{3+}

		Al III					Si IV				
		λ_{Pred}	λ_{Exp}	I	$gf(5/2)$	$gf(3/2)$	λ_{Pred}	λ_{Exp}	I	$gf(5/2)$	$gf(3/2)$
$(3s3d^3D)$	$^4D_{7/2}$	165 79*	–	–	5 62	–	–	–	–	–	–
	$^4D_{5/2}$	165 56*	–	–	3 11	5 90	122 31	122 36	1 0	4 78	9 35
	$^4D_{3/2}$	165 47	165 47	2 0	3 51	0 12	122 17	122 21	1 0	1 55	1 79
	$^4D_{1/2}$	165 38	165 32	2 0	–	4 61	–	–	–	–	–
$(3p^2\ ^3P)$ + $(3s3d^1D)$	$^2P_{1/2}$	165 14	165 17	1 0	–	8 65	–	–	–	–	–
	$^2P_{3/2}$	164 72	164 76	1 0	7 48	0 55	–	–	–	–	–
$(3s3d^3D)$	$^2D_{3/2}$	164 43	164 44	5 0	19 00	23 60	121 50	121 43	1 0	29 22	15 00
	$^2D_{5/2}$	164 24*	164 20	4 0	34 67	8 22	121 28	121 33	2 0	35 31	8 09
	$^2P_{3/2}$	164 04	164 05 W	8 0	20 80	19 23	121 12	121 14	1 0	13 43	33 54
	$^2P_{1/2}$	163 52	163 52	8 0	–	38 98	120 88	120 85	5 0	–	45 33
	$^2F_{7/2}$	164 62*	164 57	4 0	36 27	–	121 65	121 57	2 0	34 56	–
	$^2F_{5/2}$	164 93*	164 87	4 0	6 93	27 41	121 89	121 78	2 0	7 53	23 86
$(3s3d^1D)$	$^2D_{3/2}$	158 19	158 46	2 0	0 58	15 31	–	–	–	–	–
	$^2P_{1/2}$	157 43	157 36#	1 0	–	1 12	–	–	–	–	–
	$^2P_{3/2}$	157 10	157 04#	1 0	0 25	0 32	–	–	–	–	–

* Calculated levels (see text)

\# An accuracy of ± 0 05 Å

gf values × 10^{-3}

W Features which coincide with a background feature

in table 4.5. If we subtract from the experimental level energies the value of the the $2p^6 3d$ state above the ground state we arrive at the values listed in the λ_{pred} column of table 4.12 for those levels with J=1/2 or 3/2 In the case of upper levels with J=5/2,7/2 this procedure is obviously not applicable and the classification is based on the following semi-empirical approach (levels marked as * in table 4 12). Where levels with J = 1/2, and 3/2 of a multiplet were previously measured e.g., the $(3s3d^3D)^4D_{1/2,3/2}$ levels, the corresponding calculated MCDF values were shifted so as to be brought into agreement with these measured values The calculated fine structure splitting of the rest of the multiplet i.e $^4D_{5/2,7/2}$ was then simply added in order to predict their positions. In the case of the $^2F_{5/2,7/2}$ levels we assumed that their calculated energies had to be shifted by the same quantity as in the previous case and hence obtained predicted positions for the $2p^6 3d \rightarrow 2p^5 3s3d\ ^2F$ lines. The good agreement observed between measured and predicted positions justifies the method used to obtain the latter

The ground state transition in Si IV to $(^3D)\ ^2P_{1/2,3/2}$ reported as very broad in the previous section has since been partially resolved into its two fine structure overlapping components By estimating the fine structure splitting from the observed line profile, the positions of the $2p^6 3d\ ^2D \rightarrow (^3D)\ ^2P_{1/2,3/2}$ lines were predicted The line at 120 95Å remains unclassified, although our calculations suggest that it could be due to perturbation by $(3p^2\ ^1S)^2P$ and could therefore also contribute to the very broad resonance observed in ground state absorption Calculated gf values have also been obtained for these transitions and are reported in table 4.12

As can be noticed from the spectra presented in Fig (4 5) and Fig.(4.6) all the prominent features observed in this experiment have been assigned, however there remain a number of weak lines in each spectrum that do not appear to be continuum background source features and hence are considered Al or Si lines. These are listed in table

4 13. We have not been able to assign these weak features which may be due to transitions from other excited states in Al III and Si IV or absorption in other ionisation stages

TABLE 4 13

Unidentified absorption lines in spectra of aluminium and silicon laser produced plasmas obtained with a Tungsten laser produced plasma.

Al III		Si IV.	
λ(Å)	I	λ(Å)	I
174.62	1.0	127.88	3.0
174.25	1.0	127.54	4 0
173.95	1 0	127.34	4 0
173.25	1.0	126.71	1.0
171.92	1.0	125.40	2.0
171.57	1.0	119 75	1 0
166.04	1 0	119.65	1.0
165.66	2.0	...	
161.46	1.0	.....	
161.16	1 0	.. ...	
160.99	1.0	.....	
159.55	2 0	.....	
159 32	1.0	.. ..	
159.08	3.0	....	

4 6 XUV LASER CONSIDERATIONS

This section examines the research carried out recently by a number of groups relating to proposed XUV laser schemes based on core excited autoionizing levels in neutral sodium and sodium like ions The XUV laser aspects of this research are related to the observation made by Harris (1980) concerning the possible use of metastable levels of alkali-like atoms and ions as storage levels for store and transfer laser schemes As was noted by McGuire (1976), see also McGuire and Duguay (1977), a few of the energy levels of neutral sodium and sodium like Mg^{+} which lie above the lower continuum and also possess reasonably large radiative yields are potentially of interest in the construction of XUV lasers. Depending on the rate of excitation relative to

the Auger transition rate of the level, these levels may be excited either directly (see McGuire and Duguay 1977), or by store and transfer from some metastable level, Harris (1980).

Because of their metastability against autoionization, the core-excited quartet levels of alkali-metal ions and alkali-like metal-ions are of interest for the construction of XUV Lasers. Recently Holmgren et al (1985) established 15 quartet levels in the $2p^5 3s3p$, 3s3d and 3s4s configurations of the sodium atom from some 28 newly identified transitions. The spectra were recorded using a pulsed hollow-cathode discharge; metastable atoms were produced in the $(2p^5 3s3p)\,^4D_{1/2}$ and $(2p^5 3s3p)\,^4S_{3/2}$ levels of neutral sodium A tunable laser was then used to excite these atoms to levels in the $2p^5 3s3d$ and $2p^5 3s4s$ configurations, as described in section 4 2 of this chapter.

Because of the various effects which contribute to the complexity of the sodium like spectra, the observed levels are not pure quartet states. Because of the spin-orbit interaction significant mixing between quartet and doublet levels would be expected. This opens up two additional decay channels besides radiative transitions within the quartet manifold The first of these channels is autoionization, the second being extreme ultraviolet (XUV) transitions to some of the lower doublet levels in the normal $2p^6 nl$ term system of neutral sodium or the sodium like ion Only the quartet levels of highest L and within a given configuration cannot mix with doublet levels (since there would be no similar J level) For example the single transition $3p\,^4D_{11/2}$ - $3d\,^4F_{9/2}$ at 3882Å was observed and its lifetime measured using the beam-foil technique (Berry et al 1984) Harris et al (1984) has shown that for certain of the mixed quartets autoionization rates could be expected to be low This would be the case for those quartet levels which primarily mix with doublet levels which are forbidden to

autoionize because of selection rules for L and parity, the requirement being that both L and parity be both odd or both even and that J-L=1/2, for example the odd-parity $2p^5 3s3d\ ^2D$ states It is this particular mixing which also opens the above mentioned XUV decay branch for example $2p^6 3d\ ^2D \rightarrow 2p^5 3s3d\ ^4D$ Because of these decay characteristics, several schemes involving the quartet levels of neutral sodium have been proposed for the construction of an XUV laser operating at around 370Å (see Rothenberg and Harris 1981 Falcone et al 1982, Falcone and Pedrotti 1982 and Pedrotti et al 1985) The various schemes depend on the transition probabilities for the various decay channels which, in turn, depend critically on the detailed composition of the quartet levels. Holmgren et al (1986) give theoretical transition probabilities for both radiative and autoionizing decay modes. These were calculated in a superposition of configurations Hartree-Fock approximation with empirically adjusted Slater parameters using the RCN/RCG computer program of Cowan (1981).

Engstrom et al (1985) have reported experimental work using the beam foil technique and have measured the mean lifetimes of all eight identified quartet levels in the $2p^5 3s3d$ and $2p^5 3s4s$ configurations of Na I. They then used experimental lifetimes to test the theoretical predictions of Holmgren et al (1986). The authors found agreement between theory and experiment to within a factor of 2

Based upon the early photoabsorption measurements of Sugar et al (1979) and their own work Holmgren et al (1985) define several XUV lasers of the store-transfer type proposed by Harris (1980). One example is a 379Å laser in which the population stored in the quasi-metastable level $(2p^5 3s3p)\ ^4S_{3/2}$ is transferred to the upper laser level $(2p^5 3s3d)\ ^4D_{3/2}$ Other possible XUV lasers in neutral sodium and singly ionized magnesium have been similarly described. These are also based on population storage in the level $(2p^5 3s3p)\ ^4S_{3/2}$ and make

use of levels in the $2p^5 3s3d$ configuration The lower level for the XUV transition in all cases is the $(2p^6 3d)^2D$ level

Fig.(4.10) shows the same set of levels for a similar lasing system scaled isoelectronically to the Al^{2+} and Si^{3+} ions. The new data for the core excited autoionizing levels in both Al^{2+} and Si^{3+} presented here will permit the scaling of the suggested scheme to shorter wavelengths, although a great deal of further investigation is still required for both the $2p^5 3s3p$ and $2p^5 3s3d$ configurations in sodium like ions, for example the autoionizing rates for the levels in both configurations as well as the life times. Fig.(4 10) shows only the possibility of isoelectronic scaling of the neutral sodium scheme at 379Å, assuming isoelectronic scaling of other parameters Fig (4.10) shows that with successful isoelectronic scaling of the 379Å laser scheme further along the sequence to Al^{2+} and Si^{3+} laser transitions at 165.47 and 122.21Å are potentially achievable. The fact that we have observed transitions between the $2p^6 3d$ level and the upper $2p^5 3s3d$ levels in emission (Fig.4.6.b) in Si^{3+} may also be significant in this regard and shows that for many of these levels in Si^{3+} the XUV decay channel is open.

One other aspect of the XUV laser research on these levels has been the use of laser produced plasmas as sources of VUV radiation to pump short wavelength lasers The suggestion was first proposed by Duguay (1975) and was taken further by Caro et al (1984) and more recently by Young et al (1987)

Clearly the construction of such lasers using aluminium or silicon laser produced plasmas requires further work. However, the work presented here has shown for the first time that for both of the sodium like ions Al^{2+} and Si^{3+} the $2p^5 3s3p$ and $2p^5 3s3d$ configurations are accessible by collisional excitation and photoabsorption which opens up the possibility of a more detailed study of these levels

and in particular, the XUV laser implications of this research

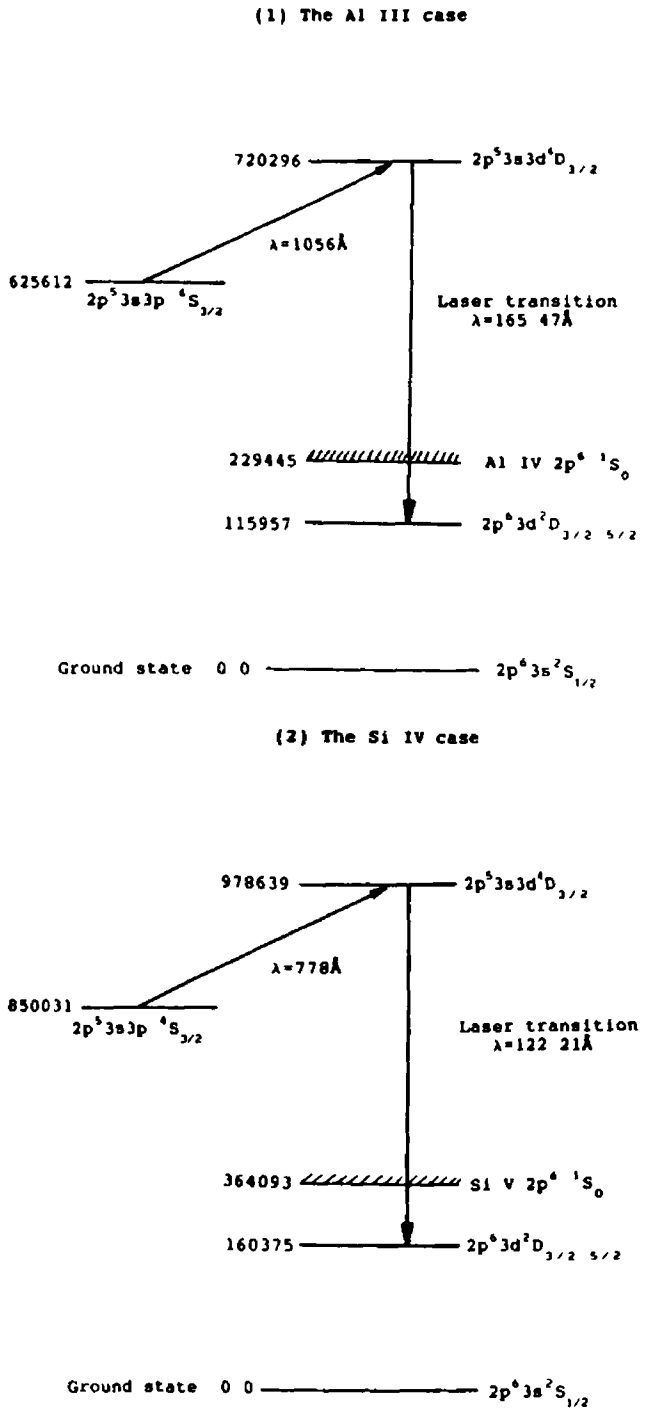

FIG 4 10

Proposed XUV laser schemes for neutral sodium scaled isoelectronically to the Al III and Si IV ions.

4 7 REFERENCES

Berry, H G Desesquelles, J Cheng, K T and Schectman, R.M. Phys. Rev A **18**, 546-551 (1978).

Berry, H G, Hallin, R Sjodin, R. and Gaillard, M Phys Lett. **50A**, 191 (1984)

Brilly J. Kennedy E.T and Mosnier J.P J.Phys.B **21**,3685 (1988)

Brilly J. Kennedy E T. and Mosnier J.P *Proceedings of the ninth international conference on Vacuum ultraviolet radiation physics VUV-9 University of Hawaii 1989* Phys. Scr **40**, 30, (1990).

Burkhalter, P G. Nagel, D.J and Cowan, R.D Phys Rev. A. **11**, 782 (1975).

Colombant, D and Tonon, G.F J. Appl Phys. **44**, 8, (1973).

Connerade, J.P. Garton, W.R S and Mansfield, M W D Astrophys. J **165**. 203 (1971).

Cowan, R.D. *The Theory of Atomic Structure and Spectra* (U. California Press, Berkeley, Calif., 1981), Secs 8-1, 16-1 and 18-7.

Cowan, R.D Opt Lett. **9**, 168-170 (1984).

Das, B.P and Grant, I P. J. Phys B **19**, L 7 (1986)

Engstrom, L Young, L Somerville L P and Berry, H G Phys. Rev. A **32**, 1468-1471 (1985)

Esteva, J.M. and Mehlman, G Astrophys J. **193**, 747-753 (1974)

Falcone, R W , Holmgren, D.E and Pedrotti, AIP Conf Proc. **90**, 287-295 (1982)

Falcone, R.W and Pedrotti, K D Opt. Lett **7**, 74-76 (1982)

Feldman, U. and Cohen, L., J Opt. Soc. Am **57**, 1128-1129 (1967)

Finkenthal M. Litman A. Mandelbaum P Stutman D and Schwob J L. J Opt.Soc Am B5, 1640 (1988)

Froese Fisher C C J Phys **53**, 184, (1975 a)

Froese Fisher C C. J Phys **53**, 338, (1975.b).

Froese Fisher C. Phys Rev. A. **34**, 3 (1986).

Grant I P , Mayers D F and Pyper N C J.Phys B **9**, 2777

(1976).
Grant I P , McKenzie B J , Norrington P M , Mayers D R and Pyper N C , Comput Phys Commun **21**, 207 (1980)
Hansen, J E. J Phys B **8**, 2759, (1975).
Harris S.E Opt.Lett 5, 1 (1980)
Harris, S E., Walker, D.J., Caro, R G., Mendelsohn, A.J and Cowan, R.D. Opt. Lett **9**, 168-170 (1984)
Harris S.E. J Opt Soc.Am. **B2**, 1942 (1985)
Holmgren, D.E., Falcone, R.W., Walker, D J and Harris, S E Opt. Lett. **9**, 85-87 (1982).
Holmgren D.E., Walker D J., King D.A. and Harris S E Phys Rev A. **31**, 677 (1985)
Lucatorto, T B., and McIlrath, T J Phys. Rev Lett **37**, 7, (1976).
McGuire, E.J. Phys. Rev. A **14**, 1402-1410 (1976)
McGuire, E.J and Duguay, M A Appl Opt. **16**, 83-88 (1977)
Martin, W C and Zalubas, R J. Phys Chem Ref Data **9**, 1, (1979).
Mehlman, G,, Weiss, A.W. and Esteva, J.M. Astrophys J. **209**, 640-641 (1976).
Mosnier J.P., Brilly . and Kennedy E.T J Physique C-9, 219 (1987).
Pedrotti, K.D., Mendelsohn, A.J , Falcone, R.W., Young, J.F. and Harris, S E J. Opt. Soc. Am. B **2**, 1942-1947 (1985).
Pegg, D.J., Haselton, H.H , Thoe, R S , Griffin, P M , Brown, M D. and Sellin, I A.Phys. Rev A **12**, 1330-1339 (1975)
Richards, R K and Griffin, D C in *Short Wavelength Coherent Radiation Generation and Applications*, Attwood, D T and Bokor J. eds , AIP Conf Proc **147**, 343 (1986)
Sugar J , Lucatorto T B , McIlrath T J and Weiss A W Opt. Lett **4**, 4 (1979)
Warden, E S and Moos, H W Appl Opt **16**, 1902 (1977)
Wolff, H.W Radler, K Sonntag, B and Haensel R Zeitschreift fur Physik **157**, 353 (1972)

CHAPTER FIVE THE ARGON ISOELECTRONIC SEQUENCE

5 1 INTRODUCTION

The argon sequence comprises ions of those elements following argon in the periodic table which have the ground state electronic structure of $3s^2 3p^6\ {}^1S_0$ The sequence contains, among others, the spectra of Ca III, Sc IV, Ti V and V VI; two of these spectra Sc IV and Ti V have been studied experimentally during this work. Absorption spectra of both scandium and titanium laser produced plasmas are shown in fig.(5.1.a.b) along with comparison spectra of the back lighting continua used. A target of calcium was also used in the series of experiments with several attempts being made to record the absorption spectrum of a calcium laser produced plasma; however, these attempts were unsuccessful

The scandium and titanium spectra reported here were recorded in the 80-250Å wavelength region Because of the ground state electronic configuration of argon like ions we expect the absorption spectra of these ions to exhibit analogous structures to those observed in the neon like spectra reported in chapter three We would therefore expect the argon like spectra to contain strong Rydberg series arising from ground state transitions which involve the outer 3p electrons, these transitions take the form $3s^2 3p^6 \rightarrow 3s^2 3p^5 ns,nd$ and converge on the $^2P_{1/2}$ and $^2P_{3/2}$ limits We would also expect to observe resonances to shorter wavelengths than the outer 3p transitions which arise due to the excitation of one of the inner shell 3s electrons As in the case of the neon like isoelectronic sequence these levels will for the most part have an autoionizing character.

This chapter describes very briefly the results of work which was carried out on those elements following argon in the periodic table The spectra presented here were

acquired during a preliminary survey of that part of the periodic table. The intention was to return and perform a more detailed study at a later stage. However, a more detailed study was never conducted and so the spectra reported here are the only spectra of the respective elements recorded. For reasons of weakness, lack of reference wavelengths and comparison spectra, no detailed analysis of any of the observed features will be given here. However, each of the spectra studied contains many strong absorption features which can be attributed to argon like and potassium like scandium and titanium ions respectively, the individual spectra are discussed in the next two sections of this chapter.

5.2 THE ABSORPTION SPECTRA OF A SCANDIUM LASER PLASMA.

The absorption spectrum of a scandium laser produced plasma is shown above in Fig.(5.1.a), directly beneath this spectrum (with which it may be compared) is a hafnium emission spectrum recorded at the time of the experiment. The spectrum was obtained using a hafnium continuum as the backlighting source. The continuum was generated by focusing approximately 50% of the laser output onto the surface of the hafnium target using the 6cm focal length spherical element of the lens combination. The absorption spectrum shown in Fig.(5.1.a) covers the approximate wavelength region 260-80Å. The spectrum was recorded using the experimental technique which has been outlined in detail in chapter two. The two rotating target configuration was employed; the scandium target comprised a thin (0.01mm thick) disc of the material cut from a foil which was then attached to an aluminium former by means of adhesive. The spectrum was recorded using a 6cm focal length cylindrical lens which was de-focused by 5mm to produce the absorbing scandium plasma. The laser beam was divided equally between the two targets and 150 laser shots were required to produce sufficient plate blackning.

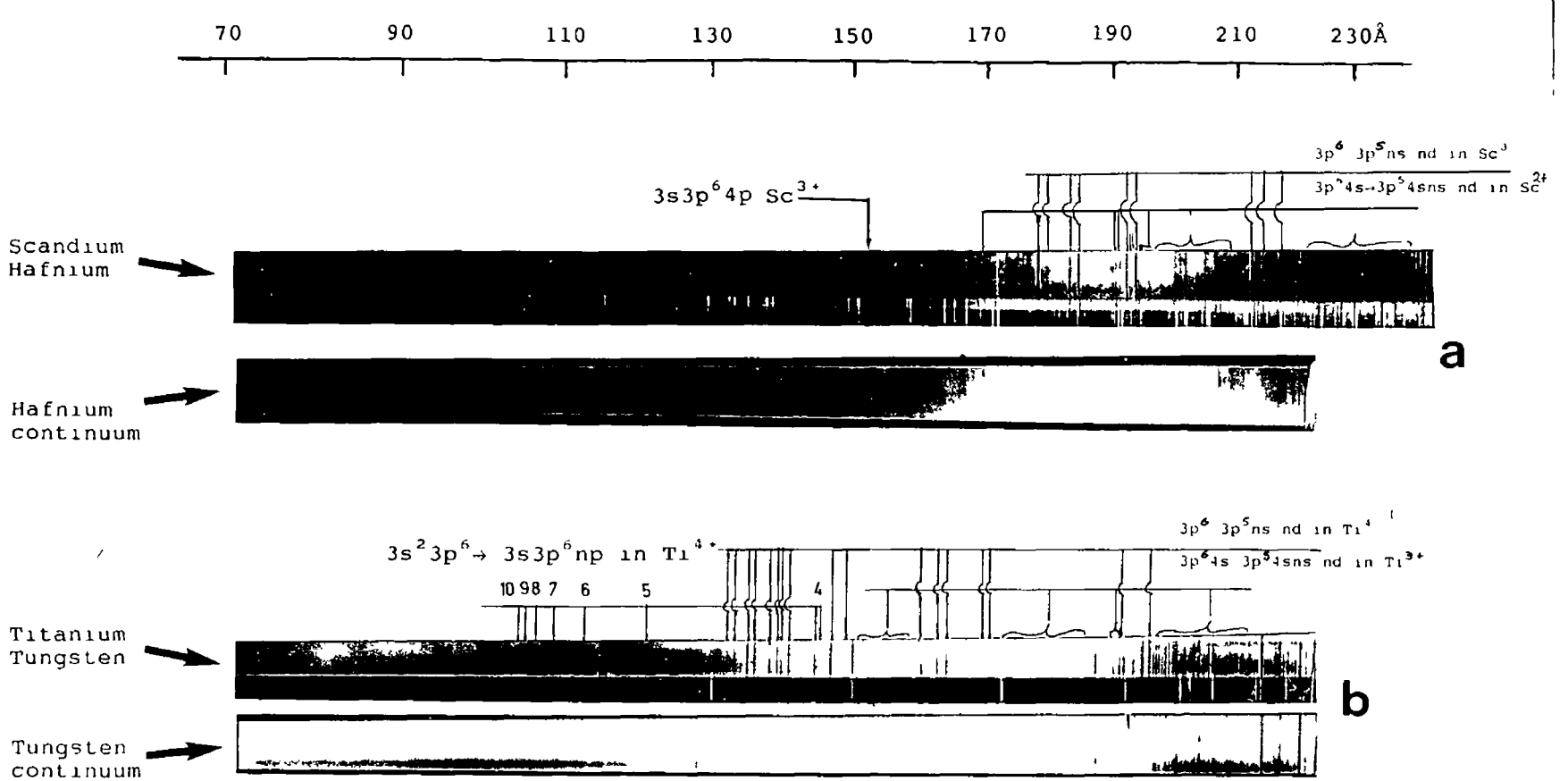

FIG 5 1

Absorption spectra of Sc and Ti laser produced plasmas in the 70-230Å region Also shown are comparison continuum spectra (See Text)

It was expected, from a consideration of ionization energies, that the argon like ion Sc IV would dominate in the absorbing scandium plasma. We therefore expected to observe a spectrum which contained several members of the principal series which arise due to excitations involving the outermost 3p electrons. These structures are to be found between 417Å and the $^2P_{1/2}$ and $^2P_{3/2}$ limits, located at approximately 168Å (Sugar and Corliss 1980). Several members of the principal series are indicated in the spectrum shown in Fig.(5.1.a) to wavelengths longer than 175Å and are absent from the comparison continuum spectrum. These lines are well known having been studied previously in emission by Smitt (1973). Several less intense structures are also noticeable from a close examination of this region of the spectrum shown in Fig.(5.1.a). These weaker features do not seem to belong to the argon like Sc^{3+} ion and are therefore possibly due to the lower stage potassium like Sc^{2+} ion. It would not be unexpected to observe an absorption spectrum which contained contributions from both of these ions, as the cylindrical lens used to create the scandium plasma was de-focused by 5mm. The analogous case of the aluminium spectra discussed in chapters three and four would also seem to lend credence to the contention regarding the weaker features in this region of the spectrum.

Above the limits of the principal series lies the region where we expect to find the autoionizing resonances which arise due to the excitation of one of the inner 3s subshell electrons. Kastner et al (1977) studied autoionizing structures in high voltage spark discharge spectra of the argon like ions Ca III, Sc IV, Ti V, V VI, Cr VII and Fe IX. Kastner et al reported the observation of the Sc^{3+} $3s3p^6 4p\ ^1P$ level at 153.21Å; close examination of this region of the spectrum shown in Fig.(5.1.a) reveals that there is a relatively strong absorption feature present which coincides with the feature reported by Kastner et al (1977). However with regard to other, higher members of the autoionizing series, this entire region of the spectrum is weak and

ambiguous containing many absorption features Most of these, for the most part weak and broad, absorption structures can be attributed to the background hafnium continuum, or to features in the weak overlapping BeO reference spectrum. The weakness and ambiguity of this region of the spectrum precludes the classification of further autoionizing features in the Sc IV spectrum

5 3 THE ABSORPTION SPECTRUM OF A TITANIUM LASER PLASMA

The absorption spectrum of a titanium laser produced plasma is shown in Fig (5.1 b). The wavelength range covered by the spectrum is approximately 230-70Å. The spectrum was recorded as described above except that a tungsten laser plasma provided the backlighting source. The cylindrical lens used was de-focused by 5mm and approximately 120 laser shots were required to record the spectrum shown. As with the scandium spectrum discussed above the titanium spectrum contains many strong resonances in the 130-230Å region. These resonances can to a large extent be identified as the principal series transitions observed previously in emission by Svensson and Ekberg (1968) and more recently by Svensson (1976) The lines in question arise from excitations of one of the outer 3p subshell electrons in transitions of the type $3s^2 3p^6 \rightarrow 3s^2 3p^5 ns,nd$. In the spectrum of Fig (5.1.b) these lines are strong and well defined and are found to wavelengths longer than 130Å. Many of the features found in this wavelength region are listed by Corliss and Sugar (1979)

As with the case of the scandium spectrum of Fig (5 1 a) the observed structures to the long wavelength end of the spectrum appear to be more complicated than would otherwise be expected from the straight forward excitation of a single outer 3p electron. Much of the long wavelength absorption seen is clearly due to the background tungsten continuum source which contains many

strong lines in this region However, it is also more than likely that much of this extra titanium absorption which is considerably weaker than the known Ti^{4+} features arises from the lower stage Ti^{3+} ion Again there is a direct analogy between the titanium spectrum of Fig (5 1.b) and the silicon spectra discussed in chapters three and four. It seems most likely that this weaker absorption arises from transitions to core excited states within the potassium like Ti^{3+} ion.

Above the principal series limits in Ti V we expect to find evidence of autoionizing structures in the continuum due to the excitation of an inner 3s electron in transitions of the type $3s^2 3p^6 \rightarrow 3s3p^6np$. The lowest lying of these states are the $3s3p^6 4p\ ^{1,3}P$ levels which lie below the $^2P_{1/2}$ limit of the T V ion. This region of the Ti V spectrum was previously studied by Kastner et al (1977) using a high voltage spark source They observed the autoionizing series through n=11, the features being observed as strong absorption lines and covering the wavelength range 145-103Å In even earlier work Svensson and Ekberg (1968) identified the n=4 ^1P member as an emission feature. From an examination of this wavelength region of the spectrum shown in Fig.(5 1.b) we have been able to classify the two $3s3p^6 4p\ ^{1,3}P$ levels as relatively strong absorption features at 145Å These two features are well defined and lie in the spectrum among the higher members of the principal series which are also seen as strong absorption features in this region. Also seen in the spectrum as a relatively strong absorption line is the $3s3p^6 5p\ ^1P$ level at approximately 120Å. In all we notice in the spectrum shown in Fig.(5.1 b) the presence of six members of the series, those members with n=6,7,8 and 9 appear in the spectrum as weak absorption features However, due to the lack of reference wavelengths in this region together with the general weakness of the spectrum it is not possible to present a listing of accurately measured features for the Ti V autoionizing series. However, the wavelengths of the features which were measured with a ruler from an

enlarged photographic print of the region having a dispersion of 0.15Å/mm were found to agree to within ±0.05Å with the values listed by Kastner et al (1977).

---

5 4 REFERENCES

Corliss, C. and Sugar, J J.Phys Chem Ref Data. 8, 1, (1979).

Kastner, S.O. Crooker, A.M Behring, W.E and Cohen, L. Phys Rev.A. 16, 2, (1977).

Smitt, R. Phys.Scr. 8, 292, (1973).

Sugar, J and Corless, C. J.Phys.Chem Ref Data 9, 2, (1980).

Svensson, L.A. and Ekberg J.O. Ark.Fys. 37, 65, (1968).

Svensson, L A Phys.Scr 13, 235, (1976)

CHAPTER SIX THE Kr, Br AND Se, ISOELECTRONIC SEQUENCES

6 1 INTRODUCTION

This chapter describes work which was carried out on laser plasmas of those elements which follow krypton in the periodic table. We report here the absorption spectra of strontium, yttrium and zirconium laser produced plasmas which were acquired using the experimental method discussed in chapter two. As might be expected in the absorption spectra of plasmas of these elements absorption features due to the Kr like ions of some of the above elements have been observed. The dominant absorption in Kr like ions arises from excitations of the outer most 4p subshell. These absorption structures are for the most part well known for all of the ions studied in this work. In the absorption spectrum of the strontium plasma the lines due to the principal series in the Sr^{2+} ion are weak and lie to relatively long wavelengths This element was found to be difficult to work with as it is reactive and thus oxidizes rapidly in air The strontium spectrum is the weakest of the three spectra reported along this isoelectronic sequence and contains only a few very weak lines for which no measurements are presented.

The work reported in this chapter is centered around the absorption observations in ions of yttrium In the yttrium spectra we have observed strong resonance absorption which, by comparison with previous work, can be attributed to the Kr like ion Y IV and to the Br like ion Y V, there is also a contribution from the higher ion stage Y VI. The spectra cover the wavelength range 280-80Å, the longer wavelength region of the spectrum is dominated by the principal series absorption in both Y IV and Y V. The most striking aspect of the yttrium spectrum

is the presence of a group of relatively strong absorption features in the 90Å region These features lie so far above the ionization limits of Y IV, Y V and Y VI that they cannot be due to outer subshell absorption in any of these ions An analysis of these features is presented with the aid of a series of multi configurational Dirac Fock calculations of inner shell structures in a number of Yttrium ions

The zirconium spectrum presented here is dominated by absorption due to the Zr^{4+} ion; this absorption is strong and has been observed previously by other workers, (Reader and Acquista 1979). None of the zirconium spectra recorded show any evidence of absorption at shorter wavelengths

6 2 THE ELEMENTS FOLLOWING KRYPTON PREVIOUS WORK

Ions along the krypton isoelectronic sequence have the ground state electronic configuration $3d^{10}4s^{2}4p^{6}\ {}^{1}S_0$ with the lowest lying configurations giving rise to the $4p^{5}(4d+5s)$ group of lines. Because of the high binding energy of the closed shell $4p^{6}$ configuration these lines all lie in the vacuum ultraviolet region for those members of the sequence which follow neutral krypton, i.e , Rb II, Sr III, Y IV, Zr V . . The Kr sequence has recently become of interest in proposals which seek to use ions along this sequence as possible media for x-ray lasers Clark et al (1986) have proposed x-ray laser schemes in which the upper levels of the laser transition are populated by multi photon excitation Boyer et al (1984) carried out experiments using an Ar F laser operating at λ=193nm with $I=10^{14}-10^{15}Wcm^{-2}$ and reported several cases of multiple ionization of atoms In order to produce many of the observed stages of ionization it was required that the atoms in question absorb as many as 99 photons Boyer et al (1984) have also observed stimulated emission at 93nm in Kr gas using the same

intense laser. The mechanism by which the population was built up seems to be as follows: Ground state Kr with the configuration $4s^2 4p^6$ is excited to the $4s4p^6 4d$ state by the absorption of four of the laser photons with λ=193nm.

$$Kr(4s^2 4p^6) + 4\gamma(193nm) \rightarrow Kr(4s4p^6 4d) \qquad \text{eq.6.1}$$

Thus a population inversion is established between the $4s4p^6 4d$ state and the $4s^2 4p^5 4d$ state from which stimulated emission occurs thus.

$$Kr(4s4p^6 4d) \rightarrow Kr(4s^2 4p^5 4d) + \gamma(93nm) \qquad \text{eq.6.2}$$

The mechanisms studied by Clark et al (1986) along the Kr sequence involve either core excited or multiply excited levels which are proposed to be populated by high intensity lasers. Because of the lack of experimental data along the Kr sequence many of the energy level structures for the ions along the sequence were calculated *ab initio* by the authors. A proposed experimental set up consisting of a magnetically confined laser produced plasma probed by a high powered pico-second laser has been designed to study such laser schemes in ions along the Kr sequence, (Suckewer et al 1985); the arrangement was briefly discussed in chapter one, section 1.4.

With the exception of neutral krypton no member of the Kr sequence has been studied in absorption in the VUV region. The VUV photoabsorption spectrum of neutral krypton was first studied by Madden and Codling (1965). They observed the principal series absorption due to the excitation of a single outer 4p electron to upper levels of the type $4s^2 4p^5 ns$ and nd. Also seen were series due to inner shell (4s) excitations as well as lines which were the result of transitions involving the simultaneous excitation of two of the outer 4p electrons.

Reader et al (1972) carried out emission studies of the first six ions of the krypton sequence, Rb II, Sr III, Y IV, Zr V, Nb VI and Mo VII. For each of the above ions the authors studied the principal series $4p^6 \rightarrow 4p^5 ns,nd$, together with inner 4s subshell excitations in three of

the ions Zr V, Nb VI and Mo VII. The authors also compared the observed spectra along the isoelectronic sequence and derived the ionization energies in each case A more detailed study of the Rb II spectrum was carried out by Reader (1974) using a pulsed radio frequency discharge as the light source with the spectra recorded on a 10.7m normal incidence spectrograph Reader (1974) classified some 600 lines arising from transitions between 165 levels below the ionization limit of the ion. Reader and Acquista (1979) and Epstein and Reader (1982) carried out similar studies on the ions Zr V and Y IV respectively. In both cases the spectra were studied using 10.7m normal and grazing incidence spectrographs For both ions about 600 lines were observed from transitions between various levels lying below the ionization limits, thus completing the classifications for a number of configurations in each of the ions Khan et al (1981) also studied the spectrum of Zr^{4+} and observed 164 lines which were classified as transitions between excited states of that ion

Many studies in emission using sparks discharges, laser produced plasmas and tokamaks have been carried out on the higher members of the Kr sequence Chaghtai (1970) studied vacuum spark spectra of Zr, Nb and Mo and presented data for the Kr like ions Zr V, Nb VI and Mo VII Chaghtai (1970) carried out a term analysis and classified many new lines arising from outer shell transitions in each of the ions Shujauddn et al (1982) conducted a similar study of the Nb VI spectrum recording the spectrum between 260 and 1830Å and analyzing the level structure and configurations of the ion Even-Zohar and Fraenkel (1972) carried out studies of ions of Ru, Rh, Pd and Ag which were isoelectronic to Br I, Kr I, Rb I and Sr I. They used a three electrode vacuum spark and observed lines due to transitions which for the most part were due to excitations of the outer 4p shell. O'Sullivan et al (1984) and Costello and O'Sullivan (1984) studied features in the spectra of Kr like Ag and Cd observed in

the emission spectra of laser produced plasmas Kr like ions of Sr, Zr, Mo, and Ru have also been studied using tokamaks, see Finkenthal et al (1981) and Wyart (1988)

Spectra of neutral and of ionized species other than Kr like ions of the elements which follow krypton in the periodic table have also been studied For example, neutral rubidium and strontium were studied in absorption using a synchrotron to back light the vapor column, (Mansfield and Connerade 1975.a.b) The VUV emission spectrum of Y III was extensively studied by Epstein and Reader (1974), also, the emission spectrum of Y V was examined by Reader and Epstein (1972), while the spectrum and energy levels of Y VI were published by Persson and Reader (1986).

6 3 THE ABSORPTION SPECTRUM OF A STRONTIUM LASER PLASMA

The absorption spectrum of a strontium laser produced plasma is shown in Fig (6 1 a) along with a comparison tungsten emission spectrum recorded at the time of the experiment The spectrum was recorded using two rotating targets by the method described in chapter five, section 5 2 Several experiments were carried out using a strontium plasma as the absorbing medium However, these experiments were for the most part unsuccessful, the strongest strontium absorption spectrum recorded was that of Fig (6.1 a).

The spectrum shown in Fig (6 1 a) is an extremely weak spectrum showing only slight evidence of absorption features which by comparison with the continuum may be assigned to ions of strontium The spectrum is so weak in fact, that an enlarged photographic print of the wavelength region which contains the strontium absorption features shows the lines in question to have faded completely into the background.

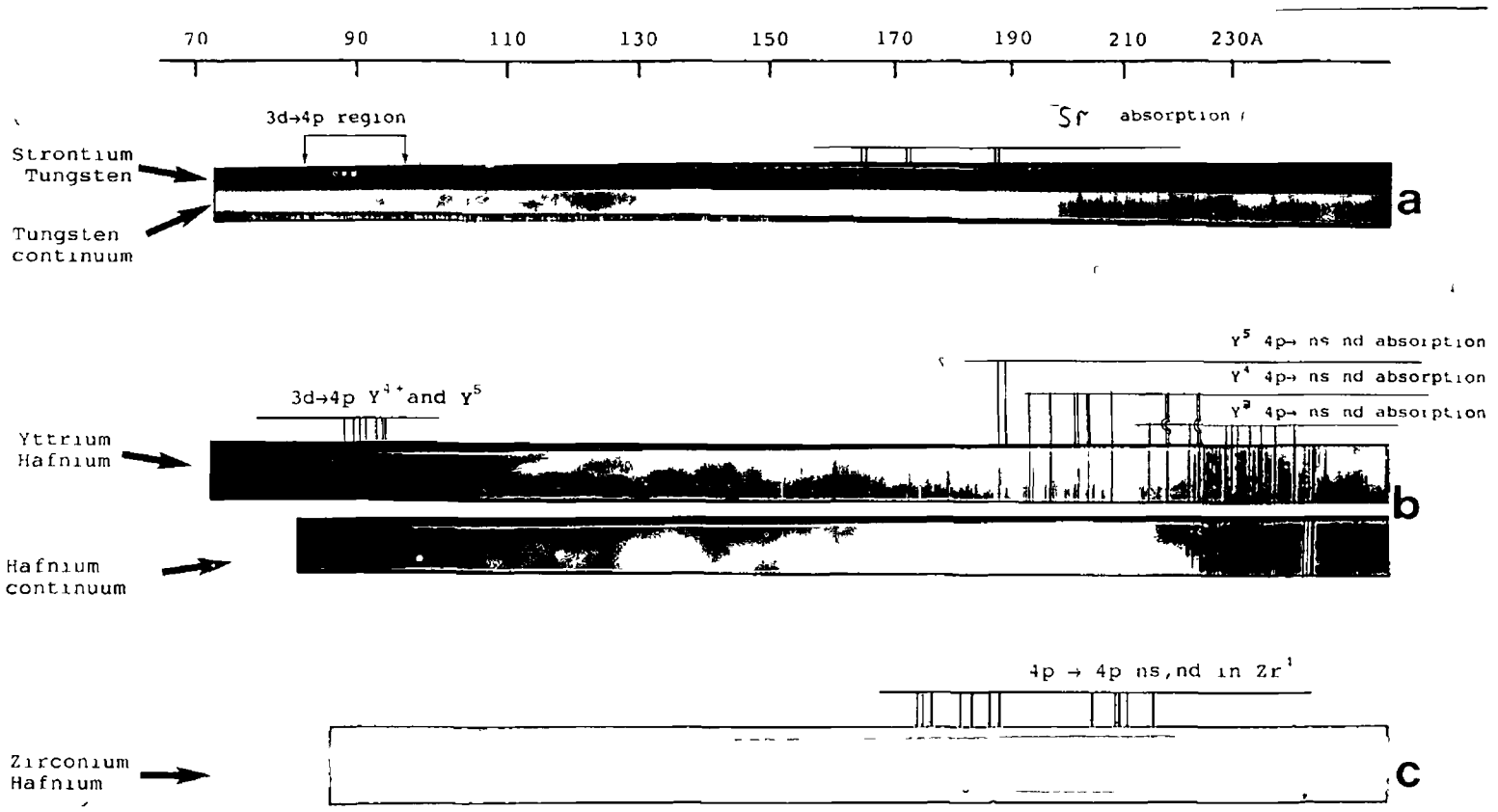

FIG 6 1

Absorption spectra of Sr, Y and Zr laser produced plasmas in the 70-230Å region Also shown are comparison continuum spectra (See Text)

However, from a study of contact prints of the plate in question the following may be stated. There are two regions of the spectrum shown in Fig.(6.1.a) which exhibit weak absorption structures when compared with a comparison tungsten continuum spectrum. At longer wavelengths 150-190Å there appear to be six distinct absorption features which appear in the spectrum as three pairs of lines, these structures are extremely weak and are just discernible from the background. To the shorter wavelength end of the spectrum there are six equally very weak absorption features in the 80-90Å region.

As was stated above no reference was recorded during the experiment and as a consequence of this coupled with the weakness of the features in question only an estimate of the wavelengths may be given. There appear to be two lines at 165Å, a second pair at 172Å and a third pair located at 188Å. The ionization potential for Sr III is given by Reader et al (1972) as 42.87eV which would indicate that the absorbing plasma perhaps contains the ions Sr III, Sr IV, Sr V and possibly Sr VI. The features seen to the longer wavelength end of the spectrum are almost certainly due to transitions in one or more of the ion stages higher than the Kr like Sr^{2+} ion. Persson (1978) and more recently Persson and Wahlstrom (1984) have carried out extensive emission studies of Sr IV and Sr V respectively, in neither case were there features in the 150-190Å wavelength region. This would seem to indicate that the features in question arise due to inner shell transitions in one or more of the lower ion stages of strontium, or from outer shell transitions in one of the higher stages. It was felt that the poor quality of the primary data did not justify a more detailed investigation of these structures.

The structures which appear in the 80-90Å region are likely to arise due to the promotion of an inner 3d subshell electron to the 4p subshell in a mixture of the ion stages Sr IV and Sr V. Because of the overall

weakness of the spectrum together with the lack of measured wavelengths for the observed features no specific calculations for this type of transition in any of the strontium ions likely to absorb in the plasma were carried out. However, a tentative analysis has been carried out for what appear to be entirely analogous features observed in the absorption spectrum of a yttrium laser produced plasma That work is discussed in the next section of this chapter and would seem to indicate that the above tentative suggestion may be considered reasonable

6 4 THE ABSORPTION SPECTRUM OF A YTTRIUM LASER PLASMA

Fig.(6.1.b) shows the absorption spectrum of a yttrium laser produced plasma in the 70-250Å wavelength region The absorption experiments carried out on yttrium laser produced plasmas were as described in previous sections of this thesis, using the two rotating target configuration A number of different experiments were carried out under varying conditions. The variations in experimental procedure were largely centered around changing the focusing conditions of the cylindrical lens or the proportion of the incident laser beam directed to each of the targets A 6cm plano cylindrical lens was used to create the absorbing ion column and in general 100-200 laser shots were required to obtain a satisfactory plate exposure Of the many experiments which were carried out using a yttrium laser plasma as the absorbing medium, only two spectra were recorded which show substantial strong yttrium absorption. Both spectra show yttrium absorption to the long wavelength and short wavelength ends of the spectrum. The spectrum shown in Fig (6 1.b) is the strongest of the spectra recorded and shows absorption in the 150-250Å wavelength range which arises from excitations involving an outer 4p electron in a number of different ion stages of yttrium

Also observed in the spectrum in the 90Å region are a number of relatively strong absorption structures which appear to be due to 3d→4p excitations in more than one ion stage present in the absorbing plasma

As with the case of the strontium spectra discussed in the previous section, experimental difficulties encountered during the yttrium work resulted in some of the spectra being recorded without an overlapping set of emission references. On other of the weaker spectra recorded, only that portion of the spectrum to wavelengths longer than 150Å contain overlapping reference lines For this reason those absorption structures which lie to the short wavelength end of the spectrum shown in Fig.(6.1.b) were measured indirectly and as a consequence of this there is a relatively large error in the measured wavelengths which has been estimated at $\Delta\lambda=\pm 0.1$Å, although the estimated error for the wavelength differences between the structures may be considered as ±0.05Å or better

The absorption features shown in the spectrum of Fig (6 1.b) were assigned to ions of yttrium by comparison with a hafnium spectrum recorded at the time of the experiment and covering the same wavelength range The yttrium spectrum may be divided into two distinct wavelength regions The long wavelength absorption which is observed beyond 150Å is for the most part well known and can be attributed to 4p subshell absorption in a number of ion stages of yttrium, Y IV, Y V and Y VI, by comparison with previously published measurements. A list of some of the observed absorption features attributed to yttrium ions together with literature values are given in table 6.1 below. The absorption seen to the shorter wavelength end of the spectrum 82-90Å is reported here for the first time and is thought to arise due to inner shell 3d→4p excitations in the ion stages Y V and Y VI

TABLE 6 1

Table of some of the strongest lines observed in the XUV photoabsorption spectrum of a yttrium laser produced plasma. (See text).

Ion.	Transition	λ_{Meas}(Å).	λ_{Lit}(Å).
Y IV	$4p^6 \rightarrow 4p^5 6d$	242.34	242.301
Y IV	$4p^6 \rightarrow 4p^5 6d$	235.75	235.769
Y IV	$4p^6 \rightarrow 4p^5 7d$	229.76	229 783
Y IV	$4p^6 \rightarrow 4p^5 7d.$	228.89	228.940
Y V	$4p^5 \rightarrow 4p^4 6s$	224.67	224 723
Y V	$4p^5 \rightarrow 4p^4 5d.$	224.49	224.564
Y IV	$4p^6 \rightarrow 4p^5 8d$	221 70	221.711
Y V	$4p^5 \rightarrow 4p^4 6s.$	217.87	217 855
Y V	$4p^5 \rightarrow 4p^4 5d$	217.56	217 564
Y IV	$4p^6 \rightarrow 4p^5 10d$	214 48	214.509
Y VI	$4p^4 \rightarrow 4p^3 6s$	188.22	188.211
Y VI	$4p^4 \rightarrow 4p^3 6s.$	186.76	186 782

λ_{Meas}(Å): Measured wavelengths of this work ($\Delta\lambda$=±0 05Å).
λ_{Lit} (Å): Values taken from the literature.

The first problem in the analysis of the short wavelength features was to ascertain which of the ion stages of yttrium were in fact present in the absorbing plasma In order to do this the long wavelength absorption was measured and the wavelength values compared with previously measured emission spectra of yttrium ions reported in the literature The emission spectrum of Y IV was recorded in detail by Epstein and Reader (1982), some 560 lines were classified in the wavelength region 210-5000Å. Many strong resonance lines due to excitations from the outer 4p subshell of Y IV were recorded below 500Å, these are the principal series transitions $4p^6 \rightarrow 4p^5 ns,nd$, many of which appear in the spectrum shown in Fig.(6.1.b). The most detailed studies of the Br like Y V ion were carried out by Reader and Epstein (1972) and by Zahid-Ali et al (1975) in the latter study about 50 lines between 180 and 250Å were classified The

transitions were for the most part from the $4p^5$ ground states to upper levels of the type $4p^4$5d,6d,6s,7s As with the Y IV case many of these lines have been observed and measured in the spectrum shown in Fig.(6 1 b). Persson and Reader (1986) studied the spectrum of five times ionized yttrium Y VI using a sliding spark discharge in the wavelength range 160-2500Å and have reported and classified a total of 900 lines arising from transitions between 101 odd and 69 even parity levels within the ion. Most of the lines which lie below 250Å are described as being extremely weak with the exception of a few $4p^4 \rightarrow 4p^3$6s lines, two of which have been observed in the 186Å region of the spectrum shown in Fig.(6 1.b), see also table 6 1.

From the above discussion it reasonable to assume that lines observed in Fig.(6.1 b) in the 90Å region arise from transitions within one or more of the ion stages Y IV, Y V or Y VI. Also it is likely that the spectrum shown in Fig.(6.1.b) contains no contribution from the higher ion stage Y VII due to the relatively high (92.5eV) ionization potential for the lower stage Y VI ion. Also from the above discussion of the known levels of the Y IV, Y V and Y VI ions it is clear that the short wavelength structures observed in the spectrum in Fig.(6.1.b) and in more detail in Fig (6 2 a b) do not arise from transitions involving the outer 4p subshell in any of the above mentioned yttrium ions.

The attempt to assign the short wavelength features therefore proceeded on the assumption that the features were due to inner shell transitions in Y IV, Y V or Y VI, or from a mixture of all of these ions Initial calculations ruled out 4s subshell excitations, as lines resulting from transitions of the type $4s^2 4p^m \rightarrow 4s4p^m np$, n=5,6.. in Y IV, Y V and Y VI fall well outside of the wavelength range of interest. From this the conclusion must be that the observed short wavelength structures arise from transitions involving the inner 3d subshell

and are therefore of the type 3d→np,nf with n=4,5 . in Y IV, Y V or Y VI or in more than one of the ions involved. Inner subshell excitations involving the 3p subshell were calculated for all of the above ions and found to lie to extremely short wavelengths (30Å) and were therefore ruled out

The calculations carried out here were confined to single and double electron excitations which involved the inner 3d subshell in Y IV, Y V and Y VI The calculations were carried out using the MCDF code of Grant et al (1980) In each case the ground state of the ion was optimised in a single separate optimum level (OL) program run in order to provide more accurate values for the transitions. The determination of the upper levels involved the inclusion in the program of all levels of interest in a single extended average level (EAL) calculation. In order to establish the oscillator strengths for the transitions the ground state together with all of the upper levels were included in a single run of the program. The results of these calculations are listed in the tables which follow

Mansfield and Audley (1988) carried out similar calculations involving inner 3d excitations along the yttrium isonuclear sequence up to and including Y VI, using the code of Cowan (1981) The type of transition possible for the 3d electron take the form 3d→np,nf, for the np series only n≥5 is possible for the neutral atom and the ions Y II, Y III and Y IV But for the higher members of the sequence the vacancy in the outer 4p subshell allows 3d→4p excitations to become possible for Y V and subsequent members of the sequence. Table 6.2 lists the calculated values for the 3d→5p,4f transitions in the Y IV ion along with calculated oscillator strengths.

TABLE 6 2

Calculation of $3d^{10}4s^24p^6 \rightarrow 3d^94s^24p^65p,4f$ transitions in the Y IV ion.

configuration	λ_{MA}(Å)	λ_{TW}(Å)	gf_{MA}	gf_{TW}
$3d^95p$	72 398	72.58	0 0248	0.0071
$3d^95p$	71.708	71 79	0 0222	0.0060
$3d^95p$	71.604	71 68	0.0001	0.0000
$3d^94f$	68.736	68 98	0.0047	0 0013
$3d^94f$	68.706	68.96	0.0652	0 0107
$3d^94f$	67.993	68 15	0.0509	0 0094

MA are results of Mansfield and Audley (1988).

TW are results of this work.

The table illustrates the comparison between the calculations of Mansfield and Audley (1988) and those of this work. The table serves to illustrate two points of interest. Firstly, there is a good agreement between the two sets of calculated values, this is particularly seen in the wavelength columns. The gf values are also in relative agreement in that each set of data predicts the same transitions to be either weak or strong. The large numerical differences in the gf values of each set of calculations may be understood by noting that in such codes there are a number of factors which govern the computation of gf values The number of configurations used in each calculation together with the type of calculation carried out e.g., relativistic or not, and the inherent differences in the codes used Also there are the difficulties associated with calculating gf values within a relativistic framework, see for example Grant (1974) The second point of interest is that the calculations show that excitations of a 3d electron to 5p,4f levels fall to much shorter wavelengths than the wavelengths of the features of interest This has been found in agreement with Mansfield and Audley to be the case for this type of transition in all members of the yttrium isonuclear sequence from Y I to Y VII for which calculations were carried out In each member of the sequence the predicted wavelengths of the 3d→5p,4f

transitions lie below 77Å and move to progressively shorter wavelengths with increasing ionization

3d→4p transitions:

The only calculated values which lie in the wavelength range of the observed features are those resulting from 3d→4p transitions in the ions Y V and Y VI In Y V the 4p subshell has a vacancy which results in that ion having the ground state $3d^{10}4s^{2}4p^{5}\ {}^{2}P_{1/2,3/2}$ Thus transitions of the type $3d^{10}4s^{2}4p^{5}\rightarrow\ 3d^{9}4s^{2}4p^{6}$ become possible However, the detailed calculated prediction of three absorption lines does not agree with the observation of some 15 absorption structures shown in Fig (6.2.a b) In the Y VI ion there is also a vacancy in the outer 4p subshell, the ground state of this ion is $3d^{10}4s^{2}4p^{4}$ and again as in the Y V case transitions of the type $3d^{10}4s^{2}4p^{4}\rightarrow\ 3d^{9}4s^{2}4p^{5}$ are possible Because the ground state of Y VI is $3d^{10}4s^{2}4p^{4}$ there are in fact five possible levels of the ground configuration; these are, $^{3}P_{0}$, $^{3}P_{1}$, $^{3}P_{2}$, $^{1}D_{2}$ and $^{1}S_{0}$ which results in a great many possible transitions between these levels and the upper $3d^{9}4s^{2}4p^{5}$ levels. The calculations carried out here show that the resulting transitions lie in the wavelength range 96-89Å we therefore appear to have observed some of the transitions from levels of the ground configuration in Y VI to upper $3d^{9}4s^{2}4p^{5}$ states. Table 6.3 lists the calculated energy values and percentage composition of the five levels of the ground configuration of Y VI It may be seen from an inspection of the table that the highest of these configurations, the $^{1}S_{0}$ level lies some 50000cm^{-1} above the lowest $^{3}P_{2}$ level It is therefore clear that all of the levels of the ground configuration are accessible within a plasma containing Y VI ions through collisional and photoexcitation processes This may be stated with some certainty by reference to the work of chapter four and the case of absorption from the $2p^{5}3p$ and $2p^{5}3d$ states in Al III and Si IV. It may be recalled that in Al III the lowest of the excited states ($2p^{5}3p$) lies some 54000cm^{-1} above the ground state, while

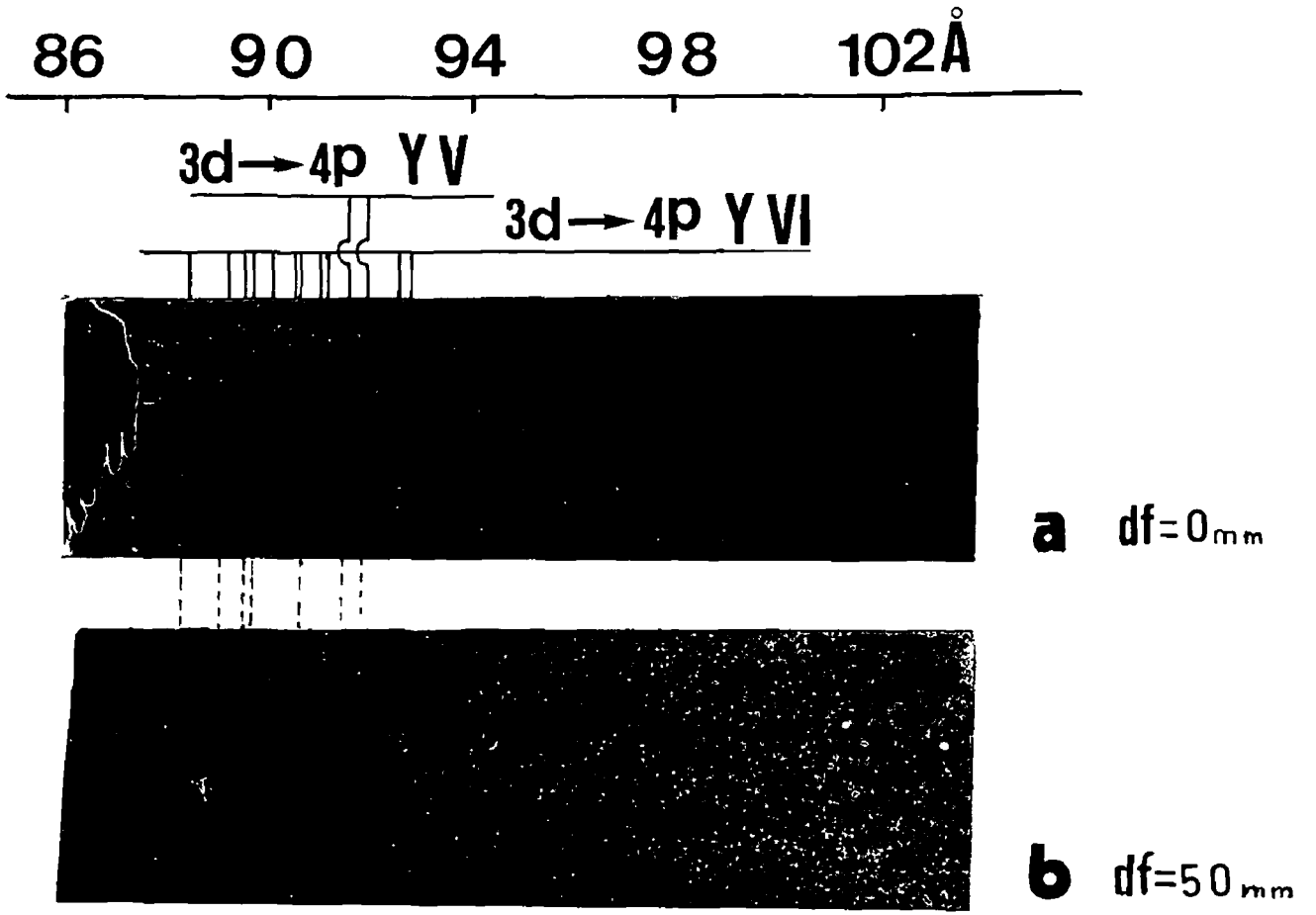

FIG 62

Short wavelength features in the absorption spectrum of a yttrium laser produced plasma at 90Å which has been assigned to the Y^{4+} and Y^{5+} ions. (See text)

the $2p^5 3d$ state lies a further $62000cm^{-1}$ above the first excited state, i.e., $116000cm^{-1}$ above the $2p^6 3s$ ground state. In the case of the sodium like Si IV ion similar excitations were observed and in this case the energy intervals involved were correspondingly greater. We may therefore conclude that all of the possible transitions from all five levels of the ground configuration in Y VI are likely candidates for the absorption seen in the 90Å region of the spectra shown in Fig's.(6.1 and 6.2).

TABLE 6.3

Calculated energy level values (cm^{-1}) and percentage compositions for the $4s^2 4p^4$ ground configuration in Y VI.

J	(a) E(Cal).	(a) %Composition.	(b) E(Cal).	(b) %Composition.
0	10634	89% ^3P, 11% ^1S.	10407	62% ^3P, 38% ^1S.
	50176	89% ^1S, 11% ^3P.	57820	62% ^1S, 38% ^3P.
1	10709	100% ^3P.	11114	100% ^3P.
2	0	92% ^3P, 8% ^1D	0	87% ^3P, 13% ^1D.
	23567	92% ^1D, 8% ^3P	26783	87% ^1D, 13% ^3P.

(a). Are results of Zalubas et al (1976).

(b). Are results of this work.

The calculated values for the $3d^{10}4s^2 4p^5 \rightarrow 3d^9 4s^2 4p^6$ transitions in Y V are listed below in table 6.4. For Y V the calculations predict three lines as a result of transitions between the two ground state levels and the upper levels. Of the three predicted lines two have relatively large oscillator strengths when compared with the third and so from the calculations we might expect that only these two strong features resulting from the 3d→4p excitation would be seen in the absorption spectrum of Y V. An inspection of the spectra shown in Fig.(6.2.a.b) shows two such lines (the strongest in the region) to be present and therefore the above argument

allows us to assign the two strongest lines to the transitions $3d^{10}4p^5\ {}^2P_{3/2} \rightarrow 3d^9 4p^6\ {}^2D_{5/2}$ and $3d^{10}4p^5\ {}^2P_{1/2} \rightarrow 3d^9 4p^6\ {}^2D_{3/2}$ in the Y V ion The features are given estimated relative intensities of 10 to indicate that they are the strongest lines in the region

TABLE 6 4

Classification of features in the Y V absorption spectrum due to the $3d^{10}4p^5 \rightarrow 3d^9 4p^6$ transitions.

$d^{10} \rightarrow d^9 4p$	λ^*_{obs}(Å)	I^*	λ^*_{cal}(Å)	gf^*	λ_{MA}(Å)	$gf_{(MA)}$
$^2P_{3/2} \rightarrow {}^2D_{5/2}$	91.82	10 0	92 06	0 045	92 30	0 2467
$^2P_{1/2} \rightarrow {}^2D_{3/2}$	91 48	10.0	91.69	0.040	91.97	0.1376
$^2P_{3/2} \rightarrow {}^2D_{3/2}$	.....	...	90.63	0.007	91.01	0 0278

*· results of this work

MA. results of Mansfield and Audley (1988)

$\Delta\lambda = \pm 0$ 10Å for the observed wavelengths

A further experimental observation which serves to support the assignments of table 6.4 together with the contention that both the Y V and Y VI ions were present in the absorbing plasma is seen from a study of Fig.(6.2) In Fig (6 2 a.b) it can be seen that there are substantial differences between the two spectra (**a**) and (**b**), these differences are seen in both the intensity of the individual lines and also in the number of lines in each of the spectra In particular two relatively strong lines seen to the long wavelength side of the group in spectrum (**a**) are not seen in spectrum (**b**). There is also a noticeable difference in both the intensity and number of shorter wavelength features in spectrum (**b**) when compared to spectrum (**a**) The only difference in experimental conditions between the two spectra in Fig (6.2) was that of the degree of focusing of the portion of the incident laser beam used to create the absorbing yttrium plasma. The spectrum shown in Fig (6 2 a) was recorded using a 6cm focal length plano

cylindrical lens tightly focused onto the yttrium target surface to create the absorbing plasma, while for the spectrum shown in Fig (6.2 b) the lens was displaced along the incident laser beam axis by 5mm, all other factors (number of laser shots etc.) were kept constant between the two experiments. The conclusion must be that the absorbing plasma of Fig (6 2 a) contained a greater density of the higher ion stage Y^{5+} than did the absorbing plasma of Fig.(6.2 b). Thus with successive de-focusing of the lens used to create the absorbing plasma the density of Y^{5+} ions within the absorbing ion column is reduced A similar effect has already been discussed in chapter four of this thesis for the sodium like ions Al^{2+} and Si^{3+}, where the dominant ion density within the absorbing plasma was made to shift from Ne like to sodium like by changing the focusing conditions of the lens used to create the absorbing plasma In the spectra shown in Fig (6.2.a.b) the strongest lines in this region of the spectrum which we have assigned to 3d→4p transitions in the Y^{4+} ion remain by far the strongest lines in the spectrum of Fig.(6 2 b) thus strongly suggesting that they originate in the lower stage Y^{4+} ion. The exception to the above observation is also seen in Fig.(6.2 a.b) where two lines which presumably belong to Y VI are seen to become stronger with de-focusing A tentative suggestion to account for this apparent anomaly is to assume that for Y VI successive de-focusing of the lens used to create the absorbing plasma results in a greater proportion of Y VI ions being in the lower of the ground levels The effect is thus that of an apparent increase in path length for those Y VI ions in the lower ground levels. Therefore on the basis of the above tentative argument we may suggest that the strongest of the Y VI lines in Fig (6 2.a b) arises from the lower levels of the ground configuration i e , from the three ^3P levels.

In summary therefore, it may be said that all but two of the features seen in the spectra of Fig (6 2 a.b) are

assigned to the Y^{5+} ion. A full list of all of the calculated values for the $3d^{10}4s^24p^4 \rightarrow 3d^94s^24p^5$ transitions is given below in table 6 5. Listed are calculated wavelengths and gf values for the transitions together with observed wavelengths of the absorption features. The assignments listed may be considered tentative given the degree of error in the measured values along with the general weakness of the observed structures The assignment of these lines to the Y^{5+} ion may be considered reasonable from the results of extensive calculations which were carried out for various two electron excitations in a number of different ion stages In all cases it was found that the resulting calculated values lay well beyond the wavelength range of interest

TABLE 6 5

Calculated and observed wavelengths in the Y VI 3d→4p transition array. (See text for details).

	Transition.	λCal(Å).	gf(10^{-2})	λObs(Å)	I(Ar Uts)
(1)	$^3P_0 \rightarrow {}^1P_1$	95.31	0 68		
(2)	$^3P_0 \rightarrow {}^3P_1$	94 44	0 17		
(3)	$^3P_2 \rightarrow {}^1D_2$	93 68	0.92		
(4)	$^3P_2 \rightarrow {}^1F_3$	93.57	0.03	92 80	5.0
(5)	$^3P_0 \rightarrow {}^3D_1$	92 57	4 17		
(6)	$^3P_2 \rightarrow {}^3D_2$	92 56	0.05		
(7)	$^3P_2 \rightarrow {}^3D_2$	92 31	0.44	92.57	5.0
(8)	$^3P_2 \rightarrow {}^1D_2$	92 27	0 14		
(9)	$^3P_2 \rightarrow {}^3D_3$	91 08	0 23		
(10)	$^3P_2 \rightarrow {}^3P_1$	91 75	0 07		
(11)	$^3P_2 \rightarrow {}^3P_2$	91 73	0 06		
(12)	$^1D_2 \rightarrow {}^1D_2$	91 39	1 70		
(13)	$^1D_2 \rightarrow {}^1F_3$	91.28	6 79		
(14)	$^1S_0 \rightarrow {}^1P_1$	91.25	4 29	91 00	1 0
(15)	$^3P_2 \rightarrow {}^3F_3$	91.21	8.77		
(16)	$^3P_1 \rightarrow {}^1P_1$	91 19	0 37		

Continued.. ...

Table 6.5 Continued.. ...

(17)	$^3P_1 \rightarrow {}^3D_2$	90 93	5 03		
(18)	$^3P_2 \rightarrow {}^3F_2$	90 79	0.39	91 81	1 0
(19)	$^1S_0 \rightarrow {}^3P_1$	90 45	0 14		
(20)	$^3P_1 \rightarrow {}^3P_1$	90 39	3 49		
(21)	$^3P_1 \rightarrow {}^3P_2$	90 38	0.88	90 81	1 0
(22)	$^1D_2 \rightarrow {}^1P_1$	90.33	0.14		
(23)	$^1D_2 \rightarrow {}^3D_2$	90 08	0 81		
(24)	$^3P_2 \rightarrow {}^3D_1$	89.98	0 23		
(25)	$^1D_2 \rightarrow {}^3D_3$	89.86	0.07	89 35	7.0
(26)	$^1D_2 \rightarrow {}^3P_1$	89 55	1.37		
(27)	$^1D_2 \rightarrow {}^3P_2$	89.53	1.69	89.16	7.0
(28)	$^3P_1 \rightarrow {}^3F_2$	89.46	0 01		
(29)	$^1D_2 \rightarrow {}^3F_3$	89.03	0 00		
(30)	$^1S_0 \rightarrow {}^3D_1$	88.73	0.64	88.75	1 0
(31)	$^3P_1 \rightarrow {}^3D_1$	88.67	0.03	88 60	1 0
(32)	$^1D_2 \rightarrow {}^3F_2$	88.64	0.11	88 26	1.0
(33)	$^1D_2 \rightarrow {}^3D_1$	87 86	0.10	87 83	2 0
(34)	.. ..		.	87.10	1.0
(35)	. . . . . .		..	86.57	1.0

6 5 THE ABSORPTION SPECTRUM OF A ZIRCONIUM LASER PLASMA

Also studied as a part of this work was the absorption spectrum of a zirconium laser produced plasma The experiment was carried out several times. However, only one spectrum containing a substantial number of intense absorption features arising from zirconium ions was recorded This spectrum is shown in Fig (6 1 c), it was recorded using the two laser plasma absorption technique described in previous sections with the following experimental conditions. A hafnium plasma was used to provide the back lighting continuum and both backlighting and absorbing plasmas were created using two plano convex 6cm focal length spherical lenses to focus the incident ruby laser In the case of the absorbing zirconium plasma the spherical lens element used was de-focused by 5mm

The spectrum was recorded with the expenditure of 130 laser shots, the incident laser beam was equally divided between both elements of the lens combination.

The spectrum shown in Fig.(6.1 c) covers the wavelength range 80-255Å and contains several strong resonance lines in the 170-220Å region A detailed comparison between the spectrum of Fig (6.1.c) and a hafnium emission spectrum recorded during the experiment shows that these resonances arise due to absorption by species within the zirconium plasma A comparison with the available literature further shows that all of the observed absorption structures attributable to zirconium ions may be readily assigned to previously observed resonance lines arising from the principal series transitions $3d^{10}4s^{2}4p^{6} \rightarrow 3d^{9}4s^{2}4p^{5}ns,nd$ in the krypton like Zr^{4+} ion. Zr^{4+} was previously studied in emission by Reader and Epstein (1972) and in more detail by Reader and Acquista (1979), with additions to the spectrum being published by Khan et al (1981). The comparison between the observed wavelengths published by the above mentioned workers together with the measured list of zirconium lines of the spectrum shown in Fig.(6 1.c) shows that all of the structures observed during this work have been previously observed and classified. Table 6.6 below is a line listing for some of the strong lines in the spectrum of Fig.(6.1 c) which were confirmed as Zr V features by comparison with published work

TABLE 6 6

Table of some of the strongest lines observed in the XUV photoabsorption spectrum of a zirconium laser produced plasma. (See text).

Ion.	Transition.	λ_{Meas}(Å)	λ_{Lit}(Å)
Zr V	$4p^6 \rightarrow 4p^5 5d.$	216.32	216 307
Zr V	$4p^6 \rightarrow 4p^5 6s.$	211.35	211.339
Zr V	$4p^6 \rightarrow 4p^5 5d$	209.83	209 872
Zr V	$4p^6 \rightarrow 4p^5 6s.$	204.75	204.798
Zr V	$4p^6 \rightarrow 4p^5 6d.$	187.95	188 027
Zr V	$4p^6 \rightarrow 4p^5 7s.$	186.11	186.146
Zr V	$4p^6 \rightarrow 4p^5 6d$	183.01	183 042
Zr V	$4p^6 \rightarrow 4p^5 7s.$	181 03	180 988
Zr V	$4s \rightarrow 5p.$	174.27	174.286

λ_{Meas}(Å): Measured wavelengths of this work ($\Delta\lambda$=±0 05Å).

λ_{Lit} (Å): Wavelengths obtained from published work.

6 6 REFERENCES

Boyer, K Egger, H Luk, T S Pummer, H and Rhodes, C K J. Opt. Soc. Am. B. **2**, 3, (1984)

Chaghtai, M S Z Phys Scr **1**, 31, (1970)

Clark, C.W Littman, M.G. Miles, R. McIllrath, T J. Skinner, C H. Suckewer, S. and Valeo, E. J. Opt. Soc. Am **3**, 371, (1986)

Costello, J.T. and O'Sullivan, G. J Phys. B. At. Mol. Phys **17**, 4477, (1984).

Cowan, R D *The theory of atomic structure and spectra* University of California Press. (1981)

Epstein, G.E. and Reader, J J. Opt. Soc. Am **65**, 3, (1975)

Epstein, G.E. and Reader, J. J Opt. Soc. Am **72**, 4, (1982).

Even-Zohar, M. and Fraenkel, B S. J. Phys. B. At. Mol. Phys. **5**, 1596, (1972).

Finkenthal, M. Bell, R.E. Moos, H.W Bhatia, A.K Marmar, E.S. Terry, J L. and Rice, J E Phys. Lett **82A** 3, (1981).

Grant, I P. J. Phys. B. **7**, 1458, (1974).

Grant, I.P. McKenzie, B.J. Norrington, P.H. Mayers, D.F and Pyper, N C. Comput Phys. Commun **21**, 207, (1980).

Khan Z.A Rahimullah, K. and Chaghtai, M S Z Phys. Scr. **23**,843, (1981)

Madden, R.P and Codling, K. Astrophys. J. **141**, 364, (1965).

Mansfield, M W.D and Audley, D Private communication (1988).

Mansfield, M.W D. and Connerade, J.P. Proc Roy Soc Lond. A **342**, 421-430 (1975).

Mansfield, M W D. and Connerade, J P. Proc. Roy Soc Lond. A **344**, 303-309 (1975).

O'Sullivan, G. Costello, J T and Carroll, P K J Phys B. At.Mol.Phys. **17**, 345, (1984).

Persson, W Phys. Scr **17**, 387, (1978)

Persson, W and Wahlstron, C G Physica Scripta **30**, 169-185, (1984)

Persson, W and Reader, J J Opt Soc. Am 3, 7, (1986)
Reader, J J Opt Soc Am 65, 3, (1975)
Reader, J and Acquesta, N J Opt Soc Am. 69, 2, (1979)
Reader, J Epstein, G.E and Ekberg, J.O J. Opt Soc Am 62, 2, (1972)
Reader, J and Epstein, G E J. Opt. Soc Am 62, 5, (1972).
Shujauddin, Q Chaghtai, M.S.Z. Mushtaq, A and Tauheed, A Phys. Scr. 26, 91-96, (1982)
Suckewer, S Skinner, C.H. Milchberg, H Keane, C and Voorhees, D. Phys Rev. Lett. 55, 1753, (1985)
Wyart,J F Phys. Scr. 37, 66, (1988)
Zahid-Ali, Chaghtai, M.S.Z. and Singh, S.P. J Phys. B At. Mol. Phys. 8, 2, (1975).
Zalubas, R. Reader, J. and Corless, C.H J. Opt Soc Am 66, 35, (1976).

CHAPTER SEVEN THE XENON ISOELECTRONIC SEQUENCE

7 1 INTRODUCTION

Numerous VUV studies of the rare earth elements have been carried out in recent years both in emission and absorption. The simplest type of experiment which may be carried out is the straightforward recording of VUV absorption spectra using either thin films of the solid material or the metal vapor. Koch et al (1977) and Radtke (1979) have between them carried out studies of the elements from Z=54-68 In each case the 4d photoabsorption spectrum resulted in a giant resonance ranging in width from 70eV for the lightest (Xe Z=54) to 15eV for the heaviest (Eu with Z=68). The 4d photoabsorption spectra of compounds of many of these elements have also been studied (Dehmer and Starace 1972, Suzuki et al 1975, Connerade et al 1980 and Connerade and Pantelouris 1984).

VUV emission spectra of rare earth laser produced plasmas from solid metal targets and from solid targets made from a low Z substrate containing only a small percentage of rare earth material (≃1%) have been studied (O'Sullivan 1980, 1987) The emission spectra from the solid targets were found to be dominated by intense continuum emission (Carroll et al 1978, 1980). For those targets composed of the low Z substrate the emission spectra were found to be very different The spectra were found to be dominated by a 4d→4f unresolved transition array (UTA) approximately 10-15eV wide in the 100Å region (Carroll and O'Sullivan 1982).

The many studies of these elements using solids, vapors, compounds and laser plasmas in the VUV region have resulted in the observation of spectra for which an explanation requires consideration of the degree of

collapse of the 4f wave function Little work has been carried out on rare earth ions in absorption prior to the work reported here. The only study reported to date Ba^{+}, Ba^{2+} (Lucatorto et al 1981) resulted in an unexpected and complex spectrum which has given rise to considerable theoretical debate in the literature Following this debate and the various attempts at explanation of the Ba^{2+} result, the further extension of the xenon isoelectronic sequence in absorption to higher stages of ionization would be expected to make a valuable contribution to the understanding of the rare earths and the Xe sequence as a whole.

The work described in this chapter was concerned with attempting to record unambiguous photo absorption spectra of the third, fourth and fifth members of the xenon isoelectronic sequence, Ba^{2+} La^{3+} and Ce^{4+} Our study of these ions has been largely successful. In the case of La^{3+} and Ba^{2+} we can report the successful recording of spectra containing discrete structure in the 4d excitation region of each of these ions. The XUV absorption spectra of lanthanum laser produced plasmas were extensively studied under varying experimental conditions. A group of well defined broad discreet absorption structures in the 95Å region were found to be the principal absorption features of these spectra; an analysis of these features is presented. The observation of this particular spectrum is the first experimental data on 4d photoabsorption for La^{3+}.

The Ce^{4+} spectrum has proven the most elusive of the spectra studied along the Xe sequence However, we have been able to record the absorption spectrum of a cerium laser produced plasma, and although this spectrum is extremely weak, we have found evidence of discrete structure in the 80Å region

Some work has also been carried out on higher members of the sequence and absorption spectra of both Pr and Nd laser produced plasmas are reported here for the first

time.

The most difficult of all the elements to work with was barium, its rapid oxidation during the pumping process presented difficulties which are briefly discussed

7 2 GIANT RESONANCES AND WAVE FUNCTION COLLAPSE

Before presenting details of specific results obtained along the Xe sequence it is pertinent to discuss the atomic structure of those elements which follow xenon in the periodic table and the expected and observed nature of their absorption spectra. Many successful studies have been carried out on elements in the transition regions of the periodic table In these elements atomic d and f orbitals can make a sudden transition from being hydrogenic to being fully collapsed This transition involves a large reduction in the mean orbital radius and results in qualitative changes in those physical processes which are sensitive to orbital size, for example, photoexcitation cross sections; see for example Clark and Lucatorto (1987). The collapse of atomic orbitals is caused by a shift, as the charge on the nucleus Z increases, in the balance between repulsive centrifugal and attractive atomic forces acting on the electron. For a particular element the balance may be changed by an alteration of the core or valence orbitals or by the formation of a molecular bond These elements are therefore characterized by unusual sensitivity of gross orbital properties to external perturbations Giant resonances associated with orbital collapse are manifested in some of the principal mechanisms of excitation of transition region elements For the sake of brevity the scope of this chapter will be confined to xenon and the elements which follow it in the periodic table.

Lukirskii and Zimkina (1963) and independently Ederer

(1964) and Haensel et al (1969) studied the photoionization continuum of xenon above the 4d threshold. Prior to these experiments it had been thought that continuous absorption should decrease uniformly with increasing energy after the initial rise just above the threshold. Ederer (1964) found that there was little absorption immediately above the threshold but that the absorption rose to a peak some 30eV higher and then fell away. The effect was described as the *delayed onset* of continuous absorption. An early explanation was provided by Cooper (1964) in terms of the independent particle model. He pointed out the importance of the angular momentum potential barrier for the out going $\ell=3$ electron. The effect of the $\ell(\ell+1)\hbar^2/2mer^2$ term in the Schrodinger equation makes the atom seem to possess a *hard* center which tends to keep electrons with $\ell>0$ away from the core. At threshold the continuum wave function hardly penetrates the core and as a result the spatial over lap between the initial and final state functions is very small. As the kinetic energy of the out going electron increases its ability to penetrate the barrier increases and the overlap becomes larger. Numerous examples of delayed onset have been observed by several groups using synchrotron radiation. In fact it has been observed that any atom in which a high angular momentum channel can be reached by photoabsorption will exhibit some form of delayed onset, (Connerade 1978).

The formation of the neutral rare earth elements is due to the filling of the 4f shell. The first attempt at explaining why the filling of successive subshells should suddenly transfer to an inner subshell of the atom for certain values of atomic number was first made by Goeppert Mayer (1941). She pointed out that the properties of these atoms depend on the sudden decrease in energy and size of the 4f wave function at the beginning of this group of elements. This is known as the collapse of the 4f orbital and has been discussed above. The effective potential is determined by the atomic central potential $V_{Coulomb}(r)$ and the centrifugal term

$\ell(\ell+1)\hbar^2/2mer^2$ and is given by the equation

$$V_{eff}(r) = V_{Coulomb}(r) + \ell(\ell+1)\hbar^2/\ 2mer^2 \qquad \text{Eq.(7.1).}$$

For f electrons of heavy atoms such as the rare earths $V_{eff}(r)$ consists of two potential wells separated by a potential barrier, the so called *double valley potential*

Fig.(7.1) below shows a schematic diagram of such a double valley potential, the sketch is divided into different regions where the electron experiences different forces acting upon it.

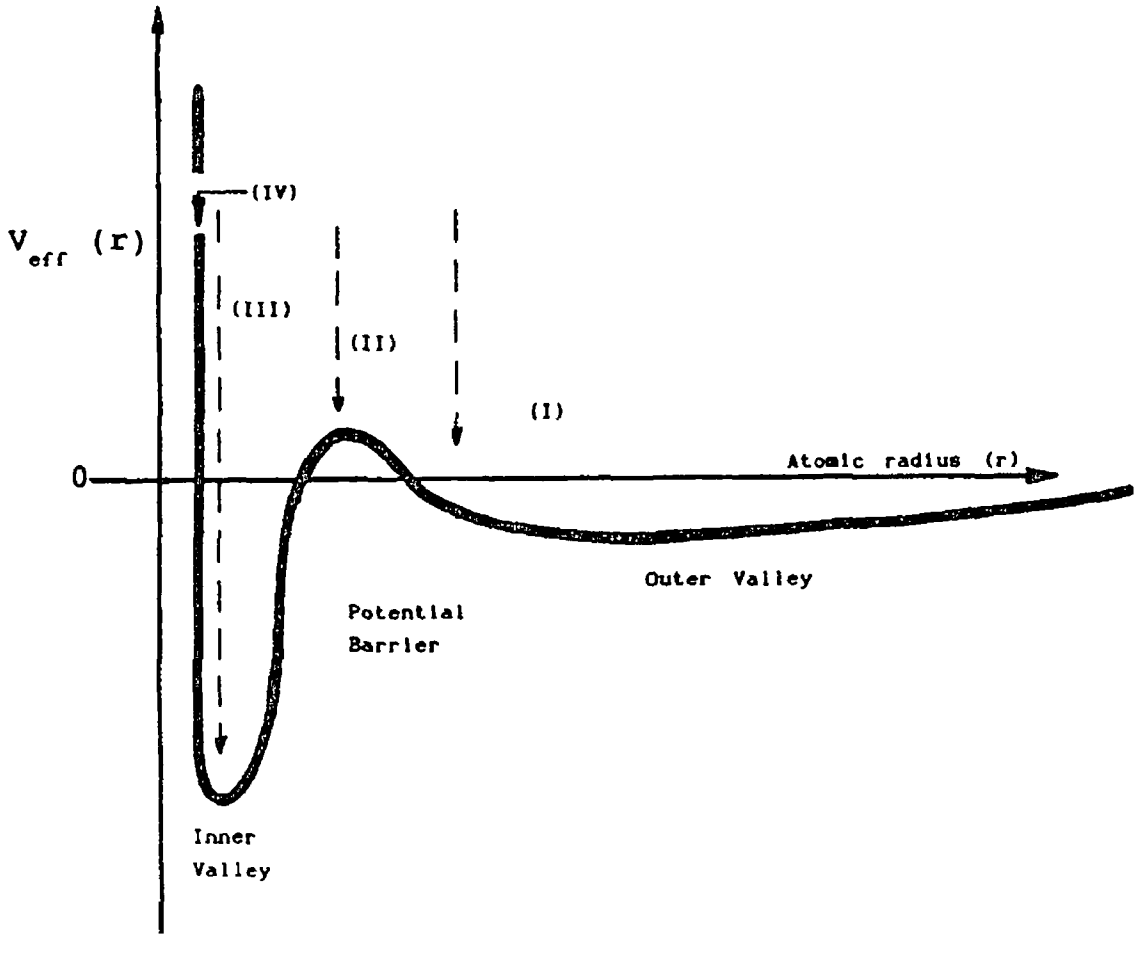

FIG (7 1)
Shows schematic representation of a double valley potential and the division into different regions dominated by different terms (Not to scale see text)

The discussion of the effective potential of the rare earth elements given below follows the treatment of Connerade (1978) and more recently that of Mansfield

(1987). The regions of the effective potential I, II, III and IV are described below. The exact form of the effective potential for any arbitrary atomic structure can be established by a calculation but may differ substantially for different configurations of the same atom. However, assuming that $V_{eff}(r)$ roughly takes the form shown above in Fig (7.1) then we may state the following Starting from large values of r, and moving towards the nucleus we first encounter the shallow well region (region I the outer valley). In this first region the potential is dominated by the Coulomb term for the Z-1 electrons in the field of which an outer electron moves. Further inwards the repulsive centrifugal term of the effective potential $\ell(\ell+1)\hbar^2/2m_e r^2$ takes over and $V_{eff}(r)$ rises sharply (region II, the outer centrifugal rise) The electron then begins to penetrate the atom and screening drops sharply so that the electron is exposed to a much stronger nuclear field (region III, the penetration of screening). However, because of the fast increase of the $1/r^2$ dependence at small values of the atomic radius, the repulsive term takes over again and dominates $V_{eff}(r)$ at small r (region IV, the inner centrifugal rise). The outer well is broad and shallow and is therefore capable of supporting a Rydberg series of nf bound states The inner well, on the other hand, is much narrower and deepens with increasing nuclear charge. For lighter elements it is not deep enough to support any bound state and all nf wave functions reside in the outer well. The first bound state of the inner well for f electrons in neutral atoms appears near Z=58, leading to sudden collapse of the 4f wave function from the outer into the inner well

Over the years there have been many studies of both atoms and ions with Z=54→70 in the region of the 4d→nf,εf excitations; see for example, Connerade (1978), Karazija (1981), Lucatorto et al (1982), Mansfield (1987) and O'Sullivan (1987) The spectra are characterized by strong absorption peaks above the 4d ionization limits with widths ranging from 15→70eV and also by weaker

absorption lines in the discrete excitation region For lighter elements in the group such as neutral xenon which has been studied extensively in the XUV and is well understood, (Hansen 1980, Wendin and Starace 1978, Zangwill and Soven 1980) the potential barrier keeps low energy f orbitals outside the region where the 4d wave functions are confined. As a result the peaks in the observed absorption spectra arise from delayed onsets of 4d→f transitions which become intense only at energies high enough for the final state f electrons to surmount the potential barrier, (Cooper 1964) For the heaver elements following xenon (Z≥56) the explanation of the observed absorption spectra becomes more complicated. Since for these elements the inner well is deep enough to hold the collapsed 4f orbital, the overlap between the 4d and 4f orbitals should increase dramatically, while the overlap between the 4d and higher nf orbitals remains small because the potential barrier still acts to prevent low energy f wave functions from entering the inner region Thus the spectra should exhibit delayed onsets of photoionizations, but in addition there should be strong absorption features due to 4d→4f transitions, but these are not observed Their absence from the observed spectra is generally explained as being due to the raising of the $4d \rightarrow 4f\,^1P$ discrete level into the f continuum as a result of strong exchange effects (Dehmer et al 1971). The strong giant resonance peaks above the ionization limits in the observed spectra are interpreted as evidence of a strong interaction between the $4f\,^1P$ level and the continuum.

7 3 THE XENON LIKE SEQUENCE PREVIOUS WORK

Along the xenon isoelectronic sequence the inner well is expected to become deeper and deeper with increasing nuclear charge. At some point, the inner well should be deep enough to support a bound state of its own and the 4f orbital is therefore collapsed into it. As a result of

this the xenon sequence is of considerable theoretical interest at the present time It was the observation by Lucatorto et al (1981) of the 4d absorption spectra of the isonuclear sequence consisting of Ba, Ba^{+} and Ba^{2+} which renewed interest in the xenon sequence The VUV photoabsorption spectra of the 4d subshell in the Ba isonuclear sequence observed by Lucatorto et al (1981) is shown in Fig.(7.2) They found that the spectra of Ba and Ba^{+} showed typical strong absorption peaks above the 4d ionization limits and weak resonance lines below them The spectrum of Ba^{2+} on the other hand was found to be entirely different. The absorption cross section for Ba^{2+} starts from a sizable value (approximately 30Mb) at the 4d threshold and decreases monotonically afterwards (up to about 160eV). At the same time, several strong resonance lines appear in the discrete excitation region The sudden change in the spectra from Ba^{+} to Ba^{2+} is clearly related to the collapse or degree of collapse of the 4f orbital. However, a detailed interpretation of this spectrum presented considerable theoretical difficulty. The experimental and theoretical work which has been carried out to date is discussed below.

The Ba^{2+} spectrum was recorded using the technique of resonant laser driven ionization (RLDI). It is appropriate here to give a brief outline of the technique and specific experimental conditions under which the barium isonuclear sequence spectra were obtained The RLDI technique produces large populations of ions by irradiating a dense atomic vapor (10^{15}atoms cm^{-3}) with a

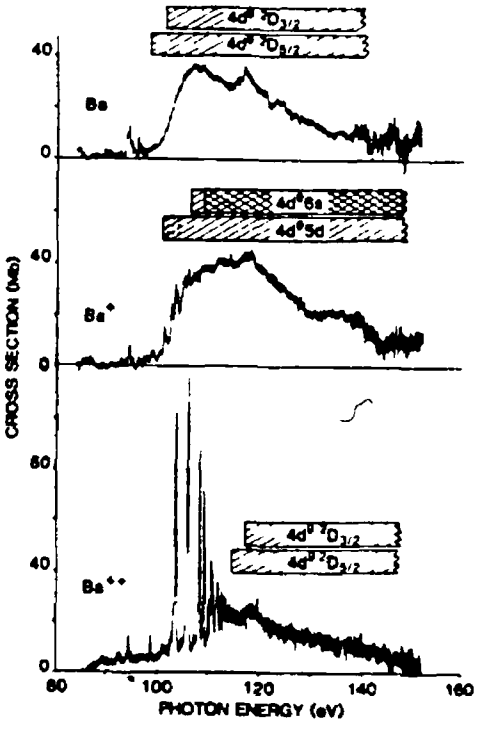

FIG (7 2)

Shows the photoabsorption spectrum of the isonuclear sequence Ba, Ba^{+} and Ba^{2+} in the 80 to 160eV range. Plotted are cross sections of the photoexcitation of a 4d electron along the sequence. The striking difference in the Ba^{2+} spectrum indicates a partial contraction of the 4f orbital. (after Lucatorto et al 1981)

long pulse ($1\mu s$) laser tuned to an atomic resonance transition; the technique has been discussed previously in chapter one. The neutral barium spectrum of Fig (7.2) was recorded by photographic measurement of the absorption of VUV radiation by a column of barium vapor produced in a heat pipe oven. The spectrum of Ba^{+} was recorded by delaying the VUV pulse with respect to a pulse from the dye laser tuned to the 553 7nm resonance line of Ba ($6s^2\ ^1S \rightarrow 6s6p\ ^1P$) which completely ionized the barium vapor. A second laser tuned to the 493.5nm resonance line of Ba^{+} ($6s^2S \rightarrow 6p^2P$) produced virtually complete ionization of the Ba^{+} column. The absorption spectrum of Ba^{2+} was thus observed by firing the VUV pulse after the two dye laser pulses

The RLDI technique has the advantage of permitting

measurements on ground state, excited state and ionized species using the same apparatus The technique has the considerable disadvantage of not being applicable to ion stages higher than 2+. The lack of short wavelength laser technology prevents this. Therefore the extension of absorption studies along the Xe isoelectronic sequence to La^{3+} and Ce^{4+} could not be carried out using the RLDI technique in its present form.

The absorption spectrum of Ba^{2+} differs from that of the neutral atom and Ba^{+} in that there is still a strong feature in the continuum but a major part of the absorption strength has moved into the bound region (Fig.7 2) This has been interpreted as evidence for the collapse or partial collapse of the 4f wave function between Ba and Ba^{2+} therefore leading to better overlap between 4d and nf with larger dipole matrix elements as a consequence The theoretical interpretation of the Ba^{2+} spectrum has been the subject of a great many publications since its observation. Most theoretical work carried out has focused on the experimental results (i.e, the Ba^{2+} spectrum) or on the expected behaviour of the 4d photoabsorption cross section further along the Xe I sequence This work is reviewed in what follows

While the sudden change in the spectra observed in moving along the Ba isonuclear sequence appears to result from orbital collapse occurring for Ba^{2+}, the interpretation of these observations was not very clear According to earlier discussions on the collapse phenomenon in rare earth atoms (Dehmer et al 1971, Wendin and Starace 1978), even after the 4f orbital is collapsed transitions to higher nf levels (n≥5) remain suppressed by the potential barrier. As a result Lucatorto et al (1981) expected to see in their 4d photoabsorption spectrum of Ba^{2+} only one strong line associated with the $4d^{9}4f^{1}P$ level and not four lines as were observed. Based on a configuration average Hartree Fock (HF) model they showed that the $4d^{9}4f^{1}P$ level was below the ionization threshold, and interpreted the Ba^{2+} spectrum as being due to the partial

collapse of the 4f orbital. This partial collapse view was also supported to a certain extent by Connerade and Mansfield (1982) who suggested that the $4f^1P$ level exhibits a *"collapse of the second kind"* and that the nf wave functions are hybridized (i.e., that they contain comparable amplitude in both outer and inner wells) resulting in strong absorption from $4d \rightarrow nf^1P$ transitions. However, contrary to the results of Lucatorto et al (1981) their configuration interaction (CI) results showed that the $4f^1P$ level was imbedded in the continuum They gave the energy of the $4d^9 4f^1P$ state of Ba^{2+} as 118 4eV which is higher than the experimental $^2D_{5/2}$ and $^2D_{3/2}$ threshold energies of 114 7eV and 117.2eV respectively given by Lucatorto et al (1981) They concluded that the observed resonance lines actually come from $4d \rightarrow 5f, 6f \ldots ^1P$ transitions.

Kelly et al (1982) calculated the photoionization of the 4d subshells of Ba and Ba^{2+} using a Hartree-Fock approximation with and without the inclusion of relaxation effects. They concluded that Hartree-Fock calculations can give reasonable photoionization results for a complicated system such as the $4d^{10}$ subshell of barium They also suggested that relaxation effects can in cases such as neutral barium be very important in cross section calculations. Nuroh et al (1982) performed calculations for the photoabsorption spectra of Ba, Ba^+ and Ba^{2+} near the 4d ionization threshold using the time dependent local density approximation, these calculations provided results which were in quantitative agreement with the experimental data of Lucatorto et al (1981). The results of Nuroh et al also suggested that the sharp resonant structures below threshold in Ba^{2+} are due to transitions to hybridized f states which are strongly modified by electron electron interactions, which is consistent with the term-dependent Hartree Fock calculations of Connerade and Mansfield (1982), but they were able to predict the detailed spectral distribution Kucas et al (1983) used a Hartree Fock model to study the 4d photoabsorption spectrum of Ba^{2+} and showed that the

strong absorption lines in the spectrum of Ba^{2+} correspond to excitations of a 4d electron in the Rydberg nf series

Calculations have also been carried out for higher members of the sequence. As one progresses further along the Xe sequence with increasing ionization, these calculations (Cheng and Froese Fischer 1983, Cheng and Johnson 1983) predict that the oscillator strength will be concentrated in the $4d^{10} \rightarrow 4d^9 4f\ ^1P$ transition with the result that basically only one very strong line should be observed in the bound region, the situation is illustrated in Fig (7.3). These calculations further predicted that the continuum absorption should be very weak Cheng and Froese Fischer (1983) considered the collapse of the 4f orbital for xenon like ions in the region of the 4d→nf, εf excitations also using a term dependent Hartree Fock technique They have found the 4f orbital to be strongly term dependent. In particular they found that for Ba^{2+} the 4f orbital is collapsed in the $4d^9 4f\ ^3P$ and ^3D states but that it is only partially collapsed for the ^1P state. They concluded that the appearance of intense absorption lines in the observed spectrum of Ba III is due to the partial collapse of the 4f orbital in the $4d \rightarrow f\ ^1P$ channel. The analysis was extended to include other ions of the xenon isoelectronic sequence and theoretical absorption spectra were generated for the sequence from Xe to Nd^{6+} The calculated spectra of Fig.(7 3) show that after the 4f orbital has completely collapsed for high degrees of ionization along the isoelectronic sequence the bulk of the absorption oscillator strength is expected to be concentrated in the $4d \rightarrow 4f\ ^1P$ transition. Cheng and Johnson (1983) used the relativistic random phase approximation to study photoionization of the inner 4d shells of Xe, Cs^+, Ba^{2+} and La^{3+}. They calculated total cross sections, partial cross sections, branching ratios and angular-distribution asymmetry parameters and studied their systematic trends along the Xe sequence

The most successful calculation of the Ba^{2+} spectrum to date is that published by Clark (1984) (see also Clark and Lucatorto 1987) who carried out a type of multiconfigurational HF calculation including spin-orbit interaction with some correlation in the initial and final state. His work has revealed that the role of true

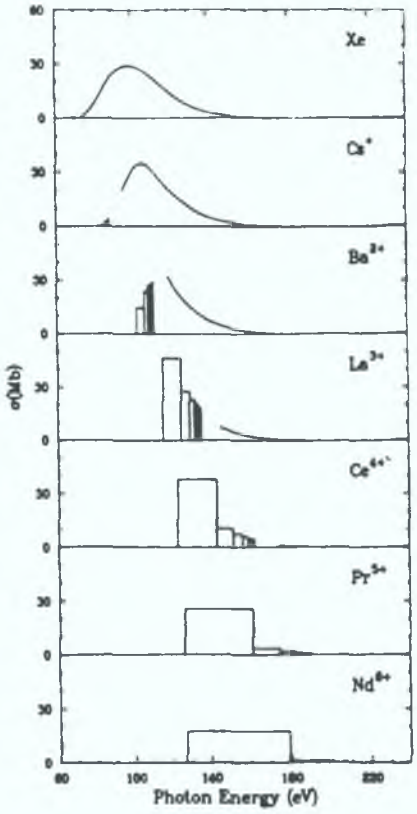

FIG.(7.3).

Shows theoretical absorption spectra for the first seven members of the xenon-like sequence. The rectangles represent the effective oscillator strength distributions of Cheng and Froese Fischer (1983) and the 4d→nf ^{1}P transitions (n=4-9). The continuum cross sections are random phase approximation results of Cheng and Johnson (1983).

collective effects in the 4d photoabsorption spectrum of Ba^{2+} is minor. His analysis showed that the most significant departures from independent particle behaviour are in fact due to correlations involving the 5p not the 4d shell, their importance is magnified by the delicate balance of opposing single particle forces. His re-evaluation of ionization limits revealed the presence of Beutler Fano structures in the experimental data of Lucatorto et al (1981).

7 4 THE XENON LIKE SEQUENCE PRESENT WORK

Our primary motivation in studying the absorption spectra of La^{3+} and Ce^{4+} was the work of Lucatorto et al (1981) It was clear from that work that the RLDI technique could not be applied to record the 4d absorption spectra of these higher members of the Xe sequence It was also clear from the theoretical discussions in the literature that the Ba^{2+} spectrum was not entirely understood and that similar spectra of La^{3+} and Ce^{4+} if observed would be a useful extension to the available experimental data for the Xe sequence and might serve to shed some light on the Ba^{2+} case. Our studies were carried out along the isoelectronic sequence; in this way systematic trends in the photoabsorption spectra are not complicated by the change in the electronic structure, as would be the case for an isonuclear sequence.

7.4.a) The Ba III spectrum.

The first element studied in absorption was lanthanum This element is harder than barium and oxidizes less rapidly, and so was an ideal candidate for use as an absorber target in the experimental arrangement described in chapter two Experiments using the flat target and later the rotating target configurations were carried out using lanthanum targets In the spectra obtained using both target variations we observed the presence of a series of discrete structures in the 95Å region Examination and measurement of these features suggested that they might be analogous to the Ba^{2+} features reported by Lucatorto et al (1981) It was also clear that a barium plasma should be studied in an attempt to provide an isoelectronic comparison and to reproduce the spectrum of Ba^{2+} recorded with the RLDI technique. The detailed discussion of the absorption spectra recorded here is given in order of increasing atomic number the discussion therefore beginning with a description of the work carried out using barium targets.

The barium experiments:

We have recorded numerous plates containing absorption spectra of barium laser produced plasmas These spectra were recorded using the flat and rotating target configurations outlined in previous chapters and which employed various degrees of de-focusing of the cylindrical lens used to create the absorbing column of Ba ions Two different continuum producing targets (tungsten and hafnium) were also used during this work It should be noted here that throughout the work described in this chapter the lenses used were either plano spherical or plano cylindrical and were of 6cm focal length.

Each of the Ba absorption spectra recorded during this work was found to be extremely weak and throughout the work this weakness in the Ba spectra persisted regardless of experimental conditions. The only common feature in each of the Ba spectra recorded was the observation of the strongest pair of lines in the 105eV region which were assigned (Lucatorto et al 1981, Clark 1984) to the $4d^9 4f\,^1P$ and $4d^9 5f\,^1P$ in Ba^{2+} respectively These two lines were seen as outstanding features in the absorption spectra of Lucatorto et al (1981). The various absorption spectra of barium laser produced plasmas recorded here may be loosely categorized into two distinct groups. On the one hand, we have those spectra of Ba^{2+} which show the four strong features observed by Lucatorto et al (1981), an example of this is shown in Fig (7 4) The features of this spectrum are in agreement with the original Ba^{2+} work. On the other hand, we have produced many absorption spectra of barium laser produced plasmas containing Ba^{2+} in which apparently only three members of this strong quartet of lines are observed to be present The most intense example of this second type of Ba^{2+} spectrum is shown in Fig.(7 5)

TABLE 7 1

Discrete features in the 4d→nf region of the Ba III absorption spectrum.

$E^{TW}_{(eV)}$	I(Arb Uts)	$E^{a,b}_{(eV)}$	Level*	gf Value*
103.16	2 0	.....	. ....	....
103.65	10 0	103 68[a,b]	$4d^9 4f^1P$	0.539
105.49	5.0	.. ...	. ..	. ..
106 02	10 0	106 06[a,b]	$4d^9 5f^1P$	0 555
106.56	2.0	. .	.	. ..
106.76	5 0	. ...	...	...
. .	..	107 22[b]	$4d^9{}_{5/2}\ 6f_{5/2}$	0 022
107 37	2.0	.	.	.
. ....	..	107.75[b]	$4d^9{}_{3/2}\ 7p_{1/2}$	0 0083
. ..	...	108.36[b]	$4d^9\ 6f^1P$	0 341
108 44	2.0	..		..
108.63	5.0	.	.. .	
109 24	2 0	109 24[a,b]	$4d^9 7f^1P$	0 207
. .	.	110 26[a,b]	$4d^9 8f^1P$	0 111
. .	.	110 60[b]	$4d^9{}_{3/2}\ 6f_{5/2}$	0 196
.	. .	110 90[a,b]	$4d^9{}_{3/2}\ 7f_{5/2}$	0 140
.. .	.	111 91[a]	.	. .

I = Intensity taking the strongest line as 10 0 and were estimated from a photographic print

TW are experimental values of this work

a,b are experimental values of Lucatorto et al (1981) and of Clark (1984), who re-evaluated the original data

* assignments and oscillator strengths of Clark (1984)

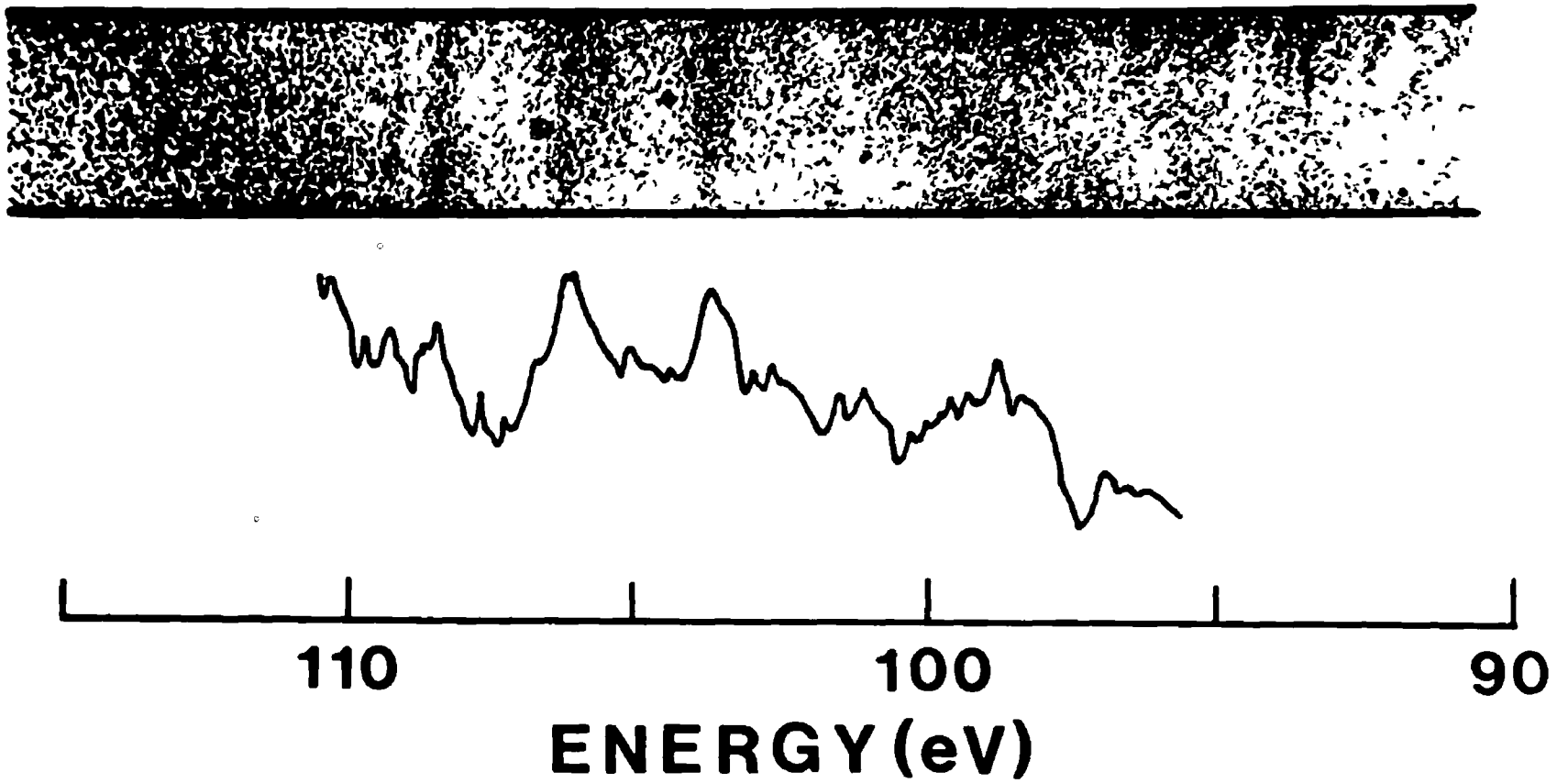

FIG 7 4

Absorption spectrum of Ba^{2+} showing the four principal features of the 4d→nf absorption. Below is shown a densitometer trace. (See text).

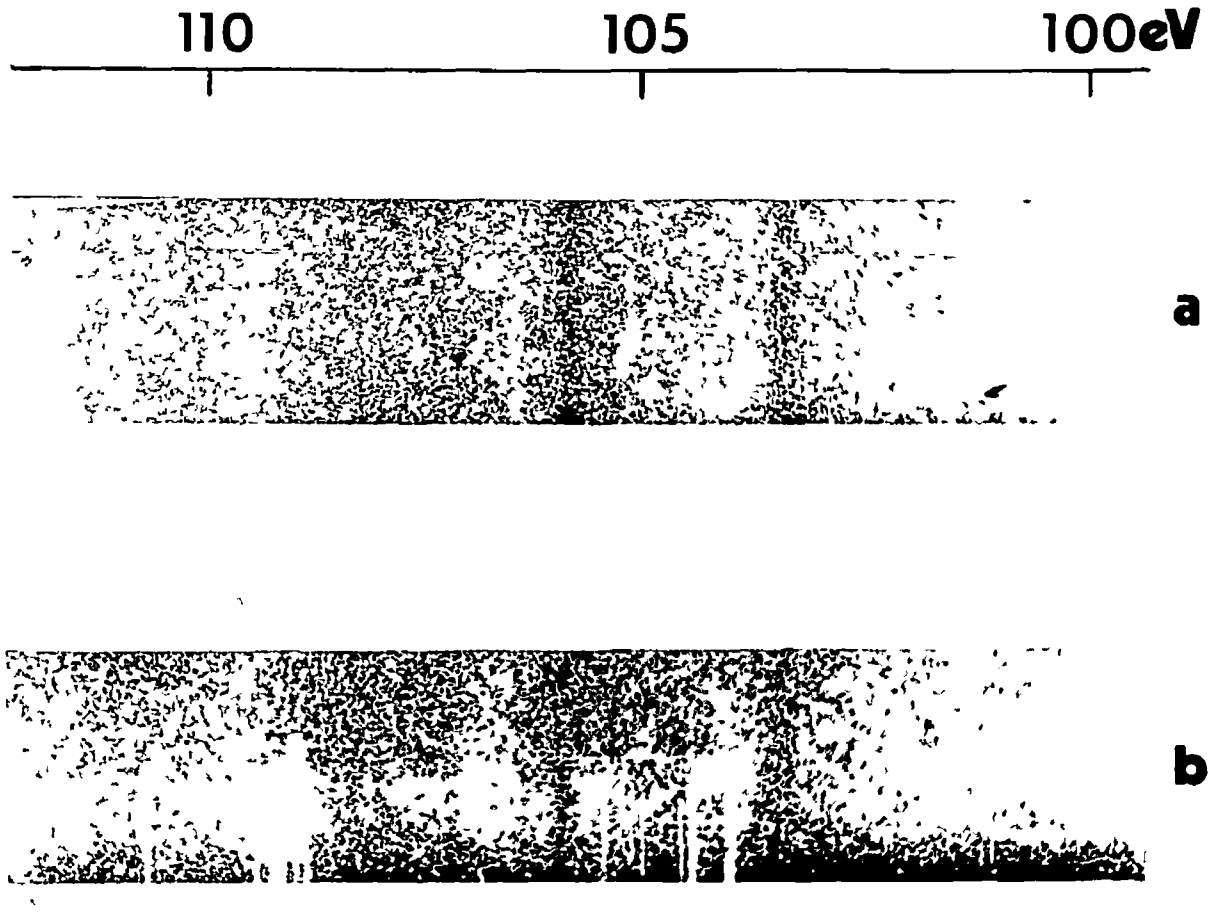

FIG 7 5

Two spectra showing strong Ba^{2} absorption (See text)

In their paper Lucatorto, et al list thirteen lines observed between 94.0 and 114eV. The strongest of these lines being at 103.68, 106.06, 108.36 and 109.24eV. These four lines are particularly strong and have been assigned to $4d^{10} \rightarrow 4d^{9}4f,5f,6f$ and $7f\,^{1}P$ transitions in Ba^{2+}.

The absorption spectrum of Ba^{2+} shown in Fig.(7.5) shows most of this discrete structure to be present. However, the intensity of the features is considerably weaker than the RLDI spectrum shown in Fig.(7.2). Fig.(7.5) is by far the most intense spectrum of Ba^{2+} of either type which we have recorded. The main features of the spectrum are expected to be the four particularly strong discreet features reported previously. However, our spectrum shows only three of these lines as strong features the feature listed by Lucatorto et al (1981) as being at 108.36eV is conspicuously absent from our spectrum.

The missing feature has been assigned (Clark 1984) to the $4d^{10} \rightarrow 4d^{9}6f\,^{1}P$ transition in Ba^{2+} and has a calculated oscillator strength (Clark 1984) of 0.341 while the line located at 109.24eV and listed in the same work as the $4d^{10} \rightarrow 4d^{9}7f\,^{1}P$ with a calculated oscillator strength of 0.207 is apparently visible in the spectrum of Fig.(7.5). This clearly represents a puzzle as to why the n=7 member of a Rydberg series should be visible in an absorption spectrum when the n=6 member is absent.

In an effort to explore this anomaly the spectrum shown in Fig.(7.5) was measured carefully. Because of the relative weakness of this particular plate when compared with those plates reproduced in chapter's three and four the measurements were carried out using an enlarged photographic print of the region between 89.0 and 114.0eV. The dispersion of the photographic print was sufficiently large to allow an error in the measurements of the features of ±0.05eV to be quoted. Every absorption feature in the region was measured and the results are presented in table 7.1 above along with a list of

measured features given by Lucatorto et al (1981) and assignments based on the reevaluation of the original data and subsequent analysis of Clark (1984). A total of seventeen absorption features of varying intensity and width have been observed in this energy region. For those features common to the work reported here and to the measurements of Lucatorto et al (1981) and Clark (1984) good agreement has been found

A close inspection of the energy region where the missing $6f\,^1P$ feature should be reveals that at the position of 108.36eV there is no feature However there are two sharp and weak lines in the immediate region of the missing resonance. These lines have been measured at 108 44eV and 108 63eV There are also other lines of various intensities which have been measured throughout the energy range 94-114eV and which do not correspond to measured features in the Ba^{2+} spectrum of Lucatorto et al (1981) Comparison with absorption spectra of laser produced plasmas of other materials also obtained using a hafnium continuum reveal that the extra features in the region are not continuum lines The conclusion must therefore be that the spectrum contains absorption features from the higher ion stage Ba^{3+} Following the trend of the Ba isonuclear sequence absorption features in the 4d spectrum of Ba^{3+} are expected to be found in the same energy region A tentative suggestion put forward to explain the absence of the $4d^9 6f\,^1P$ feature in the Ba^{2+} spectrum is to assume that each of the features seen in the spectrum of Fig.(7 5) at energies higher than the Ba^{2+} $4d^9 5f\,^1P$ resonance in fact originate in the higher stage Ba^{3+} ion An explanation of the apparent disparity in the strengths of the 6f and 7f features in Ba^{2+} might be that coincidence of a Ba^{3+} absorption feature with the $4d^9 7f$ resonance of Ba^{2+} enhances this weak feature but due to the lack of a similar feature coinciding with $4d^9 6f$ resonance, this line because of its low oscillator strength, is not observed above the background on the plate It may also be said here that it was found to be particularly easy to ionize barium Even

with a weakly focused laser beam large populations of barium ions are created, the spectrum shown in Fig (7.4), which most closely resembles the original result of Lucatorto et al was recorded with an extremely de-focused laser beam (df≈2-3cm) used to create the absorbing plasma. The spectrum of Fig (7.5) was recorded using a much less de-focused laser beam, in which case there was not a sufficient path length of Ba^{2+} ions to enable the weaker members of the nf series to be observed in the spectrum, this further strengthens the above argument

Experiments performed along this sequence were in general found to be difficult to carry out and on average there was a poor success rate when compared to other absorption studies. Barium was the most difficult material to work with. The Ba spectra were recorded using both flat target and rotating target configurations The spectrum shown in Fig (7 5) was acquired using the flat target set up The barium target was extremely difficult to work with, it tarnishes rapidly in air and even in the vacuum used which was normally better than 10^{-4}torr, builds up a thick oxide layer This build up of oxide was the result of the time taken to evacuate the system to the working pressure Barium is also an extremely soft target and suffered considerable surface damage even with a de-focused laser beam resulting in comparatively large amounts of debris being thrown back from the target surface onto the inner surface of the glass window of the target chamber The rapid oxidation and softness of the barium target surface may well account for the relatively poor success rate of the barium absorption experiments

The net result of the physical nature of the barium target was that the inner surface of the target chamber window became coated with a film of barium oxide and as the experiment progressed this window became opaque taking on the appearance frosted glass The effect of this was to reduce the intensity of each portion of the incident laser beam reaching the targets. The intensity of that portion of the laser beam focused by the

spherical element of the lens combination passing through the glass was high enough to almost totally clean a path through to the continuum producing target and was thus un-affected by the oxide layer. That portion of the incident laser beam directed to the barium target by the cylindrical element was severely attenuated. This drop was noticeable by eye even after fifty shots while the intensity of the continuum remained almost constant Thus with little or no intensity in the absorber target beam after say fifty shots we effectively had no absorbing plasma being created on the barium target surface. The effect on the photographic plate used in recording the spectra was to swamp any information recorded in the early stages of the experiment Under these conditions we would expect to find either no absorption spectrum at all (which was common) or a very weak affair with the less intense members of the discrete structure missing, this result was equally common.

The use of two spherical lenses was employed in the hope that the intensity of both portions of the laser beam would be equalised at the inner surface of the target chamber window. However, for barium we found that a well focused laser beam on the surface resulted in considerably more target damage and a far more attenuated beam reaching both targets Also this lens configuration required de-focusing of the beam in order to obtain a sufficient density of Ba^{2+} in the absorbing plasma. This again led to the problem of different intensities of the incident laser beam at the inner surface of the target chamber window as before It is the consideration of this author that the experimental arrangement used to obtain the absorption spectrum of La^{3+} is not suitable for the recording of the analogous Ba^{2+} spectrum Recording of this spectrum will require a radical re-design of the existing target chamber set up.

7.4.b). The La IV spectrum.

Lanthanum has been extensively studied over the course of this work and many strong absorption spectra of laser

produced lanthanum plasmas have been obtained. The most detailed of the spectra recorded to date is shown below in Fig (7 6) which was recorded using the rotating target arrangement described in chapter two. It is however, pertinent to outline the precise details of the arrangement used to record the La^{3+} spectrum. A hafnium or tungsten target was used to yield the hot plasma which acted as the source of background continuum while a 5mm long line focus was formed on an adjacent lanthanum target by using the cylindrical element of the lens combination. The resulting spectra were recorded photographically on the 2m grazing incidence spectrograph using SWR plates.

The lanthanum absorption spectrum was found to contain a number of discrete features which were assumed to be analogous to the Ba^{2+} features observed by Lucatorto et al (1981) and discussed above. The observation of rare gas like ions as the dominant ionization stages in laser produced plasmas has been discussed in previous chapters of this thesis, and has been a feature of the absorption studies throughout this work, (see chapter four). It was thus reasonable to assume that the predominant absorbing species in the lanthanum plasma was La^{3+} The series of experiments carried out on barium targets also supported the assumption that the dominant ion within the lanthanum plasma was La^{3+}. To further check this point the focusing conditions of that portion of the incident laser beam on the lanthanum target were varied by changing both the lens type (i.e , both cylindrical and spherical lenses were used) and the lens to target distance In these experiments it was found that the discrete features displayed the same behaviour i e. they either grew or diminished in intensity as a group. The spectrum of Fig.(7 6) shows a group of discrete features in the 95Å region which are entirely analogous to the Ba^{2+} structures discussed above. Six strong features and several other weaker features are seen in this area of the spectrum The energies of the lines in this region are presented in table 7.2.

TABLE 7 2

Identification of features in the La^{3+} spectrum. LS coupling is used to label the levels but most of the configuration labels have little significance, see text. Intensities are visual estimates. Only transitions with the gf value of more than 0.01 are included.

Transition $4d^{10}\ ^1S_0 \rightarrow 4d^9nl\ J=1$	E_{calc} (eV)	gf	FWHM (eV)	$E_{obs.}$ (eV)	Intensity.	gf[a]
4f ^3D	102.8	0.02	0 018			
6p ^1P	117.3	0.01	0 004[b]			
4f ^1P	121.0	3 98	1 4	-		4.315(4f)
5f ^3D	125.7	0 88	0.36	125.1	10	
7p ^1P	126.3	0.05	0 002[b]	126 0[c]	0-1	
5f ^1P	128.2	0.76	0.31	127 6	8	1.297(5f)
7p ^1P	129 0	0.02	0 0005[b]	128.8	1	
6f ^3D	130 4	0 36	0 20	129.7	10	
8p ^1P	130 4	0.60	0.22[b]			
7f ^3D	132.1	0 01	0.004	131.7[c]	0-1	
6f ^1P	133.0	0.51	0.25	132.5	8	0.591(6f)
8p ^1P	133 1	0.03	0 003[b]			
8f ^1P	134 0	0 32	0 16	133 65	6	0 321(7f)
9f ^1P	134 0	0 02	0 011			
7f ^1P	135.2	0 16	0 086	135.25	4	0 194(8f)
10f ^1P	135.7	0.28	0.16		5	0.127(9f)

a) Cheng and Froese Fischer (1983). No spin-orbit interaction included. The configuration label in parentheses.

b.) The decay of np basis states has not been included

c.) Weak feature only observed on some plates.

d) Feature possibly double.

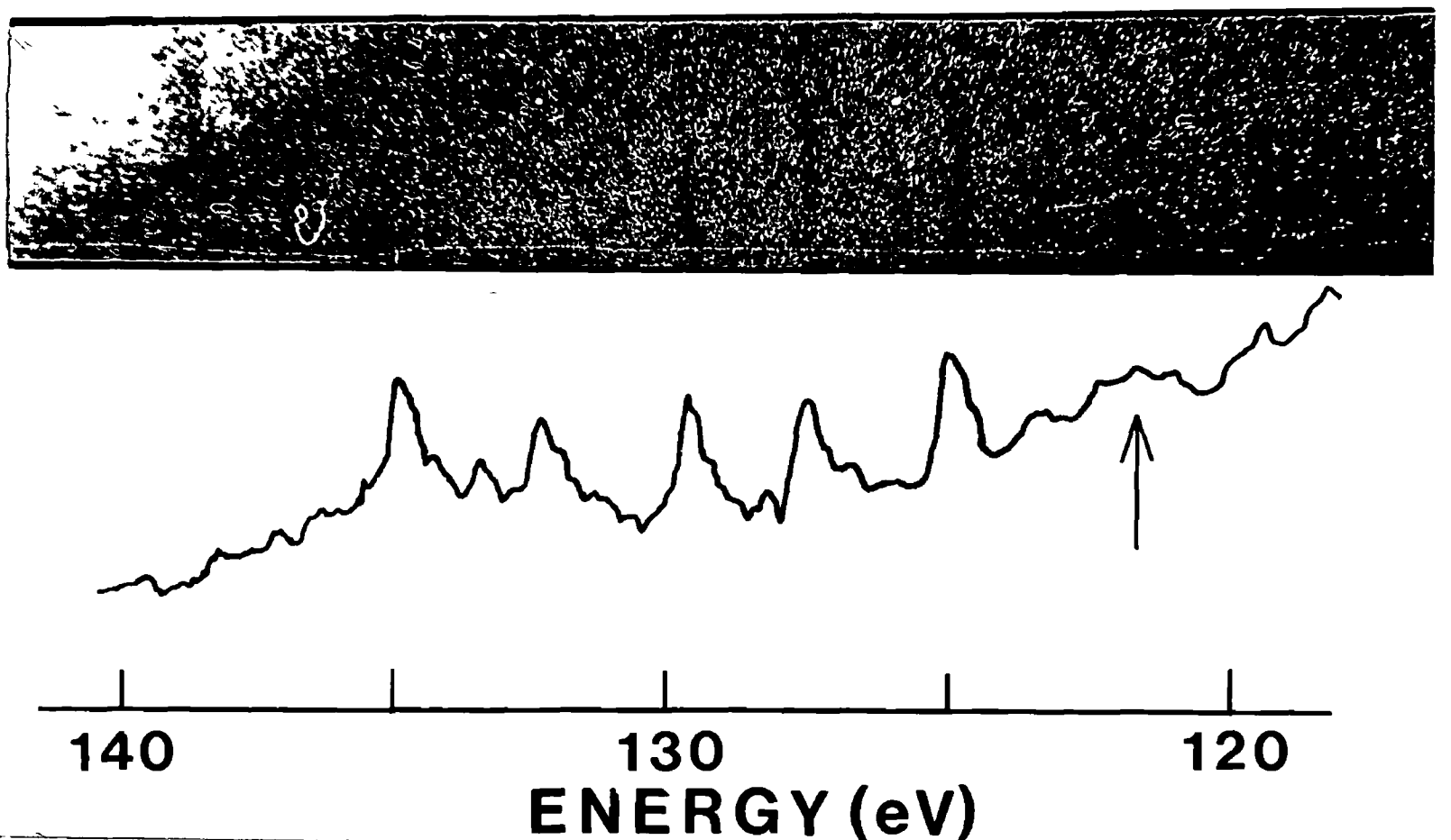

FIG 7 6

The absorption spectrum of a lanthanum laser produced plasma showing strong absorption in the La IV ion, (see text)

The analysis of the La IV spectrum which is presented here was carried out at the Zeeman Laboratory (Amsterdam) by Prof. J.E Hansen and has recently been published (Hansen, Brilly, Kennedy and O'Sullivan 1989), with the precise calculational details expected to follow in the near future, Hansen (1990).

To interpret the La^{3+} spectrum he carried out calculations of the energy level positions and intensities using the suite of programs written by Cowan (1981). The energy level positions and oscillator strengths were determined in a CI calculation using a discretized continuum (Cowan: Chapter 18). Calculations were carried out for Ba^{2+} in order to test the quality of the approach subsequently applied to La^{3+}. A number of bound $4d^9 5s^2 5p^6 \varepsilon f$ HF(E_{av}) and np functions as well as continuum $4d^9 5s^2 5p^6 \varepsilon f$ HF(E_{av}) functions were used as basis states in an expansion which gave energy levels and oscillator strengths for the transitions $4d^{10} \rightarrow 4d^9 nf/np$ using a HF calculation for the ground state. Good agreement was obtained with the calculation due to Clark (1984) as well as with the experiment of Lucatorto et al (1981), with regard to both energy level positions and intensities keeping the accuracy of the photographic plate as an intensity detector in mind.

The leading eigenvector components are all rather small in this basis and, in particular, no level has a large 4f(E_{av}) (collapsed) component (the lowest f ^1P level has a 4f(E_{av}) component of less than 0.1). One consequence is that no oscillator strength is particularly large. This can also be seen from the fact that the nominally weaker transitions to np states are of roughly the same strength. Another consequence will be discussed later. Table 7.2 shows the results of the equivalent calculation for La^{3+} compared to the experimental results. The labels used in Table 7.2 are the largest LS component in the particular level. Many of these are much smaller than 50% and have therefore little significance. This can also be seen from the apparently random order of the higher nf ^1P

labels (see also Clark 1984) The lowest f ^{1}P state here has a dominant 4f(E_{av}) (collapsed) component of 50% with an associated oscillator strength of 4 0 This indicates that the interaction with the εf continuum is less important in La^{3+} and that a limited CI expansion consequently should be more accurate than in Ba^{++}. We also note that the gf values are in quite good agreement with those determined by Cheng and Froese Fischer (1983) using HF(^{1}P) wave functions (without spin-orbit interaction) Nevertheless, assuming the same accuracy in the energy level predictions in La^{3+} as in Ba^{2+} we do not observe a strong feature at the position predicted for 4f ^{1}P (see Fig.7.6). However, if we assume that the transition to 4f ^{1}P is not present there is good agreement between our predictions and the observed transitions starting with 5f^{3}D. Attempts to identify the lowest observed resonance with 4f ^{1}P do not lead to agreement with regard to either energy or oscillator strength for the observed features so we are faced with the situation that the strong resonance predicted by us and by others apparently is absent on our plates.

Several potential explanations of this puzzle were explored. One was based on the observation that the 4f orbital, which in the beginning of the sequence is less strongly bound than 5p, with increasing ionization becomes the more tightly bound at which point the $4d^{10}5s^25p^6$ state ceases to be the ground state We believe that this has not yet occurred for La^{3+} Hansen has carried out calculations which show that, even in the presence of a $4d^{10}5s^25p^54f$ state close to the ground state, the $4d^94f$ ^{1}P resonance in La^{3+} would simply be distributed over a finite number of strong transitions which would still be observable

Considering the experimental spectrum in Fig (7 6) we noticed that the observed transitions have widths larger than the instrumental The final states $4d^95s^25p^6nf,np$ are far above the first ionization limit of La^{3+} which is associated with the $4d^{10}5s^25p^5$ configuration. We have

therefore considered the autoionization widths of these resonances using the perturbation approach described by Cowan (1981, Chapter 18). Previously Cheng and Johnson (1983) considered the autoionization of those $4d^9\ ^2D_{3/2}$ nf levels for which decay to the $^2D_{5/2}$ threshold is possible but these authors did not take into account the decays from $4d^95s^25p^64f$ to $4d^{10}5s^25p^5\varepsilon\ell$ This is determined by the electrostatic R^k $(4f5p,4d\varepsilon\ell)$ integral which can be large if 4f is collapsed while the integrals associated with the decay of the higher nf resonances will be much smaller The widths of the resonances have been estimated using the eigenvectors determined already in conjunction with R^k integrals connecting the bound nf basis states to the $5s^25p^44f\varepsilon\ell$ and $5s5p^6\varepsilon\ell$ continua (decay to $5s^25p^44f\varepsilon\ell$ continua was found to be less important). The results cannot be considered more than a first approximation to the real widths but since the largest interaction integral is due to the $4f(E_{av})$ component the main features of the calculation will probably be correct The complete results are expected to be published in the near future (Hansen 1990).

The calculated width of the 4f ^1P state in La^{3+} (Table 7 2) is between 1 and 2 eV It should be pointed out that this calculation assumes that the interaction with the continuum does not lead to an asymmetric, Beutler-Fano, line profile If that assumption is wrong and there are perhaps indications for the other resonances in Fig 7 6 that this is the case, the intensity will be distributed over an even wider range than our calculation indicates This makes it more likely that the reason for the disappearance of the resonance is that its autoionization width has become so large that it is spread out over too extensive a wavelength range to make it visible on a photographic plate with its limited dynamic range

It should be noted that the (collapsed) 4f $HF(E_{av})$ orbital in <u>both</u> Ba^{2+} and La^{3+} leads to autoionization widths of the same order of magnitude The reason that the lowest f ^1P state in Ba^{2+} is narrow enough to be

readily observed in absorption is thus that the 4f orbital in the ^1P state in Ba^{2+} is only slightly collapsed which is reflected in the small 4f(Eav) components in the bound levels mentioned earlier This is one reason for the success of Clark's calculation which does not include autoionization. In La^{3+} the 4f ^1P orbital has collapsed further with the result that the autoionization width has increased by a factor of around 20. Still the fact that the 4f(Eav) component in the lowest state is only 50% means that even here complete collapse in the ^1P state has not yet taken place The very gradual collapse we propose agrees with the results of the calculations of Cheng and Froese Fischer.

Similar behaviour can be expected in other cases of inner shell excitation where $\Delta n=0$ One example is 5d excitations in the actinides where 5f collapses Here the electrostatic integral involved is R^k $(5d\varepsilon\ell, 5fn\ell)$ A case, where we do not expect a similar effect, is the 2p → 3d excitations in the Fe group elements where the integral is $R^k(3\ell 3\ell, 2p\varepsilon\ell)$.

In conclusion, we have shown that the collapse of the 4f orbital in the Xe I isoelectronic sequence leads eventually to very large autoionization widths for the $4d^9 4f$ ^1P resonance This in turn leads to the *"disappearance"* of this resonance. Higher up in the isoelectronic sequence the degeneracy between 5p and 4f will change the appearance of the spectrum further.

7.4.c) The Ce V Spectrum.

Ce V has proved to be the most elusive of the xenon like spectra so far studied. The spectrum is extremely weak and despite numerous attempts at improvement the spectrum still remains to be recorded with the same strength as either the lanthanum or barium spectra reported above Shown in Fig.(7.7.a-f) are the best spectra recorded to date for each of the elements studied up to Nd The cerium spectrum shows a degree of discrete structure in the 80Å region which seems analogous to the Barium and

Lanthanum spectra discussed above It is not possible due to the weakness of the spectrum to give precise wavelengths for any of the discrete structure However, table 7 3 contains the wavelengths of six weak and broad absorption features measured between 75 and 93Å. The wavelengths were measured from an enlarged photographic print of the region on which only faint traces of the absorption features could be seen For this reason the wavelength accuracy in given as $\Delta\lambda=\pm 0.1$Å.

TABLE 7 3

Weak and broad features observed in the absorption spectrum of a cerium laser produced plasma. The wavelength accuracy is given as $\Delta\lambda=\pm 0.1$Å.

λ(Å)	Description
92.6	Very Weak
91 8	.... ..
89.0	.. .
83.7	..... .
76.8	.. .
75.8	....

The spectrum shown in Fig.(7 7.c) was obtained using a hafnium continuum to backlight a plasma created with a de-focused spherical lens on the surface of an adjacent cerium target, while the spectrum shown in Fig (7 7.d) was obtained using the self absorption technique With this method a plasma is created using a single spherical lens which is substantially de-focused and thus the cooler outer regions of the plasma will absorb the continuum produced by the warmer central region of the plasma.

7.4.d) Absorption spectra of Pr and Nd laser plasmas

Both Praseodymium and Neodymium plasmas have been studied in both emission and absorption. However, very little can be reported at this time. In reviewing some of the old work in preparation for the writing of this thesis and in the light of the lanthanum analysis presented above, some very early absorption studies of Nd Plasmas were re-evaluated. The spectra shown in Fig.(7 7 e f) shows

some evidence (although only just) of broad absorption features in the 80Å region of the Nd and Pr spectra There is no evidence to suggest that the observed weak structures in spectra of either praseodynium or neodynium plasmas are due to 4d-nf features in the xenon like ions of these elements The complex nature of the atomic structure of both of these elements together with the unknown ionic composition of the laser plasmas studied precludes this The spectra are presented here with the observation that in this particular wavelength region we have noted what might possibly be broad absorption features, only further more detailed work will elaborate on the point

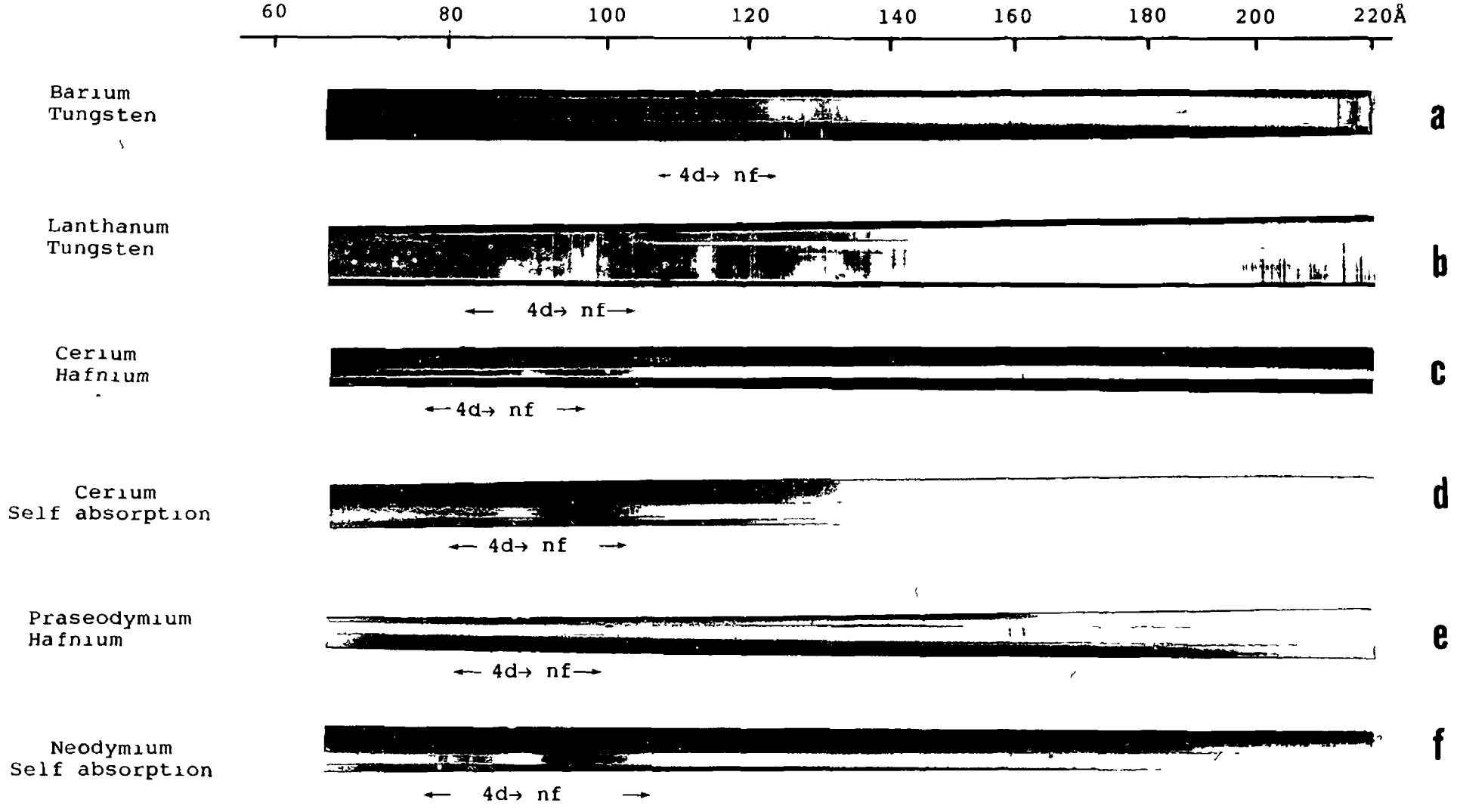

FIG 7 7

XUV absorption spectra of members of the xenon isoelectronic sequence (See text)

Fig (7 7.a b c.d e f)

7 5 REFERENCES

Carroll, P.K Kennedy E T and O'Sullivan G Opt Lett **2**, 72, (1978)

Carroll, P.K. Kennedy E T. and O'Sullivan G Appl Opt. **19**, 1454, (1980).

Carroll, P K. and O'Sullivan G Phys Rev A **25**, 275, (1982).

Cheng KT and Froese Fischer C Phys Rev A **28**, 5, (1983).

Cheng KT. and Johnson WR Phys. Rev. A **28**, 5, (1983)

Clark C W J. Opt. Soc. Am B1, 626 (1984)

Clark C.W and Lucatorto T B NATO ASI *"Giant resonances in atoms molecules and solids"* Plenum N Y. (1987)

Connerade, J.P. Contemp. Phys **19**, 5, (1978).

Connerade, J P and Pantelouris, M Baig, M A Martin, M.A.P. and Cukier, M J Phys B At Mol. Phys **13**, L357, (1980)

Connerade JP and Mansfield MWD Phys. Rev Lett **48**, 131, (1982).

Connerade, J.P and Pantelouris, M J Phys B. At Mol Phys. **17**, L173, (1984)

Cooper, J W Phys. Rev Lett **13**, 762, (1964).

Cowan R D. *"The theory of atomic structure and spectra "* (University of California Press, Berkeley) 1981

Dehmer, J.L. Starace, A F. Fano, U. Sugar, J. and Cooper, J.W. Phys Rev. Lett **26**, 1512, (1971).

Dehmer, J L and Starace, A F. Phys. Rev B **5**, 1792, (1972)

Ederer, D L Phys Rev Lett **13**, 760, (1964)

Geoppert Mayer Phys Rev. **60**, 184, (1941).

Haensel, R Keitel, G. Schreiber, P and Kunz, C. Phys Rev. A. **177**, 62, (1969)

Hansen J.E., Phys. Scrip. (1980) and references therein

Hansen J E Brilly J. Kennedy E T. and O'Sullivan G. Phys Rev. Lett. **63**, 1934, (1989).

Hansen J E (1990) To be submitted

Kelly HP. Carter SL. and Norum BE Phys Rev. A **25**, 4, (1982).

Koch, E E. Kunz, C and Sonntag, B. Phys Rep. **29**, 153, (1977)

Kucas S Karıosıene A and Karazıya R Lıet. Fız Rınkınys 23, 34 (1983); Translatıon ın Sov Phys Coll (USA) 28. 36 (1983)

Lucatorto TB. McIlrath T J. Sugar J and Younger SM Phys. Rev. Lett. **47**, 16, (1981).

Lucatorto, T B. McIlrath, T.J. Hıll, W T. and Clark, C.W ın *X-ray and Atomıc Inner-Shell Physıcs* B. Crasemann Ed. (Amerıcan Instıtute of Physıcs, New York p 584, (1982).

Lukırskıı, A P and Zımkına, T M Bull Acad. Scı USSR Phys Ser. **27**, 808, (1963).

Mansfıeld, M W.D NATO ASI *"Gıant resonances ın atoms molecules and solıds"* Plenum N.Y. (1987)

Nuroh K. Stolt MJ. and Zaramba E Phys Rev. Lett **49**, 862, (1982)

O'Sullıvan, G Ph.D Thesıs *Unıversıty College Dublın* (1980). Unpublıshed

O'Sullıvan, G. NATO ASI *"Gıant resonances ın atoms molecules and solıds"* Plenum N Y (1987)

Radtke, E.-R J. Phys B. At. Mol. Phys **12**, 77, (1979)

Suzukı, S Ishıı, T and Sagawa, T. J Phys Soc Japan **38**, 156, (1978).

Wendın G. and Starace A.F J Phys B 11 4119 (1978)

Zangwıll A. and Soven P Phys Rev Lett. 45, 204 (1980)

CHAPTER EIGHT COMMENTS AND CONCLUSIONS

8 1 COMMENTS AND CONCLUSIONS

This chapter concludes the thesis by briefly summarising the work which has been described in detail in the preceding seven chapters In each of the chapters dealing with specific experimental results we have produced for the most part new and interesting spectra, many of which have been analysed using MCDF calculations (Grant et al 1980) and in many cases have been the subject of publication. The main conclusion of this thesis must therefore be. that the dual laser produced plasma technique used here has proven itself to be very efficient in obtaining VUV and soft x-ray photoabsorption spectra of manifoldly charged ions, thus enabling studies along extended isoelectronic and isonuclear sequences to be carried out.

In chapter two we have described the versatile technique used to record the many new absorption spectra reported throughout this thesis During this work the two laser produced plasma technique has been modified considerably since it was first used by Carroll and Kennedy (1977) to record the VUV photoabsorption spectrum of Li^{+}. The major modifications to the technique included the design of a target chamber large enough to accommodate the two cylindrical targets used in the experiments The two separated and rotating targets were connected to motors outside of the target chamber which in turn were controlled by computer software. The computer control was also extended to the firing of the ruby laser used to create the plasmas which was synchronised with the step wise rotation of the targets, thus making the system more controllable and hence, more reproducible. Improvements

in the control of the relative positions of each of the plasmas with respect to each other as well as with respect to the entrance slit of the spectrograph served to further enhance the system The number of absorption spectra produced during this work testifies to the usefulness and reproducibility of the system in its present form

In chapter three we have presented new absorption spectra of the neon like ions Mg III, Al IV and Si V The absorption spectrum of an aluminium laser produced plasma reported in chapter three is the first unambiguous VUV absorption spectrum of the Al^{3+} ion to show clearly the autoionizing series due to the excitation of one of the inner 2s subshell electrons. The work carried out on silicon resulted in the VUV absorption spectrum of the neon like Si^{4+} ion also being recorded for the first time. Also recorded in the Si V spectrum was, we believe, the first experimental observation of forced autoionization in a laser produced plasma.

In the work reported in chapter four new EUV absorption spectra of the sodium like ions Al III and Si IV were recorded, (Mosnier et al 1988, Brilly et al 1988, Brilly et al 1989). The 2p subshell excitation spectra of sodium like aluminium and silicon were found to be quite complex due to the perturbation of the 3snd and 3sns series. In particular it was shown that because of electrostatic mixing the $3p^2$ configuration acts as a strong perturber of the $2p^5 3s3d$ configuration A detailed analysis of core excited autoionizing transitions from both the ground state and excited states in both Al III and Si IV has been given The work on sodium like ions illustrated that by simply moving the lens used to create the absorbing plasma the dominant ionic species within the plasma could be changed thus allowing absorption studies along isonuclear sequences to be carried out. Under the particular experimental conditions used the even parity $2p^5 3s3p$ states in both Al III and Si IV were also made accessible to XUV photoabsorption spectroscopy

The work presented in chapter five was concerned with the recording of absorption spectra of members of the argon like sequence. Laser plasmas of two elements following argon in the periodic table (scandium and titanium) were studied, in both cases the presence in the spectra of absorption features arising from the argon like ions Sc IV and Ti V was confirmed. This work has also shown that absorption features arising from other ions of both scandium and titanium were also present in the spectra It was argued, by comparison with the work of chapter four and by the number and complexity of the weaker absorption features that they were most likely to be due to the potassium like ions Sc III and Ti IV. The close analogy between the spectra reported in chapter five and the neon and sodium like spectra of chapters three and four was also pointed out.

The Krypton like isoelectronic sequence was the subject of chapter six VUV absorption spectra of strontium, yttrium and zirconium laser produced plasmas were recorded Absorption features were observed in the spectra of each of the plasmas studied. In particular, the zirconium spectrum was dominated by the Zr V ion With the exception of yttrium the spectra recorded were weak and contained little which was not previously known. The main portion of the chapter was concerned with the yttrium absorption spectrum which showed evidence of outer 4p subshell absorption in the Y IV, Y V and Y VI ions at wavelengths longer than 150Å. In the 90Å region of the spectrum we observed several discrete absorption structures which were assigned, with the help of atomic structure calculations, to 3d→4p transitions in the Y V and Y VI ions.

Chapter seven reports results for the xenon like isoelectronic sequence. Work was carried out on Ba III, La IV and Ce V The work on the Ba III spectrum was found to be in agreement with the observations of Lucatorto et al (1981), we further extended the absorption studies

along the sequence to the next member La IV. The La IV spectrum recorded was found to contain several discrete absorption structures in the 130eV region. These structures were analysed (Hansen et al 1989) as $4d^{10} \rightarrow 4d^{9}nf,np$ transitions The analysis was able to show that the 4f transition which was expected to be the strongest absorption feature in the spectrum was in fact absent from the spectrum. The conclusion drawn from this was that the 4f orbital in Ba^{2+} was only partially collapsed Some evidence for analogous short wavelength absorption structures was also observed in the absorption and emission spectra of cerium laser produced plasmas and also in weak emission spectra of neodynium and preaseodynium laser plasmas, however, due to the weakness of these spectra the evidence remains inconclusive

8 2 SUGGESTIONS FOR FUTURE WORK

All of the spectra discussed in the preceding chapters of this thesis could be improved upon. Improvements in the intensity of the individual spectra together with improvements in the measurement of specific spectral features and the extension of the wavelength ranges of study could be easily envisaged There are also a number of spectra which have been discussed, in particular the spectra described in chapters five and six, which were only weakly recorded and which could almost certainly be considered as candidates for further investigation. Also worthy of further investigation are the higher members of some, if not all, of the isoelectronic sequences studied in the previous chapters, in particular the xenon like sequence might be mentioned in this regard

In particular the spectra of Si V and La IV would be interesting spectra to study further. However, future work on these spectra with the present experimental set up would probably not result in any new information being obtained Further studies of the spectra of these ions would only be productive if carried out with a

photoelectric detection system rather than the photographic plate detector used throughout this work. The application of such a detection system to the study of the spectra discussed in the previous chapters of this thesis would result in photoabsorption spectra which contain considerably more information. In particular such detection systems have been successful in obtaining information concerning relative intensities and photoionization cross sections. Such computer interfaced CCD area detectors produce spectral information which can be stored and manipulated in a computer and are therefore a much more versatile detector; these detectors were briefly described in chapter one, (section 1.3, see also Cromer et al 1985, Cooper 1989). Such detectors for the VUV region are set to completely replace the photographic plate as the primary method of detection for this spectral region. Such a system is currently under development in this laboratory (Corcoran 1990) and if employed to study some of the spectra described in the preceding chapters of this thesis then a wealth of new information may well be obtained.

If we consider for example the case of the n=3 member of the autoionizing series in Si V as recorded in the single plasma experiment discussed in chapter three, then there is clearly scope for further work. The profile of this member was seen to change with changing plasma conditions, the feature was also found to be an example of forced autoionization. If a photoelectric detection system was employed in a detailed study of this feature it would probably be possible to acquire an interesting series of observations concerning the precise relationship between the degree of focusing of the laser used to create the plasma and the shape of the profile of the n=3 member in Si V. In other members of the neon like sequence studied, Mg III and Al IV we have observed strong Beutler Fano profiles in the spectra, a photoelectric detection system could be used in the determination of the Fano parameters q and Γ for these profiles. A similar system was employed by Jannitti et al

(1984) using a dual laser produced plasma technique to study the absorption spectrum of a carbon laser produced plasma and study the profile shape of the $1s^2 \rightarrow 2s2p$ resonance in helium like carbon

There is also room for improvement at the front end of the spectrograph, for example, the positional control of the two targets used in the experiment could be further refined by the inclusion of micrometer like target position controllers. The laser power of the present experimental set up could also be increased. A more powerful laser would be an advantage and find a useful application in the present system, however, a more practical approach would seem to be the incorporation of a second laser system into the arrangement A second laser would allow time resolved experiments of the type reported by Carroll and Costello (1986) to be carried out, which would further extend and enhance the current experimental arrangement

In short, there are many areas of the work described above where improvements and advances could be made. There are equally many spectra reported in the chapters of this thesis which could be further studied, either in more detail in the wavelength range discussed or in a different or extended wavelength region or both. The work reported in this thesis has shown that with a relatively simple experimental set up consisting of a low power Q-switched ruby laser and a 2m grazing incidence spectrograph, a valuable wealth of previously unreported photoabsorption spectra of ionized species were recorded. Clearly further new and equally interesting results remain to be uncovered in the field of absorption spectroscopy of ionized species.

8 3 REFERENCES

Brılly, J Mosnıer, J.P and Kennedy, E T. J Phys. B. **21**, 3685, (1988)

Brılly, J. Mosnıer, J P. and Kennedy, E.T. *Proceedıngs of the 9th Internatıonal Conference on Vacuum Ultravıolet Radıatıon Physıcs VUV-9* Physıca. Scrıpta (1990). To be Publıshed.

Carroll, P K. and Costello, J.T. Phys Rev. Lett. **57**, 1581, (1986).

Carroll, P K and Kennedy, E T Phys Rev Lett. **38**, 1068, (1977).

Cooper et al Phys. Rev. A. (1990).

Corcoran, R. M.Sc. Thesıs (Dublın. Cıty Unıversıty.). (1990). Unpublıshed work.

Cromer, C.L. Brıdges, J M Roberts, J R and Lucatorto, T.B Appl. Opt. **24**, 2996, (1985)

Grant, I.P McKenzıe, B J. Norrıngton, P H. Mayers, D.F and Pyper, N.C. Comput Phys. Commun. **21**, 207, (1980)

Hansen, J E. Brılly, J. Kennedy, E.T and O'Sullıvan, G. Phys Rev Lett **63**, 1934, (1989)

Jannıttı, E., Nıcolosı, P and Tondello, G. Opt. Commun **50**, 255, (1984).

Lucatorto, T B, McIllrath, T.J. Sugar, J and Younger, S.M Phys Rev Lett. **47**, 1124, (1981).

Mosnıer, J P Brılly, J. and Kennedy, E.T J De. Physıque **C9**, 219, (1988)

APPENDIX ONE

AP-1.1 INTRODUCTION.

In chapter three section 3.5 we discussed a series of emission spectra of silicon laser produced plasmas in which the shape of the 2s→3p resonance in Si^{4+} was seen to alter with changing plasma conditions, while no similar effect was noted for the 2s→4p feature As was discussed in chapter three this particular feature seems to be a case of forced autoionization which explains the unexpected observation of a Beutler Fano line shape associated with a Si^{4+} feature measured below the ionization limit of the Si^{4+} ion. However, this does not provide an explanation for the apparent alteration of the profile shape with changing plasma conditions In this appendix we offer a series of interesting ideas which may further assist in the explanation of this curious result

AP-1.2. Electron density gradients within the plasma.

The series of spectra shown in Fig.(3 3.a.b.c) were recorded by focusing the output of the laser onto the surface of a silicon target. Each of the spectra was the result of a progressive de-focusing of the incident laser beam from being tightly focused to being de-focused by 5mm, with the same number of laser shots (150) taken in each case Fig.(3 3.a) shows the 2s→3p feature to have a distinct Beutler Fano line shape, this had been previously established by a series of dual plasma absorption experiments using tungsten and hafnium point plasmas to backlight silicon absorbing plasmas created with both spherical and cylindrical lenses. In Fig.(3.3.b) this same feature is seen to take on the appearance of single broad absorption structure with an emission like feature superimposed along its center Fig (3 3.c) is similar to Fig.(3.3.b) except that the effect is more pronounced The point to be argued is whether or not the central portion of the feature is due to emission within the plasma or whether it may be

considered as the reduced absorption region of the original Beutler Fano line shape of Fig.(3 3 a), Fig (3 1 c) and Fig (3 2 b)

The first idea discussed argues in a qualitative manner that the central portion of the profile is the reduced absorption region of the asymmetric 2s→3p resonance in Si^{4+}.

As the lens used to create the silicon plasma is progressively de-focused the plasma increases in size, the average electron density is therefore expected to decrease However, in an expanding laser produced plasma of this size we would also expect an electron density gradient to pertain across the plasma, with those ions in the outer region of the plasma being subjected to a somewhat lower electron density than those ions in the center of the plasma It may therefore be possible to suggest that in the silicon plasma created by successive de-focusing we have effectively two types of Si^{4+} ion. The first type of ion is subjected to an electron density which is sufficiently high to cause a lowering of the ionization limit such that the $2s2p^6 3p^1P$ level appears autoionizing The second type of ion finds itself subject to an electron density which is not sufficient to cause a lowering of the ionization energy by the amount necessary to cause the $2s2p^6 3p^1P$ level to appear autoionizing In this second case the $2s2p^6 3p^1P$ feature may be considered simply as a conventional bound state and should therefore appear in the spectra of Fig (3 3 b c) as a conventional absorption feature If this is the case then the superposition of the two types of absorption profile at the same energy position within the spectrum might conceivably be expected to give rise to the altered profile shape seen to emerge in Fig (3 3.b c) with progressive de-focusing

A typical Beutler Fano resonance of the type observed during this work exhibits a line profile which has an increased absorption region on the low energy side and a

reduced absorption region on the high energy side of the profile. A typical absorption profile shows only increased absorption across the width of the profile with no reduced absorption component Clearly if two such features lie exactly at the same energy in the spectrum then the reduced absorption region of the Beutler Fano profile must suffer a loss of intensity due to the presence of the superimposed absorption profile. This is effectively saying that both features may be thought of as competing for the same continuum at the same energy position in the spectrum This loss of intensity will be clearly more noticeable where the reduced absorption wing of the Beutler Fano profile tails off into the underlying continuum, i e., to the short wavelength side of the profile. It may therefore be imagined that the superposition of the two profiles might give rise to a combination profile which would have the apparent shape of the feature seen in Fig (3.3 b c) Clearly the combination of the two profiles will depend on the number densities of the two types of Si^{4+} ions. It will also be expected that with further de-focusing the plasma will further broaden out and the electron density further decrease such that there will be only a small number of Si^{4+} ions which have a depressed limit, and in this case we would expect to see only a single absorption profile with no trace of a reduced absorption region at or about its center, as the amount by which the lens is de-focused increases

Another idea which might be advanced is to suggest that the feature seen in the spectra of Fig (3 3) could also be interpreted, at first sight, as the emergence of a second absorption feature to the high energy side of the main Fano structure associated with the 2s→3p resonance However, a careful study of the literature relating to all of the ion stages known to be present in the plasma, from a study of the emission spectrum of Fig (3.3 a) revealed no transition with an energy corresponding to that of the high energy absorption structure Also no such second absorption structure was observed to the high

energy side of the 2s→3p resonance in those spectra recorded using the two plasma technique, as might be expected if such a level existed

AP-1.3: Lasing at 74.96Å.

We now argue that the central portion of the feature of Fig (3.3 b c) is in fact due to emission within the silicon plasma The following idea is very much a tentative suggestion put forward to explain the curious line shape. We suggest here that we are in fact observing gain at 74.96Å In a recent paper Harris (1989) has suggested that a population inversion is not a prerequisite for lasing to take place He has considered a four level laser system in which the two upper levels are purely lifetime broadened and decay to an identical continuum. In such a system the absorption profile of the lower level will have an asymmetric Beutler Fano line shape while for the stimulated emission from the upper level there will be a conventional emission line profile and an absence of the interference which gives rise to the Beutler Fano shape resonance The situation is described graphically in Fig.(AP-1) below

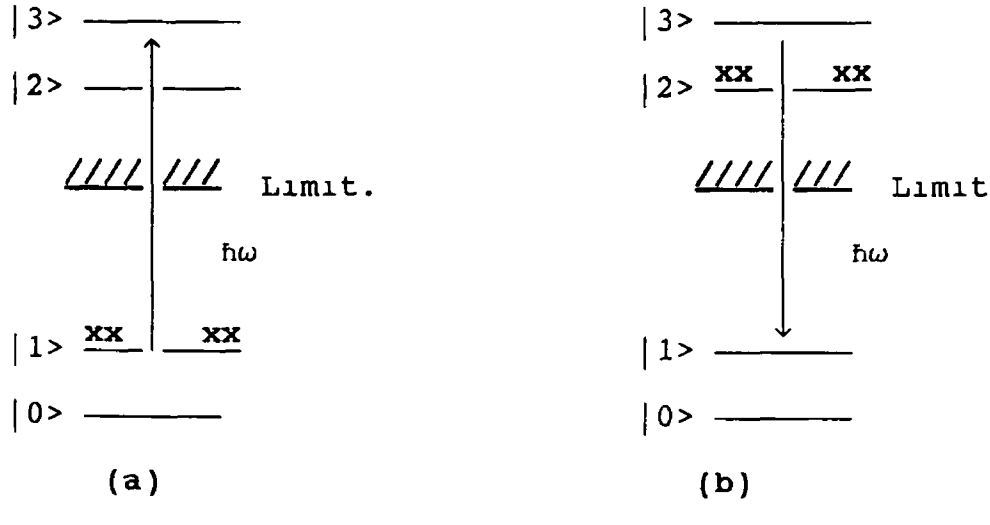

FIG AP-1

(a) Lasing without inversion: atoms in the lower level |1> absorb radiation of ħω and are excited to form a pseudo bound system consisting of an ion and electron (b) atoms in level |2> may autoionize and are stimulated to the lower level (|1>) thus gain is observed at the frequency ħω. (After Harris 1989).

Atoms in level |1> absorb radiation and are subsequently excited to the upper level |2> Because level |2> lies

above the ionization limit of the atom the absorption profile of the $|1\rangle \rightarrow |2\rangle$ transition will be Beutler Fano in shape with increased absorption on the low energy side and a reduced absorption region on the high energy side. Atoms which are initially in level $|2\rangle$ may undergo a stimulated emission to the lower level $|1\rangle$ and in the case of the emission profile there will be no associated asymmetric shape It is therefore possible to observe a gain cross section at frequencies where the absorption cross section is zero and therefore to obtain laser amplification under conditions where the lower-level population exceeds the upper-level population, i e , lasing without inversion. Arkhipkin and Hiller (1983) have shown that a discrete level above the ionization limit (such as the 2s→3p level in Si^{4+}) which exhibits a typical Fano structure will exhibit no such interference in emission They point out that in Fano's theory (Fano 1961) the equation describing the frequency dependence of an autoionizing resonance fails to take account of the autoionizing state population. The Fano theory is considered a good approximation for gases and vapors where lifetimes of such autoionizing states are typically of the order of 10^{-11} to 10^{-13} sec. However, for plasmas the situation is different and a steady state autoionizing state is quite possible due to processes such as electron impact pumping or to recombination processes Arkhipkin and Hiller (1983) have derived an expression for the absorption index and find that it contains a term which may be interpreted as the stimulated emission cross section for the autoionizing level

If the above situation is applied to the Si^{4+} ion then level $|1\rangle$ becomes the ground state and the upper level $|2\rangle$ is taken to be the $2s2p^6 3p\,^1P$ state One observation which might help in support of the argument relates to the intensity of the central portion of the feature In the experiment each of the spectra were recorded with the same number of shots (150) and as can be seen in Fig (3.3) every emission line which is common to each of

the three spectra is observed to diminish in intensity with progressive de-focusing, as might be expected This is particularly well seen in the case of the two emission lines to the short wavelength side of the feature both of which are not seen to self absorb and which both decrease in intensity between Fig (3 3.a) and Fig.(3.3.c) The central emission like region of the autoionizing feature on the other hand is seen to maintain its intensity between Fig.(3.3.b) and Fig.(3.3 c) and does not suffer the same decrease in intensity observed for other features in the region. If the emission part of the feature is the result of gain at 74 93Å then this result would not be un expected due to the increased path length through the plasma as a result of progressive de-focusing of the incident laser beam

Another argument in favor of the emission case may be put forward as follows It is possible that if the central portion of the feature were the reduced absorption region of a fano structure, then an emission line, from some or other ion stage of silicon present in the plasma and having the same wavelength as the feature may be considerably, though artificially enhanced in intensity as a result of the superposition of the two features A similar enhancement of an emission feature *sitting on* the reduced absorption wing of a Beutler Fano structure was reported in chapter three section 3.4 b for the Al^{3+} 2s→3p feature where an emission spectrum overlapped the absorption spectrum and both were well defined. However, for the silicon case there does not seem to be a candidate emission line in any of the ion stages known to be present in the plasmas studied which would correspond to the wavelength of the central portion of the feature This may be seen by reference to the published compilations of known emission lines in ions of silicon below 2000Å given in Kelly (1986), see also Martin and Zalubas (1983). The above discussion would not however, offer an explanation for the observation of the short wavelength absorption portion of the feature observed in the spectra of Fig.(3.3.b.c).

AP-1.4: Configuration interaction.

The third idea put forward to account for the line shape anomaly in the 2s→3p feature in Si^{4+} involves the concept of configuration interaction The $2s2p^6 3p^1P$ level and the higher members of the $2p^5ns,nd$ series have the same parity, therefore configuration interaction between the 2s→3p and $2p^5ns,nd$ levels is possible. However, in the case of the Si^{4+} ion it is also a requirement that the higher members of the $2p^5ns,nd$ series remain discrete, i e , that the ionization limit remain un-shifted In support of the configuration interaction argument it may be stated that a calculation carried out for the P^{5+} ion shows a substantial configuration interaction between the 2s→3p level and certain of the $2p^5ns,nd$ levels, n=4,5,6. However, the requirement that the high n states remain discrete would seem to be contradicted by the arguments put forward in favor of the electron density gradient proposal and by the dual plasma observations of chapter three

The above discussions may be considered as a series of interesting, though tentative, proposals although it is clear that this particular observation would require further experimental investigation Of particular interest in this regard would be the observation of silicon spectra created with even further de-focused laser beams Such spectra could decide the case one way or the other If the central feature is seen to disappear with further de-focusing of the laser beam leaving only a broad absorption feature then the density gradient idea might be considered the more reasonable However, if on the other hand, the central feature is seen to enhance with further progressive de-focusing then the case for stimulated emission would appear to be strengthened Density traces of plates containing stronger spectra than those shown in Fig.(3 3) would be required. Density traces of the spectra shown in Fig (3 3) have been made during this work with the densitometer set to its maximum sensitivity, however, the weakness of the spectra

resulted in traces which were uninformative.

A further series of similar de-focusing experiments performed using an aluminium target might also serve as a useful comparison to the silicon work. Clearly the search for the 2s→3p level in the P^{5+} ion and the comparison of the experimental wavelength of this feature with with the calculated value would also be a further interesting study. This proposed series of experiments highlights the need for sensitive detectors in the XUV region and in particular shows that the above series of experiments, depending as the do on intensity information, would be best conducted using a solid state detector of the CCD type.

REFERENCES

Arkhipkin, V.G. and Hiller, Yu. I Phys. Lett. A 98 1,2 (1983)

Fano, U Phys. Rev. A **124**, 1861 (1961).

Harris, S E. Phys. Rev Lett 62. 9 1033. (1989).

Kelly, R.L. J. Phys. Chem Ref. Data. **16**, 1 (1987)

Martin, W.C and Zalubas, R J. Phys. Chem. Ref Data **12**, 123 (1983)

ACKNOWLEDGMENTS

The author wishes to express his heart felt thanks to all those people who, whether known to them or not, made contributions, substantial, financial and otherwise, to the final version of this work. Firstly I would like to offer my thanks to Prof. Eugene T Kennedy whose unfailing and inexhaustible enthusiasm for this area of experimental physics has been inspiring. I thank him for his forbearance, frankness, attention to detail, approachability and his sense of humour.

To the other members of the spectroscopy group, past and present, I offer my gratitude for the years of ebullient good fellowship and many evenings of merriment at the local hostelry. In particular I am indebted to Jim Cooke, John Costello, Richie Corcoran, Dave Evans, Jean Paul Mosnier, Ciaran Mythen and Gerry O'Sullivan for everything.

To members of the technical staff of various departments of the university, I declare myself grateful In this matter I would like to mention specifically Mr Tommy Walsh of the mechanical engineering department for his crafting, to exact specifications, of the target chamber and other components used in this work. Also to David O' Callaghan and Dave Carney of the Communications department for the efficient and careful preparation of many of the prints and line drawings which appear in this thesis I would also like to express my gratitude to Mr Alan Hughes and the technical staff of the physics department for many useful discussions regarding the finer points of electronics and instrumentation.

I would also like to take this opportunity to thank very much Prof. P K Carroll and the members of the spectroscopy group of University College Dublin, for the use of equipment and facilities and in particular Dr G. O'Sullivan for extremely useful discussions. I am particularly indebted to Dr J P Mosnier of Dublin City University for his analysis and assistance in the work presented in chapter four Also my thanks go to Prof. M.W D Mansfield of University College Cork, for private communications. I would also like to express my thanks to Prof J E Hansen of the Zeeman Laboratory Amsterdam, for his analysis of the lanthanum spectrum. I remain grateful

I would also like to thank Barbara Drew for typing various sections of this thesis and for showing an ability to decipher a difficult style of handwriting, she's to be commended Lastly I must thank Linda, Traudi, Michelle, Olive, Karen and Lorrette who provided me with tea, sympathy and shoulders to cry on, at critical periods during this work